University of Southampton

FACULTY OF NATURAL AND ENVIRONMENTAL SCIENCES

SCHOOL OF OCEAN AND EARTH SCIENCE

Submarine mega-slides from the Norwegian Continental margin and their relationship to periods of climatic change

by

Camilla Watts

Thesis for the degree of Doctor of Philosophy

OCTOBER 2017

Graduate School of Ocean and Earth Sciences,

National Oceanography Centre, Southampton

This Ph.D. dissertation by

Camilla Watts

Has been produced under the supervision of the following persons:

Supervisors:

Prof. Peter J Talling

Dr. James E. Hunt

Prof. Paul Wilson

Chair of Advisory Panel:

Prof. Alan Kemp

University of Southampton

Abstract

FACULTY OF NATURAL AND ENVIRONMENTAL SCIENCES

SCHOOL OF OCEAN AND EARTH SCIENCE

Doctor of Philosophy

By Camilla Watts

Submarine landslides can be orders of magnitude larger than their terrestrial counterparts. The largest of these submarine slides have the potential to generate devastating pan-oceanic tsunamis. For example, the Storegga Slide that occurred on the Norwegian Margin around 8,200 years ago, contained over 3,000 km^3 of material. This slide produced a tsunami that has been detected on coastlines across the North Atlantic, reaching 5 m above sea level across much of Scotland. This landslide was the most recent in a series of mega-slides from the same location, during the last 2.74 Ma. The triggering of these slides has been linked to major deglaciations of the Quaternary period, yet only the 8.2 ka Storegga Slide has been accurately dated. Within the context of modern rates of climate change, this link between large slides and glacial cycles requires further evaluation.

This thesis seeks to understand the timing of these mega-slides, by using a sediment core that captured the distal deposit of the last two slides from the Storegga Slide Complex. It is shown that the penultimate (Tampen) slide occurred at 55.9 ± 4 ka BP, rather than at ~130 ka BP as previously thought. The Tampen Slide is thus much younger than previously thought, and occurred during early period of MIS 3, following a significant deglaciation at the end of MIS 4. We therefore show that the last two mega-slides (Tampen and Storegga Slides) both occurred a few thousand years after periods of significant warming. By showing that the Tampen Slide is much younger than previously thought, this work suggests that mega-slide recurrence times may be shorter than previously thought.

Finally, a new slide deposit from the Lofoten Contourite Drift is dated. We show that this slide occurred ~5,500 year ago during a period of relative climate stability, suggesting that slide occurrence is not always linked to climate cycles. This work highlights our incomplete understanding of submarine slide preconditioning and triggering.

Table of Contents

Table of Tables

Table of Figures

Research Thesis: Declaration of Authorship

Print name: Camilla Watts

Title of thesis: Submarine mega-slides from the Norwegian continental margin and their relationship to periods of climatic change

I declare that this thesis and the work presented in it are my own and has been generated by me as the result of my own original research.

I confirm that:

This work was done wholly or mainly while in candidature for a research degree at this University;

Where any part of this thesis has previously been submitted for a degree or any other qualification at this University or any other institution, this has been clearly stated;

Where I have consulted the published work of others, this is always clearly attributed;

Where I have quoted from the work of others, the source is always given. With the exception of such quotations, this thesis is entirely my own work;

I have acknowledged all main sources of help;

Where the thesis is based on work done by myself jointly with others, I have made clear exactly what was done by others and what I have contributed myself;

Parts of this work have been published as:

Pope, E., Talling, P.J., Hunt, J.E., Dowdeswell, J.A., Allin, J.R., Cartigny, M.J., Long, D., Mozzato, A., Stanford, J.D., Tappin, D.R., Watts, C.J., 2016. Long- term dynamics of the marine based Barents Sea Ice Sheet from a 140,000 year record. Quaternary Science Reviews 105, 55-66.

Signature: Date:

Acknowledgements

I would like to acknowledge my mother, Liz Watts, for her unending support and encouragement. I would like to thank my supervisors, Peter Talling, James Hunt and Paul Wilson for their advice and guidance in producing this thesis. Particular thanks to my honorary supervisor Dave Tappin, whose encouragement, enthusiasm and support was essential in completing this work, it would not have been completed without you. Special thanks for Mike Clare for his assistance in improving this thesis, and help with working in R. Mark Vardy was particularly helpful with digitising and processing analogue 3.5 kHZ data, which took a significant amount of time and effort, contributed to by Shun Wen and Lewis Bailey. Thanks to Vicki Taylor, for helping to pick and count foraminifera, Anya Crocker for the help interpreting stable isotope work and Dave Long for the help both on the cruise and after.

This project has been generously supported by additional research grants, which have contributed greatly to the conclusions. The first was a grant from the National Isotope Geoscience Laboratory, for the stable isotope work which was supported by Prof. Melanie Leng, who was very helpful in writing the grant, and deciding suitable sampling strategies. The tephra work was supported by a grant from the Quaternary Research Association, and took place under the supervision of Prof. Siwan Davies of Swansea University. This was an invaluable tool for this core stratigraphy. A special mention for Dan and John in the rock prep lab, who spent a week prepping samples for me at the last minute. Much of this work took place in BOSCORF, with the support of Suzanne Maclachlan for the non-destructive core analysis, and help with many of the methods and data interpretation. Chuang Xuan and Tim van Peer were instrumental in the palaeomagnetic analysis, particular thanks to Tim for pushing me to pursue this route.

The Ph.D. was made enjoyable by my office mates, Will, Alessandro, Josh, Ed and Zoe, and the rest of the sedimentology research group, including Matthieu, Esther, Age, Jamie and Sophie in addition to my Ph.D. colleagues Hannah, Eric, Neela, James, Stu, Cris and Maya. My deepest gratitude to Nico, for the last few months of this Ph.D., which have been a challenge. Finally, a special mention for Malory who made the final months of writing, and the viva, particularly memorable.

Definitions and Abbreviations

ΔR Radiocarbon Reservoir Correction

^{14}C Radiocarbon

AF Alternating Field

AMS Accelerator Mass Spectrometry

ARM Anhysteretic Remanent Magnetism

Cal BP Calibrated years Before Present (Present refers to 1950)

ChRM Characteristic Remanent Magnetism

FMAZ Faroe Marine Ash Zone (Basaltic)

GSR Greenland-Scotland Ridge

ICP-MS Inductively Coupled Plasma Mass Spectrometry

Ka Thousand years

Ma Million years

MSE Mean Squared Error

NAAZ North Atlantic Ash Zone (Rhyolitic)

NADW North Atlantic Deep Water

NRM Natural Remanent Magnetism

NSOW Nordic Seas Overflow Water

ODP Ocean Drilling Program

REE Rare Earth Element

RPI Relative Palaeointensity

SSC Storegga Slide Complex

TAU Tephra Analysis Unit

µXRF Micro-X-Ray Fluorescence

Chapter 1 Introduction

1.1 Rationale

Submarine landslides are a significant geohazard, and a threat to both population and infrastructure. One of the best studied large submarine landslides, the Storegga Slide, generated a tsunami that was up to 25 m high in the Shetland Islands, and 3-6 m high around parts of the Scottish coastline (Smith *et al*., 1985; Dawson *et al*., 1988; Dawson and Smith, 2000; Tooley and Smith, 2005; Bondevik *et al*., 2012). Tsunami deposits have been identified in Norway, Denmark, the Faroe Islands and Greenland (Bondevik *et al*., 1997; Grauert *et al*., 2001; Wagner and Bennike, 2007; Fruergaard *et al*., 2015). A repeat of this event would be one of the most damaging geological hazards the UK and Europe could face. The Storegga Slide occurred 8,170 years ago, but at least four older slides have been identified within the vicinity of this slide scar. These preceding slides are thought to have occurred over the last 0.5 Ma (Million Years). A better understanding of the timing of these slides helps to understand preconditioning and potential triggering factors, and the recurrence rates of such events.

1.2 Project Aims

This thesis initially precisely dates two turbidites believed to be sourced from the Storegga Slide Complex. The Storegga Slide Complex (SSC) refers to the region of the Norwegian Continental shelf from which the headwalls of at least five buried slides have been identified (the Holocene Storegga Slide (8.2 ka B P), the Tampen Slide (0.13 Ma), Slide R (0.3 Ma) and the Møre Slide (~0.4 Ma) Evans *et al*., 1996; King *et al*., 1996). The turbidite from the Holocene Storegga Slide has been dated from marine records to 7,075 ± 35 14C years (7476-7630 Cal BP (Paull et al., 2010)) and 7,250 ± 250 14C years (7259-8220 Cal BP(Haflidason *et al*., 2004; Haflidason, *et al*., 2005)). This is well supported by multiple dates from terrestrial deposits of the resultant tsunami, which have placed the age of the event at 8,120 - 8,175 years Cal BP. This quality of dating is made possible by the combination of marine and terrestrial dates, and the benefit of the recent age of the slide. The tsunami deposits were largely preserved in uplifted lakes, which were close to sea level at the time of the slide, or preserved as sandy horizons in coastal peat bogs (Dawson and Smith, 2000; Smith *et al*., 2004; Bondevik *et al*., 2005; Wagner and Bennike, 2007; Dawson *et al*., 2011; Long *et al*., 2016). The likelihood of finding tsunami deposits for older slides in such lake or peat bog settings is low due to the scouring action of Pleistocene ice sheets.

The older slides from the Storegga Slide Complex do not have such good quality dating control, as none of these older slide deposits have been penetrated by sediment cores. The dates of these

older slides have been derived through the correlation of seismic packages into the slide scars, resulting in low quality age control. For example, the penultimate slide from the Storegga Slide Complex, the Tampen Slide, was dated using this method to between 30-130 ka BP (Berg *et al*., 2005; Bryn *et al*., 2005). This Ph.D. aims to determine more tightly constrained age, and reduce the uncertainty in age estimates for an older slide from the Storegga Slide Complex: the Tampen Slide. Furthermore, it seeks to place the Tampen Slide within a high resolution stable isotope stratigraphy, allowing an assessment of when within the glacial cycle the slide was triggered. This is important for enhancing our understanding of the role of climate changes in preconditioning submarine slopes to fail. Previously, the Storegga Slide Complex slides have been correlated to major glacial-interglacial transitions, with a short delay after peak warming (Bryn *et al*., 2003, 2005). This raises the prospect that some more Arctic slopes, where there has been significant anthropogenic warming could be, could be at enhanced risk of large-scale failure. Only through accurate dating of older slides can this risk be properly assessed and quantified.

1.3 Thesis outline and key science questions

This section sets out the motivation behind this thesis, the need for this research, and the key questions it seeks to answer.

1.3.1 Research drivers: why study Nordic Submarine Landslides?

Submarine landslides are one of the most voluminous transport mechanisms on Earth, capable of relocating thousands of cubic kilometres of material into the deep sea. A frequent effect of these rapid failures, is the generation of tsunami waves (Lindholm *et al*., 2005; Løvholt *et al*., 2005). These waves can be of comparable size to those generated at subduction zones, such as the recent events in the Indian Ocean and Japan (Bondevik *et al*., 2005). The risk presented by submarine landslide generated tsunamis is both significant and difficult to predict. As such, their occurrence is not limited to active tectonic margins, they can occur in regions of the world unaccustomed to geohazards, with little to no disaster preparation or public education, and without a history of building tsunami resistant infrastructure. It has been demonstrated that not all large slides produce tsunamis (Løvholt *et al*., 2017), yet the debris flows or turbidity currents generated from modest failures, still pose a threat to offshore infrastructure.

Understanding the frequency of these events represents the first step towards effective mitigation. The UK uses the risk matrix outlined in the UK Risk Register to define a framework for handling major emergencies that could affect the UK (The UK Cabinet Office, 2017). The National

Risk Register has an accepted minimum threshold for the frequency of events, before mitigation and recovery measures are considered. For the UK, this threshold is a frequency exceeding a 1 in 20,000 chance of occurring in the next five years. Therefore, for a geological risk to be included, the frequency must exceed 1/100,000 years. The likelihood and severity of each risk is assessed by experts within the relevant field before inclusion. To date, the tsunami risk for the UK has not been included within the National Risk Register.

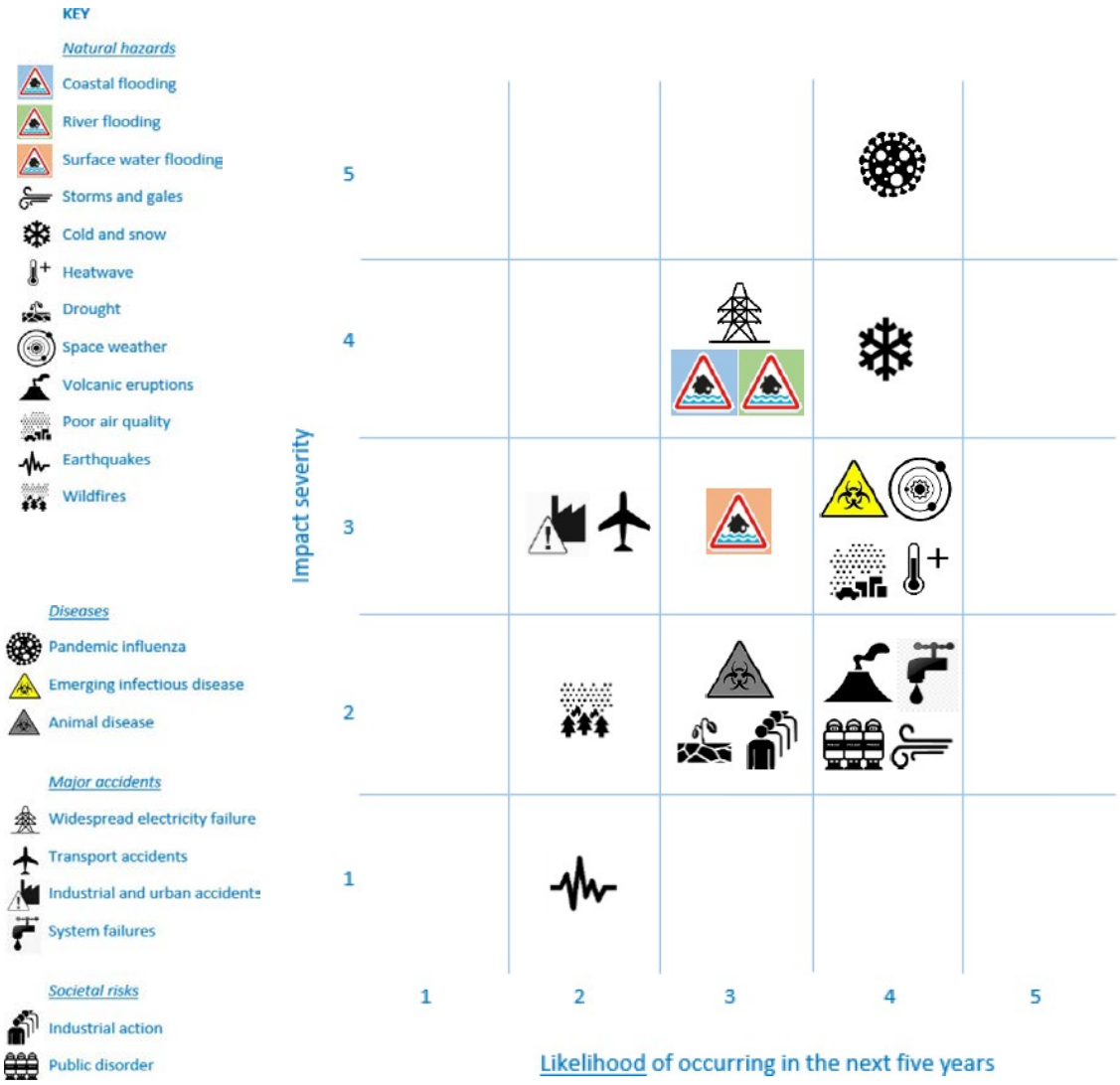

Figure 1.1: Risk matrix for the UK from the National Risk Register, 2017 (UK Cabinet Office). For inclusion, a risk must be defined as an event that would have serious effect on the security on the UK, its people or the environment in which we live. Risks are given a likelihood score, on the probability of their occurrence over the next five years, and an impact severity score. The impact severity is based on likely fatalities, casualties, social disruption, economic damage and psychological impact on the population.

The National Risk Register is reviewed every two years, and reflects the changing world situation and emerging threats, for instance, the 2017 revision now includes the increased risk of the Zika virus, and pervasive cyber-attacks. The 2017 risk matrix is shown in Figure 1.1.

A tsunami striking UK and European coastlines is a unique hazard, quite unlike coastal flooding and storm surges. Tsunamis travel vast distances, at great speeds, and are capable of transporting debris within the waves once on shore. They are rarely one wave, but a sequence of several, and will amplify in height as they ingress wide-mouthed estuaries and inlets.

The Holocene Storegga Slide has been comprehensively investigated, with associated tsunami deposits located across Scotland, the northern UK, Shetlands, Greenland, the Faroes, Norway and Denmark (Bondevik *et al*., 1997; Dawson and Smith, 2000; Grauert *et al*., 2001; Smith *et al*., 2004; Tooley and Smith, 2005; Wagner and Bennike, 2007; Fruergaard *et al*., 2015). The previous slides from the Storegga Slide Complex have not been as accurately dated, but the repetitive failures have been linked with previous glacial-interglacial transitions (Bryn *et al*., 2003, 2005; Solheim *et al*., 2005). Dating errors for older slides are substantial (>50,000 years), and can be improved with analysis of both seismic evidence and sediment cores (Solheim *et al*., 2005; Urlaub *et al*., 2013). Within the context of modern climate change, a re-evaluation of the slide history should be considered, and the potential link between significant environmental change and slide triggering tested. This is essential for understanding the future risk, and what role, if any, global climate change could play in the frequency of geohazards affecting the UK.

The key drivers for this research are to (1) improve on the dates for pre-Holocene events from the Storegga Slide Complex and reduce the error associated with their dates, (2) to evaluate the dates within the context of glacial-interglacial transitions (Bryn *et al*., 2005; Solheim *et al*., 2005), (3) to document a further landslide deposit from the more northerly Lofoten Basin, to add to the growing database of accurately dated submarine landslides. It is only through increasing the number and quality of dated slide deposits that risk can be accurately assessed (Urlaub *et al*., 2013; Pope *et al*., 2015).

1.3.2 Why study turbidites associated with submarine landslides?

Submarine landslides can be orders of magnitude larger than terrestrial landslides, and are a globally important sediment transport process (Haflidason *et al*., 2005; Wynn *et al*., 2010; Urlaub *et al*., 2013; Talling, 2014; Pope *et al*., 2015). Unlike terrestrial landslides, the slopes that fail occur on remarkably low gradients of < 2° (Urlaub *et al*., 2013). Submarine landslides have been documented to be involved in the relocation of several thousand cubic kilometres of material in one event, and mix with seawater to form turbidity currents, which can travel for several hundred kilometres (Talling *et al*., 2007; Talling *et al*., 2012; Hunt *et al*., 2013). One of the largest known, geologically recent slides on Earth is the Holocene Storegga Slide, with a volume of 2,500 -3,400 km3 (Bugge, 1983; Bugge *et al*., 1987; Evans *et al*., 1996; King *et al*., 1996; Haflidason *et al*., 2005).

The turbidity currents formed from submarine landslides become thinner, less voluminous and less energetic with distance, and can travel across the surface of sediment without causing significant erosion (Hunt *et al*., 2013; Hunt, 2017). A turbidity current deposits a characteristic sedimentary unit known as a turbidite. Turbidite facies are ubiquitous across marine deposits, and a typical turbidite deposit is described with reference to an idealized turbidite deposit referred to as a Bouma sequence. The Bouma sequence describes the vertical changes in sedimentary facies with decreasing energy of the turbidite (Bouma, 1962). The identification, correlation and dating of turbidites, is the most reliable form of dating that can be applied to submarine landslides.

Within the Storegga Slide Complex and within close proximity to the Storegga and Vøring regions, the multiple landslide deposits are several hundred meters thick, with large, intact blocks of sediment reaching several kilometres across. In order to date these events using sediment core material, the head scar region is challenging to sample by normal piston coring methods as the large thickness of slide deposits within the scar prohibits coring below the most recent slide deposit without rotary drilling, which is rare in marine studies. Dating in this region is limited to applying chronological tools to the hemipelagic drape above the landslide deposit. In addition, substantial erosion results in the loss of underlying stratigraphy. The marine acquired for the Storegga Slide have all come from the sediments immediately above the slide deposit, within the post-slide drape, either within the slide scar (Bugge, 1983; Bugge *et al*., 1987; Haflidason *et al*., 2005), or from further into the Norwegian Basin above the turbidite deposit (Paull *et al*., 2010).

Turbidity currents deposit a changing combination of facies with increasing distance from the source, with an increasing mud content, resulting in thinner deposits that are more easily penetrated by piston cores. This changing flow and deposit character is justification for distal coring of large or mega-turbidites in order to penetrate the deposit and be able to apply chronostratigraphic methods both above and below the turbidite (Urlaub *et al*., 2013). Previous piston cores captured 20.47 m of turbidite mud cap from the Holocene Storegga Slide (Paull *et al*., 2010). This length of core is at the upper limit of recovery for piston coring, and to fully penetrate the deposit in this location would require a drill ship recovering rotary cores.

1.4 Regional setting

The Northern North Atlantic is defined as the area to the north of the Greenland- Scotland Ridge (GSR). The region in divided into five deep-water basins: Boreas Basin, Lofoten Basin, Molloy Basin, Norway Basin and Greenland Basin (Figure 1.2), either through the presence of the mid-Atlantic Ridge, or of the fracture zones that spread away from the active centre. Material from the Norway Basin forms the basis for chapters 3 and 4, with chapter 5 focussing on the Lofoten Basin.

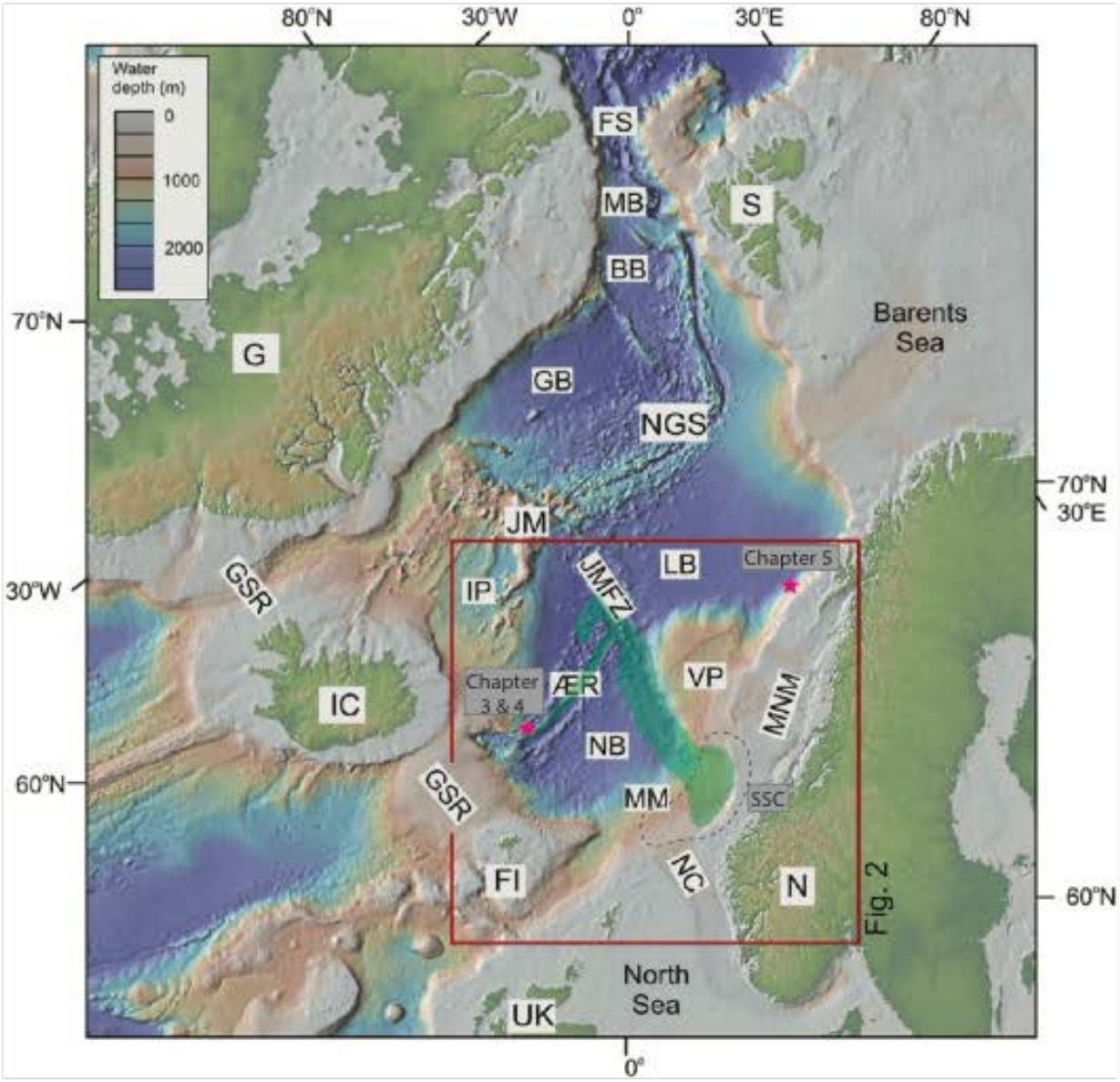

Figure 1.2: A map of the Norwegian-Greenland Sea (NGS) and neighbouring continents. Adapted from Hjelstuen et al. (2015). Red box highlights key areas discussed in thesis. Stars indicate position of cores discussed in chapters as labelled. Green outlines the location of the Holocene Storegga Slide. Dashed black line indicates position of the Storegga Slide Complex (SSC). Abbreviations: the Boreas (BB), Lofoten (LB), Norway (NB), Molloy (MB) and Greenland (GB) basins, are all at water depths of >2000 m. Red box indicates location of map in Fig. 2 (Hjelstuen et al. 2015). ÆR: Ægir Ridge; GSR: FI: Faroe Islands; FS: Fram Strait; G: Greenland; Greenland Scotland Ridge; IC: Iceland; IP: Iceland Plateau; JM: Jan Mayen; JMFZ: Jan Mayen Fracture Zone; MM: Møre Marginal High; MNM: Mid- Norwegin margin; NC: Norwegian Channel; N: Norway S: Svalbard; UK: United Kingdom; VP: Vøring Plateau. Fig. 2 refers to original paper.

The Norway Basin is located within the Norwegian Greenland Seas (NGS), with an area of 2.8 x 105 km2, reaching a maximum depth of 3,970 m. The basin is dissected by the Ægir Ridge, the location of the cores discussed in chapters 3 and 4. This spreading ridge has been extinct since the Oligocene (33.9 ± 0.1 to 23.03 ± 0.03 Ma), following a prolonged period of ultra-slow spreading (Mosar *et al.,* 2002; Hjelstuen and Andreassen, 2015). The basin is bordered to the

south by the steep Greenland-Scotland Ridge, and the north by the Jan Mayen Fracture Zone. The Jan Mayen fracture Zone forms a discontinuous raised ridge, and is connected to the seismically active Jan Mayen micro-continent. The fracture zone extends eastwards into the Storegga Slide Complex, providing a potential source of seismic activity within the slide scar (Mosar *et al*., 2002; Evans *et al*., 2005; Brothers *et al*., 2013). Iceland and the Icelandic Plateau are the western border to the Norway Basin; this active volcanic system provides regular volcanic ash to the basin, utilised in this study as a chronological tool. The eastern border, the wide Norwegian continental margin, is the source material for the Storegga slides (Bugge, 1983; Jansen *et al.,* 1987; Bugge *et al.,* 1988; Evans *et al*., 1996; Haflidason *et al*., 2004; Solheim *et al.,* 2005).

Deep water exiting the Norwegian Basin flows over the Greenland-Scotland Ridge (Hansen *et al.*, 2003) as North Atlantic Deep Water (NADW), formed through the addition of brine from sea ice formation and cooling of inflowing warm surface currents (Rasmussen *et al.*,1999). Where the current passes to the south of the Aegir Ridge core site (chapters 3 and 4) it forms the Iceland- Faroe Frontal Jet (Risebrobakken *et al.*, 2006; Bendle and Rosell-Melé, 2007). The westerly branch of the North Atlantic Current crosses the Greenland Scotland Ridge and follows the 2000 m contour (Orvik, 2002). This current bathes the Ægir Ridge coring site, which therefore records changes in current intensity, as well as fluctuations in the Icelandic Ice Sheet (IIS), and global glacial/interglacial cycles.

1.4.1 Sedimentation history of the Norwegian Continental Shelf

The sediments of the Norwegian Continental Shelf are divided into Eocene (55-16 Ma Brygge Formation) and Miocene-late Pliocene (16-4 Ma Kai Formation) sequences (Ottesen *et al*., 2005; Rise *et al*., 2005, 2006; Ottesen and Rise, 2009; Newton and Huuse, 2016). The Quaternary Period is represented by the Naust Formation, and reaches up to 1 km thick (Newton and Huuse, 2016). The Naust Formation has seen several changes in nomenclature of the units, this work adopts the names of formations from Rise *et al*. (2006, 2010). This division of the formation into five units (N, A, U, S and T, oldest to youngest), simplifies previous interpretations, and is constrained by seismic correlation of the Naust to ODP borehole 644A on the Vøring Plateau (Dahlgren *et al*., 2002). The youngest two units have been constrained using this approach, despite the considerable distance (> 300 km) between the borehole and the Storegga Slide Complex, where identified Naust surfaces have been used to date older slides. Older units have poor age constraint due to a low number of cuttings with dateable material from ODP 644A (Ottesen and Rise, 2009). These units have each been formed through the action of repeated ice sheet advances to the shelf edge, with stratified reflectors representing the hemipelagic sediments deposited during interglacials. Slides from the SSC have been sourced from the material within

the Naust, and most slides have been dated by identifying a key surface within the Naust above or below a massive slide deposit within the SSC.

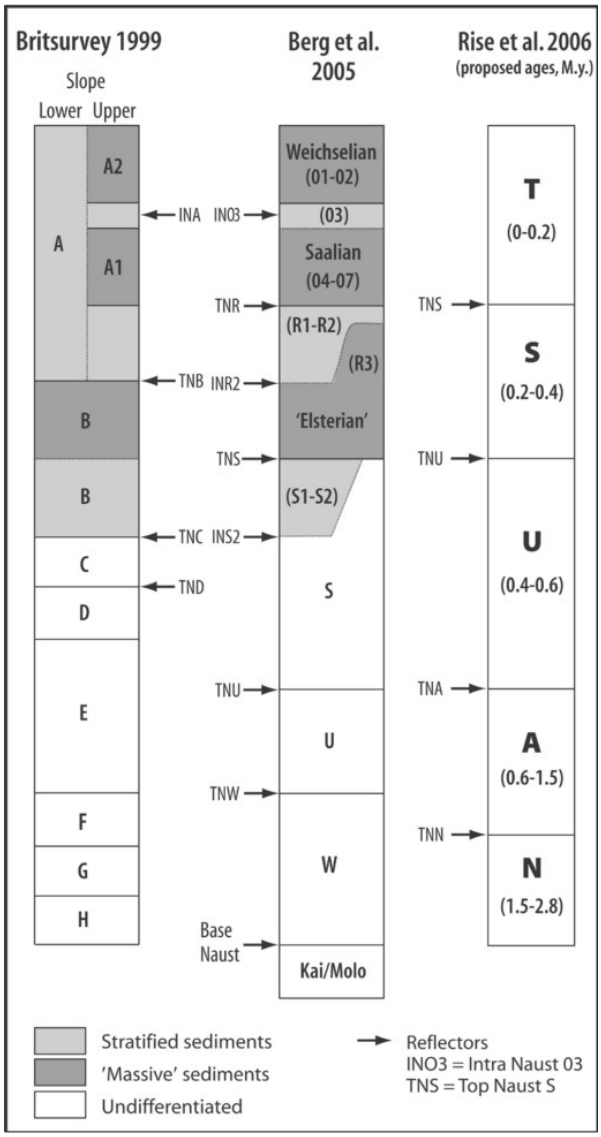

Figure 1.3: Diagram showing the Naust stratigraphy (Quaternary). Diagram reproduced from Ottesen and Rise (2009). Diagram shows the various naming conventions adopted for the Naust stratigraphy and the approximate ages of each unit.

1.5 The Storegga Slide Complex

The first detailed study of the Norwegian continental shelf and slope was carried out as part of exploration efforts for oil and gas. Holtedahl (1971) first recorded the bathymetry of the Storegga area with echo sounding in 1955, with further work detailing the Holocene Storegga slide scar morphology in 1971 and 1973 (Holtedahl, 1971 and Sellevol, 1973, detailed in Bugge, 1983). Extensive surveys conducted in 1974 first detailed the form of the slide, and in 1978 the first estimate of the slide extent and volume was made (Bugge, 1983). This estimate suggested a slide of 75 km wide and 250-300 m thick, with a volume of 800 km3. Later work by Bugge identified

three slide scars within the Storegga region: the First, Second and Third Storegga slides. These slides were broadly dated to 6,000-8,000 years ago for both the Second and Third, and 30,000-50,000 years ago for the First slide (Bugge, 1983; Bugge *et al*., 1987; Jansen *et al*., 1987).

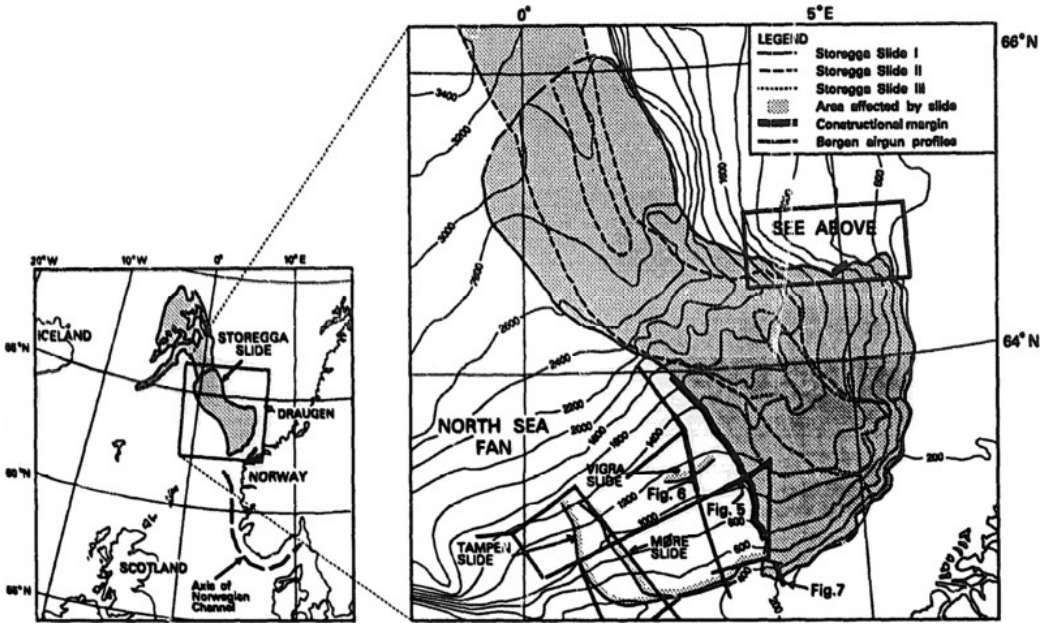

Figure 1.4: Map of the original interpretation of the three Storegga slides, reproduced from Evans et al. (1996) after Bugge, (1983). Showing location of seismic lines used to identify head scarps, and the approximate location of older scarps within the Storegga region. Slides 1-3 are named after Bugge (1983).

The Second and Third slides were later renamed, with the Second slide becoming the Holocene Storegga Slide, and the First being identified as a later failure from the Northern sector of the slide escarpment (Evans *et al*., 1996; Haflidason *et al*., 2004, 2005). The age of the First Slide was approximated using a core from the Ægir Ridge, dated by extrapolating from the age of the Vedde tephra (dated in Jansen *et al*., [1987] to 10,600 BP) to the base of the core 5.5 m below this horizon (Bugge *et al*., 1988). The headwall scarps of the First slide were identified by Evans *et al*. (1996), in addition to the deeper, buried scarps from the Tampen, Møre and Vigra slides (Figure 3.1). The revision of the First Storegga Slide from an independent, earlier event, to being part of the Holocene Storegga Slide is documented in Evans *et al*., (2002). This new interpretation was made on the basis that the First Slide deposits did not have a "well-defined sedimentary cover", as such they were more likely contemporary to the Second Storegga Slide (hereafter referred to as the Holocene Storegga Slide).

1.5.1 A history of mega-slides from the Norwegian Margin

The Storegga Slide Complex has been extensively studied through seismic methods due to both the significant geohazards risk the slide complex poses, and the oil and gas potential of the Norwegian continental margin. Large slide deposits have been identified from 2.74 Ma onwards,

with this phase of major sliding coinciding with the onset of major Northern Hemisphere glaciations at the start of the Quaternary (2.6 Ma). Each slide has been dated through correlation of seismic packages into the slide scar, and the interpretation of a late glacial to early interglacial timing is based on the thick infill of stratified, interglacial sediments within the scar for each slide (Bryn *et al*., 2005; Rise *et al*., 2005; Solheim *et al*., 2005). A significant issue with resolving the chronology of these slides is the paucity of sediment cores recovered from the central Norwegian Basin (Hjelstuen and Andreassen, 2015). The location of DSDP Site 337 on a basement high of the Ægir Ridge is not truly representative of the stratigraphy of the basin (Talwani and Eldholm, 1977). ODP Site 985 was also drilled at a shallower depth than the deep basin floor, on the edge of the Icelandic Plateau, resulting in a substantial difference in the lithology of units correlated to ODP sites on the Vøring Plateau (Hjelstuen and Andreassen, 2015).

1.5.1.1 Early to Mid-Quaternary (2.74-0.5 Ma)

Three older slide units in the Norwegian Basin are identified in this time period, labelled NBS-A, NBS-B and NBS-C. A further slide, Slide-Y is identified within the head scarp of the Storegga slides (Lawrence and Cartwright, 2009). These four older slides confirm a long history of slope failures in this area, extending throughout the entire Quaternary.

The volume of the oldest slide, Slide Y (3.6-1.8 Ma) is unknown, and underlies the colossal, largest failure, NBS-A an estimated 24,600 km^3, close to an order of magnitude larger than the Holocene Storegga Slide (Hjelstuen and Andreassen, 2015). Slide NBS-B is considered to be the same volume, with slide NBS-C estimated at a reduced 15,000 km^3. Dating for these events is based on the identification of regional reflectors, using the estimated 30 cm/ka sedimentation rate of Hjelstuen *et al*. (2007). This approach to dating the slides suggests ages of ~2.7-1.7 Ma (NBS- A), ~1.7-1.1 Ma (NBS-B) and ~ 0.5 Ma (NBS-C) summarised in Figure 1.5.

The earliest slide is coincident with notable changes in the Nordic seas: the onset of major Northern Hemisphere glaciations and a marked increase in glaciomarine sedimentation rate. Refining the ages of these slide events may shed light on the process that initiated sliding from the Storegga Slide Complex, as pre-Pleistocene mass failures have not been identified. Lawrence and Cartwright (2009) have linked the initial phase of sliding to the evacuation of siliceous oozes from large (>10 km) craters within a pre-Quaternary formation. The massive size of the subsequent slide scar created accommodation space for rapid sedimentation, and may have contributed to on-going sliding from the same location.

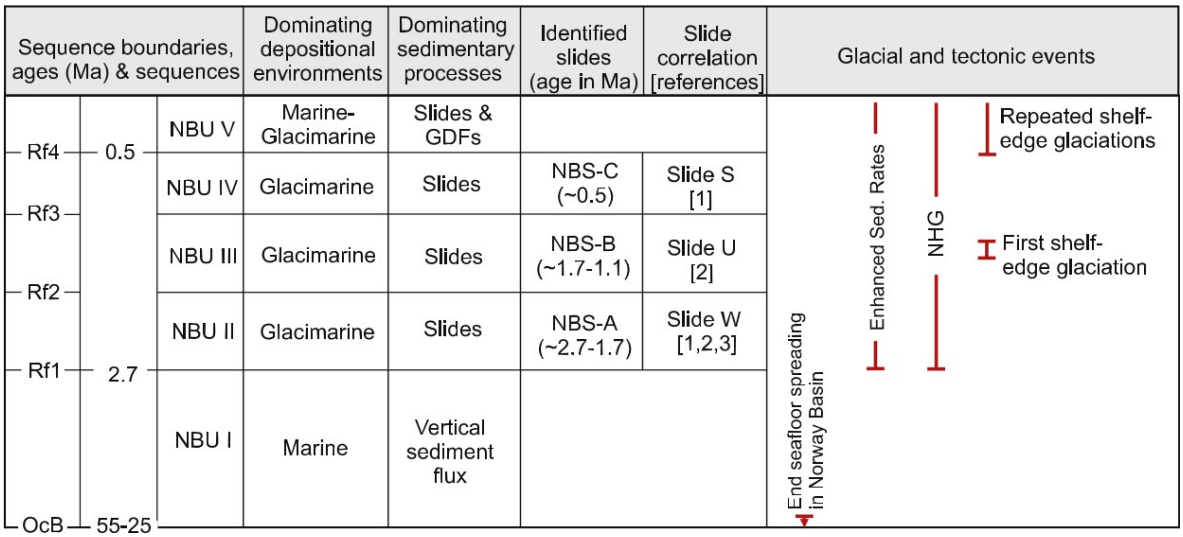

Figure 1.5: Early-Mid Quaternary stratigraphy of the Norwegian Basin, with dates of slides NBS-A, NBS-B and NBS-C. Summary figure from Hjelstuen and Andreassen (2015), showing seismostratigraphic framework (Rf1-Rf4), chronology, identified units (NBU I-NBU V), identified slide debrites (NBS-A, NBS-B, NBS-C), slide correlation and glacial and tectonic events in the study area. OcB: Oceanic Basement. NHG: Northern Hemisphere Glaciation. [1] Solheim et al. (2005), [2] Evans et al. (2005), [3] Lawrence and Carthwright (2009).

1.5.2 Late Quaternary (0.5 Ma to present)

This period constitutes the most active slide phase from the Storegga Slide Complex, with four large slides, which have been dated to c. 100,000 years apart. These slides are the Holocene Storegga Slide (8.2 ka BP), the Tampen Slide (0.13-0.15 Ma), Slide R (~0.3 Ma) and the Møre Slide (~ 0.4 Ma). Chapters 3 and 4 date the most recent two slides using turbidites captured in the Norwegian Basin, whereas the only available dates for Slide R and the Møre Slide, are based on seismic stratigraphy and correlation to ODP drill cores. The slide scars of the four older slides partially underlie the Holocene Storegga Slide scar as shown in Figure 1.6. The Sklinnadjupet and Vigrid Slide scars refer to a more northerly slide complex on the western edge of the Vøring Plateau, not discussed in this thesis.

The Holocene Storegga Slide cut anomalously deeply into the stratigraphy of the region, which complicates interpretations of the true lateral extent of each slide. The slides detailed in Figure 1.6 were identified based on the following criteria (reproduced from Solheim *et al.*, 2005):

Existence of a headwall and side walls in seismic sections formingan identifiable slide scar

Presence of seismically homogenous or chaotic deposits withinthe slide scar

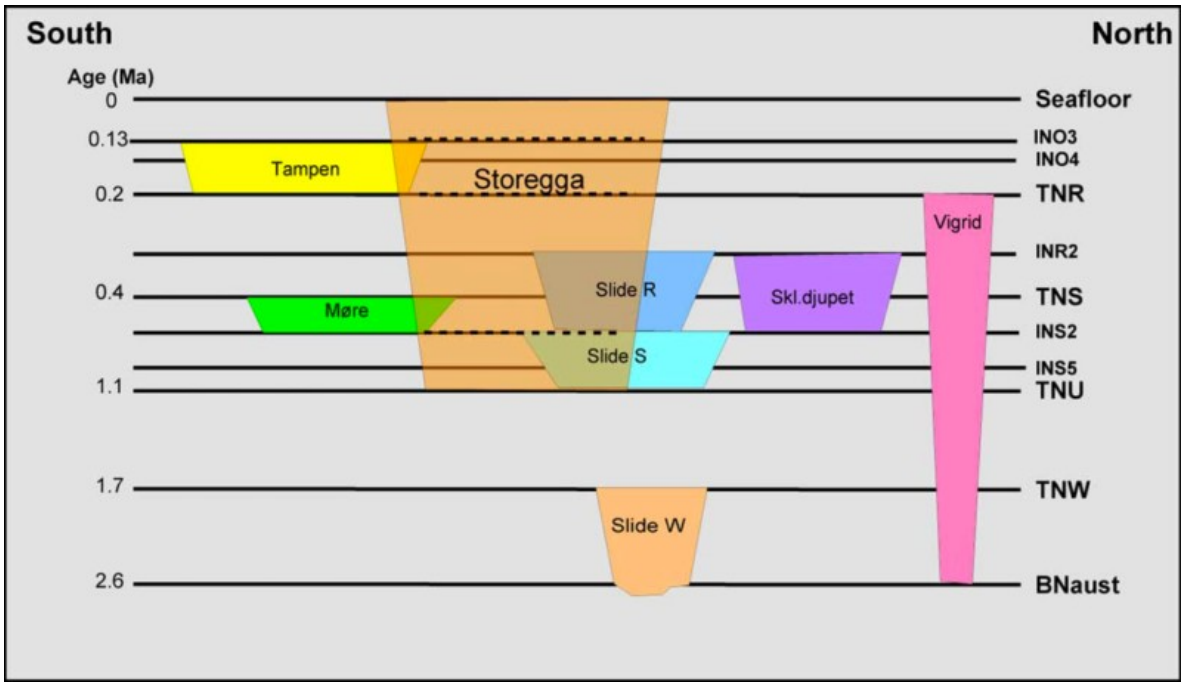

Figure 1.6: Schematic slide stratigraphy of the study area reproduced from Solheim et al. (2005). Note the use of slide nomenclature which has been updated, Slide W corresponds to NBS-A, Slide S to NBS-C. Dashed lines through the Holocene Storegga Slide indicate the most important slide planes for this Holocene slide. The Holocene Storegga Slide has cut into the scar of the Tampen, Slide R, More and Slide S sediments, and has the potential to have erased smaller slide events immediately below it.

The known dimensions of these slides are summarised in Table 1.1, including the reflectors detailed in Section 1.4.1 on the stratigraphy of the Naust formation. The table has been supplemented by the ages of the Naust units as detailed in Rise *et al*. (2006). The key failure planes of each of the slides are also identified, however many slides jump between glide planes as they progress downslope.

Table 1.1: Adapted from Solheim et al. (2005), table to show the dimensions and approximate ages of the four Storegga slides between 0.4 Ma to present. Note that the area given for the Holocene Storegga Slide is a minimum estimate for the erosive slide scar. Estimation of headwall height (a) is through using an average seismic velocity of 1.8 km/s. Failure planes are identified in Figure 1.6.

Slide Name	Scar Area (km^2)	Headwall length (km)	Headwall height [a] (m)	*Stratigraphy*	Age (Ma)	Main failure plane/zone [b]	Stratigraphy (Ma) from Rise *et al.* (2006)
Storegga	27,000	300	<250	Holocene	0.008	INO3, TNR, INS2, INS4, INS5	Late Naust T (0-0.2)
Tampen	27,000	>200	<220	INO3 or slightly earlier	~0.15- 0.13	TNR	Mid Naust T (0-0.2)

Slide R	6,800	120	60-180	Before or Early INR2	~0.3	INS2, Intra S1/S2, TNS	Mid Naust S (0.2-0.4)
More	14,000	160	50-90	Pre TNS	~0.4	Intra S2, INS2	Pre TNU (~0.4)

Improving the age control on each of these older Storegga Slides will substantially improve our understanding of the preconditioning and triggering of these events. Dating of these slides must rely on the successful coring of older marine deposits within the Norwegian Basin. The seismic stratigraphy established in Hjelstuen and Andreassen (2015) identified the Ægir Ridge as a locus of sedimentation from these slides. The Ægir Ridge should therefore be a key coring target for future work on the Storegga Slide Complex.

1.5.3 Dating limitations on the Storegga Slides

The dating of the Holocene Storegga Slide was extensively detailed in Haflidason *et al*. (2005), which utilised 89 marine sediment cores. This study identified the main phase of failure at 8,100 ± 250 Cal yrs. BP, with two subsequent small failures from the slide scar at 5,700 Cal yrs. BP and 2,500- 3,000 Cal yrs. BP. The volume of the later slide phases is restricted to c. 1 km3 of material, in comparison to the 2,500-3,200 km3 of the main phase (Haflidason *et al*., 2005). The date of 8,100 ± 250 Cal yrs BP for the main phase is confirmed by the extensive database of terrestrial tsunami deposits, which yield a date of 8,170 Cal yrs. BP (Bondevik *et al*., 2012).

The Holocene Storegga Slide is the only identified slide within the Storegga Slide Complex to have been dated using sediment core material. The work of Bugge (1983; 1987) identified a deeper slide with a postulated date of 30-50,000 yrs. BP, but this age was dismissed on seismic evidence (Evans *et al*., 2002). The older slides within the Storegga complex have been dated by correlating identifiable Naust units and reflectors into the slide scars (Berg *et al*., 2005; Solheim *et al*., 2005). Interpretations for the stratigraphy of the Ormen Lange region were based on the analysis of > 25,000 km of seismic lines (2D and 3D), complimented by a set of boreholes and targeted coring in the scar region (Berg *et al*., 2005).

1.5.4 Other large volume slides in the Nordic Seas and Arctic Ocean

The Storegga Slide Complex represents one of the most intensively studied late Quaternary slide complexes in the world. This is in part due to the unparalleled study of both slide and resultant tsunami deposits, and due to the 2005 licensing of the giant Ormen Lange gas field, which lies within the Holocene Storegga slide scar. Numerous other slide complexes have been identified

within the Nordic Seas (Evans *et al*., 2005). The key features of these slides are summarised in Table 1-2, in addition to the date derived for each slide and the method used. This table briefly summarises the state of knowledge of submarine landslides in the Nordic Seas, and demonstrates the large age uncertainties for each event. Improving the age estimates for each of these slides will develop our comprehension of preconditioning and triggering of these events. Once age estimates for each event have been obtained, similarities in slide complex behaviour can be assessed, and a comprehensive model for submarine landslide (and tsunami) risk in the Nordic Seas to be developed.

Table 1.2: Table of mapped slides from the Nordic Seas. Table details the rough extent or known dimensions, the date deduced for each slide and the method used. SS = seismic stratigraphy, where dating has been applied through seismic correlation, 14C = date generated by radiocarbon dating from a sediment core.

Name and references	Location	Description	Volume	Date (ka) and method	Glacial/ Inter-glacial/ deglacial	Notes
Trænadjupet / Nyk (Laberg *et al.*, 2002; Evans *et al.*, 2005; Allin *et al.*, 2017)	North Vøring Plateau, Lofoten Basin	Three large slides identified, located at the edge of the Træna ice stream.	5-700	2.6-3.4 (14C)	Interglacial MIS 1	Slide complex aligned with the Bivrøst Fracture Zone
			9-1100	18.6-20.9 (14C)	Deglacial MIS 2-1	
			Unknown	60-66 ka BP (M. Watts)	Glacial/ Deglacial (?) MIS 4/MIS 4-3	
Sklinnadjupet (Dahlgren *et al.*, 2002; Rise *et al.*, 2006)	West Vøring Plateau, north of Storegga	Buried slide, headwall 60 m high, 80 km long	Unknown	339-245 SS	Unknown	Rise *et al*., 2006 revised the Vigrid Slide to be part of the Sklinnadjupet Slide
Hinlopen-Yermack (Vanneste, Mienert and Bunz, 2006; Winkelmann, 2006; Winkelmann and Stein, 2007; Geissler *et al.*, 2016)	North continental slope off Svalbard	Steep headwall (1200 m), potential clathrate involvement	1250-2400	c. 30 14C of adjacent turbidite	Interglacial-Glacial MIS 3-2	Actual slide debris not dated, only dated from above, on an adjacent lobe assumed to be part of the same slide

Fram Slide **(Elger *et al.*, 2015, 2016)**	West continental slope off Svalbard	17 slides between 5 Ma to 0.68 Ma Deep slide >3 km water depth	1.7-1160 65-220	500-68 SS 60 SS	Various Glacial MIS 4	Close proximity to Spitsbergen Transform Fault and Molloy Ridge
Bear Island **(Laberg and Vorren, 1993)**	South of Bear Island	Large buried slide, 400 m headwall	1,100	< 330 SS	Unknown	
Bjørnøya Fan mega slides A, B and C **(Hjelstuen *et al.*, 2007; Safronova *et al.*, 2015)**	Each slide scar overlaps from the Bjørnøya Trough, and extends into the Lofoten Basin	Slides identified in Seismic lines only	25,500 24,500 11,600	Dated to between 1.0-0.2 Ma with c. 370 ka between events	Unknown	These slides substantially exceed the volume of Storegga.
Molloy Slide **(Freire *et al.*, 2014)**	Western Svalbard Shelf, adjacent to Molloy Hole	Deepest documented slide, low transport distance (<5 km).	65	Unknown	Unknown	Massive vertical displacement (> 3 km), adjacent to active Molloy Ridge
Jan Mayen Slide **(Laberg *et al.*, 2013)**	East sector of Jan Mayen Ridge	Large amphitheater shaped scar, bottleneck slide	60	Unknown	Unknown	Frequent volcanism and seismicity along ridge. Steep volcanic center.
Fugloy Slide North and South **(Taylor *et al.*, 2003)**	2 adjacent slides, Fugloy South is cut by Fugloy North	Comparable in size to the Andøya Slide	Unknown	Unknown, but minimal sediment cover	Deglacial-Holocene (?)	
Andøya Slide **(Laberg *et al.*, 2000)**	Immediately north of the Andøya Canyon, SE Lofoten Basin	Smaller than Trænadjupet (covers 9700 km2, to 14100 km2)	Unknown	Max 10 14C	Interglacial MIS 1	
Faroe Slides **(Nielsen and van Weering, 1998; Van Weering *et al.*, 1998; Taylor *et al.*, 2000)**	Multiple slides identified, largest is greater in volume than Storegga (Early Pliocene)	Largest Slide occurred in the early Pliocene, smaller failures c. 17 ka BP	>3,000 17 ka BP	SS 14C	Unknown Deglacial	Multiple failures identified and not yet dated.
Miller Slide **(Evans *et al.*, 2005)**	Northern end of the Faroe-Shetland Channel	Covers area of 5,700 km^2, series of flows extending over 95 km	840	c. 200 SS	Unknown	Located on the UK margin, nearly in filled slide scar

Helland Hansen Slide **(Evans *et al.*, 2005)**	SE of Sklinnadjupet, up to 13 km long, 90m thick, only terminal 20 km located	Pre-flow location not known, probably headwall to east of Helland Hansen arch	Unknown	Unknown	Mid-Pleistocene (Near base of NAUST B)	Large debris unit located, but full extent of slide unknown

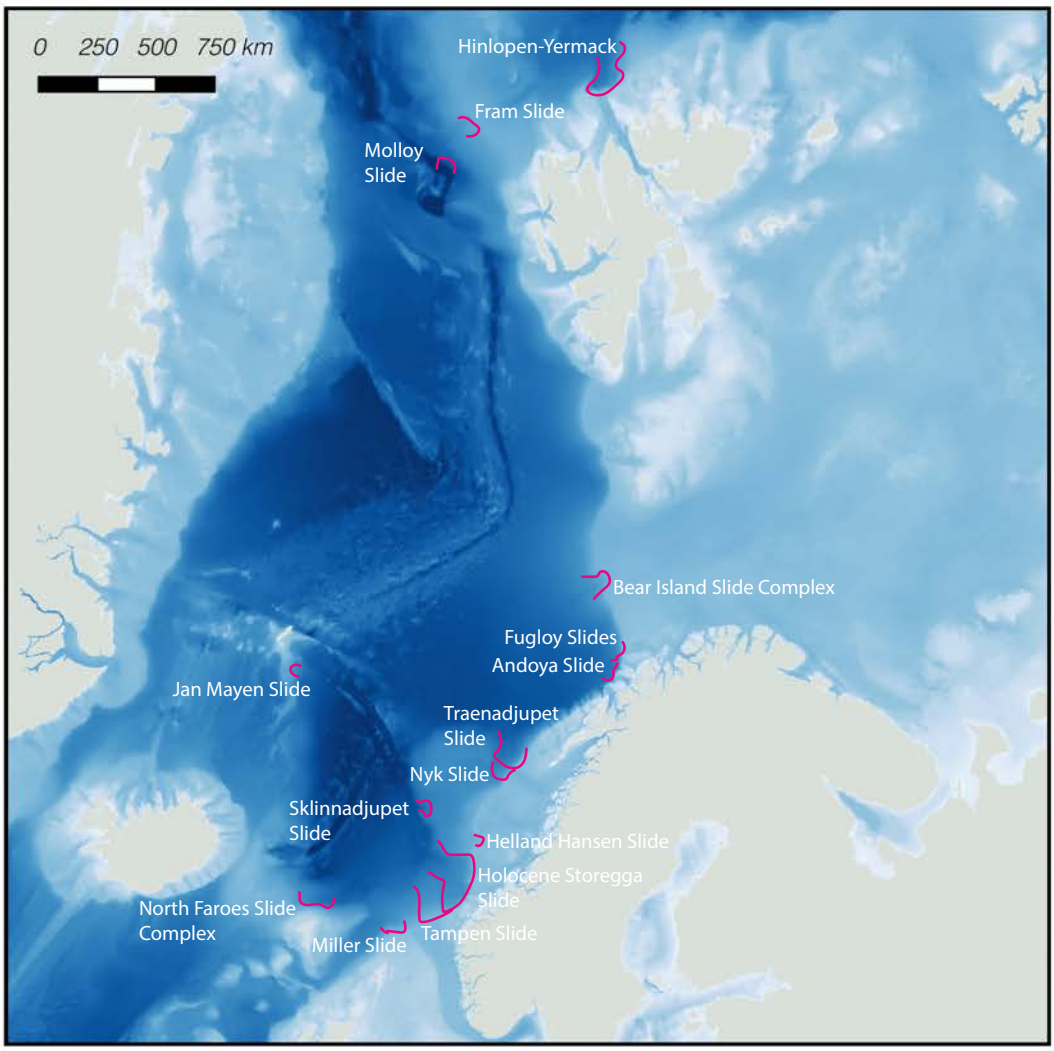

Figure 1.7: Summary map of slide complexes from the Nordic Seas (adapted from Evans et al., 2005). Locations of headwalls of palaeoslides identified in Table 1-2. Locations of tectonic features are highlighted in red. Not shown are the Bjyornoya, Fugloy, Hinlopen-Yermack and Fram Slides.

1.6 Geohazards: The Storegga Tsunami

The identification of the submarine Storegga Slide (Bugge, 1983) was closely followed by the description of a coarse sand layer found across eastern Scotland (Smith *et al.*, 1985). The horizon was initially dated to c. 7000 B.P, and attributed to an unusually large storm surge, or very rapid sea level rise (Figure 1.8; Smith *et al.*, 1985). This interpretation was revisited on the basis of the dates for the Second Storegga Slide/Holocene Storegga Slide (description after Bugge, 1983) and

the lack of any further sand layers within the region (Dawson *et al*., 1988). The agreement of the dates of the slide from Jansen *et al*. (1987) and the sand layer from multiple sites suggested a link between these two events. This interpretation was supported by modelling work, that predicted tsunami heights close to the topographic height of the known deposits when accounting for sea level change and isostatic rebound (Harbitz, 1992).

Within the UK, further tsunami deposits were located in Sutherland (Dawson and Smith, 2000), with additional deposits identified along the east coast of Scotland (Smith *et al*., 2004). The wave heights were most significant on the Shetland Islands, where the wave was calculated to have reached 25 m a.s.l (Smith *et al*., 2004; Bondevik *et al*., 2005; Bondevik *et al*., 2012). Similar deposits located on the Faroe Islands recording the passage of at least two waves, dated to 8,100-7,300 cal yrs. BP, each with a suggested height of at least 10 m (Grauert *et al*., 2001).

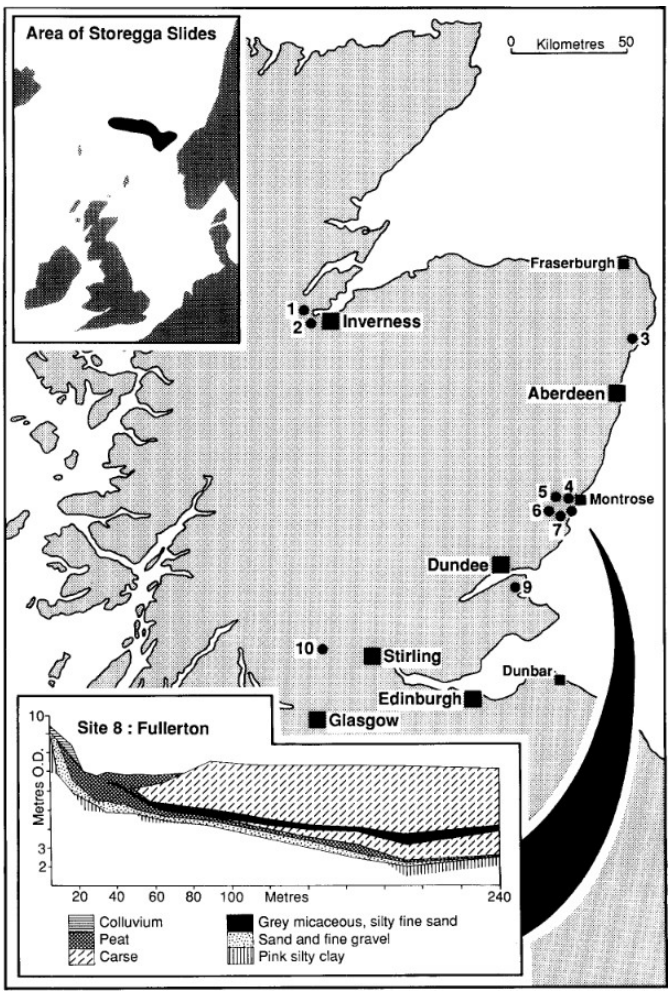

Figure 1.8: The location of the Storegga Slides and the sand layer in eastern Scotland (Taken from Dawson et al., 1988). Numbers refer to sites where the sand layer has been investigated: 1 – Barnyards; 2 – Moniac; 3 – Waterside; 4 – Puggieston; 5 - Dubton; 6 – Bonnyton; 7 – Old Montrose; 8 – Fullerton; 9 – Silver Moss; 10 – Easter Offerance.

Further evidence of a tsunami inundation was located in Norway, with evidence of multiple waves preserved in some locations (Bondevik *et al*., 1997). Bondevik identified a tsunami height of 10-11 m above the high tide mark closest to the slide scar (Figure 1.9), using a series of progressively higher altitude lake basins. Following the interpretation of widespread tsunami deposits in Scotland and Norway, further deposits were identified in additional countries across the North Atlantic.

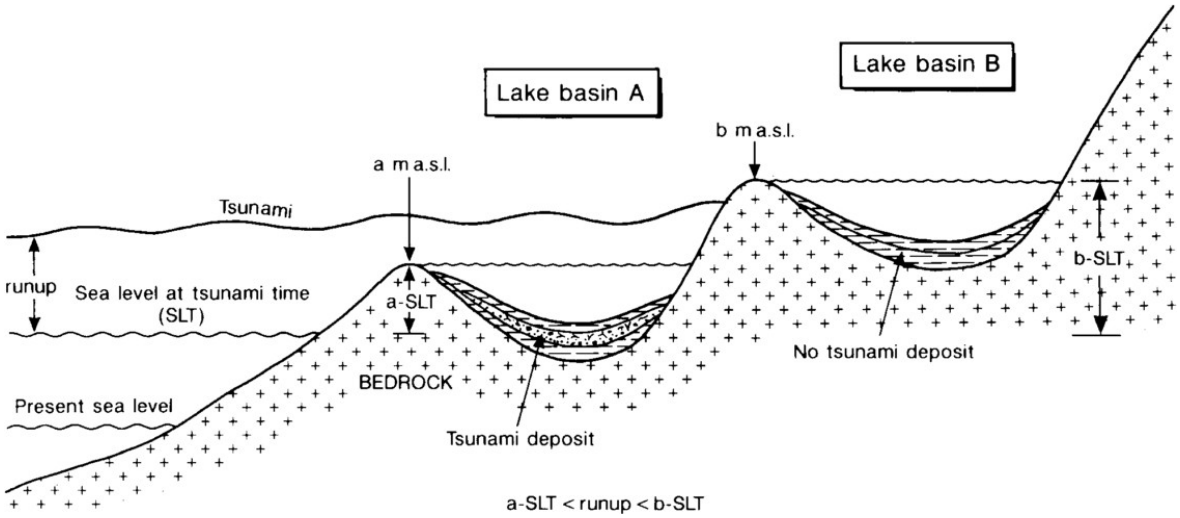

*Figure 1.9: Sketch showing how vertical run-up of the Storegga Tsunami was estimated in Bondevik et al. (1997). Tsunami deposits have been identified in Basin A, but not in Basin B. Estimated run-up is thus somewhere between the threshold of Basin A (**a** m.a.s.l.) and threshold of basin B (**b** m.a.s.l.). The smaller difference in elevation between basins A and B, the more precise is the measure of run-up estimated.*

The first evidence of the tsunami reaching East Greenland was identified in Loon Lake in 2003 (Wagner and Bennike, 2007). Loon Lake is currently 18 m a.s.l, and contains a 0.72 m thick horizon with an erosive base, composed of sands with absence of diatoms. This horizon was dated to between 8,630-7,575 cal. yrs BP, at which time the lake was 15-35 m below current sea level. A reconstruction of wave height was not possible at this location, but can was interpreted as evidence of a significant tsunami impact on the Greenland shoreline.

A palaeo-lake on Rømo, east Denmark, currently ~16 m, below sea level has also been identified as a tsunami deposit (Fruergaard *et al*., 2015). A sea level-based reconstruction of the site suggested a wave height of between 1.5-5.5 m, indicating for the first time that a Storegga sourced tsunami was capable of traversing the shallow Southern North Sea. This is interpreted as evidence that a repeat of the wave would reach the low-lying coastlines of the south-eastern North Sea.

1.6.1 The risk to modern society

A repeat of the Holocene Storegga Landslide and tsunami would be extremely damaging for the UK and Europe. Regions of high population density, with low elevation above sea level are particularly vulnerable, and these include the Danish and north Netherlands coastlines, in addition to the east coast of the UK. For the UK, major cities now occupy positions known to be vulnerable to wave heights of c. 5 m, including Aberdeen, Dundee, Edinburgh and Inverness. Further to the substantial threat to population, these locations are also the host to nationally important energy infrastructure, notable on Shetland the Sullom Voe oil terminal, on mainland Scotland the Dounreay and Torness nuclear power stations, and the Grangemouth oil refinery.

Offshore risks are also substantial, with North Sea oil platforms at risk, in addition to the Ormen Lange hydrocarbon infrastructure now located within the slide scar associated with all the Storegga Slide Complex failures. Oil and gas pipelines as well as internet communication cables run across the North Sea and would be particularly at risk where they come to shore.

The greatest element to this risk is the fact the UK is not prepared for a tsunami. For tectonically active countries, preparation and education mitigate the potential risk, but for countries located on passive margins with an infrequent but significant risk, these measures do not exist.

1.7 Key questions addressed by this thesis

1.7.1 Question 1: What was the timing of mega-slides from the Storegga Slide Complex and how accurately can this be constrained?

This research provides dates for the last two mega-slides from the Storegga Slide Complex area using mega-turbidites deposited within the Ægir Ridge. In particular, it provides a new age for the Tampen Slide. These dates provide a test of the hypothesis that mega-slides occur every ~100,000 years, and coincide with 100,000 year climate cycles, as has been previously proposed (Berg *et al*., 2005; Bryn *et al*., 2005; Solheim *et al*., 2005).

To do this, the composition and thus source area for the Ægir Ridge megaturbidites is determined. The turbidites are then dated using a multiproxy approach covering a range of methods suitable for late Quaternary marine sediments. These methods include radiocarbon dating, tephrochronology, coccolith biostratigraphy, palaeomagnetism and the analysis of IRD (Ice Rafted Debris) content to identify Heinrich layers (Chapter 3).

1.7.2 Question 2: What are the implications of submarine megaslide recurrence intervals for the UK National Risk Register?

The recurrence interval for the last two (Tampen and Storegga) mega-slides is found to be shorter than previously thought, and less than 100,000 years. The UK National Risk register considers events with recurrence intervals of less than 100,000 years. The implications for whether submarine landslide-tsunamis should be included within the UK National Risk Register are therefore subsequently discussed.

1.7.3 Question 3: How is the timing of mega-slides related to periodsof environmental and climatic change?

Chapter 4 seeks to understand how the timing of the Storegga and Tampen slides is related to variations in palaeo-ocean temperature and climatic cycles. It tests whether both the Storegga and Tampen slides occurred during periods with similar ocean temperatures and ice sheet conditions. If both slides were triggered following a delay after deglaciation, this has important implications for predicting future events.

1.7.4 Question 4: Was the landslide within the Lofoten Contourite Drift triggered at the same time as the adjacent Trænadjupet Slide

Chapter 5 dates a small slide near the Lofoten Contourite Drift, which is located 40 km north from the much larger Trenadjupet Slide. If the dates for both slide events are shown to be contemporaneous, this may suggest that regional earthquake shaking, or widespread climatic change was the trigger. We therefore discuss the significance of these landslide ages for understanding their trigger(s).

These four questions are addressed in the following chapters. Question 1 and 2 are addressed in Chapter 3, which applies a range of dating methods to a core from the Ægir Ridge. Chapter 4 builds on this new chronology, and addresses question 3. It reconstructs palaeo-oceanographic conditions around the time of the Tampen and Storegga Slide, with a focus on palaeotemperature and salinity. This helps to determine whether both slides occurred in the same part of glacial cycles. Question 4 is the subject of Chapter 5, which dates a small landslide deposit on the Lofoten Margin. This chapter tests whether both slides were triggered at the same time, potentially by a shaking due to a major regional earthquake.

Chapter 2 Methods

2.1 Introduction

This thesis is based on the analysis of a suite of sediment cores collected as part of the Natural Environment Research Council (NERC) funded Arctic Landslide Tsunami Project. The sediment cores used for this work were recovered during the 64PE391 July 2014 cruise to the Nordic Seas aboard the *RV Pelagia*. This chapter outlines the methods used to analyse those cores.

There are three key questions:

1. When were the turbidites from the Aegir Ridge deposited? A multiproxy approach to dating has been taken, with the methods used depending on the timescale involved and the material available. These methods are detailed in the chronology section, and discussed in relevant chapters.

2. What can the sampled deposits tell us about the palaeoceanographic environment during which mass transport deposits were emplaced? This is the basis of Chapter 4, which examines surface and deep-water conditions at the time of the slides; specifically, palaeotemperature, salinity and volumetric changes of the Quaternary Fennoscandian Ice Sheets (FIS).

3. What can be interpreted with respect to preconditioning and triggering of large submarine landslides? Chapter 3 presents a substantially revised date for one of the largest known submarine slides (the Tampen Slide), and this date is examined in relation to global climate records, the Fennoscandian Ice Sheet, and regional events to assess the contribution of these factors to the triggering of the slide.

This chapter introduces methods that will be used in subsequent chapters and discusses the theoretical basis and limitations of each method. These methods have been chosen to explore the emplacement timing of mass transport deposits (landslides and turbidites), and the associated environmental conditions prior to which they were emplaced. In addition, methods have been used to determine the provenance of the deposits, and tie the distal deposits to known slide scars where possible. Individual chapters contain a shortened methods section with a summary of the relevant methodological descriptions provided here.

2.2 Core collection and types of core

Coring locations were selected to target sediment successions likely to contain hemipelagic material interbedded with mass transport deposits. Whilst mass transport deposits can be detected using seismic surveys, sediment cores provide calibration for geophysical surveys. Capturing the deposits resulting from mass transport events within a hemipelagic succession is the only way to accurately determine bed thickness, to provide a date for the event, and to calibrate any interpretations made from seismic data. Sediment cores collected by piston coring methods are limited to the length of the core barrel (20 m on-board the RV Pelagia), with most cores not exceeding 15 m in length.

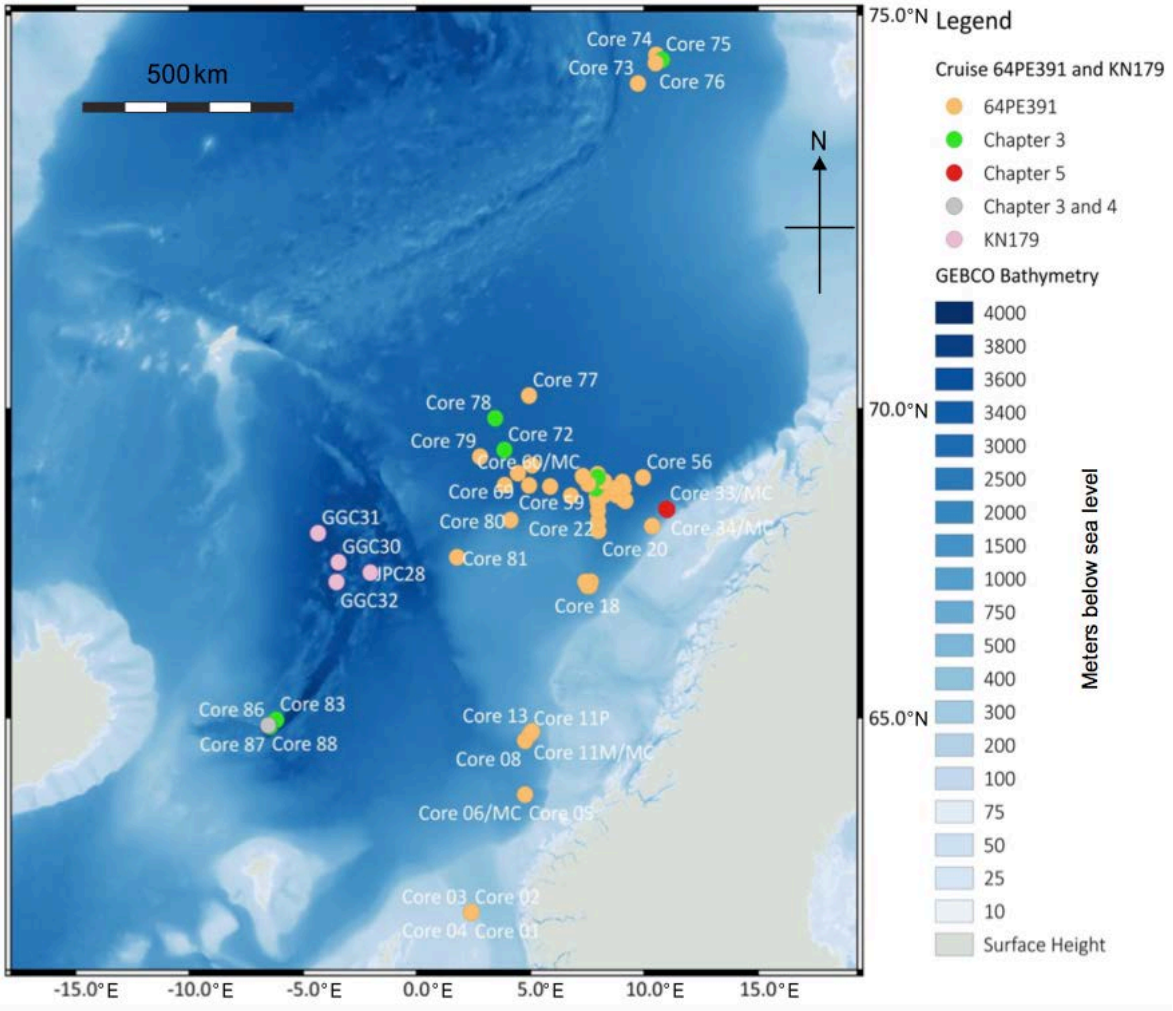

Figure 2.1: Map of coring locations in the Nordic Seas from cruise 64PE391, and cores from cruise KN179 (2004) used in this study. Cores are colour coded by chapter; chapter 3 includes both green cores from 64PE391, and a sample from JPC28 (Collected as part of cruise KN179). Core PC88 is the only core used for chapter 4. Chapter 5 focuses on the cores shown in red (PC33-38). Remaining cores are not discussed in this thesis.

Within the Nordic Seas, a typical sedimentation rate of 5 to 10 cm per 1,000 years limits the captured chronology to 75,000 to 150,000 years of hemipelagite (Hjelstuen *et al.,* 2004). The number and volume of mass transport deposits captured within a core also affect this. A hemipelagic age range that exceeds 43.5 ka BP (the limit of AMS radiocarbon dating), means a range of multiproxy chronological methods need to be used to date the hemipelagite.

This thesis is based on a series of sediment cores from the Nordic Seas (fig. 2.1), which were collected in two different ways; via piston coring and multi-coring. Piston cores are up to 18 m in length (11 cm diameter), and are much longer than multi-cores, which only sample the upper 40 cm of sediment below the sea floor (8 cm diameter). However, multi-cores recover the sediment water interface, whilst piston cores can lose the upper few centimetres of sediment immediately below the seafloor, either by compression from the coring device, or extrusion at the seafloor. Both types of core are needed to both preserve a long record, and to be sure that the most recent events are recovered. Chapters 3 and 4 focus on one core, PC88, collected from the Ægir Ridge. Chapter 5 compares cores from across the Lofoten Basin to those from the Ægir Ridge, with all chronology work for this chapter being performed on PC38.

All piston and multi-cores used for this thesis were collected during cruise 64PE391 from the Norwegian seas (Figure 2.1). This cruise ran from 1st to the 31st July 2014 and was funded under the NERC Arctic Landslide Tsunami Project. One additional sample from cruise KN179-3 (August to September 2004 (Figure 2.1)), was used as a reference for the composition of the Holocene Storegga turbidite (supplied by H. Haflidason, University of Bergen).

2.3 Core description

Cores collected were cut on deck into 1.25 m lengths and split lengthways. One half was preserved for archiving in the British Ocean Sediment Core Research Facility (BOSCORF). The archive half was used for all non-destructive instrument logging (data collection from core scanners that do not require any discrete sampling). The working half was subsampled into 2 x 2 cm u-channels, palaeomagnetic cubes (2 cm x 2 cm) or contiguous small volume samples on return to the UK.

2.3.1 Visual core logging

Visual core logging provides a rapid assessment of the facies contained within the cores. The methods detailed here for chronology and provenance rely on correct interpretation of hemipelagite and turbidite facies. Cores were first logged on-board the research vessel whilst at sea, at a scale of 1:10 cm. This involved the identification of sediment facies, boundaries

between units and sedimentary structures, and an assessment of grain size using a visual comparator. Any defects in the core, such as disturbance from the coring process were also recorded. Attention was paid to the distinction between turbidites and hemipelagic sediments (see sections 2.3.2 and 2.3.3).

All age models are built through the identification of chronological markers within the sediment that accumulates slowly. Identification of turbidite sediments within the cores is important, as all chronological methods must be performed on hemipelagic material. Hemipelagic sediment is deposited at variable rates, normally expressed in cm/ka (kilo-year = 1,000 years). Hemipelagite is gradually accumulated from the remains of foraminifera and coccolithophores, fine-grained terrigenous sediments transported in ocean currents (< 150 µm), and volcanic ash (tephra). Turbidites are deposited geologically instantaneously, recording the movement of large volume slides. Turbidite units can form significant thicknesses within the stratigraphic record, with individual events producing sediments reaching several metres in thickness. Sediments included in the final age model form an "event-free- chronology", devoid of any mass transport deposits (Ramsey, 2008), as such the thicknesses of turbiidite beds are not included in age-depth models (section 2.5).

In order to establish an accurate age of deposition for a turbidite, the upper and lower boundaries must be identified. Dating immediately above the upper surface of the turbidite is normally preferred as there is potential for erosion at the base of the turbidity current. The criteria used to define hemipelagic and turbidite units are described below.

2.3.2 Identification of hemipelagic sediments

The accurate identification of hemipelagic sediments and turbidites is essential for producing accurate age models of hemipelagic sequences. Hemipelagite forms from accumulation of both sediment and detritus that has settled vertically from the water column with a degree of lateral advection from ocean bottom currents interact with the sea floor (Stow and Tabrez, 1998; Rebesco *et al.,* 2013). Hemipelagite may be further defined as a mixture of biogenic pelagic (>10% by volume) and terrigenous/volcanigenic (>10%) material, with terrigenous/volcanigenic material comprising > 40% (by volume) or silt size of greater, and a mean grainsize of all hemipelagic material of between 5 to 15 µm. This sediment can be distinguished by its high microfossil content and variable colour between brown-yellow and pale grey-brown. Within the North Atlantic, north of the Ruddiman Belt, some fragments can be identified as Ice Rafted Debris (IRD), and are > 150 µm in size, too coarse to have been transported by bottom current activity. The Ruddiman Belt describes the region of the North Atlantic at > 50°N, within which these IRD layers are commonly identified (Ruddiman, 1977). Variations in the lithic fraction of hemipelagic

sediments are recognizable. Some layers in which the IRD content is particularly high are known as Heinrich Layers and deposited during the coldest periods recorded in the Greenland ice core record (Bond & Lotti, 1995).

2.3.3 Identification of turbidites

Turbidites represent the deposits of sediment transported by turbidity currents, a mixture of sand and/or mud generated from the run-out of a submarine landslide, volcanic island collapse, flooding events or earthquakes (Talling *et al.,* 2012). The cores collected for this work targeted the deposits of a number of previously mapped submarine landslide scars, notably, the Storegga Slide (Haflidason *et al.,* 2004; Paull *et al.,* 2010). This failure produced a large volume turbidite that fills much of the Norwegian Basin, and has been traced as far as the Ægir Ridge coring site on high-resolution sub-bottom seismic records. Turbidity currents are capable of depositing significant volumes (> 1,000 km^3) of material over short periods of time: days to months. Chapter 3 focuses on dating this duration of deposition, by separating the hemipelagic and turbidite sediments in the core. Through accurate dating, an assessment of probable preconditioning (environmental conditions prior to each slide that prime the slope to fail) and triggering factors can be made (Urlaub *et al.,* 2013). A range of dating proxies can be used within the hemipelagic sequence to construct a sedimentation rate and age-depth model, as discussed below. This allows the upper surface of a turbidite to be dated where no erosion has occurred (Urlaub *et al.,* 2013). This age-depth model can then be interrogated to determine the time of deposition for each turbidite (Ramsey, 2008).

Turbidites within core sequences are identified on the basis of their colour, composition, boundaries and structures (Shanmugam, 1997; 2000). Within the Nordic seas, hemipelagic sediments are represented by pale brown-yellow brown sediments, and turbidites as olive grey. These units are characterised by a sharp base, often undulating, and exhibit normal grading (Bouma, 1964; 1987; Sumner *et al.,* 2012). There are a range of internal characteristics that are observed that vary between the turbidites studied. Within the coarse base, graded bedding is often observed, with thick units showing cross lamination in the medium-fine sands. The fine grained turbidites may show limited lamination, nearly always with a bioturbated upper surface. Turbidite mud caps can develop oxidation fronts whereby the upper section of the mudcap is stained red-brown. Oxidation fronts are formed by the downward movement of oxidised Iron and Manganese from the top of the turbidite, which alters the composition of the affected mud cap. The composition of turbidites differs significantly from that of hemipelagites with a higher percentage of quartz and feldspars and a near complete absence of microfossils. Within some turbidite deposits, microfossils are present, but foraminifera are damaged and coccoliths are fragmented.

The term "megaturbidites" is used here based on the description of Bouma (1987) to describe beds within the Ægir Ridge. These exceptionally large volume (> 100 km^3) beds conform to the six key criteria for the definition of a megaturbidite:

(1) they are thick in comparison to the host rock; (2) they are laterally extensive; (3) different in composition to the host sediment; (4) there is no associated submarine fan geomorphology observed on the surrounding sea floor bathymetry (5) their internal structure suggests one event, or closely spaced multiple phases; (6) they form excellent regional stratigraphic markers.

The published data for the volume of the Holocene Storegga Slide ranges from 2,500-3,200 km^3 (Bugge et al., 1988; Evans et al., 1996; Bryn et al., 2003; Haflidason, Gravdal and Sejrup, 2003; Micallef *et al.,* 2009). This estimate exceeds that of other identified megaturbidites in the Eastern Mediterranean of 160 ± 10 km^3 (Rebesco *et al.,* 2000), Late Quaternary Indus Fan megaturbidites ~ 1-3 km^3 (Bourget *et al.,* 2013), the Western Mediterranean ~ 500 km^3 (Rothwell *et al.,* 1998), and the Bed 5 deposit on the Madeira Abyssal Plain ~ 162 km^3 (Wynn *et al.,* 2010; Hunt *et al.,* 2013).

2.3.4 ITRAX µXRF

Variations in down core chemistry are useful for assessing the provenance of deposits and making environmental interpretations. The ITRAX micro-X-Ray Fluorescence (µXRF) core scanner at the BOSCORF was used to progressively scan split core sections. The ITRAX is capable of analysing elemental variations at 200-1,000 µm intervals. The benefit of XRF scanning is that it is non-destructive and capable of scanning a 1.25 m core section at 0.2 mm resolution within 24 hours (Croudace *et al.,* 2006). The ITRAX allows the construction of detailed chemostratigraphic records (e.g. calcium content, controlled by surface productivity), and allows an assessment of provenance of turbidite units by comparing relative intensities of elements and ratios. Element intensities are generated from K-shell peak areas, a characteristic X-ray emission that allows the element to be identified, for the range of selected elements. Compton scatter integral and KCPS (kilo counts per second) are monitored for data validity using the Mean Squared Error (MSE). MSE measures the goodness of fit of the mathematical model to the observed measurements, and an MSE of > 5 is rejected (Croudace *et al.,* 2006). This approach minimizes the inclusion of data points influenced by high surface roughness, water content or surface height variations beyond the limits of the detector (MacLachlan *et al.,* 2015).

All ITRAX data were collected using a molybdenum (Mo) tube with a setting of 30 KHz and 30 mV, and a count time of 30 seconds. The Mo tube is the standard X- ray tube used for environmental analysis and the detection of heavy elements (Croudace *et al.,* 2006). Detection of element concentration using the ITRAX core scanner is subject to variations beyond sediment composition.

The usefulness of data is based on density, grain size and surface water saturation (Croudace *et al.,* 2006; Rothwell *et al.,* 2006; Cronan *et al.,* 2010). To minimise the effect of these aforementioned parameters, XRF measurements for comparative turbidite composition and provenance interpretations were restricted to portions of the turbidite mud-cap (<63 μm), below the oxidation front to avoid the effects of mobile elements migrating downwards (Hunt *et al*. 2015).

Down-core XRF data from the hemipelagite sequence, removed of intervening turbidites, provides a near-continuous chemostratigraphic record that can be used to correlate between cores and date the sediments by comparison to existing chronologies. XRF compositions of the turbidite mud caps are assessed below the effects of the oxidation fronts to avoid an overrepresentation of mobile elements within the sample. Once the composition of the turbidite has been established, it can be used to correlate marker beds between cores and provide information about the turbidite provenance (Pearce and Jarvis, 1995; Rothwell *et al.,* 2006; Hunt *et al.,* 2011; Hunt *et al.,* 2013). Water content and sediment grain size are highly variable across the cores used, ranging from coarse sands (>1,000 μm) to clay (<3.9 μm). All comparisons are made using elemental ratios and exclude single element comparisons. This has the advantages of reducing the effects of water content, grain size, and reducing the effect of unit-sum constraints and dilution (Weltje and Tjallingii, 2008). Ratios have been strongly advocated by past research and allow the examination of variations in carbonate content (Sr/Ca and Ca/Fe) an assessment of the original water depth of the failed source units (Si/Sr) (Croudace *et al.,* 2006). Where possible Rb has been used as a discriminator for ratios used to assess composition, due to its consistent response to excitation and similar atomic radius to aluminium (Rothwell *et al.,* 2006). Aluminium detection is limited by the use of the Mo tube and suffers poor detection accuracy due to its high attenuation rate.

The raw count of Ca can be used as a proxy for surface productivity in the North Atlantic (Brendryen *et al.,* 2010; Hibbert *et al.,* 2010; Hennekam and Lange, 2012; Jouve *et al.,* 2013; Pope *et al.,* 2016). The variations in Ca concentration are reflected in the δ18O record of the NGRIP ice core. The rapid fluctuations in temperature, identified in both the NGRIP record and sediment core Ca contentrations have successfully been used for refining existing North Atlantic sediment core chronologies (Brendryen *et al.,* 2009). In chapter 4, they will allow the timing of deposition of the turbidites to be narrowed within the constraints of the age model developed in chapter 3.

2.3.5 Magnetic Susceptibility

Magnetic susceptibility (MS) of the sediment is a useful for tool for correlating between sediment cores, and identifying lithological changes within the sediment. MS is directly influenced by the presence of magnetic minerals. With regards to the hemipelagite record, interstadial periods

show enhanced magnetic susceptibility while stadials show reduced values, as a result of the dilution of strong magnetic signal in the fine grained fraction (Rasmussen *et al.,* 1996; Rasmussen and Thomsen, 2008). The presence of IRD horizons can be detected as a reduction in magnetic susceptibility, and used as a proxy for the IRD layers (Rasmussen *et al.,* 1996). Sediment cores were analysed for magnetic susceptibility using the GeotekTM MSCL-XYZ logger at BOSCORF, at 0.5 cm intervals with a Bartington point sensor (MS2E). This technique also aids in accurate identification of boundaries due to significant differences in susceptibility, such as between basal turbidite sands and underlying hemipelagite.

2.3.6 ICP-MS composition of mud caps

Distal turbidites record a geochemical signature of their source rocks that allows a broad tectonic provenance to be assigned (McLennan *et al.,* 1993). However, the provenance of turbidites from distal basin cores can be difficult to establish. The Nordic seas are surrounded by significantly different tectonic terranes: the Mid-Atlantic Ridge, the Faroe Plateau, the Jan Mayen Microcontinent and the Fennoscandian Shield. In order to definitively distinguish between volcanic and continental sources, the composition of the rare earth elements (REEs) may be used (McLennan and Taylor, 1990). The REEs can distinguish between five key provenance types: old upper continental crust, recycled sedimentary rocks, young undifferentiated arc, young differentiated arc and exotic components (i.e. ophiolites). Within the Northern North Atlantic, turbidites in basin cores could be sourced either from Iceland, the Faroe Islands and the Mid-Atlantic Ridge (young undifferentiated arc) or the Norwegian continent (old upper continental crust/recycled sedimentary rocks). A key discriminator is the europium anomaly: a relative degree of europium enrichment in a sample relative to a standard. This anomaly can distinguish between plagioclase rich sources, as europium forms a divalent ($^{2+}$) cation, very similar in size to Ca^{2+}, it can therefore substitute for Ca^{2+} in plagioclase found within evolved magmas (Jarvis and Jarvis, 1985; Sun and McDonough, 1989; McLennan *et al.,* 1993). Observation of a positive europium anomaly in turbidite sediments is interpreted as a continentally sourced deposit.

A set of 36 bulk samples of turbidite mudcaps were selected from 6 cores from across the Nordic Seas. The turbidites had been identified through visual logging and ITRAX XRF geochemistry. These samples comprise 1 cm^3 of turbidite mud cap extracted below the oxidation front (see above). These samples were prepared for analysis by ICP-MS at the National Oceanography Centre, Southampton. Sediment samples were first dried at 40°C for two days to remove interstitial water content, then weighed to enable final calculation of concentration per dry gram. Samples were then ground in an agate pestle and mortar to ensure a homogenous sample and to enable easier dissolution. Subsamples of 0.1 g were extracted and digested overnight in sealed teflon reagent vessels in Aqua Regia (1:3 proportion of HNO_3: HCl) at 160°C. Aqua Regia

dissolves most base element sulphates, sulphides, oxides and carbonates, but only partially digests most silicate minerals (Gaudino *et al.,* 2007). To ensure complete digestion of silicates, an overnight digest of HF+$HNClO_4$ (3:2.25 ml) was followed by subsequent dry-down at 140°C, to evaporate the HF. An addition of 1 ml $HClO_4$ when this reaction was complete was made to ensure total removal of all HF, and a full dissolution of organic matter. Remaining residues were dissolved in 5ml of HCl overnight to dissolve any coarse carbonate precipitates, then weighed and stored in 30 ml high-density polyethylene bottles (mother solution). A daughter solution was made up using 0.5 ml of the mother, dried down and then re-dissolved in 5 ml 3% HNO_3 for aliquot analysis by ICP-MS (Thermo Fisher Scientific ELEMENT). An internal standard of powdered Cody Shale (SCo) was used to check the reliability of the digest method. Samples were calibrated against a set of nine rock standards (CBLK, JA2, BRR1, BIRI, JB19, BHV02, BAS206, JB3 and JG61) and blanks analyzed for each sample run to assess potential contamination and any instrumental drift. The latter was minimized by analysing samples in two batches. Full data sets are reported in the appendix.

2.4 Chronology development

Significant success in low-resolution cores has been achieved through the combination of RPI, magnetic excursions and coccolith biostratigraphies in the sub Arctic (Nowaczyk *et al.,* 1994; Nowaczyk, 1997; Knies *et al.,* 2000).

2.4.1 AMS Radiocarbon dating

Radiocarbon dating makes use of the known half-life of carbon-14; 5,730 ± 40 years, to estimate the age of younger marine sediments. Carbon-14 (^{14}C) is captured from the atmosphere by living organisms, and decays steadily after death. This decay rate allows samples deposited within the last c. 50,000 years to be accurately dated by calibrating the ratio of ^{14}C:^{12}C.

Complications with the method arise from the variable rate of ^{14}C production in the upper atmosphere (Ramsey, 2008; Reimer, 2013; Brauer *et al.,* 2014). The production rate of ^{14}C in the atmosphere varies with the change in the interaction of cosmic rays with the upper atmosphere (Stuiver, 1961; Houternmans and Suess, 1973; Masarik and Beer, 2009; Roth and Joos, 2013). This variation in production rate has an effect on the calibration of dates, which is resolved through the use of calibration curves (Reimer, 2013). All radiocarbon dates in this study have been calibrated using the Marine13 curve within the Oxcal program (Reimer and Reimer, 2006; Reimer, 2013).

Using radiocarbon to date marine sediments produces an additional complication. The marine reservoir effect refers to the difference in age between atmospheric ^{14}C and marine ^{14}C. The average age of surface ocean waters is 440 years, a result of the slow movement of water in the thermohaline circulation system. The additional 440 years is included in the calibration of radiocarbon dates when using the OxCal program. In addition to this correction, a further correction may be required, known as Delta R (ΔR), the regional reservoir correction. This correction is dependent on the location of the sample, with different ocean basins demonstrating variations in ΔR both spatially and temporally (Bondevik *et al.,* 2006; Mangerud *et al.,* 2006; Reimer and Reimer, 2006). For some regions, this has been estimated through the analysis of historic collections of marine bivalves, palaeomagnetism or tephra horizons (Ascough *et al.,* 2005). In the Norwegian seas this has been shown to vary by up to 1200 years (Voelker *et al.,* 1998a).

Radiocarbon dating is a widely used chronostratigraphic tool for marine sediments from the North Atlantic, and many studies have been performed to estimate the radiocarbon reservoir regionally (Haflidason *et al*. 2000; Waelbroeck *et al*. 2001; Thornalley *et al*. 2011). Studies in the Nordic seas have shown that this reservoir correction varies between 400-1600 years (Voelker *et al.,* 1998a). Further work is needed to constrain this effect, this work adopts the suggestion that ΔR 20 ± 30 years (Bondevik *et al.,* 2006; Mangerud *et al.,* 2006). This allows work to be compared to other dated cores in the region. All calibrated dates are expressed as "Cal BP" (calibrated years before present (1950 AD)) with conventional radiocarbon years detailed in Table 3-3, chapter 3.

All samples selected for dating were taken from hemipelagic sediments with minimal evidence for reworking at sites close to the boundaries of turbidite units. A 2-8 cm^3 sample of sediment was wet sieved through two different sieve sizes (125 µm and 250 µm). Where possible monospecific samples of the polar planktonic species *Neogloboquadrina pachyderma sinistral (nps)* were selected. Where abundance was low, mixed planktonic species, including *Orbulina universa* and *Globoquadrina bulloides* were picked. The 125-250 µm size fraction was picked for 4-20 µg of specimens under a binocular microscope. This corresponds to between 500 and 4,000 individual specimens of nps. The samples were prepared at BOSCORF and analyses were performed by the Scottish Universities Environment Research Centre (SUERC) AMS Facility, East Kilbride or Beta Analytic Inc., Miami. Dates are reported with an individual error estimate to 2σ, based on three repeat analyses per sample. Where the error is lower than ± 30 years, a conservative error estimate of ± 30 years is applied.

2.4.2 Palaeomagnetism

Radiocarbon can only provide accurate dating for the last 43,500 years. Beyond this limit, the proportion of preserved radiocarbon is too low to measure, and additional methods must be used to establish a chronology. Sediments record the intensity of the geomagnetic field, the inclination (dip of the field lines from the horizontal plane) and the declination (magnetic deviations from true north (Jovane *et al.,* 2013)). Palaeomagnetic directional and intensity signal preserved in sediments provide a method for dating over longer time periods. The strength of the Earth's magnetic field is known to vary over time, and the strength of the field at the time of deposition of sediment packages can be preserved. This strength can be reconstructed, and a chronology cam be acquired through comparison of the reconstructed variations to other well-dated reference records from around the globe (Laj *et al.,* 2000). Although the mechanism for sediment magnetisation acquisition is not fully understood, records from around the globe have been proven to correlate well and hence can be used to assist the development of chronologies (Gartner, 1977; Nowaczyk and Frederichs, 1999; Valet *et al.,* 2005; Evans *et al.,* 2007; Hambach *et al.,* 2008; Roberts *et al.,* 2013). The Earth's magnetic field behavior is well documented for the last 400 kyr (Valet, 2003; Channell *et al.,* 2009; Roberts *et al.,* 2013) and the occurrence of short-lived geomagnetic excursions within periods of low field intensity provide stratigraphic tie-points between down core records. Through comparing the intensity record generated from selected sediment cores to established records, the age for sediments can be derived.

The study cores were not split along an orientated axis when collected, and hence the acquired declination data have arbitrary values. Intensity and inclination data are discussed separately.

2.4.2.1 Palaeomagnetic Intensity

To use palaeomagnetic intensity data as a chronological tool, the relative palaeointensity (RPI) of the sediments must be calculated. RPI is estimated by normalising the Natural Remanant Magnetisation (NRM) using laboratory-induced Anhysteretic Remanant Magnetisation (ARM) of the sediments. The result can be correlated to established RPI records from around the globe. The palaeomagnetic record measures the NRM as recorded by magnetic minerals. These minerals are either sourced from terrigenous material, or from in situ bacterial production. In general, terrigenous derived materials are considered preferable for recording a strong magnetic signal.

NRM is a function of the intensity of the magnetic field, and the direction of the magnetic field at the time of deposition (Stoner and St-Onge, 2007). The normalization of NRM is essential to minimise the effects of magnetic grain size and concentration. NRM is subject to variations in the concentration of NRM-carrying grains, which is predominantly carried by 1-15 μm single domain/pseudo-single domain magnetite grains (Stoner and St-Onge, 2007). ARM and NRM

retention are dependent on the concentration and size of magnetic grains, and the use of the NRM/ARM ratio restricts the effect of the magnetic grain concentration and size variations on the record. As such NRM measurements should be normalised by ARM to acquire estimates of the relative palaeointensity record. Normalised records of intensity are referred to as Relative Palaeointensity (RPI) records (Tauxe, 1993; Guyodo and Valet, 1996; Laj *et al.,* 2000; Laj *et al.,* 2004; Valet *et al.,* 2005; Channell and Xuan, 2009), which can then be compared with reference records of palaeointensity variations such as SINT2000 (Valet *et al.,* 2005), PISO1500 (Channell *et al.,* 2009) and GLOPIS (Laj *et al.,* 2004) and the regional NAPIS-75 (Laj *et al.,* 2000).

This record of magnetic intensity across hemipelagic sequences is a powerful geochronological tool, but is often complicated by several factors. The process of Post-Depositional Remanent Magnetisation (PDRM) is responsible for "locking-in" magnetisation once sediment is buried to a certain depth. This lock-in depth restricts movement or remobilisation of magnetic grains through compaction and dewatering of the host sediment. This lock-in depth varies from 2-30 cm, and this depth is believed to relate to the thickness of the mixed layer (sediment that is loosely settled but still mobile) and sedimentation rate (Boudreau, 1994). Natural Remanent Magnetism

The production of an RPI record requires two types of magnetisation to be measured: Natural Remanent Magnetisation (NRM) and a lab-induced magnetisation such as Anhysteretic Remanent Magnetisation (ARM) that compensates for the ability of the samples to acquire magnetisation. Palaeomagnetic data were measured at the University of Southampton, on a 2G-Enterprises superconducting rock magnetometer (SRM) designed for u-channel samples. All measurements for NRM and ARM were performed at 1 cm intervals along the u-channels. The response function of the SRM pick-up coils integrates measurements over several centimetres (6-7 cm). All u-channel measurements were performed with 10-cm leader and 10-cm trailer intervals before and after the sample, respectively. The NRM was measured using stepwise alternating field (AF) demagnetisation at peak fields from 0 to 60 mT at 5mT increments, then 10 mT increments from 70-100 mT for a total of 17 steps. NRM component directions (inclination and declination) of the characteristic remanent magnetisation (ChRM) were calculated using principal component analysis (PCA) with 9 AF demagnetisation steps. Component Magnetisations were computed for the 25-60 mT range using the UPmag software (Xuan and Channell, 2009). The maximum angular deviations (MAD) values were calculated to monitor the quality of individual component direction estimates. Values of <10° are accepted as reliable (Xuan and Channell, 2009).

2.4.2.2 Anhysteretic Remanent Magnetism

Anhysteretic Remanent Magnetisation is widely used as a normaliser to generate RPI (Channell *et al.,* 1997; Laj *et al.,* 2000; Stoner *et al.,* 2002). This was measured after the full 17 step NRM demagnetisation, ARM acquisition being performed in a 100 mT peak alternating

field with a 50 μT DC bias field along the u-channel sample. ARM was then measured repeatedly following the same AF demagnetisation sequence used for NRM.

2.4.2.3 Relative Palaeointensity

RPI was then calculated within the UINT function of the UPmag software (Xuan & Channell, 2009) through normalising the NRM by ARM. RPI was calculated using the average ratio between NRM and ARM data from the 25-60 mT demagnetisation range, where (i) represents the different demagnetisation steps:

$$RPI = (1/n)*sum\ (NRMi/ARMi)$$

The hemipelagic RPI record is discussed in Chapter 3.

2.4.2.4 Magnetic excursions

In addition to variations in RPI, palaeomagnetism can provide an additional chronological tool through the identification of geomagnetic excursions. Whilst full magnetic reversals are rare, short-lived excursions from normal polarity are well documented within the Late Quaternary (Tric *et al*. 1991; Thouveny *et al*. 2004; Channell 2006, Laj and Channell, 2015). These excursions often coincide with periods of significantly lower field intensities. Within the last 250 ka, five excursions are well-documented, these are Mono Lake (32-34 ka); Laschamp (39-41 ka); Blake (115 ± 3 ka), Iceland Basin (180-188 ka); and Pringle Falls (205-225 ka). An additional excursion has been reported but (variably constrained) within the marine record: the Norwegian-Greenland Sea (NGS) excursion (72-86 ka, Nowaczyk *et al*. 1994). These excursions have been widely used in the North Atlantic as chronological markers for Late Quaternary sediments (Gartner, 1977; Nowaczyk *et al.,* 1994; Nowaczyk, 2003; Lekens *et al.,* 2009). Magnetic excursions therefore represent valuable chronostratigraphic horizons (Thouveny *et al.,* 2004; Osete *et al.,* 2012; Sier *et al.,* 2015).

The discovery that the Earth's magnetic poles have periodically reversed has allowed establishment of a series of chronological markers for the Late Quaternary (Nowaczyk and Knies, 2000; Thouveny *et al.,* 2008; Valet *et al.,* 2008; Jovane *et al.,* 2013; Channell, 2014; Laj *et al.,* 2014a). The current 'normal' polarity field configuration has existed since the Brunhes-Matuyama Boundary, 781 ka BP (Nowaczyk *et al.,* 1994; Langereis *et al.,* 1997; Channell, 2006). Inclination measures the angle between the magnetic vector and the horizontal plane. Sediments in the high north display a high angle of inclination (close to 90°), whereas sediments from the southern hemisphere display negative inclinations.

The hemipelagic sedimentation rate at the core sites (c. 3-5 cm/kyr), constrain the detection of short-lived excursions. The measurement resolution of 1 cm intervals and the SRM response function (~4.5 cm at half maximum response) will result in smoothing of short-lived events. For an

event to be clearly detected it must exceed 3 cm in duration (1,000 years [Roberts, 2008]). Additionally, with low sedimentation rates, inclination deviations are unlikely to reach the full 180° observed in high-resolution records. Here the suggestion of Jovane *et al.* (2013) is adopted, whereby a Virtual Geomagnetic Pole (VGP) movement of > 40° from the geographic pole is considered as an excursion. Each potential magnetic excursion detected in the studied cores is discussed in chapter 3. Validation is then provided by independent dating methodologies to ensure ages are comparable to known excursions in the Late Quaternary.

2.4.3 Coccolith biostratigraphy

Coccolith bioevents are routinely used as chronological markers in sediment cores (Gartner 1977; Weaver & Kuijpers 1983; Bleil & Gard 1989; Backman *et al.,* 2009; Hunt *et al.,* 2013, 2014; Pope *et al.,* 2016). They are particularly useful in the Northern North Atlantic where much work has focused on dating the horizons using either the SPECMAP (SPECtral MApping Project) protocol (Imbrie *et al.,* 1984) or in association with palaeomagnetic variations (Bleil and Gard, 1989; Nowaczyk *et al.,* 1994). Coccolith samples were prepared using a novel method whereby <1 mm^3 samples were dispersed over Scanning Electron Microscope (SEM) pads with acetone and analysed under the Hitachi TM3000 SEM in BOSCORF (Hunt *et al.,* 2011; Hunt *et al.,* 2013). This enables rapid sampling and high-resolution analysis down to 2 µm. The higher quality visualisation of coccoliths in the SEM allows for accurate species identification. For each sample, 15 fields of view were counted to a minimum of 300 specimens per sample. The relative abundance of dominant species (*E. huxleyi; G. mullerae; G. aperta; G. caribbeanica;* and *P. lacunosa*), relative abundances of further species (*C. pelagicus* and *C. leptoporous*), and first and last appearances of particular species were compared to established chronologies. Gard (1988) demonstrated a working coccolith biostratigraphy in the Arctic Ocean and Norwegian Sea, identifying a series of barren intervals interspersed with periods of high abundance and correlated both to the SPECMAP timescale (Imbrie *et al.,* 1984).

Table 2.1: Coccolith biozones of the Northern North Atlantic after Gard (1988). Initial dating performed through correlation to the SPECMAP Oxygen isotope stratigraphy (Imbrie et al., 1986). Data collected by J. Hunt.

Zone	*Definition*	***Marine Isotope Stage***	*Age (ka BP)*
N-G 1	*Recent to point of dramatic decrease in* C. pelagicus *total abundance*	*Recent to mid/lower 1*	*0-8*
N-G 2	*Predominantly barren zone, defined as the interval from where* C. pelagicus *decreases dramatically in total abundance to where* G. muellerae *(and total nannofossils) increases dramatically.*	*Mid/lower 1 to mid 4*	*8-66*
N-G 3	Gephyrocapsa mullerae *dominates over* Emiliania huxleyi. *The interval is defined from where* G. mullerae *dramatically increases in total abundance and*	*Mid 4 to lowermost 5*	*66-119*

	dominates over E. huxleyi *down to where all nannofossils disappear from the sediment. There are one or two short barren intervals within this zone. The presence of* E. huxleyi *distinguishes this zone from N-G 7 (372-423 ka BP)*		
N-G 3a	*Abundance peak of* Coccolithus pelagicus*. The upper boundary of zone 3 plus increase in abundance of* C. pelagicus*. Lower boundary defined by decrease in abundance of* C. pelagicus *and decrease in total amount of nannofossils.*	*Mid 4-5a*	*66-79*
N-G 3b	*Low total amount of nannofossils. The interval from where* C. pelagicus *and the total amount of nannofossil decreases in abundance to where* C. leptoporus *increases in relative abundance and also total abundance of nannofossils increases.*	*5b to 5d*	*79-97*
N-G 3c	*Abundance peak of* Calciduscus leptoporus*. Upper boundary from where* C. leptoporus *increases in total abundance and also total abundance of nannofossil increases. Lower boundary as for zone 3.*	*Upper part of 5e*	97 -119
N-G 4	*Mainly barren*	*Lowermost 5e to lowermost 8*	119-280

The chronology detailed in Gard (1988) highlights the latest barren zone commencing at 66 ka BP and ending at 8 ka BP with the reappearance of *Gephyrocapsa mullerae, which* dominates over *Emiliana huxleyi* (Zone NG3). Coccolith biozone NG3 (66-119 ka BP) is split into three subzones defined by changing relative abundances of *Coccolithicus pelagicus*, *Calcidiscus leptoporous* and *Gephyrocpasa mullerae* (Gard, 1988). These subzones provide three clear datum horizons at 79 ka BP, 97 ka BP and 119 ka BP (Table 2.1). Below biozone NG3 another barren zone persists from 280 ka BP to 119 ka BP. The identification of barren zones is combined with the identification of magnetic excursions in chapter 3. The correlation of barren zones or changes in species dominance, with periods of low Relative Palaeointensity and magnetic inclination, allows an age date to be unambiguously assigned to specific sediment depths.

2.4.4 Tephrochronology

The deposition of a tephra layer is geologically instantaneous, and can provide an isochronous tie-point between the marine, terrestrial and ice core records, where locations are subject to either ash clouds or prevailing winds that can transport ash over long distances. The development of the technique of tephrochronology has been a significant step forward in enabling high precision dating and assessing synchronicity between rapid climate change events in the ice core and

marine records (Svensson *et al.,* 2008). This study utilises tephra horizons to date marine sediments in combination with other chronostratigraphical methods outlined here. This work focuses less on the micro-sedimentological features of tephra deposits or volcanic processes, but uses the major element profile of tephra from the core to add valuable tie points to the chronology. Tephras are commonly found in marine sediments across the North Atlantic due to the eruptions of subglacial and subaerial volcanoes on Iceland, and the volcanic island of Jan Mayen throughout the Quaternary.

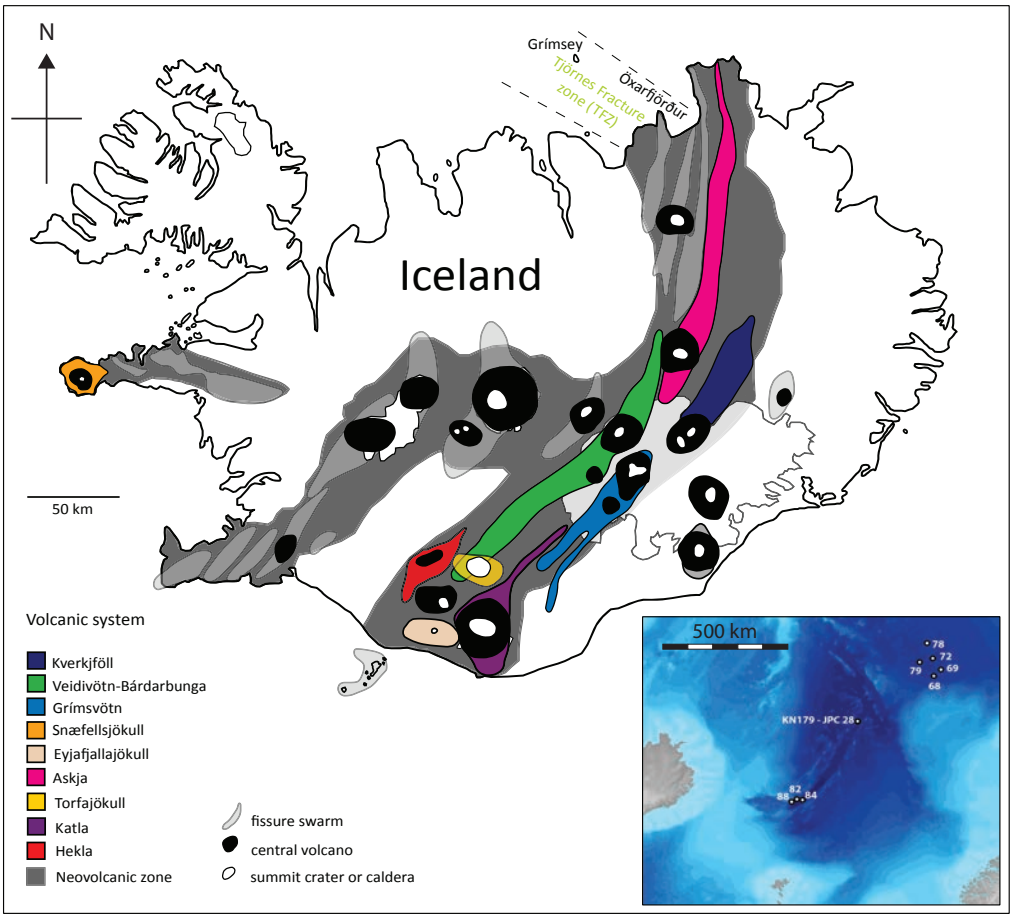

Figure 2.2: The volcanic system of Iceland (Oladottir et al. 2011, modified from Johannesson and Saemundsson, 1998). Relevant volcanic systems are shown; colours refer to each volcanic system, which is chemically distinguished in the Chapter 3. Inset shows location of cores in relation to eastern Iceland.

The North Atlantic has several well-defined tephra horizons, which have been broadly divided into two compositional groups (basaltic/rhyolitic) throughout the Late Quaternary. The first group, the North Atlantic Ash Zones (NAAZ) are the rhyolitic tephra and are numbered NAAZ I to III (Ruddiman and Glover, 1972). These three ash zones spanned the last 620 ka BP and were found in sediment cores across the North Atlantic up to 1,800 km south of Iceland. NAAZ1 is more widely known as the Vedde Tephra, dated to 12.1 ka BP (Turney, 1998; Wastegård, 2002; Gudmundsdóttir *et al.,* 2012; Lane *et al.,* 2012; Gudmundsdóttir *et al.,* 2016).

This horizon forms a valuable age marker, and has been instrumental in highlighting significant carbon-14 reservoir age variations around the Younger Dryas cooling of up to 600 years (Austin *et al.,* 2011). The NAAZ II has most recently been dated to 55,350 ± 1,184 BP and provides a valuable tie point to the Greenland Ice core records. This date is particularly useful due the upper limit of radiocarbon dating being at c. 50 ka BP. The NAAZ III was dated to 620 ka BP and is considered unlikely to be found within these cores, as piston core chronologies are not expected to reach beyond 500 ka BP. Since the work of Ruddiman and Glover (1972), numerous other tephra horizons have been identified, and tephrochronology represents the most reliable form of dating in the pre-radiocarbon period in this region (Lacasse and Garbe-Schönberg, 2001; Abbott *et al.,* 2013, 2014; Kuhs *et al.,* 2014).

The second group of tephra are known as the Faroe Marine Ash Zones are so named after their finding around or on the Faroe Islands. These horizons consist of the basaltic tephra spanning the last 50 ka BP. There are four FMAZ deposits, major tephra horizons, supplemented by numerous basaltic tephra horizons in the Nordic Seas: FMAZ I (17.78 ka BP), FMAZ II (24.55 ka BP), FMAZ III (36.9 ka BP) and FMAZ IV (46.8 ka BP) (Haflidason *et al.,* 2000; Wastegård *et al.,* 2005; Brendryen *et al.,* 2010; Abbott *et al.,* 2012; Hibbert *et al.,* 2014; Voelker and Haflidason, 2015; Wastegård and Rasmussen, 2016). Each of these ash zones was sourced from the Grimsvotn volcanic system (Jennings *et al.,* 2014; Voelker and Haflidason, 2015).

Samples for tephra analysis were taken in 1 cm contiguous slices down core and wet sieved in distilled water through a 63 µm sieve. The < 63 µm fraction was discarded. Samples were dried for 24 hours and then sieved at 150 µm. The 150 µm grain size was selected for macrotephra horizon detection as it corresponds to the IRD grain size used in this study, which was simultaneously counted alongside the tephra shards. A fraction of each sample was counted, separated using a microsplitter, for basaltic (brown) and rhyolitic (clear) tephra shards in two size fractions (80 µm - 150 µm and > 150 µm). Initially samples were counted every alternate centimetre and where shards were identified the resolution increased to every centimetre.

Where peaks in tephra concentration were identified, tephra shards were extracted using a sable paintbrush and mounted in epoxy resin on SEM slides. A minimum of 50 shards were picked from each horizon in the > 150 µm and the 80-150 µm fraction. These slides were left to cure for 24 hours, then ground by hand to a thickness of c. 50 µm to expose a minimum of 20 grains on the surface of the slide. The slides were carbon-coated in the Tephra Analysis Unit at Edinburgh University and analysed using using a Cameca SX199 electron microprobe (EPMA) equipped with five vertical WD spectrometers. Secondary standards of Lipari and BCR2g were used to correct for elemental drift (Hayward, 2012).

Marine tephra suffer from variable degrees of hydration from magmatic water during tephra formation, or post depositional hydration from pore waters, which increases over time (Pearce *et al.,* 2014). A result of hydration is that volatiles are driven off and EPMA results are rarely 100% weight % (wt%) oxide totals, the treatment of these data is a subject of contention in the tephrochronology community (Abbott *et al.,* 2011; Griggs *et al.,* 2014). Normalisation of results to 100% weight oxide values allows tephra collected from different environments to be compared (i.e. ice core: marine core), but can mask subtle differences in composition (Pearce *et al.,* 2004; Pearce *et al.,* 2008; Davies *et al.,* 2014). In order to compare results to published tephra data from different microprobes, all data were normalised to a 100% anhydrous basis and expressed as total oxide/volatile free values (Abbott *et al.,* 2011; Griggs *et al.,* 2014). Tephra analysed with total wt% below 90% were excluded.

A database of 106 known tephra from Iceland and Jan Mayen was assembled from the relevant literature (Lacasse *et al.,* 1996; Turney, 1998; Wastegård *et al.,* 2000; Lacasse and Garbe-Schönberg, 2001; Davies *et al.,* 2001; Wallrabe-Adams and Lackschewitz, 2003; Austin *et al.,* 2004; Svensson *et al.,* 2008; Brendryen, Haflidason and Sejrup, 2010, 2011, Abbott *et al.,* 2011, 2012; Gudmundsdóttir *et al.,* 2011; Gudmundsdóttir *et al.,* 2011; Abbott *et al.,* 2013; Bourne *et al.,* 2013; Austin *et al.,* 2014; Griggs *et al.,* 2014; Voelker and Haflidason, 2015; Gudmundsdóttir *et al.,* 2016; Timms *et al.,* 2016). This database was used to produce cross plots of CaO vs. FeO, K_2O vs. Ti_2O, FeO vs. K_2O and Al_2O_3 to Na_2O, which are used to define the volcanic system from the Icelandic tephra shards, originated. Cross-plots were then used to compare tephra horizon compositions between observed and reference datasets for well-dated regional eruptions. Relevant chronological information was used in conjunction with the likely volcanic system to assign a probable age to the tephra deposits located by using age estimates from high resolution marine cores (MD99 2289 and MD95 2822, or the Greenland ice core records as detailed in the INTIMATE stratigraphy literature (Lowe *et al.,* 2008; Austin and Hibbert, 2012; Davies *et al.,* 2012; Blockley *et al.,* 2014; Brauer *et al.,* 2014).

2.4.5 Ice Rafted Debris

The North Atlantic has been repeatedly affected by the discharge of massive volumes of ice during periods of rapid warming, known as Heinrich Events. It has been established that each period of ice-rafting correlates to a half period of a precessional orbital cycle (11,000 ± 1,000 years [Sarnthein *et al.,* 2001]). These regularly spaced events left a clear imprint in hemipelagic sediments within the Ruddiman Belt, the North Atlantic between 40- 64° N (Ruddiman, 1977; Hemming, 2004). Identification of these horizons can aid the development of a core chronology as they are synchronous and well-dated regionally (Sarnthein *et al.,* 2001; Rashid *et al.,* 2013). These horizons are known as Ice Rafted Debris layers (IRD layers), and can be identified through distinct

troughs in magnetic susceptibility records and the manual counting of >125 µm grains within the sediment samples.

Sampling was performed in 1 cm^3 contiguous samples throughout the hemipelagic sections of the core. The same samples were used for picking foraminifera for stable isotope analyses and tephra counting. The samples were weighed, dried at 40° for two days, and weighed again for dry weight to calculate the flux of grains per dry gram (standard unit of measurement for IRD [Dowdeswell *et al.,* 1999; Knies *et al.,* 2000]). The samples were washed through a 63 µm sieve, the < 63 µm fraction was discarded. This size fraction is not used for any of the analytical methods in this thesis. A fraction (normally 1/16th or until 300 grains were counted as a minimum) of the > 63 µm fraction was sieved at 150 µm. The > 150 µm fraction is considered too large to have been transported to the deep ocean by any method besides ice rafting.

The deposition of grains > 150 µm is interpreted as the release of glacially scoured sediment from icebergs (Ruddiman, 1977). All lithic and mineral grains were counted to identify variations in the quantity of IRD. The tephra was also counted in this grain size fraction (> 150 µm) tephra shards were not included in the IRD calculation. Grains per dry gram is the standard method of reporting IRD concentration, and significant increases in this measure are interpreted as Heinrich Events (Dowdeswell *et al.,* 1999; Knies *et al.,* 2000). Samples were counted every 2 cm with additional counts performed every 1cm where a significant increase in IRD was observed. To ensure counting accuracy 5% of the samples were recounted at random. Significant peaks in IRD were assigned to Heinrich Events 1-6 based on their stratigraphic relationship to other age markers (discussed in Chapter 3). The ages of Heinrich Events were taken from well-dated regional records and used in the final age model (Sarnthein *et al.,* 2001).

2.5 Age Model development (OxCal)

An age model describes the formal method of integrating all sources of chronological information against the depth at which they are found in the depositional sequence (Bronk Ramsey, 2007). As discussed above, age models are built using only hemipelagic sediments, and exclude rapid depositional events such as turbidites. No dating method can give an absolute date to the accuracy of a given year, but instead each date is expressed with an estimate of uncertainty (see Chapter 3 for discussion relative to each type of chronostratigraphic index). A realistic minimum analytical uncertainty for chronological methods is ± 30 years (Scott *et al.,* 2007).

Where possible, globally or regionally synchronous events are considered preferable for age model construction (such as magnetic excursions and tephra horizons), because they are free from complications related to radiocarbon calibration and reservoir correction (Lowe *et al.,* 2008;

Davies *et al.,* 2012; Brauer *et al.,* 2014; Rasmussen *et al.,* 2014). All age models described in thesis adopt the Bayesian approach used by the Oxcal model (Ramsey, 2008). The central tenet of this model rests on the prior model detailing the depth and order of the points to be used. The dates from each analysis are added as a series of likelihoods, or probability distribution functions (Ramsey, 2008; Ramsey and Lee, 2013; Bronk Ramsey *et al.,* 2015). OxCal utilises a Markov Chain Monte Carlo method of sampling and applies Bayes' theorem to produce the probability of each depth- based date. This approach produces an Agreement Index ("A"), and it is preferable for this to be >60% for each chronological marker (Bronk Ramsey, 2007). Chronological markers failing to meet the 60% threshold were rejected from the age model as they are considered statistically invalid.

Chronological markers to be included in the age model were assessed independently; these are discussed in Chapter 3. Dates were input to the Bayesian depositional model in OxCal (version 4.2, U_Sequence). Radiocarbon dates were calibrated using the Marine13 curve and a reservoir correction of 20 ± 30 years in addition to the standard ΔR of 440 years (Bondevik *et al.,* 1999; Mangerud *et al.,* 2006). Tephra dates were entered with the associated estimated uncertainty for each horizon. This uncertainty is derived from layer counting error in the ice core records or from marine sediment core dates in North Atlantic cores (see Chapter 3). Coccolith biozones are given a larger uncertainty for all horizons of at least 5,000 years. The Blake Geomagnetic Event was given an age of 114,000 ± 5,000 years to account for the long duration of this event, and the range in age estimates from terrestrial sources. All age models were built using the deposition model function in OxCal (Age-depth based), and depositional ages for turbidites were taken from interrogating the final model using the inbuilt age function of Oxcal.

2.6 Stable Isotopes

The analysis of stable isotopes is used in this thesis to establish the climatic conditions under which each turbidite was deposited. Stable carbon and oxygen isotopes within foraminiferal calcite shells are a well-established chronostratigraphic tool. The $\delta^{18}O$ ratio in biogenic calcite is driven by changes in $\delta^{18}O$ world-wide, (Shackleton & Opdyke 1973; Prell *et al*. 1986). These large magnitude changes are driven by glacial/interglacial changes and have been used to construct the Marine Isotope Stage (MIS) model used in chronostratigraphy. These MIS stages are recognisable as distinct periods of lighter (interglacial) or heavier (glacial) isotope ratios within foraminifera: odd numbers refer to warm periods such as today (MIS 1) and even numbers to cold, glacial periods (MIS 2, 4, 6, etc.). On shorter time scales, variations associated with short-lived Dansgaard-Oeschger cycles (1470 years) and Bond Cycles (5-10,000 years) can also be detected within marine sediment cores, depending on the sedimentation rate. When combined

with additional dating methods, $\delta^{18}O$ stratigraphies can be used to establish dates for marine sediments throughout the Quaternary (2.6 Ma). Short-lived warm periods in the ocean can be correlated to variations in the $\delta^{18}O$ of the Greenland ice core records, which can considerably enhance the accuracy of a stratigraphy, and allow an interpretation of the state of the ocean at the time of deposition of turbidites. This is examined in Chapter 4, where the oxygen isotope stratigraphy is used to examine a model of slide preconditioning and triggering with relation to ice sheet decay.

Variations in $\delta^{13}C$ in foraminiferal tests record the isotopic value of Dissolved Inorganic carbon (DIC) of the seawater. Changes in the DIC of seawater are driven by the global carbon cycle, increased terrestrial photosynthesis results in $\delta^{13}C$ enrichment of ocean surface waters. Carbon isotope ratios can also be affected locally by the dissociation of gas hydrates (extreme low values of $\delta^{13}C$ [Ravelo &Hillaire-Marcel 2007; Panieri *et al*. 2014]).

Contiguous samples were taken every 1 cm down core through the hemipelagite and initially dried at 40° for 48 hours. The dried samples were weighed and washed through a 63 µm sieve. From each 1 cm^3 processed sample 8 specimens of *Neogloboquadrina pachyderma* (sinistral) (*N. pachyderma* (s)) with a size between 150 and 212 µm were recovered for analysis of stable carbon and oxygen isotopes. The restriction to one size fraction limits the impact of vital effects, such as juvenile life stage, on the isotope ratio.

To develop a benthic stable isotope profile, 3 specimens of epifaunal *Cibicidoides wuellerstorfi* or 6-18 specimens of the infaunal species *Oridorsalis umbonatus* were selected. A spliced profile of benthic $\delta^{18}O$ is necessary in the Nordic Seas due to the well-established deficit of *C. wuellerstofi* in glacial and deglacial sediments in the region (Bauch *et al.,* 1996, 2000; Billups, Rabideaux and Stoffel, 2011; Telesiński *et al.,* 2015). *Cibicidoides wuellerstorfi* are regarded as an accurate indicator of bottom water properties due to its epibenthic lifestyle (Meland *et al.,* 2008). *Oridorsalis umbonatus* is infaual and as such records a partial pore water signal. Dual *Cibicidoides wuellerstorfi* and *Oridorsalis umbonatus* samples were taken from 19 separate stratigraphic positions covering glacial periods within the core. Correlations of these two benthic taxa are discussed in chapter 4.

Samples were analysed at the NERC Isotope Geosciences Laboratory, British Geological Survey in England. Analyses were performed using an *IsoPrime* dual inlet mass spectrometer plus multiprep device. Samples were loaded into glass vials and sealed, the automated system evacuates vials and delivers anhydrous phosphoric acid to the carbonate at 90°C. The evolved CO_2 is collected for 15 minutes, cryogenically cleaned and passed to the mass spectrometer.

Isotope value ($\delta^{13}C$ per mille [‰]) deviations of the isotopic ratios ($^{13}C/^{12}C$, $^{18}O/^{16}O$) were calculated relative to the (Vienna Pee Dee Belemnite (VPDB) scale using a within-run laboratory standard calibrated against NBS-19 $\delta^{13}C$ and $\delta^{18}O$.

2.7 Geophysics: Ægir Ridge 3.5 KHz sub-bottom profiles

Limited geophysical data was available for the Aegir Ridge coring site, and is used within this thesis to estimate turbidite volume and deposit extent. Sub-bottom profiles of marine sediments can reveal the nature of those sediments, and their mode of deposition be it hemipelagic or mass transport. The 3.5 KHz frequency is capable of penetrating up to 50 m below the seafloor depending on sediment compaction. Hemipelagic sediments display a stratified seismic character, whereas deposits of mass transport events are chaotic, and are represented as acoustically transparent seismic facies.

In 1990 two marine expeditions surveyed the Ægir Ridge as part of a joint Naval Research Laboratory and Hawaii Institute of Geophysics project (cruises EW9006 and EW9007 [Jung *et al.,* 1997]). The focus of these cruises was to investigate the structural geology of the ridge, and the processes linked to slow spreading centres and failed rifts (Jung and Vogt, 1997; Vogt and Jung, 2009). These expeditions collected 3.5 KHz and watergun data in a series of 92 lines crossing the ridge at 6 km intervals.

The 3.5 KHz data for this cruise was provided for analysis in the present study in analogue format by the Naval Research laboratory. These analogue rolls were digitised using a process in SegXY combined with the ship's navigation file. These converted images were then analysed in Petrel for relative bed thickness in Two Way Travel time (assumed acoustic seismic velocity of 1,800 m/s). The quality of these digitised lines is variable, but the stratigraphy of the region is demonstrated in Chapter 3. The relative bed thickness can be compared to give broad estimates of the volume of the turbidites.

Chapter 3 Two huge (>3,000 km^3) volume tsunamigenic landslides occurred offshore Norway in the last 60,000 years

Submarine landslides can be orders of magnitude larger than their sub-aerial cousins, and cause extremely dangerous tsunami. Several of the largest landslides yet found on Earth are located offshore Norway. They include the huge Storegga Slide that occurred 8,200 years ago, and involved over 3,000 km^3 of material. This mega-slide covered an area larger than Scotland, and produced a widespread tsunami. A repeat of the Storegga event would be very damaging to European coastlines, so it is important to determine the frequency and causes of such mega-slides. Previous work concluded that the recurrence interval of Storegga-like events was greater than 100,000 years, and the preceding mega-slide (Tampen Slide) occurred ~125,000 years ago. This is partly why landslide-tsunami are currently not included in the UK's National Risk Register, which considers events with shorter return times than 100,000 years. Here we show that the Tampen Slide is much younger, and occurred 52-60,000 years ago. The recurrence interval of mega-slides is thus lower than previously thought, and less than 100,000 years. Both the Tampen and Holocene Storegga slides occurred 2-10,000 years after the ice streams had retreated from the continental shelf edge, and rapid sedimentation ceased. Although small landslides can occur at other times, the early stages of deglaciations are when the threat from large landslide-tsunami is greatest.

3.1 Aims

This work investigates two mega-turbidites from the Ægir Ridge, with a primary aim to establish the provenance and timing of these events. This work produces the first date of the penultimate slide from the Storegga Slide Complex, known as the Tampen Slide. Dating of these two slides from distal deposits recovered in a sediment core will allow the hypothesis of mega-slide preconditioning and triggering to be tested, an assessment of the likely future risk, and indicate whether submarine landslide tsunamis should be included in the UK Risk Register.

3.2 Introduction

Submarine landslides are orders of magnitude larger than their terrestrial counterparts, and can potentially generate significant pan-oceanic tsunamis. The Holocene-age Storegga Slide,

which occurred 8,200 years ago on the Norwegian continental margin and mobilised 2,500-3,200 km^3 of material generated the largest tsunami known to have impacted UK shorelines (Haflidason *et al.* 2004, 2005). The tsunami had run-up heights up to 20 m in the Shetland Islands and over 5 m in the Firth of Forth (Figure 3.1; Bondevik *et al*. 1997; Dawson *et al*. 2011; Bondevik *et al*. 2012). The headwall for this failure extends 300 km across the southern Norwegian Continental Slope, and is the most recent of at least five slides from the same location in the last 500 ka. The only submarine slide from this slide complex that has been accurately dated is the Holocene Storegga Slide at 8,200 years Cal BP. The dating of older slides from this source area will help estimate their recurrence times, and thus, the hazard they pose to the UK and NW Europe. Understanding the recurrence of these slides and the possible processes that precondition and trigger them will inform the hazard posed to the giant Ormen Lange gas field that is situated within the landslide scar of the Storegga slides and represents the second largest petroleum play in Norway (Bryn *et al.,* 2005).

The most recent sediment accumulation on the Norwegian continental slope preserves a record of the history of the repeated advance and retreat of the Quaternary Fennoscandian Ice Sheet (Yoon *et al.*, 1991; Dahlgren and Vorren, 2003; Lekens *et al.*, 2006, 2009; Peck *et al.*, 2006). This package of sediment is known as the Naust Formation and spans the Quaternary period (Rise *et al.*, 2005, 2006; Stoker *et al.*, 2005; Ottesen and Rise, 2009; Ottesen *et al.*, 2012). The Norwegian shelf also hosts the scars of both the Holocene Storegga Slide and numerous other large-volume submarine landslides (Haflidason *et al.*, 2005; Laberg *et al.*, 2005; Solheim *et al.*, 2005; Laberg and Vorren, 2006; Baeten *et al.*, 2013). These slides runout into the central Norwegian Basin, while associated turbidity currents flowed south westwards along the narrow and deep Ægir Ridge. The thickness of the slide deposits in the central Norwegian Basin has proven an obstacle for sediment coring to recover records of the older slides, as thicknesses of the previously identified Storegga deposit exceed 30 m and thus cannot be penetrated by traditional piston coring methods. To accurately identify and date these slides, the thinner, distal deposits from the Ægir Ridge were cored and linked to the established record of glaciations on the Norwegian shelf. The establishment of accurate ages for each slide event allows an assessment of preconditioning and triggering factors.

The most recent Holocene Storegga Slide scar has been mapped with over 100,000 km of seismic lines (Bryn *et al.*, 2003; Haflidason *et al.*, 2005; Solheim *et al.*, 2005). These surveys also identified four previous slide scars buried beneath (Bugge, 1983; Bugge *et al.*, 1987; Evans *et al.*, 1996, 2005; King *et al.*, 1996). This repetitive failure of the continental slope has been interpreted as linked to glacial-interglacial transitions, with each major slide suggested to occur within a few thousand years of the start of an interglacial period (Bryn *et al.*, 2005; Solheim *et al.*, 2005). Excellent preservation of tsunami deposits in lakes and peat bogs

across the North Atlantic (Bondevik *et al.*, 2012) and extensive coring on top of the slide deposit (Paull *et al.*, 2010) has facilitated obtaining an accurate age estimate for the Storegga Slide. The Holocene Storegga Slide has been dated from terrestrial tsunami deposits to 8.17 cal ka BP (Bondevik *et al.*, 1998; Bondevik *et al.*, 2005; Paull *et al.*, 2010; Dawson *et al.*, 2011; Romundset and Bondevik, 2011) and offshore slide and turbidite deposits in the Norwegian Basin to 8,100 ± 250 Cal BP (Haflidason *et al.*, 2004, 2005). This age estimate coincides with the notable 8.2 ka BP climate excursion during which ice cores record a 6°C atmospheric temperature change in a few decades (hereafter the "8.2 ka event", Alley and Agustsdottir, 2005).

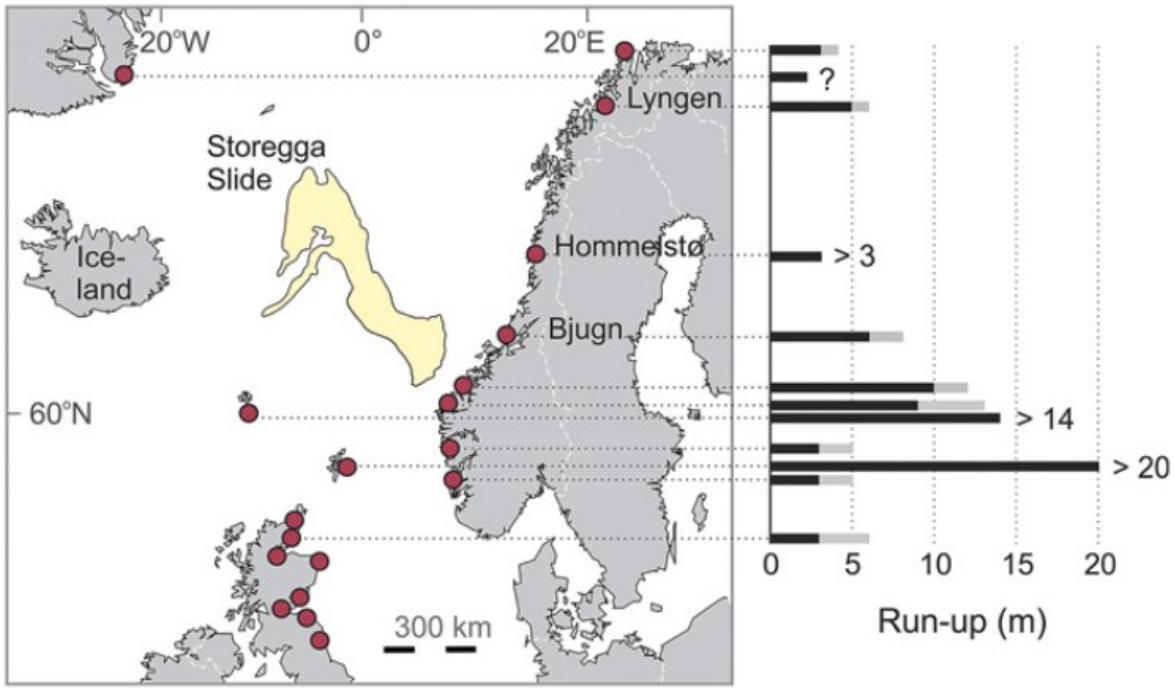

Figure 3.1: Location of tsunami deposits from the 8.2 ka BP Storegga Slide. Red dots indicate terrestrial deposits and the estimate of the waves height above sea level (black bar is the minimum height; grey bars are maximum heights). Yellow indicates the extent of known debrite and turbidite deposits from the Storegga slide (Figure 3 from Bondevik et al. (2012)).

Previous works have suggested dates for the last five slides from the Storegga region of the continental slope: Storegga (8.17 ka BP), Tampen (125 ka BP), Slide R (300 ka BP), Møre Slide (400 ka BP) and Slide S (500 ka BP). These dates broadly correlate to glacial terminations over the last 500 kyr (Figure 3.2; Solheim *et al.,* 2005). The dates for these older slides were established by identifying the seismic stratigraphy of the oldest sedimentary unit infilling the buried slide scar (Solheim *et al.*, 2005). Key reflectors were dated by identifying foraminiferal biostratigraphy from industry borehole cuttings (Figure 3.2; Berg *et al.*, 2005). Older slides have also been dated to 1.7 Ma (Slide U) and to 2.7-to-1.7 Ma (Slide W, Figure 1.5 and Table 1.1), further indicating that large-scale sliding has been a common feature along the

Norwegian margin since before major shelf edge glaciations began about 2.5 Million years (Ma) ago (Solheim *et al.*, 2005; Hjelstuen and Andreassen, 2015).

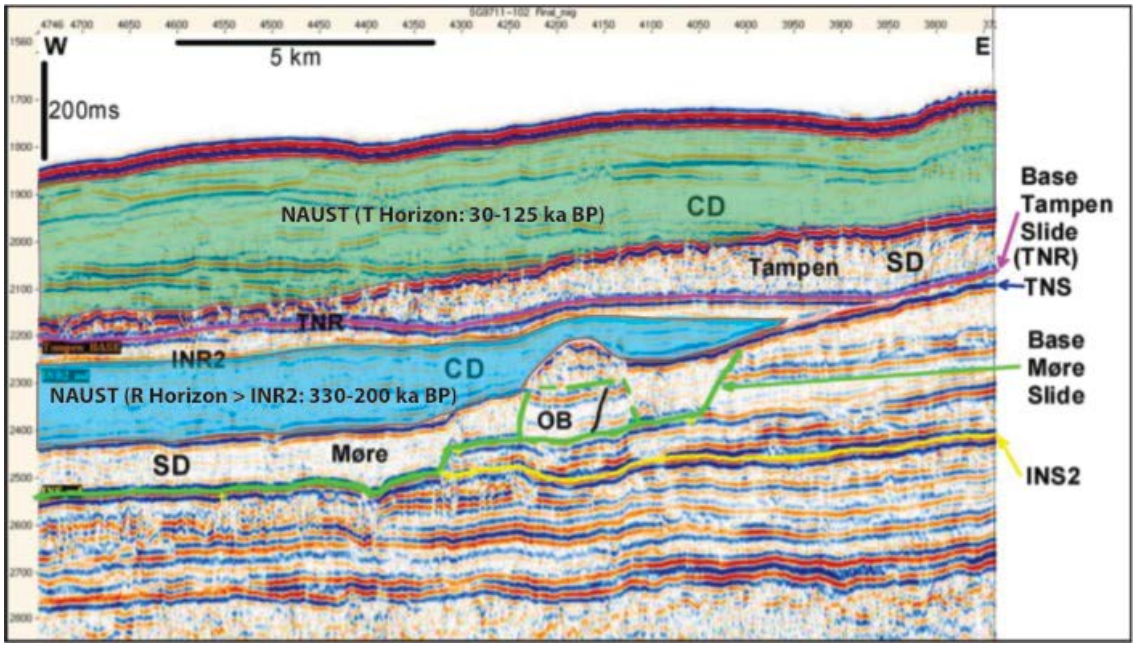

Figure 3.2: Seismic stratigraphic section from the NAUST Formation showing the deposits of the Storegga Slide Complex and the dated surfaces. Slide material and dated horizons are labelled from the text and figure adapted from Solheim et al. (2005).

Based on the dates from seismic stratigraphy and a number of borehole data, rapid sediment deposition during glacial periods was identified as an important preconditioning factor for slope failures (Figure 3.3). Triggering of the slides was attributed to environmental changes that occurred during glacial terminations and early stages of the interglacial periods. The leading model of slide generation suggests the coarse, glacial material slid over glide planes of stratified interglacial muds (Bryn *et al.*, 2003, 2005). Each slide occurred within an interglacial, suggestive of the involvement of isostatic rebound and associated seismicity (Bungum *et al.*, 2005), the build-up of pore pressure, and potentially changing ocean conditions (Lee, 2009).

A repeat of the Storegga Slide today would represent one of the worst geohazards the UK, and Northern Europe could expect. Tsunami deposits in the UK indicate major Scottish cities such as Aberdeen, Edinburgh and Dundee, would be impacted by the wave (Dawson and Smith, 2000; Bondevik *et al.*, 2012). In addition, the Sullen Voe oil terminal on Shetland and the Grangemouth oil refinery would be impacted by significant tsunami wave heights. For a risk to be considered for inclusion in the UK National Risk Register, it must have a recurrence interval of less than ~100,000 years. Current dating of the recurrence intervals of past slides in the Storegga Slide exceeds this minimum recurrence threshold, as such no risk mitigation or response planning is in place for the UK.

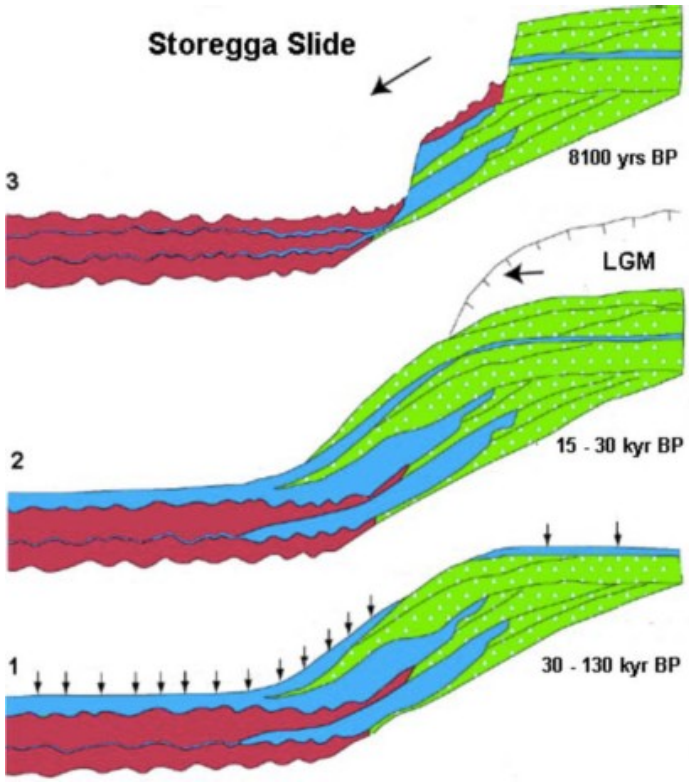

Figure 3.3: : Illustration of cyclic deposition and slides within the Ormen Lange region/Storegga Slide Complex. Green: glacial sediments; red: slide deposits; blue: marine sediments. (1) Last interglacial with deposition of soft marine clays. (2) Last Glacial Maximum (LGM) with the ice at the shelf edge and deposition of glacial sediments. (3) The Storegga Slide. The figure indicates two older slide scars from previous slides, the scars of which are filled with marine clays. The first known slide from this complex was dated to 500 kyr ago (S-Slide). The glide planes are found within seismically stratified deposits (hemipelagite) with a thick infill of stratified sediments suggests a late glacial to early interglacial occurrence. Figure suggesting the period between the 8.2 ka BP slide and the previous (Tampen) slide is 30-130 ka. Figure taken from Bryn et al. (2005).

3.3 Regional Setting

The Storegga Slide Complex lies on the Norwegian continental margin between 62.5 and 65°N (Figure 3.4). The 270 km long scar left by the Holocene Storegga Slide forms a submarine cliff < 250 m in height, and is a prominent feature of the Norwegian Shelf (Haflidason *et al.*, 2004, 2005; Solheim *et al.*, 2005).

The Norwegian Basin adjacent to the Storegga Slide Complex is a partially enclosed oceanic basin bordered by the bathymetric high of the Vøring Plateau to the east, and the Jan Mayen Fracture Zone to the north ([Figure 3.4] Eldholm, 1977; Breivik *et al.*, 2006; Mjelde *et al.*, 2008). The basin was formed as regional Cenozoic magmatism produced crustal thickening forming the Icelandic hotspot, and separated the Norwegian Greenland seas into a series of deep, bounded basins (Mosar *et al.*, 2002; Breivik *et al.*, 2006; Mjelde *et al.*, 2008). The Ægir Ridge is an extinct spreading ridge and represents the deepest region of the Norwegian Basin

that exceeds 3900 m water depth. The ridge widens north-eastwards from 40 km to 70 km between conjugate mountain chains (Vogt and Jung, 2009).

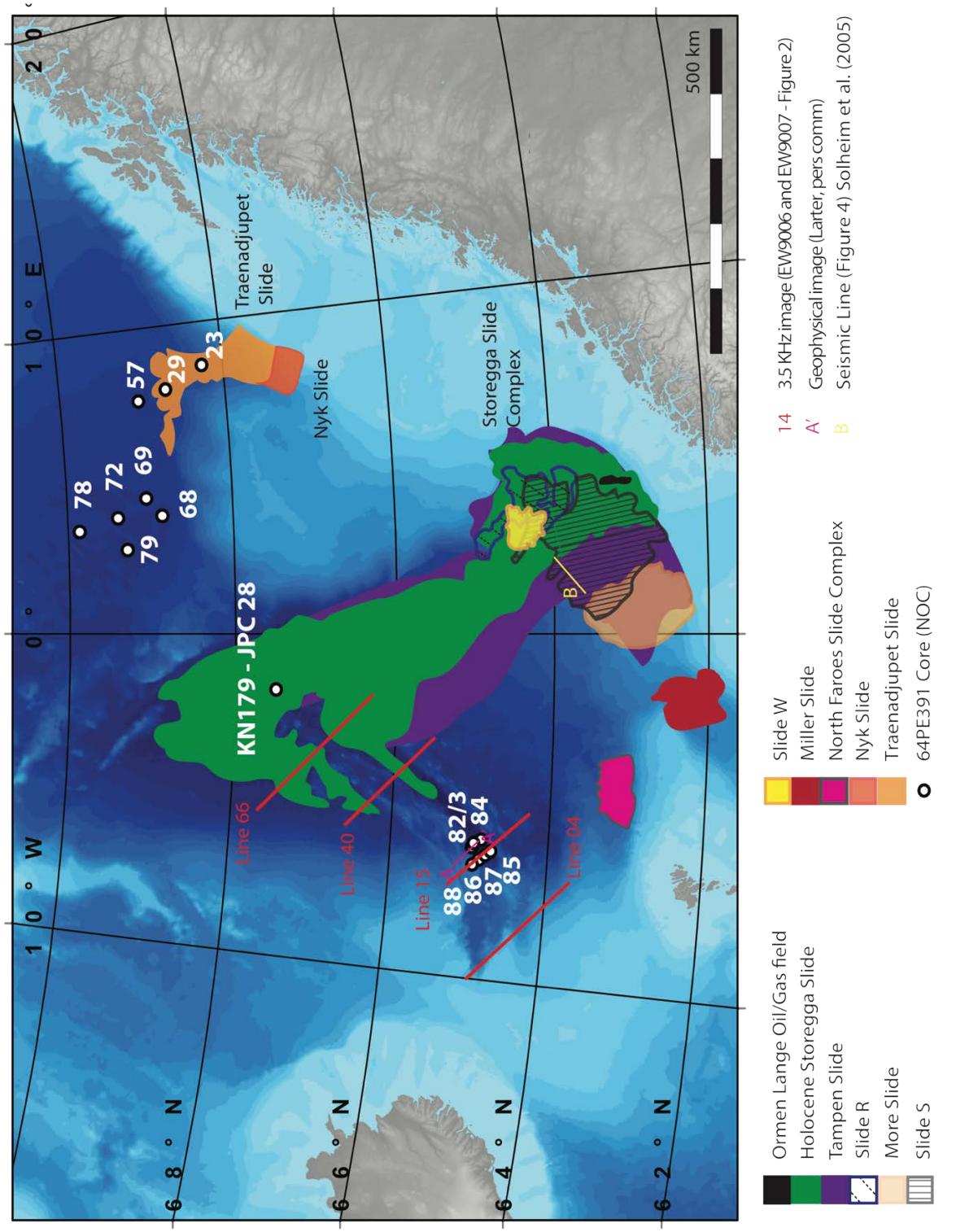

Figure 3.4: Map of the Nordic seas to show the locations of the cores discussed in this Chapter, and the sample of the central Storegga mud pond (KN179-JPC28). Coloured outlines show the known extent of each of the Storegga Slides, and the recent Trænadjupet and Nyk slides in the Lofoten Basin. Red lines indicate the chosen 3.5 kHZ sub-bottom profiles of cruise E9006 and EW9007 which illustrate the preserved stratigraphy in the Ægir Ridge.

The Ægir Ridge is a depocentre of pelagic material and mass wasting deposits from the surrounding basin margins (Jung & Vogt 1997; Vogt & Jung 2009). The ridge terminates at its south-western end against the Iceland-Faroe Ridge. Deposits from slides on the surrounding continental slopes are interbedded with hemipelagic deposits from the surface Norwegian Atlantic Current. The Norwegian Atlantic Current flows over the Faroe-Shetland Channel before following the continental margin northwards and passing over the Storegga Slide Complex (SSC) (Figure 3.3). At the southwest extent of the ridge the Icelandic Plateau forms a regional bathymetric high and a source for recent and modern volcanic inputs.

Part of the Ægir Ridge was surveyed during the July 2000 trials cruise of the RRS James Clark Ross (JR50). This cruise trialled use of the TOPAS sub-bottom profiler across the western edge of the rift. During the equipment trial two large acoustically transparent units were identified and interpreted as preliminary evidence of large turbidites within the Ægir Ridge of unknown age or origin (Figure 3.4). These trial cruise data were used to locate coring sites for a later cruise in 2014 (Figure 3.3).

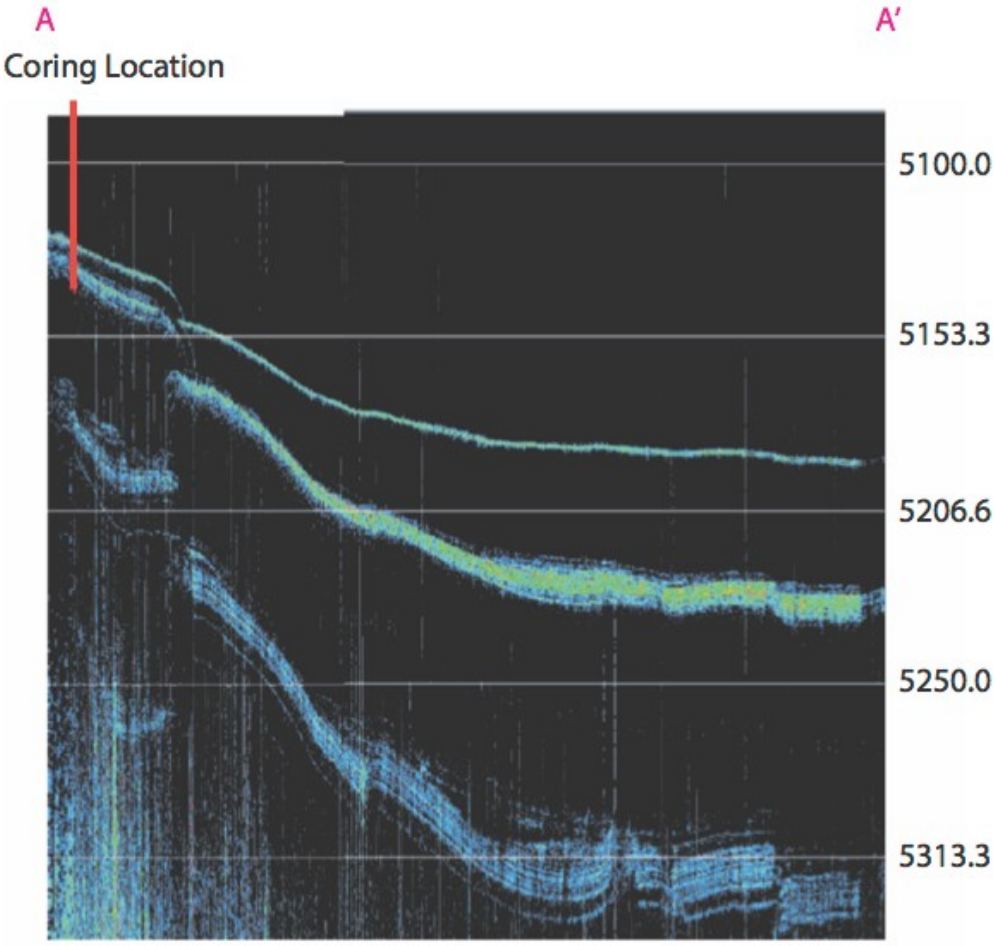

Figure 3.5: TOPAS sub-bottom profile from a JCR Trials cruise showing two large transparent units within the Ægir Ridge. A-A' labelled on Figure 3.3, Figure 3.3 provided by R. Larter (pers. comm.). Pale horizons indicate stratified hemipelagite, black units interpreted as chaotic mass transport deposits based on their transparent expression.

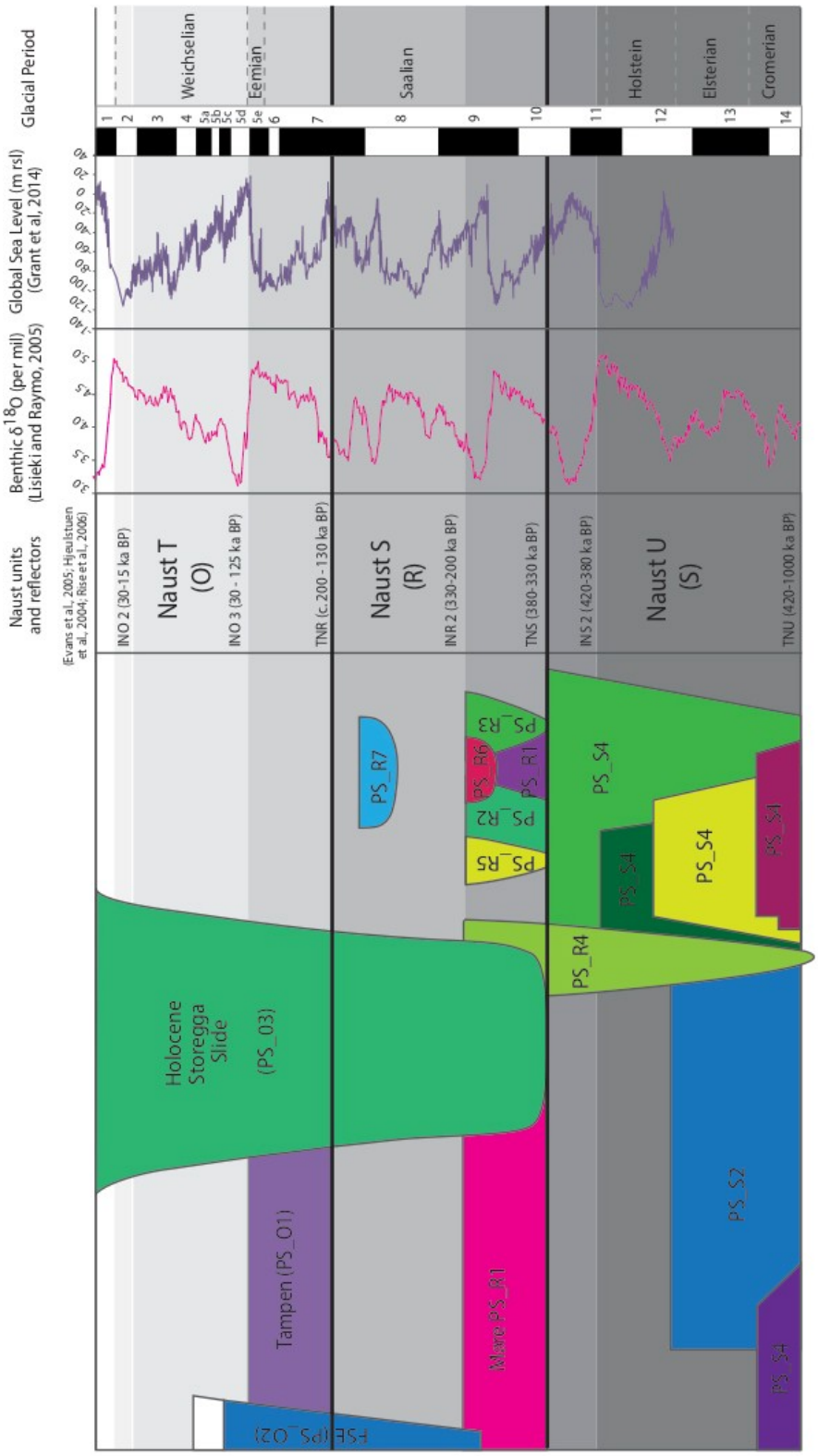

Figure 3.6: Slide stratigraphy of the Norwegian Margin aligned with global oxygen isotope curves (Lisieki and Raymo, 2005) and sea level change (Grant et al., 2014). Adapted from Bryn et al. (2005) and Solheim et al. (2005). The Naust stratigraphy is shown (Rise et al. 2009) and dates of the key reflectors within the Naust units (Berg et al., 2005) and Rise et al. (2005, 2010). Slide volumes are based on seismic interpretations (Solheim et al. 2005), the benthic global isotope curve (Lisieki and Raymo, 2005) and global sea level (Grant et al. 2014) are shown to illustrate the link between dates applied to slides through seismic correlation and major changes in ice sheet volume.

3.4 Material and Methods

3.4.1 Core Material

Seven piston cores were collected in July 2014 by the *RV Pelagia* from the southern limits of the Ægir Ridge in two short transects downslope along the western slope of the ridge (between 3,670 m and 3,799 m water depth; Table 3.1). The two shallowest cores (PC86 and PC88) recover identical stratigraphies, consisting of two metre-thick turbidites interbedded with stratified hemipelagite and thinner intervening debrite and turbidite units (Figure 3.5). This repeating stratigraphy can be correlated between the additional five core sites. Three cores (PC82, PC84 and PC88) were selected to build a robust age model. These cores were correlated visually and through non-destructive methods (Figure 3.7). Core PC88 was selected for dating as it recovered the thickest hemipelagite below the lowermost metre-thick turbidite (core details in table 3-1). Core PC84 was selected based on the expanded hemipelagic section between the two turbidites. Core PC82 was also sampled for radiocarbon dating.

Table 3.1: Details of the cores collected from the Ægir Ridge targeting the two transparent units highlighted in Figure 3.5.

Cruise Code	Core Code	Collection Date	Position	Water Depth (m)	Core Length (m)
64PE391	*Core 82*	*28/07/2014*	*64° 57.869 N, 06° 11.175 W*	*3815*	*10.04*
64PE391	*Core 83*	*28/07/2014*	*64° 57.9 N, 06° 11.167 W*	*3815*	*12.72*
64PE391	*Core 84*	*28/07/2014*	*64° 50.976 N, 06° 29.06 W*	*3799*	*12.89*
64PE391	*Core 85*	*28/07/2014*	*64° 57.495 N, 06° 27.664 W*	*3811*	*12.29*
64PE391	*Core 86*	*28/07/2014*	*64° 51.937 N, 06° 32.275 W*	*3666*	*10.42*
64PE391	*Core 87*	*29/07/2014*	*64° 51.25 N, 06° 29.916 W*	*3789*	*12.19*
64PE391	*Core 88*	*29/07/2014*	*64° 51.963 N, 06° 32.197 W*	*3670*	*13.11*

3.4.2 Methods

3.4.2.1 Core logging: visual and multi-sensor

The sediment records in each core were visually logged and categorised into sedimentary units defined by variations in grain size, colour, texture and sedimentary structures. These units were subsequently grouped into five lithofacies (Table 3.2 and Figure 3.9). Hemipelagite and turbidite facies were distinguished visually. Hemipelagite was identified as pale to dark brown, containing randomly dispersed microfossils and variable quantities of Ice Rafted Debris (IRD). Upper boundaries of turbidites are often identified above a red-brown oxidised mudcap, exhibiting intense bioturbation before returning to hemipelagite. Hemipelagite boundaries above turbidites are often gradational and heavily bioturbated . Turbidite facies

were identified with a sharp, often erosive base, visible normal grading from coarse sands to clay, and were dark olive-grey. The cores were also analysed using a *Geotek*™ Multi- Sensor Core Logger (MSCL-S at the British Oceanographic Sediment Core Research Facility [BOSCORF]) for P-wave velocity and bulk density and at 1 cm intervals in order to generate a density profile to determine if significant erosion has taken place at the base of the turbidites. Sediment cores were analysed for magnetic susceptibility and photospectral reflectance using the *Geotek*™ MSCL-XYZ logger (BOSCORF) at 0.5 cm intervals. .

3.4.2.2 AMS Radiocarbon Dating

Accelerator Mass Spectrometry (AMS) carbon-dating is a widely-used for dating marine sediments. Here this method measures the concentration of ^{14}C within the shells of foraminifera up to a maximum age of 43.5 ka BP (Reimer, 2013). A total of 11 radiocarbon dates from three cores were obtained for the Ægir Ridge chronology (Figure 3.7). Samples selected for carbon-dating comprise hemipelagic sediments with minimal evidence of reworking within 3 cm of upper turbidite boundaries.

Foraminiferal samples were picked from the 150-212 µm fraction, where possible single species samples were used (*Neogloboquadrina pachyderma sinistral* [NPS]); mixed planktonic samples (including *Globigerina bulloides* and *Orbulina universa* in addition to *NPS)* were only used where the minimum weight for AMS analysis could not be reached (20 mg). Radiocarbon ages were calibrated to calendar years using *OxCal* software utilising the marine13 calibration curve (Reimer, 2013). A 400 year global ocean reservoir correction was applied to this data (Reimer, 2013). Significant uncertainties surround calibrated radiocarbon ages in the Norwegian Sea. The unconstrained reservoir age in the North Atlantic is both large and variable (Haflidason *et al.*, 2000; Waelbroeck *et al.*, 2001; Thornalley *et al.*, 2011). This work adopts methodology of Laberg *et al.* (2002) and uses an additional regional specific delta R (ΔR) correction of 20 ± 30 years (Reimer, 2013). This allows comparison of previous carbon-dating of sediments in the Norwegian Basin. All calibrated dates are therefore expressed as calibrated years before present (Cal BP) with conventional (^{14}C years) radiocarbon years detailed in Table 3.3. Analyses were performed by the Scottish Universities Environment Research Centre (SUERC) AMS Facility, East Kilbride and Beta Analytic Inc., Miami (Table 3.3, Figure 3.7).

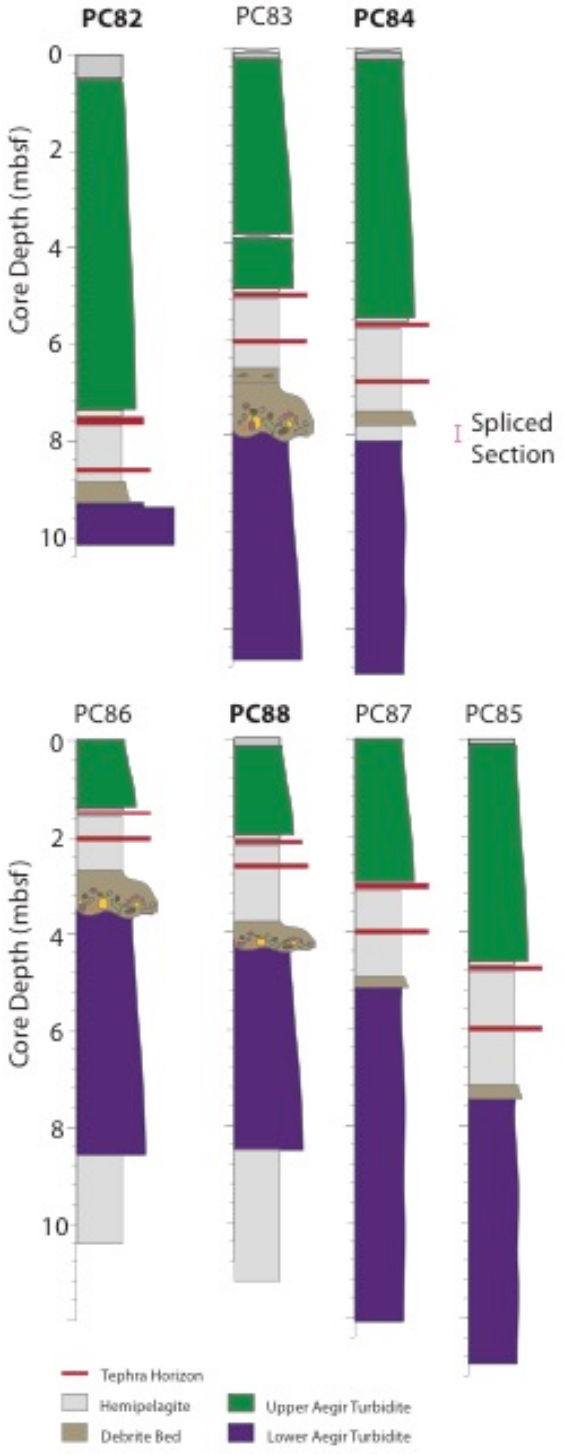

Figure 3.7: Lithological logs of cores collected from Ægir Ridge, detailed in Table 3.1. Cores are shown along the two transects, colours indicate beds that are correlated between all cores. Core labels in bold indicate those selected for radiocarbon dating..

3.4.2.3 Tephra

The North Atlantic has been subject to periodic inputs of volcanic ash from both the Icelandic and Jan Mayen volcanoes (Lacasse *et al.*, 2001; Óladóttir *et al.*, 2011; Óladóttir *et al.*, 2008;

Davies *et al*., 2010). Iceland is subdivided into ten volcanic systems (figure 2.2, p41). Eruptions from each Icelandic volcanic system and eruptions from Jan Mayen are geochemically unique, and in combination with additional stratigraphic information, characterisation of these horizons by Electron Micro Probe Analysis (EPMA) can be used to correlate marine tephra to those found in the North Greenland Ice Core Project (NGRIP) ice core record and existing sediment cores (Svensson *et al*., 2008). Once correlations have been identified an accurate date can be applied to the horizon in the sediment core. This method is particularly useful for the last 125,000 years (length of the Greenland Ice core records), and can be used for older records where a reliable tephra chronology exists (Davies *et al*., 2014). For these analyses contiguous 1 cm^3 samples were taken down core and sample preparation follows the methods of Hibbert *et al*. (2014). Tephra shard counts were undertaken every alternative centimetre. This resolution was increased to every centimetre where macro-tephra were observed. Tephra were visually identified from the >150 μm fraction and classified as brown or colourless. To assess geochemical homogeneity between size fractions and negate the potential effect of ice-rafting on tephra deposition, samples up to 5 cm either side of peaks in tephra presence were counted every centimetre spanning all identified peaks in the 80-150 μm, and >150 μm grain size fraction.

For geochemical analysis, tephra slides were prepared by picking 50 individual tephra shards and placing them on polished glass slides. The tephra shards were then mounted in two-part epoxy resin and left to cure for 48 hours. Slides were then ground to a 30 micron thickness, ensuring at least 20 glass shards were exposed for analysis. The prepared tephra slides were carbon-coated prior to major element SEM EDX composition analysis using the Cameca SX100 electron microprobe, University of Edinburgh, as discussed in Hayward (2012). Secondary standards “Lipari” and “BCR2g” were used to monitor instrumental drift, precision and accuracy. Data were normalised to a 100% anhydrous basis for comparison to existing datasets, full raw data are also reported (appendix).

Age assignment of each tephra layer was based on geochemical comparisons with a database developed for this project, of 109 Marine Isotope Stage 6 to present tephra deposits from marine, terrestrial and ice core records with excellent dating controls (full discussion section 3.6.4). Geochemical composition and existing stratigraphical information were used to determine the most likely eruption match. Confident matches were used in the final age model.

3.4.2.4 Ice Rafted Debris

The North Atlantic has been surrounded by vast ice sheets that periodically retreat and release armadas of icebergs into the central North Atlantic regions (Ruddiman, 1977;

Sarnthein *et al.,* 2001; Rashid *et al.,* 2003). These icebergs transport coarse debris that is too large to have been transported by ocean currents. The melting of these icebergs releases the debris, which deposit on the seafloor and leave characteristic horizons of coarse sediment (Ice Rafted Debris – IRD) reaching as far south as 40° N (Ruddiman, 1977). Concentrations of IRD in the hemipelagite sediments are known as Heinrich layers and occur synchronously across the North Atlantic (Rashid *et al.,* 2003). Once these horizons are identified, they can be used to date the sediments in which they are found as each horizon is named and constrained chronologically back to Heinrich Event 6 (66.5 ka BP; Hemming, 2004). Subsamples of > 150 μm grains from the hemipelagite were counted to identify variations in the quantity of IRD. The fraction was converted to the number of grains per gram of dry sediment to allow identification of Heinrich layers. Samples were counted every 2 cm, with additional counts performed every 1 cm where a significant increase in IRD was observed. Five percent of the samples were recounted to ensure precision fell within 5%. Where tephra glass counts and IRD horizons were found at the same stratigraphic horizon, this is suggestive of ice rafting, rather than primary airfall as the dominant transport mechanism for tephra, and such horizons could not be used as reliable chronological indicators.

3.4.2.5 Palaeomagnetism

Palaeomagnetic dating of sediments uses recorded variations of the intensity and direction of Earth's magnetic field over time to correlate to a well-dated regional or global reference record, or to known geomagnetic excursions (Laj *et al.,* 2000). Over the last ~2 million years the estimates of down core magnetic palaeointensity can be correlated to a reference record that allows the sediment sequence to be accurately dated. Age determination based on geomagnetic excursions is typically used for sediments with high accumulation rates, as low accumulation rates < 5 cm/kyr often cannot record short-lived excursions. Previous studies have developed a multiproxy chronology for late Quaternary sediments in the sub-Arctic records (Nowaczyk *et al.*, 1994; Nowaczyk, 1997; Nowaczyk and Knies, 2000). Low foraminifera abundance and an upper useful limit of 43.5 ka BP limit the effectiveness of AMS radiocarbon-dating for building core chronologies. Palaeomagnetism can be used to date sediments well beyond this limit, and is particularly effective when excursions are combined with additional dating methodologies. The low sedimentation rate encountered in these sediment cores have combined radiocarbon dates and coccolith biostratigraphies to validate excursions in magnetic inclination records (Nowaczyk *et al.*, 1994; Nowaczyk, 1997; Nowaczyk and Knies, 2000). This study only investigated significant excursions in the inclination (> 40° from background) that were coincident with periods of low Relative Palaeointensity (RPI).

Palaeomagnetic data were measured at the University of Southampton, on a 2G-Enterprises superconducting rock magnetometer (SRM) designed for u-channel samples. All Natural Remanent Magnetisations (NRM) measurements were performed at 1 cm intervals.

The response function of the magnetometer coils integrates measurements over several centimetres (6-7 cm). All u-channel measurements were performed with a 10 cm trailer and leader. The NRM was measured using stepwise alternating field (AF) demagnetisation at peak fields from 0 to 60 mT at 5mT increments, then 10 mT increments from 70-100 mT for a total of 17 steps. Directions (inclination and declination) of the characteristic remanent magnetisation (ChRM) were calculated by principal component analysis (PCA) with 9 AF demagnetisation steps from 20 to 60 mT. The hemipelagic record was generated using horizons identified from visual logging and ITRAX analysis. Magnetisation components were computed for the 25-60 mT range using the UPmag software (Xuan and Channell, 2009). The maximum angular deviations (MAD) values were calculated to demonstrate the integrity of individual component directions. Values with <10° are accepted as reliable.

The use of a normaliser for NRM is essential to minimise the effects of magnetic grain size and concentration. Anhysteritc remanent magnetism is widely used as a normaliser to generate RPI (Channell *et al.*, 1997; Laj *et al.*, 2000; Stoner *et al.*, 2002). This was measured after the full 17 step NRM demagnetisation, through the application of ARM acquisition in a 100 mT peak alternating field with a 50 µT DC bias field. ARM was re-acquired in a stepwise protocol mimicking the NRM steps. The RPI was then calculated within the UINT function of the UPmag software through normalising the NRM by ARM. Due to the expected low resolution of the core, Isothermal Remanent Magnetism (IRM) was not measured, as the sedimentation rate is <5 cm/kyr, therefore short-lived intervals of magnetic reversal were unlikely to be detected The RPI will then be used to correlate to regional and global stacked records of RPI such as NAPIS-75 (Laj *et al.*, 2000), SINT-200 (Guyodo and Valet, 1996) and PISO-1500 (Channell *et al.*, 2009).

3.4.2.6 Coccolith Biostratigraphy

Coccolith species and abundances were counted using a *Hitachi* TM1000 Table top SEM following the methodology in Hunt *et al*. (2013). Samples were prepared by spreading a hemipelagite over a semiconductor stub and dispersing with acetone. Prepared samples had a minimum of 300 specimens counted under x5,000 magnification. Species data were analysed in comparison to the biozones described by Gard *et al*. 1988. This work had developed a biostratigraphic framework for relative species abundances across the Norwegian and Greenland Seas, dated using the SPECMAP timescale (Imbrie *et al.*, 1984),

and by correlation with the benthic oxygen isotope curve (Gard 1988; Bleil & Gard 1989). All coccolith data was collected by James Hunt.

3.4.2.7 Age model development

The age model was constructed using *OxCal* v4.2.4 (Ramsey and Lee, 2013) and the Marine13 calibration curve (Reimer, 2013). *OxCal* uses a range of Bayesian models for deposition that allow all dating methods to be combined as a series of probability distribution functions that represent the likelihood of a sample at a given depth holding a given age (Ramsey, 2008). The deposition model function of *OxCal* uses a Markov Chain Monte Carlo (MCMC) sampling to develop a distribution of possible solutions to the age/depth model. This study adopts the P_Sequence (Poisson process) function of *OxCal* in which the deposition rate is unknown and considered inherently random. The *k* parameter (increments per unit length) was defined in centimetres due to the limited length of the hemipelagic sequence. Full data for the model is provided in Table 6.

In order to develop an age-depth model for core 88, an "event-free chronology" was created (Ramsey, 2008). This was achieved by removing all turbidites, glacigenic debris flows and the mud clast debrite from the record. The remaining hemipelagite record includes the visible tephra layers and the lag deposit contourite Each of these facies are considered appropriate to include on the basis of a high proportion of intact foraminifera within the hemipelagite sediment. This hemipelagite depth is plotted against the datum horizons discussed below. Data from each chronological method was then plotted within *OxCal*, which incorporates an estimation of error. This hemipelagite age-depth scale allows for linear interpolation between age markers based upon the changing sediment accumulation rate. This age model was was used to calculated the age of the hemipelagite at the depths where the turbidites had been removed, and provided an additional estimation of the potential uncertainty.

3.4.2.8 ITRAX XRF

The ITRAX µ-XRF core scanner at the British Ocean Sediment Core Research Facility (BOSCORF) was used to progressively scan split core sections at 500 µm intervals to construct a detailed chemostratigraphic record of the hemipelagite (Hunt *et al*. 2013), which was correlated to past climatic records (Hunt *et al*. 2013). In addition, the ITRAX micro-XRF core scanner was used to obtain geochemical compositions of the turbidites to assess sediment provenance (Hunt *et al*., 2015a, 2015b). All ITRAX data were collected using a Mo tube with a setting of 30 kV and 30 mA for quantitative XRF. Element intensities are generated from K-shell peak areas for the range of selected elements. The ITRAX core scanner data is subject to variations based on grain size and sediment surface water saturation (Croudace *et al.*, 2006;

Rothwell *et al.*, 2006; Cronan *et al.*, 2010). Although Hunt *et al*. (2015a) show a minimal effect of grain size sampling was restricted to turbidite mud caps to give maximum comparability between sites.

To minimise the effect of these parameters towards turbidite XRF compositions only the turbidite mud-cap (<63 μm) below the oxidation front was analysed for each turbidite (Hunt *et al.*, 2015a; MacLachlan *et al.*, 2015). Oxidation fronts are evident in all turbidites in the Ægir Ridge cores. Oxidation fronts form as oxygen migrates downwards from the seafloor into the turbidite mud cap. This process results in a distinctive "two-tone" turbidite consisting of a pale brown upper section, with distinctive orange brown laminations and olive-grey lower section (Jarvis and Higgs, 1987; Pearce and Jarvis, 1995). The alteration of the turbidite mud is due to the oxidation of labile organic matter and precipitation of manganese oxy- hydroxides within the fine-grained turbidite mudcaps (Jarvis and Higgs, 1987).

Elemental ratios were selected from Croudace *et al*. (2006) and are chosen to highlight variations in terrigeneous and carbonate compositions (Figure 3.25). Si/Rb, Fe/Rb and K/Rb are valuable indicators of clay mineral contents. Rb is a useful normaliser as it is concentrated in resistant minerals and often enhanced in turbidites. Rb is commonly used in micro-XRF studies as a substitute for Al, which is poorly detected with XRF core scanners due to its attenuated signal as a light element (Croudace *et al.*, 2006; Rothwell *et al.*, 2006). The use of the Sr/Ca and Sr/Si ratios offers an indication of relative aragonite content and silica content (Croudace *et al.*, 2006; Richter *et al.*, 2006; Rothwell and Croudace, 2015). With Sr/Si allowing discrimination between silicate and carbonate source material. Sr indicates a shallow water source though the inclusion of high-Sr aragonite, whilst Si is a useful terrigenous indicator (Croudace *et al.*, 2006).

The Norwegian Caledonides are a succession of nappes of late Precambrian to early Palaeozoic rocks that have undergone extensive regional metamorphism. The metamorphism is variable, progressing from ~320° to ~610° in a northerly direction. Metalliferous minerals are found at high concentrations throughout the range, including Cu and Cu-Zn volcanogenic massive sulphides (VMS) and Zn-Pb-(Cu) sedimentary exhalative deposits (SEDEX (Barrie *et al.*, 2010; Corfu *et al.*, 2014)). In association the northern Sulitjelma region hosts a large ore deposit of pyrrhotite, pyrite, chalcopyrite and sphalerite (Kullerud *et al.*, 1955; Barrie *et al.*, 2010). The economically important Pechenga Formation, north-western Russia, has a significant influence on detrital sediments in the Barents Sea region (Hanski *et al.*, 2011). The variation in metamorphic province and VMS elemental ratios is evident in sediments eroded from the continental shield and deposited as glaciomarine sediments. This geochemical

signature of the source rock can be successfully detected using the ITRAX methodology. Whilst the composition of mud caps is interpreted as indicative of the composition of source rocks that failed, they may also represent the composition of the sea floor they have eroded during transport (Pearce and Jarvis, 1992). The exceptional distance these turbidites may have travelled introduces an element of uncertainty in interpretation of the major element record. As such the interpretation of provenance is based on a multi-proxy approach including both assessments of geochemistry and suggested dates for the failures. For comparison, debris flow samples from the Bear Island Fan (Pope *et al.*, 2016) and samples from the Trænadjupet turbidite in the Lofoten Basin (this work) are included.

3.4.2.9 Inductively Coupled Plasma Mass Spectrometry (ICP-MS)

A set of 36 samples was selected from 6 cores to analyse the geochemical composition and provenance of turbidite mudcaps. Samples represent 1 cm^3 of turbidite mud extracted and prepared for ICP-MS at the National Oceanography Centre (McLennan *et al.*, 1993; Pearce and Jarvis, 1995; Hunt *et al.*, 2011). Sediment samples were dried at 40°C for two days and then ground in an agate pestle and mortar. Aliquots of 0.1g were digested overnight in sealed Teflon bombs in *aqua regia* (HCl + HNO_3, 3:1) at 160°C under reflux. This was followed by HF + HNClO digestion (3:2.25 ml) overnight and subsequent dry-down at 140°C with an addition of 1 ml HClO and subsequent dry-down to ensure complete removal of all HF. Resulting residues were dissolved in 5ml of HCl overnight under reflux, and then weighed and stored in 30 ml mother solutions of HCl. A daughter solution was made up using 0.5 ml of the mother solution, dried-down and dissolved in 3% HNO for analysis by ICP-MS. Sample compositions were calibrated against a set of nine rock standards (CBLK, JA2, BRR1, BIRI, JB19, BHV02, BAS206, JB3 and JG61), while blanks were analyzed routinely to assess potential contamination and drift of the instrumentation.

3.4.2.10 3.5 KHz sub-bottom profiles

The Ægir Ridge was extensively investigated in 1990 during two *R/V Maurice Ewing* cruises (Jung and Vogt, 1997). During this survey 92 adjacent lines of 3.5 KHz *Hydrosweep* sub-bottom profilers and watergun seismic reflection data were completed in transects six kilometres apart along the length of the Ægir Ridge (Jung and Vogt, 1997; Vogt and Jung, 2009). The water-gun seismic reflection and sub-bottom profiler data were used to evaluate the deep structure of the ridge. Within the water-gun data a thick package of acoustically transparent layers interbedded with stratified sediments was consistently observed along the ridge (Figure 4: Vogt & Jung 2009). The character of these packages is consistent with seismic records of mass wasting deposits. Here, these data were digitised and processed with IMAGE2SEGY and the ship's navigation file, using a script run through *Matlab* that converts

hardcopy seismic data to geo-referenced Seg-Y files. Re-processed data was analysed in *Petrel*. Selected lines have been shown to illustrate the continuous geometry of the deposits along the ridge. From the 3.5 KHz data, two large acoustically transparent units are visible; the volume of these deposits has been constrained through calibration of thickness of the units in cores collected along the survey line. Photographed images were stitched into continuous lines at four key locations along the ridge. Locations were chosen based on the quality of the analogue data for the site, and targeted: (1) the most distal line from the Storegga Slide; (2) a transect across the main mud pond of the slide; (3) and two equally spaced lines between the proximal and distal sites.

3.5 Results

3.5.1 Stratigraphy

The stratigraphy of all seven cores collected is remarkably consistent with two large turbidites (Upper and Lower Ægir Turbidites) interbedded with hemipelagic units (Figure 3.7). Core PC88 was chosen to develop an idealised stratigraphic model as this core contained the greatest depth of hemipelagite below the Lower Ægir Turbidite (section 3.6). The units discussed are illustrated in detail in Figure 3.8. Within the Ægir Ridge a thin hemipelagic drape (Unit 1) covers a thick turbidite (1.2-5.6 m-thick; Unit 2). Beneath Unit 2 a 1.6 m-thick hemipelagic package (Units 4, 6 and 8) are interbedded with two basaltic tephra horizons (Unit 5 and 7). In all cores except core PC84, beneath the hemipelagic Unit 8 is a small mud clast-rich debrite (Unit 9) immediately atop Unit 10 (Lower Ægir turbidite). In PC84 Units 9 and 10 are separated by a thin (13 cm) hemipelagic bed. Unit 10 is similar to Unit 2, and represented by a 5.7 m thick olive grey turbidite displaying a clear fining upwards succession from coarse sands to muds. Unit 10 was only fully penetrated in cores PC86 and PC88, and beneath this turbidite a return to hemipelagic muds interbedded with thin glacigenic debris flow deposits is observed.

3.5.2 Facies description and interpretation

The units observed in cores PC82-88 are described fully below, and divided into 6 lithofacies summarised in Table 3.2 and the following subsections. The facies detailed in Table 3.2 have been classified using the criteria described in Eyles *et al*. (1983).

3.5.2.1 Hemipelagic current sorted silts (HPC) facies

This facies appears as a distinctive pale brown/yellow moderately sorted medium grained horizon. The hemipelagic current-sorted silts are highly variable in colour, ranging from pale yellow to orange-grey. Few drop stones are visible, but IRD content is variable and concentrated into discrete horizons. The ITRAX Ca content is high (>25 Kilo Counts per Second [KCPS]), but varies down core (1-125 KCPS). Planktic and benthic foraminifera are present throughout this facies. Within this facies magnetic susceptibility is variable, (40-225 $x10^{-5}$ SI) and sand content is sporadic throughout. The X-ray images show weakly developed laminations throughout, interrupted with moderate bioturbation indicative of subtle variations in energy through time. This facies is interpreted here as representative of both interglacial and glacial hemipelagic muds.

3.5.2.2 Lag deposit contourite (LDC) facies

Well-sorted sands occur at three positions within the stratigraphy (Unit 1, Unit 20 and Unit 26 (Figure 3.8)). In each unit a sharp base is overlain by medium-coarse sand. U1 represents the modern sedimentary environment. This coarse sandy lag is present in each of the cores, and contains a high proportion of foraminifera and fresh tephra with a distinct colour change to pale yellow-brown. Some stratification is visible in Unit 1 and Unit 26, with Unit 1 showing well-developed alternating bands of coarse/medium to fine sands. Frequent foraminifera and a lack of IRD content indicates an interglacial environment as microfossil abundances in the Nordic seas are limited during cold periods. The coarser grain size of the LDC facies compared to the HPC facies is interpreted as representing a high current strength, comparable to modern conditions in the region.

3.5.2.3 Glacigenic debris flow (GDF) facies

This facies occurs seven times throughout the core (Units 12, 14, 16, 18, 22, 24 and 28), exclusively below the two mass transport deposits (Units 3 and 10) between 9.3 and 11.7 m core depth. It comprises of high-strength, matrix- supported, dense grey muds. There is a variable IRD content. Units vary between 2-and-34 cm thick and no visible foraminifera. There is evidence of stratification and weakly developed grading within the thicker units. Stratification is only visible in the X-ray scans and is poorly developed when present. The lower boundary of each unit is sharp with a marked colour change from pale brown-yellow hemipelagite to a dark greenish grey stiff clay. The upper boundary is heavily bioturbated with a clear oxidation front identified by yellow-orange clays. Units are characterised by a very low magnetic susceptibility (<50 x 10^{-5}SI), and a low Ca content (<5 KCPS). The absence of microfossils and inclusion of coarse-grained, angular material suggests these deposits have

been transported downslope and redeposited in the Ægir Ridge. These angular deposits are likely re-deposited from a proximal source or smaller local failures from within the Ægir Ridge.

Table 3.2: Summary characteristics of lithofacies of PC82 - 88.

Code	Structure	Colour (Munsell)	Texture	Boundaries	Sed. Units	Interpretation
HPD	Moderately sorted, occasional laminations, some evidence of bioturbation with IRD clasts.	9.0 YR 4.50/1.60	Sandy clay, moderate to poor sorting, occasional large clasts of IRD with infrequent sandy horizons.	Bioturbated lower boundaries.	U2, U4, U6, U8, U11, U13, U15, U17, U19, U21, U23, U25, U27, U29	Hemipelagic IRD Diamict
LDC	Stratified to structureless sands with abundant tephra and microfossils.	8.8 YR 5.70/0.70	Well sorted fine-medium sands.	Sharp base, occurs as a 12-15 cm thick horizon at the top of all cores.	U1, U20, U26	Lag deposit Contourite
GDF	Dense, well consolidated dark grey clays with abundant IRD.	Dark grey, dark greenish grey 1.5 Y 4.40/1.40	Poorly sorted, significant coarse sand and IRD component or angular clasts.	Sharp erosive base, heavily bioturbated upper boundary oxidized to orange.	U12, U14, U16, U18, U22, U24, U28	Distal Glacigenic debris flows.
HPT	Well consolidated, discontinuous horizons of dark, sandy material often with IRD.	10.0 YR 4.60/1.30 or 0.3 Y 4.10/1.40	Coarse-medium grains of volcanic glass, occasionally with abundant IRD.	Non-erosive base, often not continuous across the core. Bioturbated to the top, upper surface often accompanied by a substantial increase in benthic and planktic foraminifera.	U5, U7	Visible Tephra horizons
MCD	Sharp base, normally graded, with minimal mud cap.	Orange-brown 9.4 YR 4.70/2.40	Normally graded, significant coarse sand component in all cores.	Varies between cores (7-25 cm thick) with coarsest component composed of 3-5 cm mud clasts grading to coarse sands Sharp base,	U9	Mud-clast debrite
MTD	Coarse sands to muds, normally graded and highly sorted	Medium green-grey 0.5 Y 4.20/1.10	Normally graded, well sorted sands to muds.	Sharp erosive base to both units. Units are substantial, exceeding 1m in all cores. Upper boundaries are oxidized mud caps with evident bioturbation and no microfossils.	U3, U10	Mega - Turbidite deposit

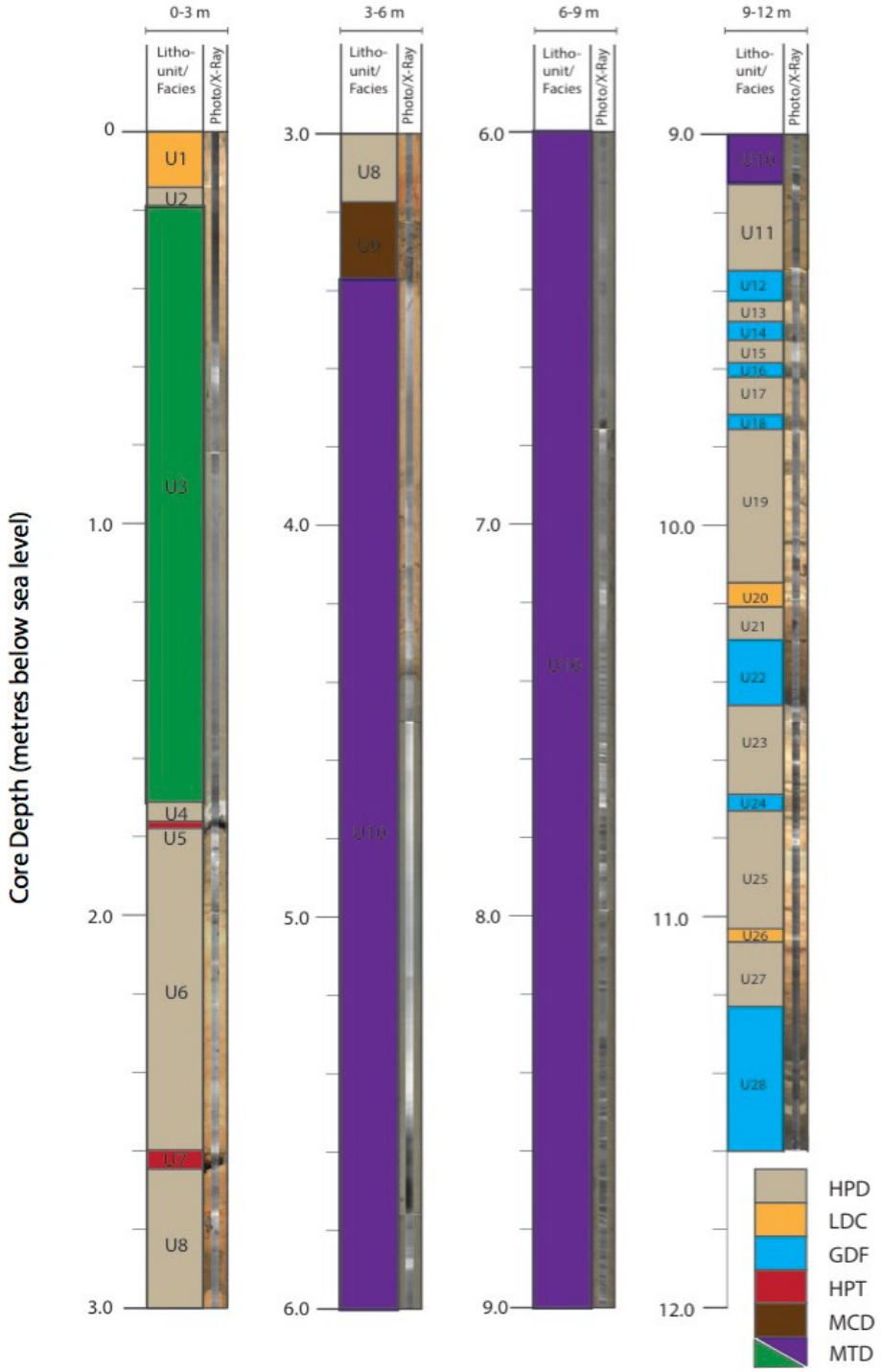

Figure 3.8: Photo and X-ray core log of PC88 showing lithofacies as detailed in Table 3.2. X-rays are from the central 2 cm of the core generated by the ITRAX. Facies abbreviations refer to section 3.5.2: HPD – Hemipelagic current sorted diamicton, LDC – Lag deposit contourite, GDF re-deposited matrix supported massive diamict, HPT – Visible tephra horizon (hemipelagic and tephra), MCD – mud clast debrite, MTD – mega turbidite deposit.

3.5.2.4 Visible tephra horizons facies (HPT)

Macro-tephra deposits are variable, and defined primarily as displaying a distinct colour change within the succesion and high content of fresh volcanic glass shards determined by microscopy. There are two examples within the core (Unit 5 and Unit 7), Unit 5 is a dark brown-black layer, present in all cores immediately below Unit 3. Unit 5 contains abundant

volcanic glass shards in addition to tachylite fragments and forams. The shards within the macrotephra horizons are variably elongate to blocky, vesicular and fluted, highly concentrated amongst background silts, and associated with high foraminiferal abundances above each visible tephra horizon, this is most evident in the increase in the presence of high numbers of *Cibicidoides wuellerstorfi* above each horizon, potentially a biological response to enhanced ash fall to the ocean surface. Unit 5 is stratigraphically below the Upper Ægir Turbidite, and is represented by a distinctive 4-cm thick black horizon with an undulating base. Unit 7 is over-consolidated, with an undulating base and composed entirely of brown glass shards. Each unit is clearly identifiable in the ITRAX data, with high values recorded for Mn, Fe and K. This is consistent with major element concentrations for volcanic glass, but may also reflect increased surface roughness of the core and a change in grain size. Unit 5 and Unit 7 each show an undulating base, considered to be conformable. Each unit is well consolidated in comparison to surrounding hemipelagite and clearly visibly in the X-ray images. The tephra appears to have undergone post-depositional alteration, resulting in early cementation of the grains and forams within the layer.

3.5.2.5 Mud clast debrite facies (MCD)

This facies is found in each core immediately above Unit 10, with the exception of core PC84 where 13-cm of hemipelagite separates Unit 10 and Unit 9 (Figure 3.7). The base of Unit 9 is undulating and therefore considered erosive. This facies is composed of mudclasts of assorted colours set in a sand rich matrix. Unit 9 fines upwards and varies from 7-to-25 cm thick. The matrix is orange-brown and supports the mud clasts. The clasts are up to 5 cm across, suggesting a proximal source. Unit 9 is interpreted as a small, locally sourced debrite, which has potentially eroded several cm from the hemipelagic record.

3.5.2.6 Mega-turbidite (MTD) facies

Each sediment core recovered two large olive-grey units (Unit 3 and Unit 10), with two cores fully penetrating both units (PC86 and PC88). Unit 3 varies from 6.5-to-1.2 m thick, and is thickest in PC82, Unit 10 is 4.6 m (PC86) and 4.8 m (PC88) thick where fully penetrated to the HPD facies below. Units 3 and 10 show a similar internal structure comprising an erosive base (Figure 3.9, E) above which there is a structureless, coarse sand with low mud content that grades into medium sands. Tephra is evident throughout both units with varying degrees of reworking.

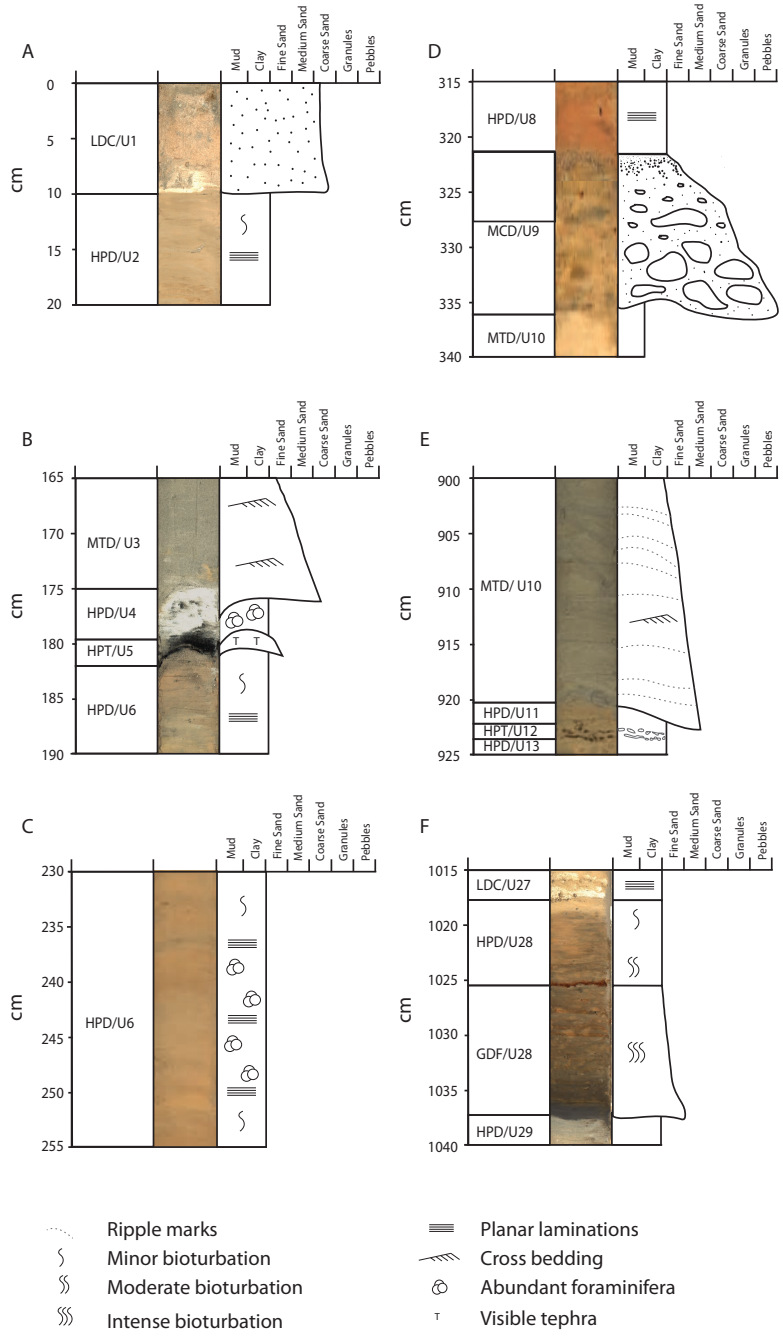

Figure 3.9: Examples of each lithofacies detailed in section 3.2 with high resolution photos and core log. A) Lag Deposit Contourite B) Visible Tephra Horizon (HPT) C) Hemipelagic Diamicton (HPD) D) Mud Clast Debrite (MCD) E) Mass Transport Deposit (MTD) F) Glacigenic Debris Flow (GDF).

Cross lamination is highlighted in both turbidites by subtle variations in colour and grain size and is clearly visible on the X-ray images (Figure 3.8). A consistent feature of this facies in each unit is a lack of foraminifera, which return at the top of the unit. These facies indicate rapid deposition under a waning current and are interpreted as mega-turbidite deposits (MTD) on the basis of their thickness, sedimentary structure, composition and homogeneity, with no evidence of multiple stages of flow (Bouma, 1987; Rebesco *et al.*, 2000; Minisini *et al.*, 2007). The units can be traced in the seismic reflection data throughout the Ægir Ridge and Norwegian Basin and both are substantially thicker than the encompassing stratified

units, conforming to the descriptive terms and criteria for megaturbidites in Bouma (1987). In both Units 3 and 10, in all sediment cores the cross-laminated sand grades to a laminated silt facies, overlain by a substantial mud cap. This mud cap is partially oxidised, as evidenced by a distinct colour change from olive-grey to orange brown demarked with occasional dark brown horizons.

3.6 Chronology

3.6.1 Radiocarbon

Chronological constraints for the uppermost stratigraphy are provided by 12 radiocarbon dates across three sediment cores (Figure 3.7, Table 3). All dates in PC84 and PC88 are in stratigraphic order. PC82 contains two dates above the Upper Ægir Turbidite, which are reversed. The deeper date (5,170 ± 30 14C yrs BP) is 300 years younger than the date 7 cm above (5,480 ± 30 14C yrs BP) which could indicate bioturbation or sample contamination. The upper-most date (Beta – 405940, 5,480 ± 30 14C yrs BP) is considered more reliable on the basis of the larger sample size (20.4 mg : 7.3 mg).

Table 3.3: Radiocarbon dates from all cores in the Ægir Ridge core suite from Beta Analytic and SUERC. Calibrated ages are expressed as a 1 sigma age range. Mixed sample types are mixed planktic species only. NPS refer to single species samples of Neogloboquadrina pachyderma sinistral.

Core	Lab Code	Total Depth	Type	Weight	Sample	^{14}C AGE (error)	From	To
PC88	Beta – 401319	1.98 - 1.99	Mixed	17.7	Beta - 7	17570 (60)	20480	20905
PC88	Beta – 401317	2.08 - 2.10	Mixed	21	Beta - 5	33500 (230)	36366	38117
PC88	Beta – 401318	2.64-2.66	Mixed	16	Beta - 6	40170 (480)	42712	44371
PC88	Beta – 401320	9.19 - 9.20	Mixed	11	Beta - 8	> 43500 BP	n/a	n/a
PC82	Beta – 405939	0.03-0.04	Mixed	20.4	Beta - 40	5480 (30)	5718	5927
PC82	Beta – 405940	0.11-0.12	Mixed	7.3	Beta - 41	5170 (30)	5418	5605
PC82	Beta – 405941	7.34 - 7.35	Mixed	11.1	Beta - 42	9510 (30)	10224	10472
PC82	SUERC-67168	8.52-8.53	NPS	10.2	ARB	48846 (2118)	45222	55629
PC84	SUERC-67169	6.21-6.22	NPS	10.5	ARF	22064 (87)	25736	26081
PC84	SUERC-67170	6.61-6.62	NPS	10.6	ARG	33128 (313)	35972	37872
PC84	SUERC-67174	7.29-7.30	NPS	6.1	ARI	> 43500 BP	n/a	n/a
PC84	SUERC-67175	7.51-7.52	NPS	10.9	ARJ	> 43500 BP	n/a	n/a

All dates were calibrated using OxCal and the Marine13 curve (Reimer, 2013) using the OxCal program (Ramsey, 2008). The considerable uncertainty surrounding the reservoir correction in this region has been well established (Haflidason *et al.*, 2000; Waelbroeck *et al.*, 2001; Thornalley *et al.*, 2011). Full data are reported in Table 3.3. The lowermost radiocarbon date in Core 88 (Figure 3.7) was above Unit 9 (Figure 3.8) and yielded a calibrated date of between 42,712 – 44,371 years Cal BP, in addition a date from Core 82 taken above Unit 9 yielded 45,222 – 55,629 years Cal BP which as the upper limit of the method. On this basis, Unit 9 is interpreted as lying just beyond the limits of the radiocarbon method (43,500 years Cal BP).

Palaeomagnetism

3.6.1.1 RPI (Relative Palaeointensity)

The relative palaeointensity (RPI) curve compares well to the regional NAPIS-75 stack (Laj *et al.*, 2000), and the longer records of the PISO-1500 stack (Channell *et al.,* 2009) and the SINT-200 stack (Guyodo and Valet, 1996). The curve generated is compared to these three palaeointensity stacks in Figure 3.10. With additional constraints for the upper section of the core provided by the calibrated radiocarbon dates, the correlation of periods of low intensity is possible. The low intensity periods in the core between 110-140 cm correlate to the low intensities observed in all stacked records surrounding the Laschamp Excursion, falling between 37 and 42 ka BP. The low between 210 cm and 250 cm lies just below the lower turbidite and correlates to the lowermost period of low intensity in the NAPIS stack (58 – 65 ka BP). Between 290 and 325 cm the correlation is less obvious, but interpreted as lying beyond the limit of the NAPIS stack (75 ka BP). The lower resolution SINT-2000 record and PISO-1500 show a period of flat intensities that are tentatively correlated to those in the Ægir Ridge record. The lowermost section of core displays very low intensities, with the exception of an anomalous spike at 369 cm. This low intensity period starts at 352 cm and continues to the base of the record. This agrees well with the 98 – 124 ka BP section of both the SINT and PISO records. Beyond 124 ka BP, both SINT and PISO records show a marked increase in the strength of the RPI. However, this age does not seem to be reached in the Ægir Ridge record, which terminates c. 120 ka BP.

3.6.1.2 Palaeomagnetic excursions

Within the palaeomagnetic inclination record, several significant excursions from the average inclination of PC88 are observed. The average angle of inclination for a consistent section of hemipelagite was calculated as 83 ° (225-290 cm hemipelagic depth). The modern inclination estimate for the latitude of PC88 is 75° (taken from magnetic model WMM2015). Any deviation from the calculated average of 83° is examined here in combination with

palaeointensity and stratigraphic information to determine of the deviation can be accepted as a palaeomagnetic excursion and used in the final age model. Due to some uncertainty over core rotation when splitting, the deviations in inclination are expressed as an average over the core depths where the excursion exceeds 20° difference from the average (83°) in comparison to an average of 10cm either side of the event, thus eliminating issues of core sections having rotated, and the effect of section breaks. All potential excursions discussed are labelled on Figure 3.10.

The Mono Lake (25.5-27 ka BP) excursion is not considered present (Nowaczyk and Knies, 2000; Laj *et al.,* 2014a), as here is no period of low intensity between 70 and 90 cm hemipelagic depth (Figure 3.10), which covers the potential location of a c. 26 ka BP excursion based on radiocarbon dates (Table 2). The Zijderveld plot does not show any significant deviation in inclination across this depth (Figure 3.11). The most significant inclination excursion relating to this event lies at 81 cm hemipelagic depth (Figure 3.10), yet the inclination reaches a low of 67.77° compared to an average of the 10 cm either side of the "event" of 80.18°. This lies within 1 standard deviation of the average inclination for the hemipelagic record (average: 65.89° ± 24.49° [1 SD]). This, together with a lack of directional change in the Zijderveld plot (Figure 3.11), suggests this excursion is not well recorded at this site.

A broad low period in the RPI record between 110 – 140 cm hemipelagic depth is coincident with a deviation in the inclination record over a 20 cm average of 69.4° to a maximum low of 34.7° at 125 cm. This correlates to the low period surrounding the Laschamp Event (as detailed in the NAPIS record (Laj *et al.,* 2000). There is a distinct tephra layer present within all cores as a well-consolidated dark brown horizon with an uneven base (Unit 7, section 3.5.2.6). This tephra correlates to the Faroe Marine Ash Zone 4 tephra, dated to 46,800 ± 1,000 BP (Wastegård *et al*. 2006; Wastegård & Rasmussen 2016 [section 3.6.4]), and is located 4 cm below the identified excursion. The low values of RPI and the reduction of recorded inclination is strong evidence of an excursion, supported by the Zijderveld plot (Figure 3.11) which shows a clear change in direction from the background samples. When considered with the chronostratigraphical evidence from the tephra deposit, this excursion is considered to be the Laschamp event.

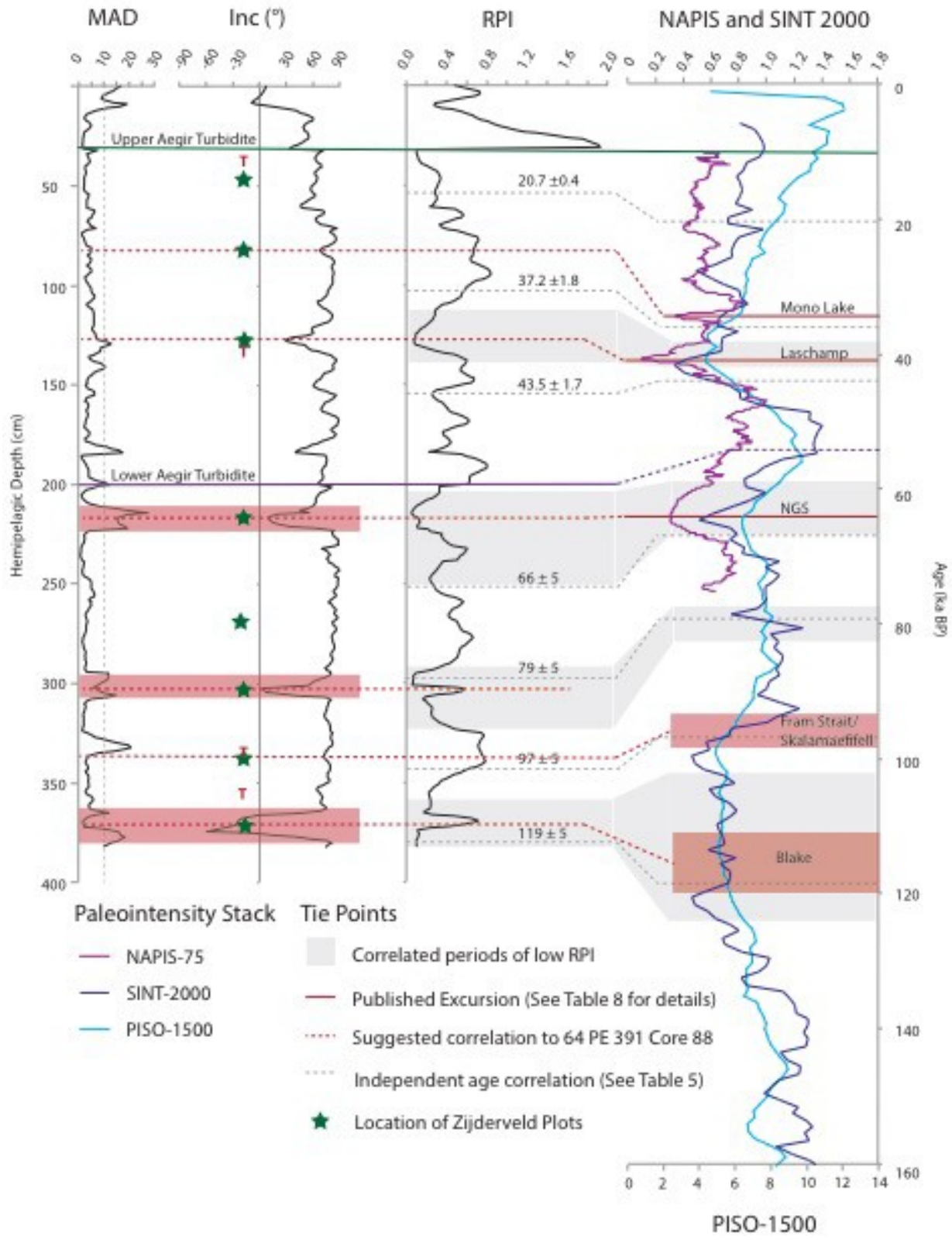

Figure 3.10: : Summary figure of palaeomagnetism of core 88 in comparison to reference data sets. Maximum Angle of Declination, Inclination and calculated Relative Palaeointensity (RPI) of hemipelagic sequence of core 88. Composite plot of stacked palaeointensity records SINT – 2000 (Valet et al. (2005)), PISO-1500 (Channel et al. (2009)) and NAPIS-75 (Laj et al. (2000)). Only the depth of the Blake geomagnetic excursion was used in the final age model. Brown bars indicate the range of uncertainty in dated records and broader inclination excursions identified within the core.

The Ægir Ridge record shows a marked reduction in RPI between 210-250 cm, in addition to a sharp change in inclination at 216 – 221 cm depth. The average inclination over this period is 18° in comparison to a local average of 70.97°. The Zijderveld plot shows a substantial change from background directions. This potential excursion occurs 8 cm below a significant and widely dispersed tephra horizon (geochemistry below). This feature in PC88 is potentially the Norwegian Greenland Sea excursion, but the reported dates for this excursion are uncertain, with a wide range of reported dates within Arctic sediments from 55-76 ka BP (Lekens *et al.*, 2009). Additionally, the excursion was used in Lekens (2009) to date core MD-2283, with a date of 73 ka BP applied based on Nowaczyk (1994) and a study of cores from the Yermack Plateau. Thouveny *et al.* (2004) correlates the excursion to an anomalous declination swing at 74 ka BP. Although all indicators suggest this is an excursion, it is not recognised here due to the absence of a narrow constraint on dating. The potential date for this excursion it is not suitable for inclusion in the age model due to the highlighted uncertainties, however It does indicate the deposition of the Lower Ægir Turbidite occurred after 55 ka BP, which is the youngest date applied to the excursion in published records.

At 302 cm, another significant excursion in inclination occurs, and may relate to the Fram Strait/Skalamaefifell excursion would fall within the declining intensities in the SINT and PISO records of RPI between 91-96 ka BP. This excursion cannot be confirmed as the maximum change in inclination is coincident with a section break in the core. There is a small change in inclination at 334 cm from an average of 79.1° to a peak low of 72°. This is also coincident with a clear tephra horizon and interpreted as the effects of a high concentration of large tephra grains.

The base of the core records both a marked RPI low and a period of high negative values between 366-376 cm. This is clearly recorded in the Zijderveld plots (Figure 3.11), and a minimum inclination of -59.67°. This potentially correlates to the Blake Event, which is variably dated from records across Europe and has an unusually long average duration of 5 kyr. The Blake Event has been well dated within a speleothem record from Northern Spain and yielded a date of 116.5 ± 0.7 kyr to 112.0 ± 1.9 kyr (Osete *et al.*, 2012). Marine records have indicated an age from Mediterranean cores of 115-120 kyr (Tric *et al.*, 1991; Thouveny *et al.*, 2004). The Thouveny *et al.* (2004) record indicates the Blake Event is characterised by two high amplitude swings in declination, lasting from 115.0 -122 ka BP, consistent with observations from PC88 (Figure 3.10). This event can be confirmed through the combined use of coccolith biostratigraphy and the positive identification of the lower boundary of sub-zone NG-3c (section 3.6.3). This bio- stratigraphic horizon marks the start of a barren period that persists until 280 ka BP. The end date of the excursion is widely reported as 115 ka BP (Thouveny *et al.*, 2004; Osete *et al.*, 2012), which is applied to the point in the hemipelagic

record at which the excursion returns to normal inclination values at 366 cm. For the purposes of the age model, this event is given an error of 5 ka to encompass the young age suggested from the speleothem record of Osete *et al.*, (2012).

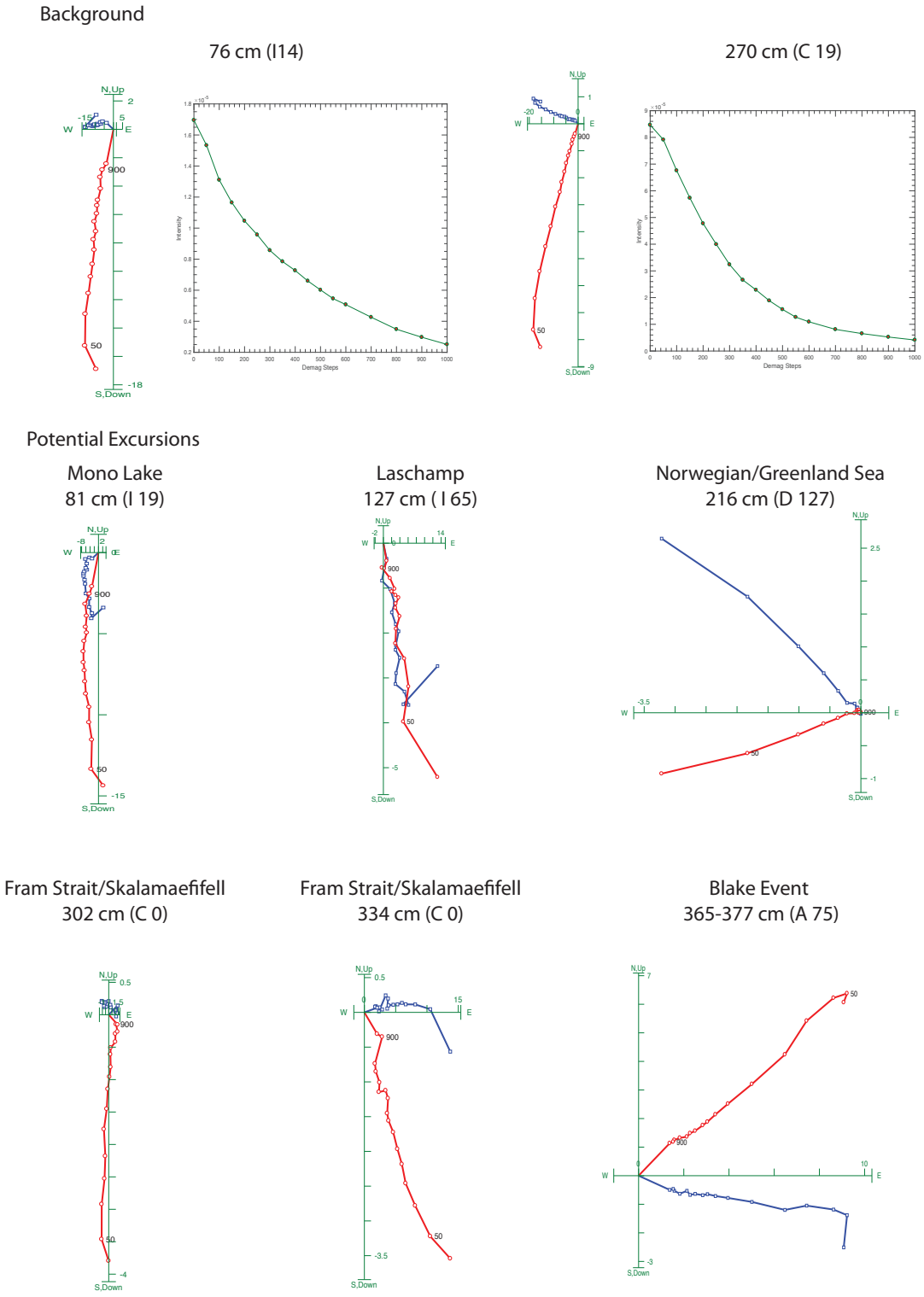

Figure 3.11: Zijderveld plots of potential excursions identified in the hemipelagic record of core 88. Only the Blake Excursion was accepted on the basis of stratigraphical agreement with the coccolith NG-3c horizon and a period of sustained low geomagnetic intensity.

3.6.2 Coccolith Biostratigraphy

This chronology of the stratigraphic record can be independently calibrated using the coccolith biostratigraphy for the North Atlantic. The coccolith biostratigraphy from PC88 was compared to the expected North Atlantic record of Gard (1988) detailed in Table 3.4 below, and compiled by J. Hunt. Coccolith biostratigraphic datum horizons have been established using the oxygen isotope based SPECMAP timescale of Imbrie *et al*. (1984). This method was successfully used in Pope *et al.* (2016) to date marine sediments from the Bear Island Fan. The coccolith biozones N-G 1 to N-G 3 were clearly identified in the hemipelagic record (Figure 3.12). The three subzones of coccolith sub-zone N-G 3 were all identified, allowing further refinement of the lower section of the record. Within the *OxCal* age model, coccolith horizons are given an estimated error of 5 ka due to the low resolution dating detailed in the SPECMAP timescale (Imbrie *et al.,* 1984; Hunt *et al.*, 2013; Pope *et al.*, 2016).

Table 3.4: Definitions of coccolith biozones and ages assigned after Gard (1988) and Backman et al. (2009), depth in core refers to hemipelagic depth (cm) and refers to the start of the listed zone. Data collected by J. Hunt.

ZONE	DEFINITION	MARINE ISOTOPE STAGE	AGE (KA BP)	DEPTH IN CORE (CM)
N-G 1	Recent to point of dramatic decrease in *C. pelagicus* total abundance	Recent to mid/lower 1	0-8	N/A
N-G 2	Predominantly barren zone, defined as the interval from where *C. pelagicus* decreases dramatically in total abundance to where *G.muellerae* increases dramatically	Mid/lower 1 to mid 4	8-66	251
N-G 3	*Gephyrocapsa mullerae* dominates over *Emilianiahuxleyi*. The interval is defined from where *G.mullerae* dramatically increases in totalabundance and dominates over *E. huxleyi* down to where all nannofossils disappear from the sediment. The presence of *E. huxleyi* distinguishes this zone from N-G 7 (372- 423 ka BP)	Mid 4 to lowermost 5	66-119	Sub divided below
N-G 3A	Abundance peak of *C. pelagicus*. Lower boundary defined by decrease in abundance of *C. pelagicus* and total amount of nannofossils.	Mid 4-5a	66-79	289
N-G 3B	Low amount of nannofossils. *C. pelagicus* and total nannofossils decrease to lower boundary then increase in relative *C. leptoporus* and total nannofossil abundance.	5b to 5d	79-97	338
N-G 3C	Abundance peak of *C. leptoporus*. Upper boundary from where *C. leptoporus* increases in total abundance and also total abundance of nannofossils increases. Lower boundary as for zone 3.	Upper part of 5e	97 - 119	372

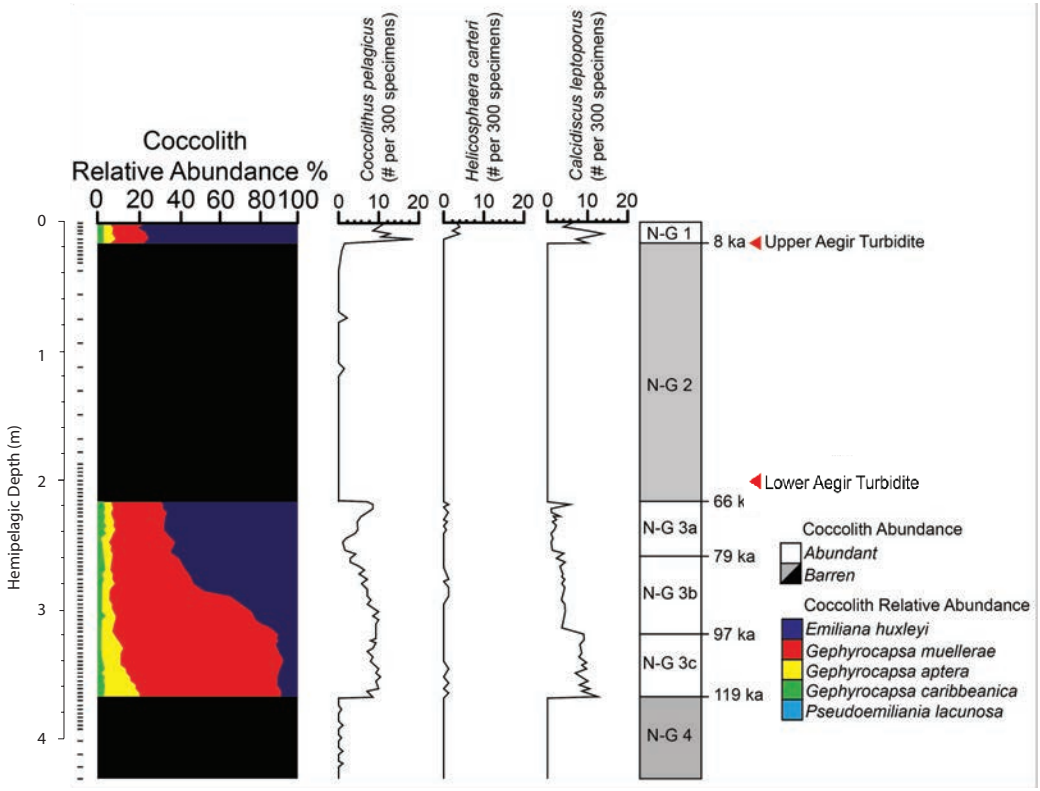

Figure 3.12: Summary figure of coccolith biostratigraphy from core 88. Figure shows the relative abundance of coccolith species down core, and the identified biostratigraphic horizons as identified in Table 3.4. Dashed lines indicate sampling positions. Data collected and figure produced by J. Hunt.

3.6.3 Tephrochronology

Six distinct tephra peaks were identified in addition to a high concentration of tephra shards within the Lower Ægir Turbidite, a total of seven tephra horizons are discussed (Figure 3.13). Tephra horizons are identified by the hemipelagic depth of the peak shard concentration in cm, with the tephra from within the Lower Ægir Turbidite given the depth of the turbidite base: 201 cm (Figure 3.12 and Table 5). The two visible tephra horizons are described in section 3.5.2.6 (Unit 5/34 cm and Unit 7/129 cm). Of the seven horizons, two were basaltic, four rhyolitic and turbidite tephra showed a mixed composition. Shard concentrations were high in all deposits and summarised in Table 3.5.

Major element geochemistry of tephra grains from Icelandic volcanoes is well defined (Óladóttir *et al.*, 2011; Óladóttir *et al.*, 2008; Davies *et al.*, 2010). Using these established compositional fields, it is possible to identify the volcanic system, specific eruption dates are assigned with consideration of other stratigraphical data. Full tephra analytical data are reported in the digital Appendix 1a.

Both turbidites contain a high proportion of fresh glass shards were present within the >150 µm fraction; retaining fine fluted shard morphology. Reworked tephra are not commonly used in dating, yet the stratigraphical information is potentially highly significant to this

study, and the analyses from within the Lower Ægir Turbidite are assessed. The inclusion of fresh, minimally reworked shards suggests that primary air-fall tephra from concurrent or closely timed eruptions were entrained within the turbidity current.

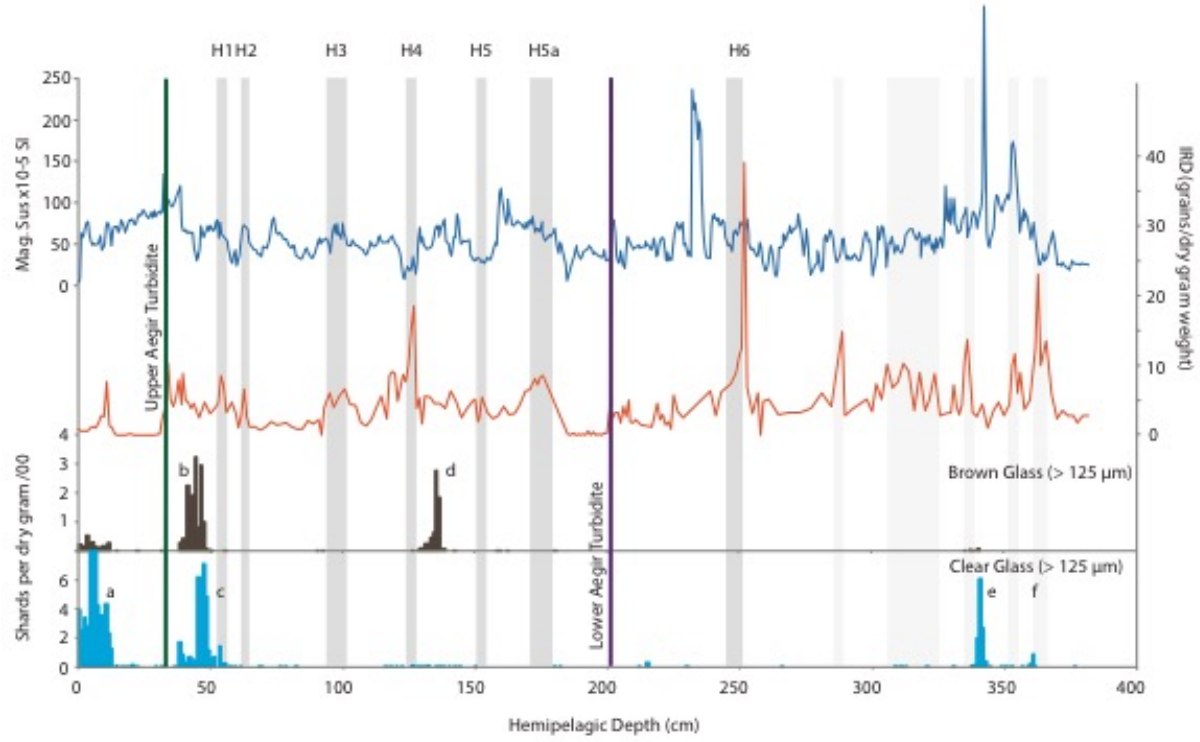

Figure 3.13: Down core profile of Ice Rafted Debris (IRD shown in orange), magnetic susceptibility (blue), and glass shards (clear and brown).Positions of the Upper and Lower Ægir turbidites are shown Horizon labels: (a) 19 cm tephra, (b)34 cm tephra, (c) 40 cm tephra, (d) 129 cm tephra, (e) 334 cm tephra, (f) 354 cm tephra. Horizon b correlates to unit 5, and horizon d to unit 7, both visible tephra horizons between the Ægir turbidites (section 3.5.2.6). Dark grey bars indicate interpreted position of Heinrich Events 1-6. Pale grey bars in lower section of core indicate probable older Heinrich Events which are not used in the stratigraphy.

In total, 160 single-glass shard analyses were performed by electron microprobe (including 31 from the Lower Ægir Turbidite). The number of shards analysed per horizon ranged from 6 to 31 depending on the variable shard concentrations of each horizon. The shards analysed showed some evidence of post-emplacement hydration, most noticeably in the tephra from the Lower Ægir Turbidite; these results are discussed separately. Of the remaining 129 analyses, 43 fell below the 97% total weight oxides (wt%) analytical total threshold, of which 28 were from the two older tephra horizons (334 and 354 cm). This is consistent with a greater degree of hydration in older tephra. For comparison to existing datasets, all data were normalised to a 100% anhydrous basis before plotting, assuming that the hydration represents a dilution of the original signal and not modification of the original geochemical composition (Jennings *et al.*, 2014). Tephra data are summarised in Table 5, full raw data are reported in the appendix.

Tephra were first characterised through assessing the SiO_2 content versus the total alkali (Na_2O + K_2O wt. %) and compared to a standard total alkali-silica (TAS) plot for volcanic glasses (Figure 3.13; Le Maitre *et al.*, 1989). Four of the tephra horizons had a rhyolitic composition according to the Le Maitre *et al.*, (1989) classification (Figure 3.14 (a)). Three of these demonstrate a mild alkali-low-alkali composition typical of calc-alkaline off-rift volcanism (82/137) from the Western Divergent Zone (WDZ), Eastern Divergent Zone (EDZ) and Southern Transgressive Zone (STZ). These grains fall into the transitional alkali description of Jakobsson (2008), shown in Figure 3.14 (b). The remaining rhyolitic grains were typical of tholeiitic silicic volcanism in Iceland sourced from the central volcanic zones (the Western Rift Zone (WRZ), Eastern Rift Zone (ERZ) and Mid-Icelandic Belt (MIL), see Figure 2.2, Chapter 2). Two basaltic populations were analysed, both falling within the tholeiitic Icelandic composition (Le Maitre *et al.*, 1989). These basaltic tholeiitic series are characterised by a high Fe and Ti, and low Al and Ca (Óladóttir *et al.*, 2011).

3.6.3.1 Tephra Horizons

19 cm Horizon (6, 10 and 19 cm samples grouped together, Unit 1)

Unit 1 is a complex deposit of coarse tephra shards and foraminifera, the tephra concentration was broadly divided to three horizons (6, 10 and 19 cm), but is coalesced here to one horizon on the basis of geochemical similarity. This tephra is referred to as the 19cm tephra due to the highest concentation of shards within the 19 cm horizon. These tephra were recovered from within the winnowed lag deposit in Unit 1 (Figure 3.8). The shard concentration profile formed a broad peak with distinct elevations in tephra shard counts at 6, 10 and 19 cm hemipelagite depths (Figure 3.13). There are two geochemical populations within this grouped deposit (observed in each of the 6, 10 and 19 cm depths), described here as populations 1 and 2. This tephra horizon overlies the Upper Ægir turbidite, and shard concentrations are consistently above 3000 shards per gram (Figure 3.13). This tephra exhibited the highest concentration of shards throughout the sequence, with a maximum of 27,265 shards per gram (Table 3.5). As existing age control on the core limits the age to < 8,200 years Cal BP, these compositions were compared to all known Holocene tephra from Iceland (Figure 3.17). Shards are fluted or have bubble wall morphologies with a significant proportion of large shards (>250 μm). The potassium enrichment for population 1 indicates a rift source, population 2 is consistent with off-rift volcanism (Figure 3.16). The key difference between the two populations were that population 1 has a higher TiO_2 content (0.85 ± 0.104 % to 0.27 ± 0.009 %), a lower Na_2O (3.91± 0.19% to 5.44 ± 0.23%) and a higher CaO (2.72 ± 0.48 % to 1.36 ± 0.07%). The range of compositions for population 1 falls within the observed values of the Askja 1875 compositions of Pilcher (2005), Oldfield *et al.*, (2005) and Larsen *et*

al., (1999), as shown in Figure 3.17. The published date of the Askja 1875 eruption is included in the age model. Population 2 composition is remarkably similar to both the 12,100 years BP Vedde tephra and the 8,050 years Cal BP Suderoy tephra (Pilcher *et al.*, 2005, Figure 3.17). It is not possible to discriminate between these two eruptions on the basis of major element geochemistry alone. However, other stratigraphic information from the core supports a Suderoy as the probable source (Table 3.6), as this tephra is stratigraphically above the Upper Ægir turbidite. Thus, the tephra could represent the Suderoy eruption, but given the broad nature of this tephra profile, and the likely winnowed nature of the deposit, it is not included within the age model.

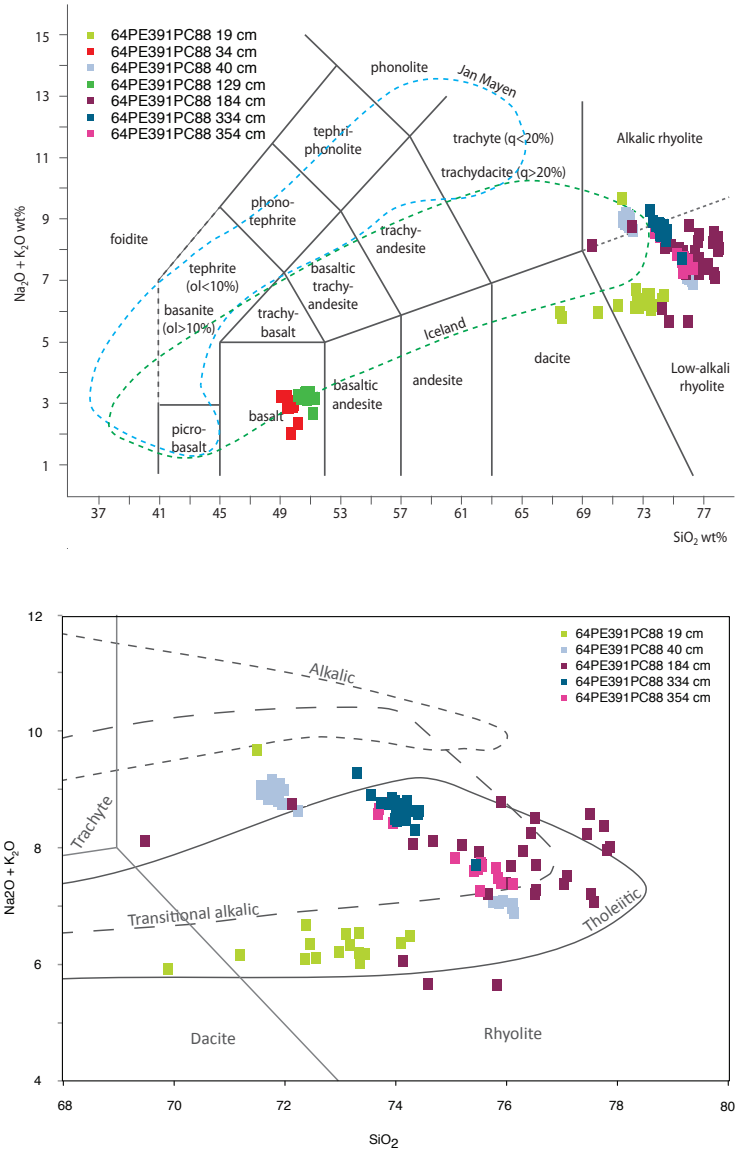

Figure 3.14: Total Alkali Silica (TAS) plot after Le Maître et al.1989 showing complete range of tephra analysed from core 88. Jan Mayen and Icelandic composition fields are taken from Gjerløw et al., 2016. (b) Icelandic series classification of tephra horizons from core 88 showing the rhyolite/dacite/trachyte fields defined by Le Maître et al. (1989), Icelandic series fields are defined in Jakobsson et al. (2008).

Table 3.5: Summary of tephra horizon characteristics and dates assigned based on geochemical comparison to existing datasets. N= number of shards analysed

Horizon	Sub-Pop.	No.	Shards/ dgw	Potassium Enrichment (Rift/Off-Rift: modal av.)	Volcanic System	Eruption/ Date
19 cm	1	44	27,265	0.032-0.034 Rift	Askja	1875
19 cm	2	8	27,265	0.048-0.05 Off rift	Katla	Suderoy/ 8.05 ka BP
34 cm	N/A	9	879	N/A	Grímsvötn	Saksunarvatn/ 10.3 ka BP
40 cm	1	13	7,108	0.05-0.052 Off Rift	Katla	Vedde/12.1 ± 0.4 ka BP
40 cm	2	6	7,108	0.034-0.036 Rift	Askja	Askja/11.5 ka BP
129 cm	1	12	2,778	N/A	Grímsvötn	FMAZ4/46.8 ka BP
129 cm	2	1	2,778	N/A	Grímsvötn	Unknown
201 cm	N/A	31	N/A	Mixed	N/A	None
334 cm	1	13	6,073	0.038-0.040 Rift	Hekla, Torfajökull or Öræfajökull	95.4 ka BP (?)
334 cm	2	3	6,073		Eyjafjallajökul or Katla	Unknown
354 cm	N/A	18	879	0.05-0.052 Off Rift	None	116.4 ka BP(?)

34 cm (Visible tephra horizon, Unit 5, Figure 3.8)

This horizon forms a distinctive 4-8 cm thick black bed, immediately below the Storegga Turbidite (Unit 5, Figure 3.8 and Figure 3.13). Shards are dark brown and vesicular, a radiocarbon date has been obtained from within the horizon in core PC82 of 10,298 ± 108 years Cal BP (Figure 3.7). The tephra are identified as being sourced the Grímsvötn volcanic system (Óladóttir *et al.*, (2008); Óladóttir *et al.*, (2011) Figure 3.15). Compositions of all known basaltic tephra within the range 0-12,500 years Cal BP were compared to the deposit. Given this excellent age control from the AMS radiocarbon date, the horizon was expected to correlate well to the Saksunarvatn ash dated to 10,297 ± 89 Cal BP (Andrews *et al.*, 2002; Rasmussen *et al.*, 2006; Thornalley *et al.*, 2011; Gudmundsdóttir *et al.*, 2016). Work on the North Icelandic Shelf has observed the Saksunarvatn tephra as a similar 4 cm thick visible horizon (Gudmundsdóttir *et* al., 2016). However, the composition of the tephra does not overlap with the main body of the Saksunarvatn tephra detailed in Figure 3.18, but shares more similarity with the Saksunarvatn composition analyses presented in Lind *et al*. (2013) and an unknown Grímsvötn eruption from the same sediment core modelled to c. 10,000 years Cal BP. Recent work suggests the Saksunarvatn tephra is not a single phase eruption, but a series of closely spaced Grímsvötn eruptions; therefore this tephra may represent a component of a broader more complicated Saksunarvatn eruption (Johannsdottir, 2007;

Jennings *et al.*, 2014; Thordarson, 2014). On the basis of the radiocarbon date and indicated compositional link to the Saksunarvatn tephra, this horizon is suggested to correlate to the Saksunarvatn eruption dated to 10,249 ± 50 years BP and included within the age model. Further work would improve the quality of this match.

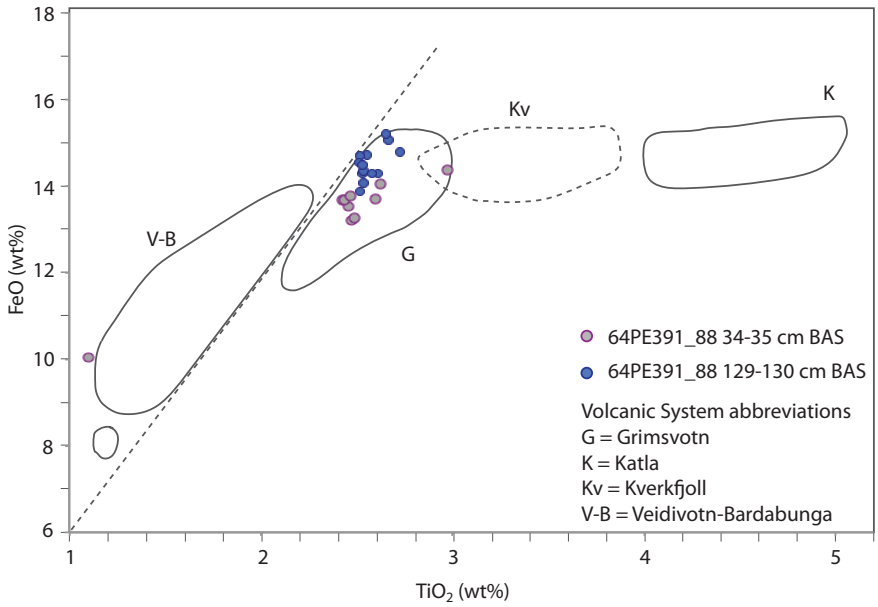

Figure 3.15: Assignment of volcanic system for basaltic tephra grains. Boundaries for volcanic systems are based on Öladottir et al.(2008) for Katla, and Öladottir et al. (2011) for Kverkfjöll, Grímsvötn and Veiðivötn-Bárðarbunga. Figure adapted from Voelker and Haflidason (2015).

40 cm

This tephra spans a zone from 42 to 38 cm depth, terminating at the base of the Storegga turbidite. Samples were selected from a 1 cm wide peak in rhyolitic shard concentration (7108 shards/gram) at 40 cm. Volcanic glass shards have a fluted and platy morphology with occasional large bubble shards. There is no clear correlation to an increase in IRD and the horizons are stratigraphically located above a radiocarbon date of 20,700 ± 400 Cal BP. All compositions of previously identified rhyolitic tephra from 10 ka BP to 20 ka BP were compared to this sample. The potassium enrichment shows a clear bimodal population (Figure 3.16), with 13 shards forming a homogenous cluster (population 1, 40 cm samples, Figure 3.16) consistent with off-rift volcanism and strong affinity to the Katla volcanic system and the Vedde Ash deposit dated to 12,100 years Cal BP. Population 2 is clearly distinguished from population 1 by the higher Al_2O_3 content (13.11 ± 0.23 % to 11.82 ± 0.11 %, Figure 3.15), and the lower SiO_2 (70.6 ± 1.03 to 73.77 ± 0.87 %), and the significantly higher total alkali value of 8.78 ± 0.27 % to 6.81 ± 0.15 %. The lower potassium enrichment of population 2 is characteristic of a rift Icelandic system and is related here to the widespread Askja 10 ka Cal BP tephra (Figure 3.17: Davies *et al.*, 2003; Pilcher *et al.*, 2005). This bimodal pattern of population within 40 cm tephra has been observed in other locations where the Askja and

Vedde tephra are present. A potential terrestrial equivalent tephra was found as a bi-modal deposit on the Lofoten Islands (Pilcher *et al.*, 2005) in association with the 12.1 ka BP Vedde tephra. The depth and date of the Vedde tephra are included in the age model.

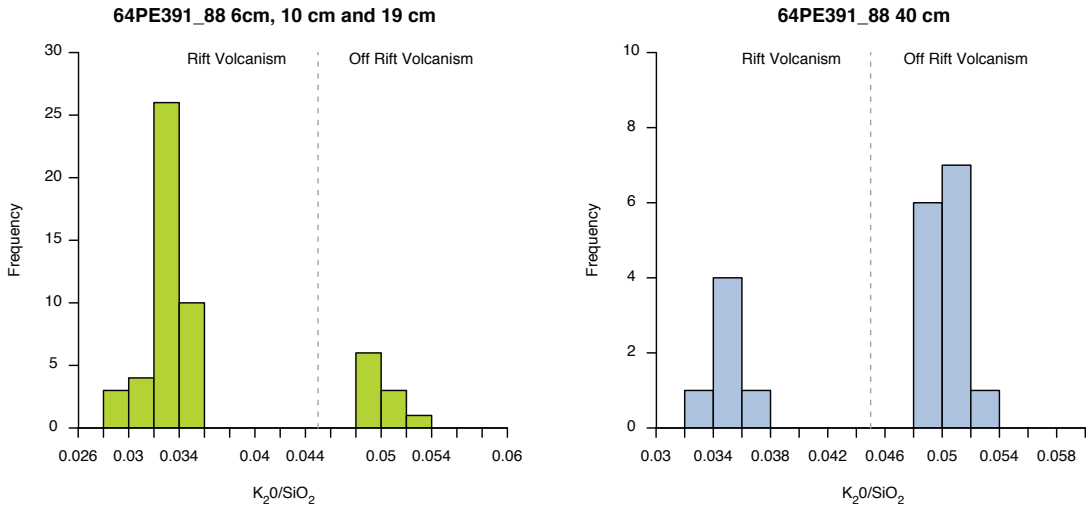

Figure 3.16: Potassium enrichment frequency histogram for rhyolitic tephra horizons at 6, 10 and 19 cm (left) and 40 cm (right).

129 cm

This tephra forms an unusual horizon in all cores from the Ægir Ridge. The horizon is over-consolidated, and difficult to wash due to "overgrowths" of glass-rich material around the forams, but forms a distinct peak in the shard concentration record (Figure 3.13). The glass shard counts were impaired by this effect, but the horizon forms a 2-6 cm thick dark brown undulating layer within each core. The 129 cm horizon has a geochemical composition with a strong affinity to the Grímsvötn volcanic system (Figure 3.15). There two geochemical populations with the 129 cm tephra (Figure 3.18 (d)), whereby Population 1 shows higher SiO_2 (50.26 ± 0.44 to 49.75 ± 0.41 %) and lower Al_2O_3 (13.1 ± 0.16 to 12.83 ± 0.096 %) than Population 2, which is characterised as lower Na_2O (2.2 to 2.77 ± 0.09), this may be an anomalous result as no other elemental concentrations show a significant difference. The horizon has a radiocarbon date of 44,300 – 42,705 years Cal BP below the tephra in core 88, and a date in core 82 of 48,846 ± 2,118 ^{14}C years BP (53,680 – 43,273 Cal BP). The identification of the Laschamp Event above this horizon (Section 3.6.2.2) and the radiocarbon dates suggest the tephra is too old to be the Faroe Marine Ash Zone 3 (FMAZ3) tephra. Indeed, it is a poor geochemical match to FMAZ3, whilst both populations are an excellent geochemical match to FMAZ4, dated to 46,800 ± 1,000 years BP (Voelker and Haflidason, 2015; Wastegård and Rasmussen, 2016). This age marker is used in the final age model.

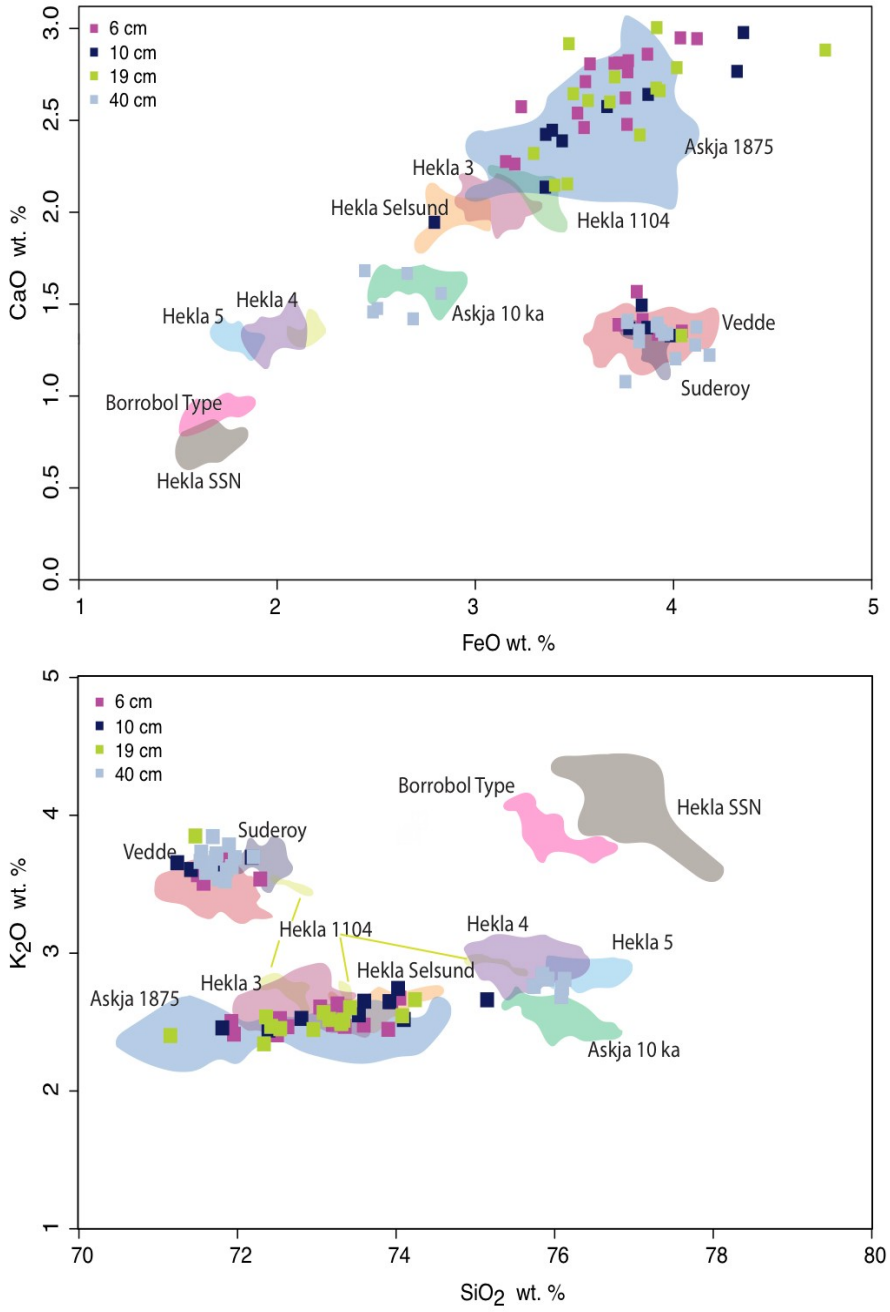

Figure 3.17: : Overlay of younger (< 43.5 ka BP) tephra over known and dated regional tephra deposits: Hekla 1104 (Gudmundsdottir et al. (2011), Hekla 3 (Gudmundsdottir et al. (2011), Boygle et al. (1994), Zillen et al. (2001), Lawson et al. (2007)), Hekla 4 (Wastegard et al. (2001), Zillen et al. (2001), Pilcher et al. (2005), Swindles et al. (2006), Gudmundsdottir et al. (2011)), Hekla 5 (Pilcher et al. (2005), Gudmundsdottir et al. (2011)), Hekla-Selsund (Wastegard et al. (2001), Dugmore et al. (1992 and 1997), Zillen et al. (2001)), Suderoy (Pilcher et al. (2005), Askja 10 ka (Gudmundsdottir et al. (2011), Pilcher et al. (2005)), Hekla SSn (Boygle et al. (1994) and Pilcher et al. (2005)), Vedde (Lane et al. (2012) and Gudmundsdottir (2011)), Borrobol Type (Gudmundsdottir et al. (2011).

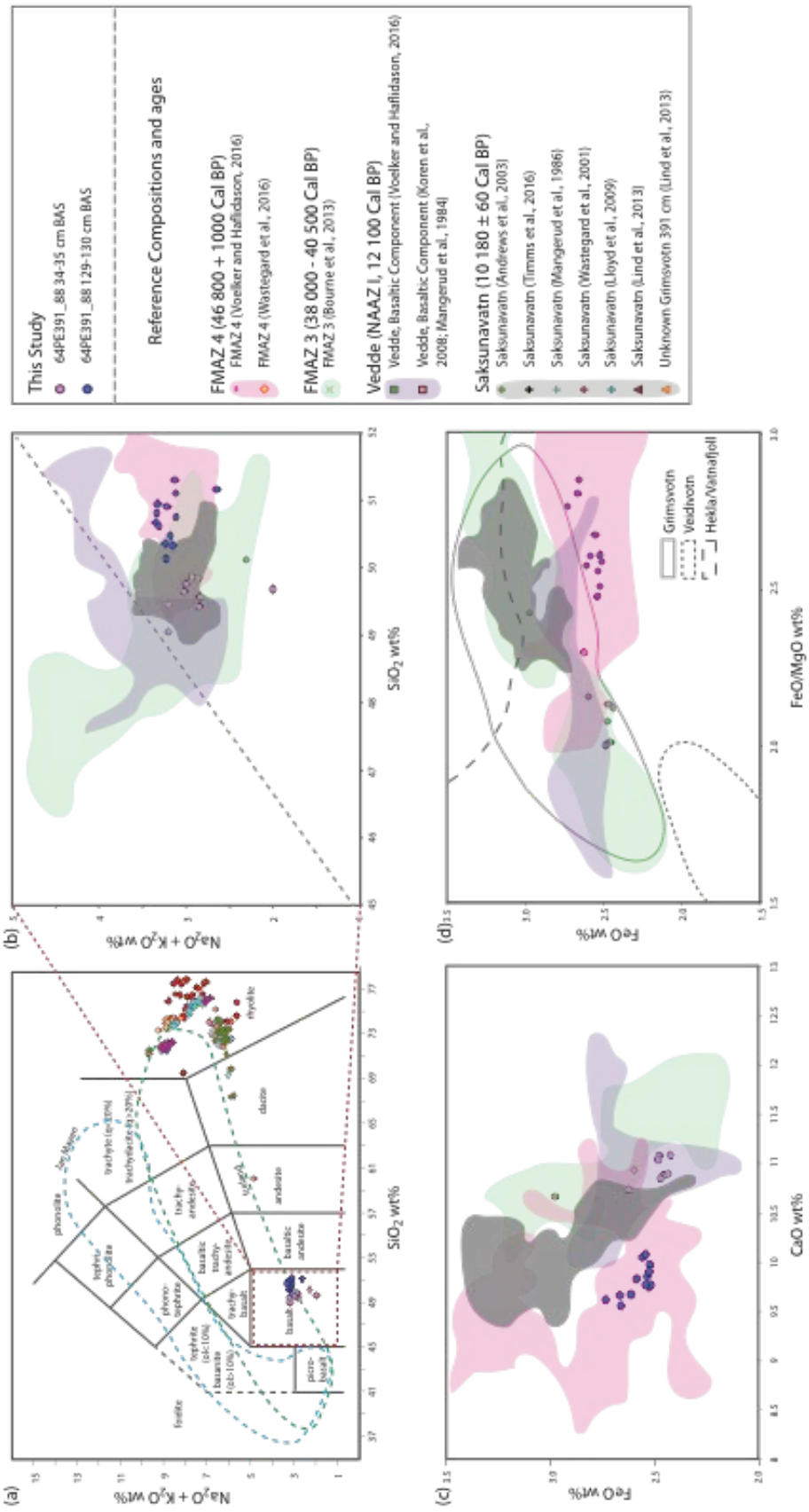

Figure 3.18: Analysis of basaltic tephra shards from core 88. (a) TAS plot for all tephra, enlarged section shows the basaltic horizons (34 and 129 cm) in comparison to regional records from NGRIP and marine sediment archives. The FMAZ 3 data is taken from Bourne et al. (2013). C and D show major element comparisons for Saksunarvatn and FMAZ 3 and 4.

201 cm

This tephra was picked from within the Lower Ægir Turbidite, with only rhyolitic samples were analysed. Tephra showed few signs of reworking, with glass shards appearing as fresh with a bubble wall or platy morphology. The tephra showed a highly heterogeneous population, illustrated by the potassium enrichment (Figure 3.20) and a large spread in the major element results. The tephra split broadly into four groups (A-D) and were compared to all previously analysed records of the North Atlantic Ash Zone 2 (NAAZ2) tephra, on the basis of the alternate dating methods used on PC88 (Figure 3.19).

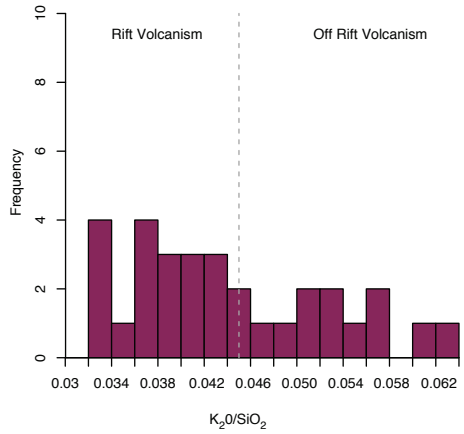

Figure 3.19: Potassium enrichment of the 184 cm tephra showing variable sources for the tephra within the turbidite.

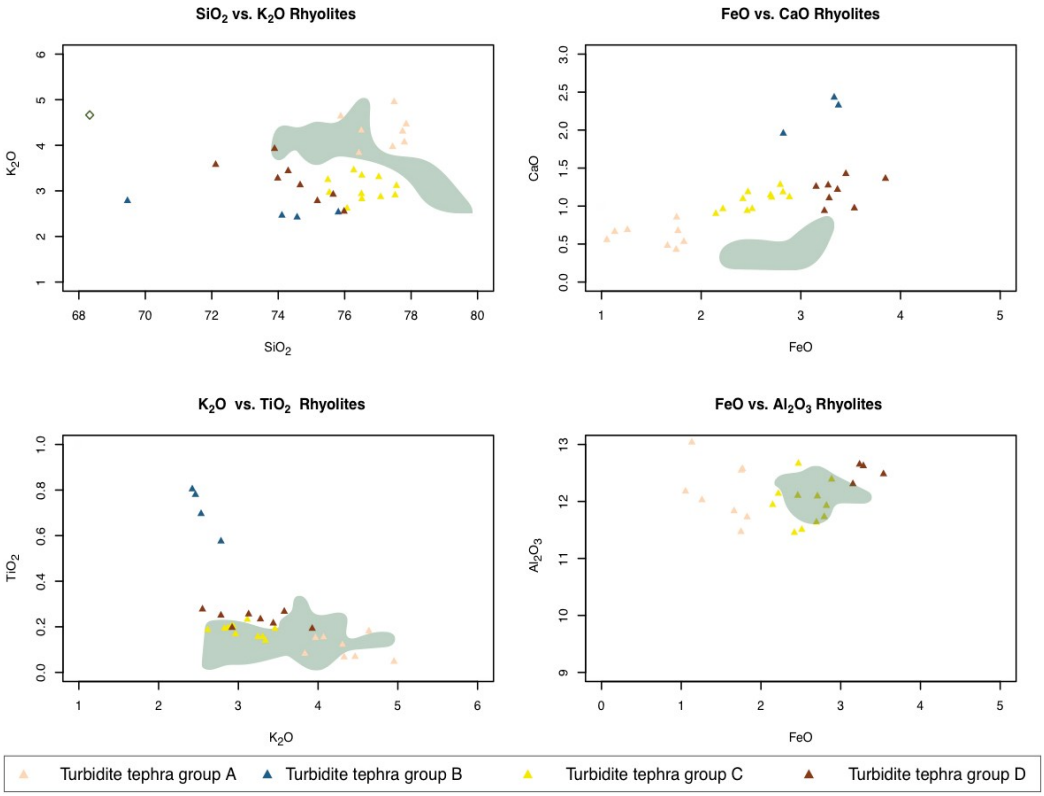

Figure 3.20: Comparison of regional NAAZ2 (55 ka BP) tephra to turbidite tephra. NAAZ 2 compositions are taken from Gronvald et al. (1995), Lacasse et al. (2001), Voelker and Haflidason (2015) and Wastegard et al. (2006).

Figure 3.20 shows the 184 cm tephra in comparison to known NAAZ2 compositions. Population 3 shows overlap with the composition of a sub-population of the NAAZ2 tephra from the Greenland Basin (Voelker and Haflidason, 2015) in the FeO vs Al_2O_3 and K_2O vs TIO fields (Figure 3.20). The relationship is not strong enough to be considered significant.

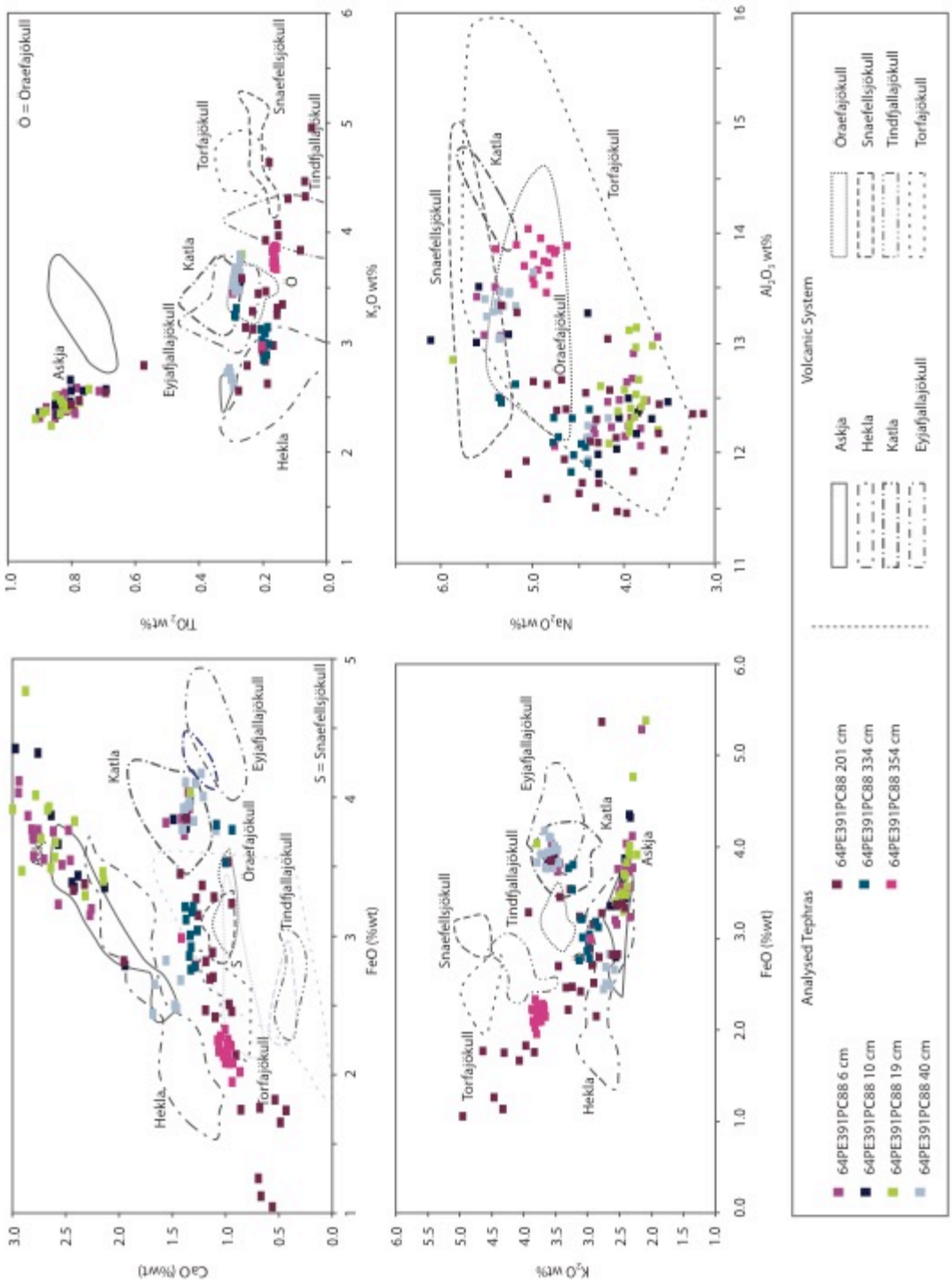

Figure 3.21: Major element geochemistry of analysed tephra in comparison to geochemical fields typical of each volcanic system on Iceland.

334 cm

This tephra horizon at 334 cm in the core forms a clear peak of 6,073 shards per gram dry weight (gdw). This tephra horizon is coincident with a marked increase in IRD, which has been tentatively suggested as Heinrich Event 8, dated to c. 90,000 years Cal BP (Figure 3.12 (Heinrich, 1988)). As such there is a strong possibility this tephra has been ice rafted. The horizon has two populations (1-2), and both show a degree of heterogeneity consistent with ice rafting. Analytical totals from the EPMA for each of the populations are considerably lower than the ideal 97% minimum total (A = 96.2 ± 1.17 %, B= 96.93 ± 1.45 %), consistent with a greater degree of hydration with age.

The 334 cm horizon is found 4 cm above the base of coccolith biozone N-G 3B representing a date of 97,000 years Cal BP (Gard, 1988; Backman *et al.*, 2009; Pope *et al.*, 2016). The time constraints provided by the coccolith biozone for this horizon provided strong age control, and all tephra horizons within the database dated from 80-125 ka BP were tested for correlation (Figure 3.22). The bimodal composition of the ash layer represents some challenges for correlation.

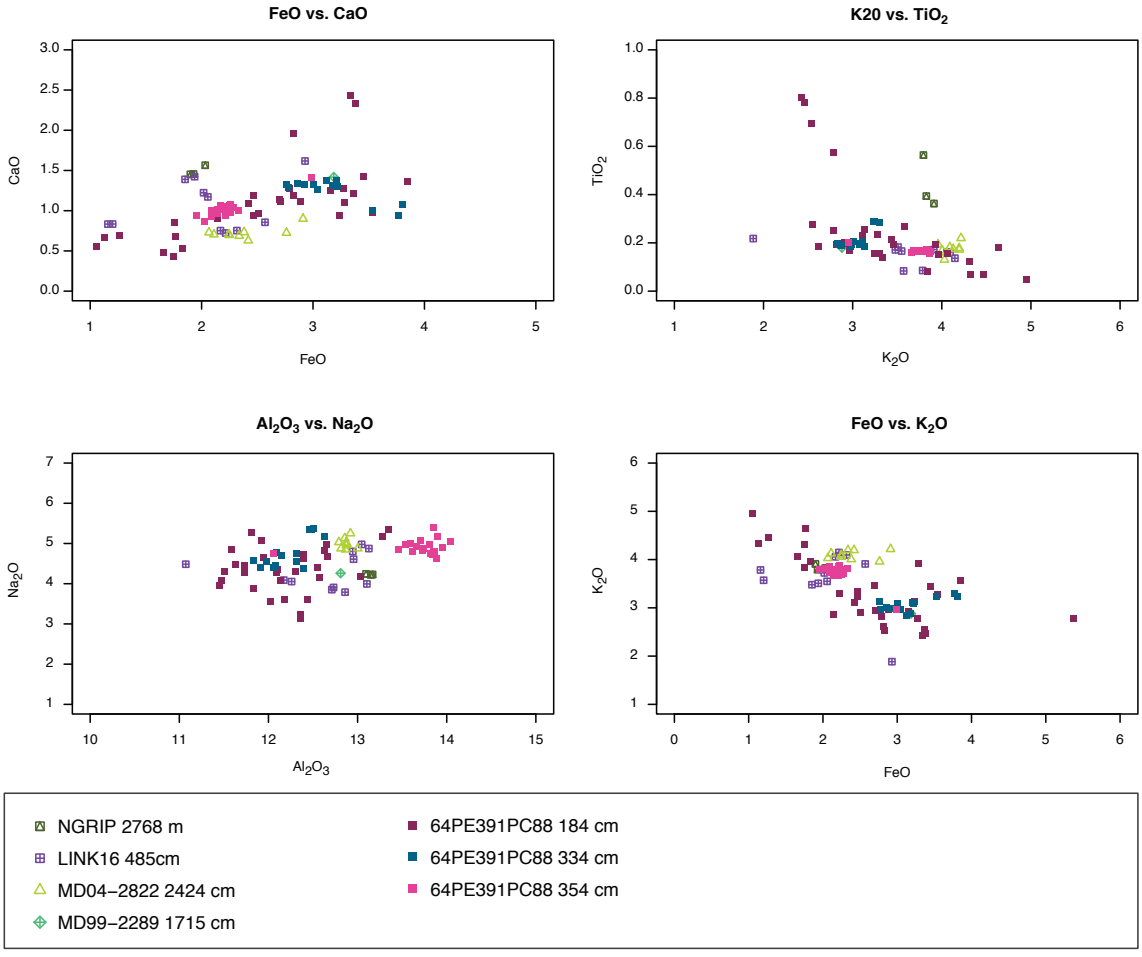

Figure 3.22: Comparison of the 334 cm tephra to MIS 5 a and 5b tephra, illustrating the potential link to a 95.4 ka BP tephra (MD99-2289, 1715 cm) dated in Brendryen et al. (2010).

The major element chemistry of both populations are consistent with a low alkali rhyolite from the Transitional Icelandic series of Jakobsson *et al.* (2008). The modal potassium enrichment value of 0.05-0.052 (Figure 3.23) demonstrates a clear off-rift source, but the value was spread between 0.036 and 0.046, indicating a potential ice-rafted origin, and suggesting a volcano from the WDZ, EDZ or MIL (Figure 3.21). Population 1 forms the majority of the grains, and is distinguished from the three grains of Population 2 by higher SiO_2 (72.71 ± 1.02% to 71.5 ± 1.06 %, Figure 3.22), lower TiO_2 (0.19 ± 0.006 % to 0.28 ± 0.003 %) and lower FeO (2.89 ± 0.18% to 5.59 ± 0.16 %). Population 1 was sourced from either the Hekla, Torfajökull or Öræfajökull system, with the strongest degree of overlap with the late Quaternary Hekla fields (Figure 3.21). Population 2 shows a strong affinity to the Eyjafjallajökull and Katla system. Neither population can be clearly assigned, this is expected within older eruptions (Lacasse and Garbe-Schönberg, 2001; Wallrabe-Adams and Lackschewitz, 2003; Hibbert *et al.*, 2014; Jennings *et al.*, 2014; Kuhs *et al.*, 2014).

A potential link can be suggested between the 334 cm rhyolite and the rhyolitic deposit at 1,715 cm in MD99-2289 provides a strong chronological link (suggested age 95.4 ka BP, MIS 5b; Brendryen *et al.* 2010). This relationship would be further strengthened by the future analysis of the brown shard component within the 334 cm horizon.

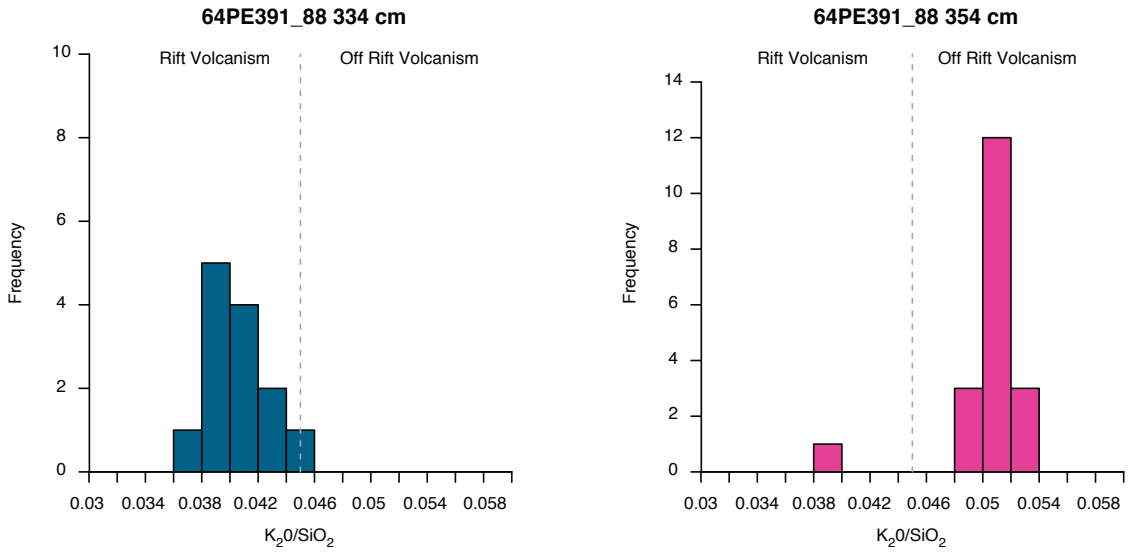

Figure 3.23: Potassium enrichment frequency plots for the two oldest rhyolitic horizons below the lower turbidite to show rift or off rift source for volcanism.

354 cm

This horizon is located 19 cm above the top of the coccolith horizon N-G 3C (119 ka and 16 cm below the base of the N-G 3B (97 ka), with an approximate age of 105 ka (Figure 3.13). The horizon is coincident with a marked increase in IRD from background levels of c. 3,000

grains per dry gram, to 12,000 grains per dry gram (Figure 3.13), raising the possibility of ice rafting as transport to the site. The tephra is a low alkali rhyolite (Le Maitre *et al.* 1989; Figure 3.14) and part of the transitional alkali series (Jakobsson *et al.* 2008;Figure 3.14). The potassium enrichment of 0.05-0.052 (Figure 3.17) is indicative of a rift source, with one off-rift outlier. Tephra 354 cm shows a low SiO_2 (70.29 ± 0.53 %), a high Al_2O_3 (13.08 ± 0.14 %) and a high K_2O (5.58 ± 0.06 %) with no clear affinity to a particular volcanic system. The total weight percentages for this horizon are consistently low (all <97%, average 94.95 ± 0.6%), consistent with older tephra horizons. The 354 cm horizon shares a similarity with the MD04-2822 2490 cm (116,400 ± 4,000 years Cal BP, Abbott *et al.*, 2013) and the 2,424 cm horizon (91,320 ± 2,410 years Cal BP, Abbott *et al.*, 2013); neither is an exact match. Further analysis of trace elements may enhance this interpretation; the horizon is not included in the age model due to this ambiguity.

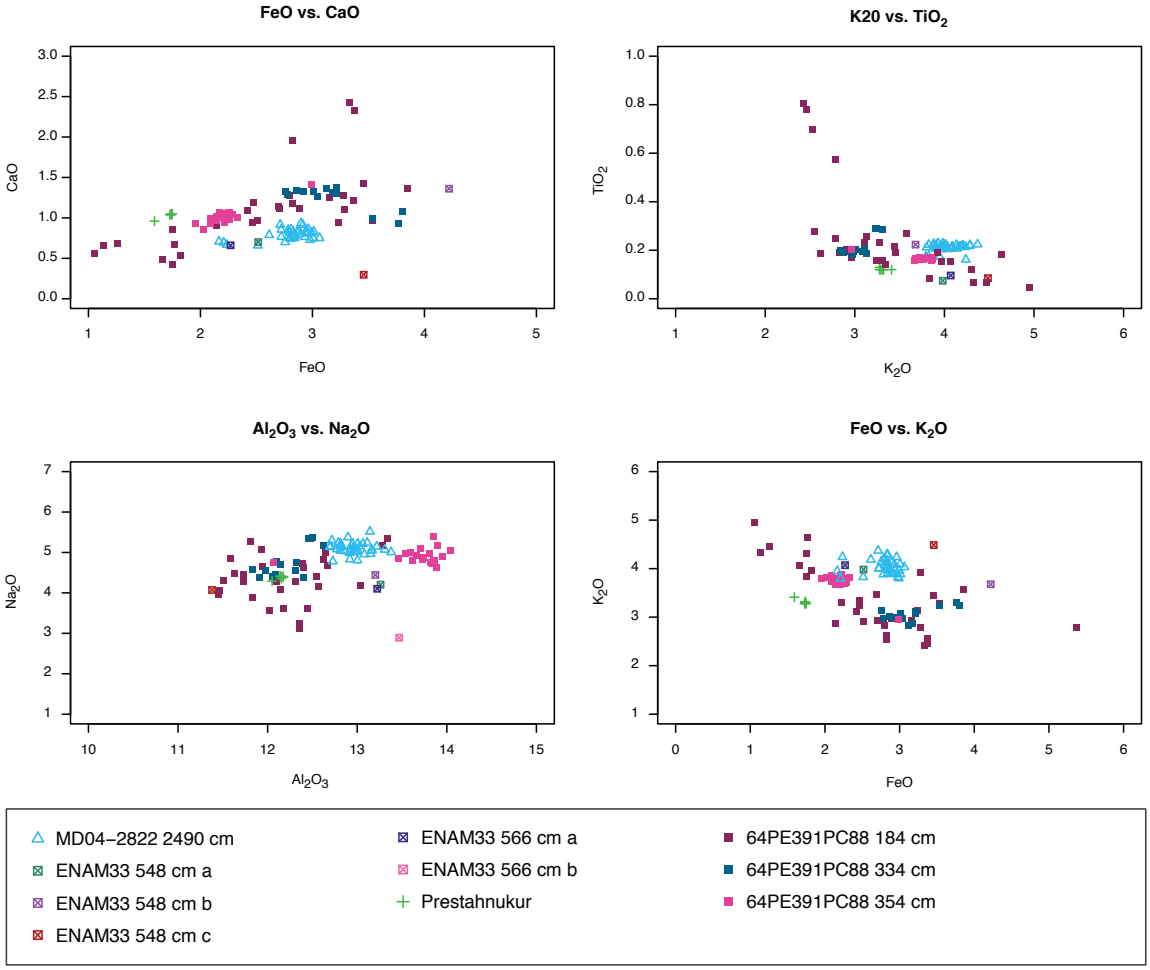

Figure 3.24: Cross plots to illustrate potential matches for the 354 cm tephra. No firm comparison can be made to any MIS 5c, 5d, 5e or MIS 6 known tephra.

3.6.1 IRD Horizons

IRD was found throughout the hemipelagite with variable concentrations. IRD results were plotted every 2 cm, with higher resolution (every 1 cm) sample counts across periods of high concentrations of IRD (Figure 3.13). Significant peaks were identified as Heinrich Events and used as age markers according to Heinrich Event stratigraphy from the North Atlantic taken from Sarnthein *et al.* (2001) and Rashid *et al.* (2003). Heinrich Event 3 was not considered as clearly expressed and not included in the age model. Heinrich Event 6 was the lowermost horizon used in the chronology as the date is close to the base of coccolith zone N-G 2 dated to 66 ka BP. The base of N-G 2 was detected at 251 cm hemipelagic depth, and the mid-point of the increase in IRD was 249 cm hemipelagic depth. Due to the poorly constrained nature of older Heinrich events, those beyond H6 were not used in the age model but are highlighted in Figure 3.13 in pale grey for reference. The magnetic susceptibility of cores in the North Atlantic has been shown to relate to Heinrich events (Rasmussen *et al.*, 1996; Abrantes *et al.*, 1998; Kuijpers *et al.*, 1998). Periods of low magnetic susceptibility are caused by the dilution of the magnetic signal by large grains where the geology of the source area is non-magnetic, but for strongly magnetic domains can be represented by a spike in magnetic susceptibility. Core 88 shows a strong reduction for Heinrich Event 4, but none of the other Heinrich events are characterised by magnetic susceptibility.Full IRD data can be found in the digital Appendix 2a.

3.7 Final Age Model: a new slide chronology

All datum horizons identified that were used in the final age model (OxCal online) are detailed in Table 3.6. The model can be interrogated for dates for specific hemipelagic depths (cm), to produce an estimated age with associated uncertainty. The depths representative of the base of the two mega-turbidites were 32 cm hemipelagic depth (Upper Ægir Turbidite, which was dated to 8,018 ± 2,128 Cal BP, and 201 cm hemipelagic depth for the Lower Ægir Turbidite yielding a date of 55,947 ± 3,910 Cal BP (Figure 3.25). The significant uncertainty of the dates is expected given the lower sedimentation rates and likelihood of erosion at the base of the turbidites. The earlier date is close to that of the published ages for the Holocene Storegga Slide at 8.17 Cal BP Dawson *et al.*, (2011); Bondevik *et al.*, (2012)). This suggests the model is projecting an appropriate date for Upper Ægir Turbidite.

The date of 55,947 ± 3,910 Cal BP for the Lower Ægir Turbidite represents a significant revision of the estimated age of 125 ka BP (Bryn *et al.,* 2005; Solheim *et al.,* 2005). This date is very close to the age assigned to the NAAZ 2 tephra, which forms a 20 cm thick horizon in cores 200 km to the south, and is found in nearly all cores between Iceland and the Faroes

(Kvamme *et al.*, 1989; Rasmussen *et al.*, 1996; Wastegård *et al.*, 2005). A possible explanation for not observing this tephra (dated to 55,350 ± 1,184, Svensson *et al.*, (2008)) in PC88 could be that the turbidite was deposited shortly after the NAAZ 2 eruption. The tephra may have been eroded by the passage of the Lower Ægir Turbidite and subsequently re-deposited within it (Figure 3.20).

Table 3.6: Dating horizons used in the final age model, all depths are in cm hemipelagic depth from core 88

Depth	HP Depth	Material/Proxy	^{14}C Age (ka)	Cal age BP	S.D (2σ) (ka)	Reference
185	34	Tephra - Saksunavtn		10.297	0.089	Rasmussen *et al*. (2006)
188	40	Tephra – Vedde Ash		12.121	0.114	Rasmussen *et al*. (2006)
190	54	H1 (IRD)		17.6		
190	54	14C	17.57	20.69	0.4	
200	63	H2 (IRD)	20.4-21.0	24.5		Sarnthein *et al* (2001)
236	101	H3 (IRD)	25.6-26.4	31.3		Sarnthein *et al* (2001)
241	104	14C	33.5	37.24	1.75	
263	127	H4 (IRD)	32.4-34.2	39.4		Sarnthein *et al* (2001)
265	129	Faroe Marine Ash Zone 4		46.8	1	Wastegard and Rasmunssen (2006)
288	161	14C	40.17	43.54	1.66	
312	153	H5 (IRD)		46		Rashid *et al* (2003)
917	175	H5a (IRD)		51	1.5	Brendryen *et al* (2011), Austin *et al* (2004)
975	251	Coccolith Zone NG-2 (base)		66	5	Gard (1988)
976	249	H6 (IRD)		66.5	1	Rashid *et al* (2003)
1013	289	Coccolith Zone NG-3a (base)		79	5	Gard (1988)
1078	334	Tephra		95.4		Brendryen *et al* (2010)
1082	338	Coccolith Zone NG-3b (base)		97	5	Gard (1988)
1115	372	Coccolith Zone NG-3c (base)		119	5	Gard (1988)
1116	373	Excursion - Blake Event		118.5	3.5	Thouveny *et al* (2004), Sier *et al* (2015), Tric *et al* (1991)

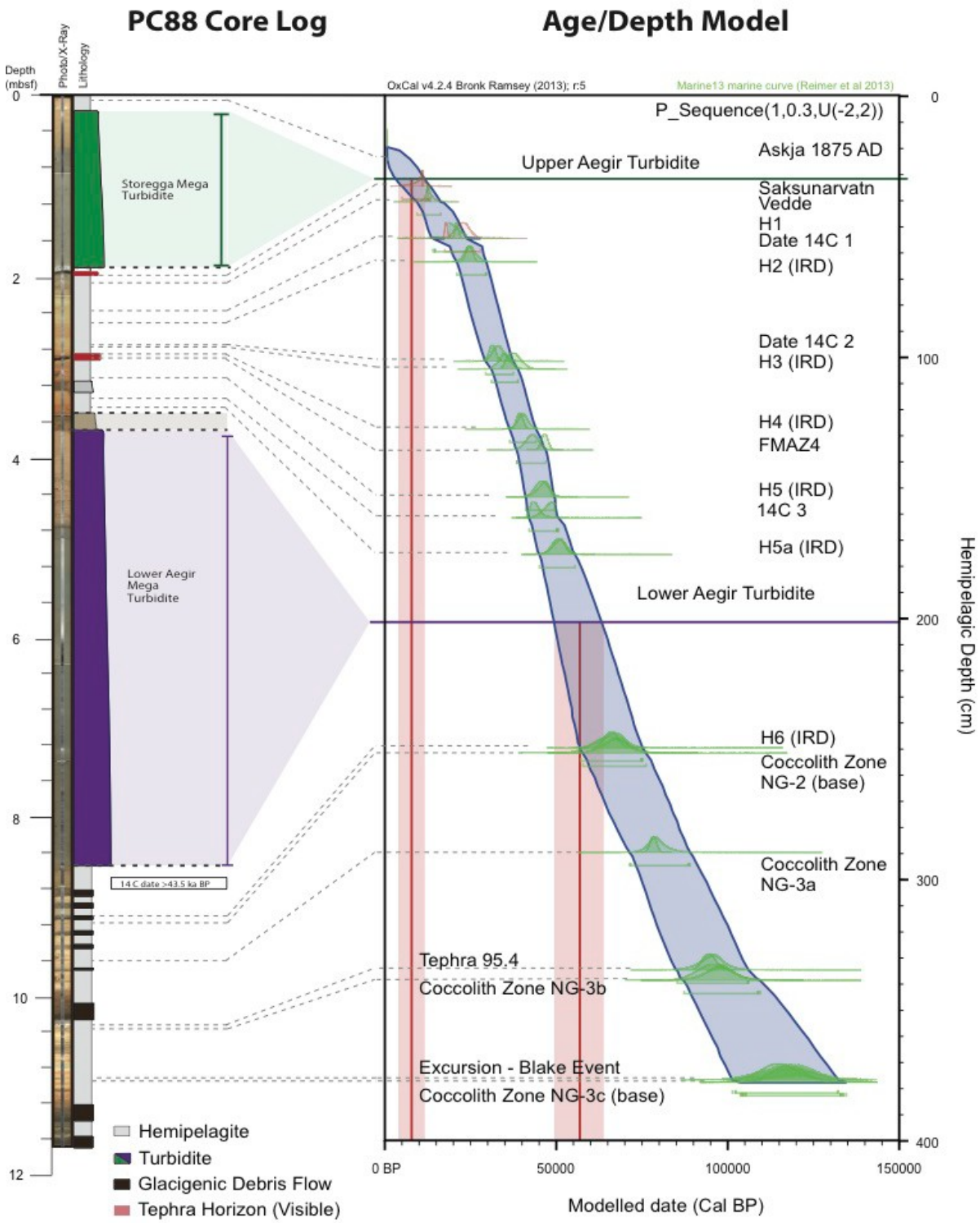

Figure 3.25: Core log and final depth model output from OxCal v4.2.4 showing the relative position of all age markers and the depths of the two megaturbidites. The red markers indicate chronological markers with a less than 60% agreement. Red vertical bars indicate the full potential age range of the two megaturbidites.

This work has demonstrated a more consistent hemipelagic sedimentation rate, in comparison to the sedimentation rate for core MD99–2283, a well-dated record of environmental change in the Nordic seas. The ages for core MD99-2283 were used to date the reflectors found above the Lower Ægir Turbidite (Lekens *et al*.2009b; Haflidason *et al.* 2004; Nygård *et al.* 2005). This record is discussed in Lekens *et al.* (2009), and utilises the

same dates as this work for Heinrich events 2-4 and the Laschamp Event. Below this date, the chronology relies on correlation of the $\delta^{18}O$ record to the SPECMAP timescale (Imbrie *et al.*, 1984).

Importantly, within MD99-2283, the interpretation of the Norwegian Greenland Sea excursion (73 ka BP) and the Iceland Basin excursion (dated to 180 ka BP) were not confirmed by additional dating methods such as tephra or coccolith biostratigraphy. MIS4 is condensed in MD99-2283, producing a step change in sedimentation rate commencing at the end of the radiocarbon period. After 45 ka BP, the sedimentation rate for MD99-2283 doubled. Core disturbance was noted between 45-60 ka BP (Lekens *et al.,* 2009). This interpretation of palaeomagnetic inclination data from MD99-2283 explains the discrepancy between MD99-2283 and PC88. As such the dating applied in this work is preferred due to the additional dating methods used to confirm the Blake Event. Further verification could be achieved by the re-analysis of excursions identified in core MD99-2283.

3.8 Provenance

3.8.1 Rare Earth Elements

Rare earth element (REE) data were normalised to Post-Archean Australian Shield (PAAS) values (McDonough and Sun, 1995; Piper and Bau, 2013). Full results are summarised in Appendix 3. The samples from the Trænadjupet turbidite, Upper and Lower Ægir turbidites and the KN179 Storegga sample (Figure 3.26 c) show characteristics common to the upper continental crust (Taylor and McLennan, 1985; McLennan *et al.*, 1993). In contrast, the basalt standards (BRR-1 and BAS 206) show a depleted LREE and no Eu anomaly, indicating the Upper and Lower Aegir turbidites cannot be sourced from a basaltic province. An enriched LREE and Eu anomaly is indicative of an upper crustal source for the source rock.REE data can be found in full in the digitasl Appendix 1b.

McLennan and Taylor (1990) calculated three provenance components to assess the tectonic terrane source (old upper continental crust, recycled sedimentary rocks, young undifferentiated arc and young differentiated arc) for turbidites derived from these settings: the Eu/Eu* anomaly, Th/Sc and Th/U ratios. These ratios were calculated for the Upper and Lower Ægir turbidites for comparison (Table 3.7, Figure 3.26 b and c). Using the values in McLennan *et al.* (1993) the KN179 Storegga sample, and both Ægir turbidites all display an Eu/Eu* anomaly consistent with that expected for Old Upper Continental Crust (OUC) or Recycled Sedimentary Rocks (RSR) of between Eu/Eu* 0.6-0.7 (means and standard deviations: 0.664 ± 0.004, 0.707 ± 0.009, 0.675 ± 0.043 respectively).

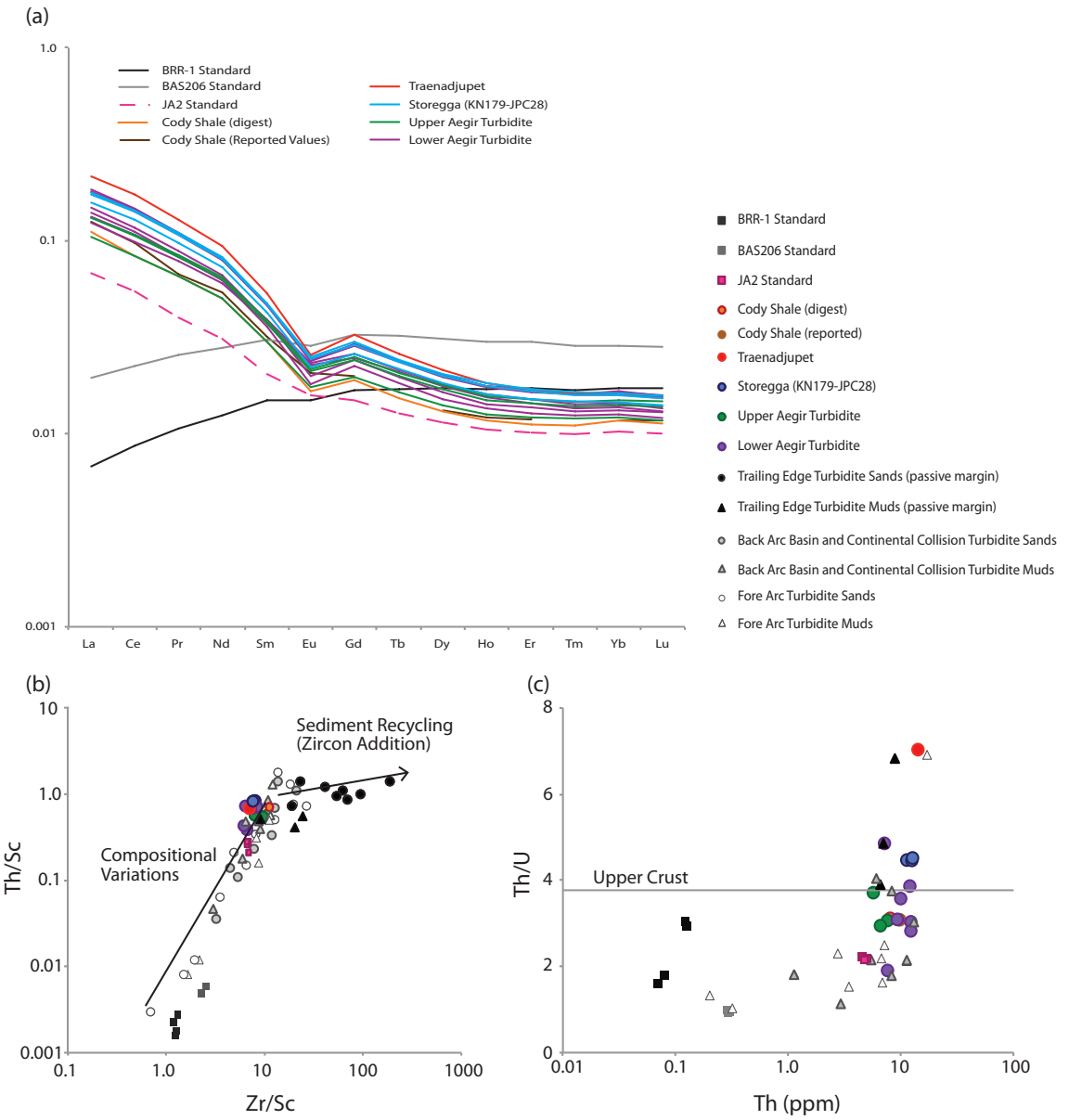

Figure 3.26: Rare earth element profiles (Normalised to chondrite values (Sun and McDonough, 1989), b and c show results in comparison to turbidite values for different tectonic terranes taken from McLennan et al. (1993).

The Th/Sc ratio also indicates an OUC origin for the Storegga Slide samples (0.822 ±0.008), the ratio for the Ægir turbidite muds is lower for both samples (Upper: 0.549 ±0.009, Lower: 0.620 ± 0.14). The lower ratio in the distal turbidites may be explained by the incorporation of carbonate-rich sediment from the basin floor and probable hydrodynamic sorting of heavy minerals during transport (Pyles *et al.*, 2013). The turbidites sampled in the Ægir Ridge have potentially experienced up to 1000 km of transport, and some dilution of the original chemical signature should be expected (Pearce and Jarvis, 1995; Pyles *et al.*, 2013). The Th/U values are consistently high (Storegga Slide: 4.489 ± 0.021, Upper Ægir Turbidite 3.247-0.418, Lower Ægir Turbidite 3.304 ± 0.926), which are broadly consistent with the value of >3.8 suggested as indicative of OUC origin (McLennan *et al.*, 1993).

Table 3.7: Provenance indicators calculated from ICP-MS acid digests of mud cap samples from the KN170-JPC28 (STOR) sample from the central Norwegian Basin, the Upper Ægir and Lower Ægir turbidites in cores 86 and 88. Reference values are summarized from McLennan et al. (1993).

	Eu/Eu* (geometric)	Eu/Eu* (arithmetic)	Th/Sc	Th/U	Probable Source
STOR1	0.660	0.642	0.816	4.513	OUC
STOR3	0.664	0.646	0.818	4.477	OUC
STOR5	0.668	0.648	0.832	4.476	OUC
L. Ægir 1 (86)	0.738	0.722	0.423	4.860	OUC
L. Ægir 2 (88)	0.644	0.626	0.726	3.021	OUC
L. Ægir 3 (88)	0.657	0.639	0.709	3.871	OUC
L. Ægir 4 (86)	0.736	0.720	0.385	1.898	OUC
L. Ægir 5 (88)	0.662	0.643	0.704	2.815	OUC
L. Ægir 6 (88)	0.653	0.635	0.720	3.562	OUC
L. Ægir 7 (88)	0.638	0.621	0.676	3.097	OUC
Trænadjupet	0.614	0.596	0.718	7.014	OUC
Upper Ægir 1	0.698	0.682	0.559	2.937	OUC
Upper Ægir 2 (88)	0.705	0.689	0.544	3.082	OUC
Upper Ægir 3 (88)	0.717	0.701	0.544	3.723	OUC
Reference values (Mclennan et al. (1993)					
Old Upper Continental Crust (OUC)		≈0.60-0.70	≈1.0	>3.8	
Recycled Sedimentary Rocks (RSR)		≈0.60-0.70	≥1.0		
Young Undifferentiated Arc (YUA)		≈ 1.0	<1.0	<3.0	
Young Differentiated Arc (YDA)		≈ 0.50-0.90	Variable	Variable	

The Th/Sc vs. Zr/Sc and Th vs. Th/U values of the Ægir ridge turbidites from PC88 were plotted against the published data for turbidite muds and sands from a range of tectonic settings (McLennan and Taylor, 1990). The use of the Zr/Sc ratio as an index of zircon enrichment is valuable in the analysis of deep sea turbidites. High Zr discriminates enrichment in zircon, while Sc is also important and preserves a signature of provenance. Th/Sc offers an estimate of igneous chemical differentiation processes due to the incompatible nature of Th (Figure 3.26 b), allowing an estimate of the degree of igneous differentiation. Passive margins hosting sediments which have undergone a more significant degree of weathering show a high Zr/Sc and lower Th/Sc enrichment. The turbidite muds from the Ægir Ridge and the KN179 Storegga sample plot amongst the samples from known

trailing edge margins (Figure 3.26 b). This indicates the Ægir turbidites must be sourced from a passive continental margin, and eliminates any basic or intermediate volcanic sources for the turbidites. Importantly this excludes Iceland or the Faroe Islands as a source for the sediments within the Ægir turbidites.

The Th/U ratio is an additional discriminator for the source of the turbidite muds. A low Th/U ratio is typical for mantle-derived rocks, whereas those from an evolved magmatic or continental source are typically enriched in U. The high degree of mobility for U results in a low Th/U ratio for sedimentary rocks derived from RSR or OUC settings (Figure 3.24c). The turbidite muds analysed in this study are comparable in Th/U and Th values for the trailing edge and continental collision turbidites. These indicators all suggest an OUC or high felsic content origin for the source material of the Ægir Ridge turbidites. The composition of these turbidites implies the slide materials were derived from the weathering of the Norwegian craton. The strong agreement between the upper and lower Ægir turbidites and the KN179 Storegga sample is interpreted here as evidence the two events were sourced from the same location. The KN179 Storegga sample therefore confirms both Ægir turbidites are distal deposits of submarine slides from the Storegga Slide Complex.

3.8.2 ITRAX XRF

The XRF geochemical analysis of the turbidite mud caps of the turbidites is discussed in relation to turbidites from three known sources, the Bear Island Fan (Pope *et al.,* 2016), the Trænadjupet slide (Allin, thesis) and the KN179-JPC28 Storegga sample as a reference for composition of slides from the Storegga Slide Complex. The Trænadjupet Turbidite Group includes samples from 6 cores containing a deposit in the Lofoten Basin dated to between 2.6 -3.9 ka BP (Allin, thesis). A series of cores was taken from the headwall of the Trænadjupet slide, and in a transect downwards across the main slide deposits within the slide scar (multi-core 23), and across the basin (piston cores 29, 57, 69, 72, 78, 68 and 79). These deposits show remarkable geochemical similarity over 400 km of turbidite run-out (Jarvis and Higgs, 1987; Pearce and Jarvis, 1995). These fields are used in Figure 2.27 to compare to the composition of the Ægir turbidites. The full database of ITRAX geochemistry used to define these fields can be found in digital Appendix 1c.

3.8.2.1 Si/Ti vs. K/Fe

High Si/Ti may indicate high silica content in source sediments, and Ti is enhanced in heavy minerals (Croudace *et al.*, 2006; Rothwell *et al.*, 2006). The presence of K is associated with detrital clays and commonly enhanced in turbidite muds. The highest Si is found in the Bear Island Group (0.177 ± 0.0178, Figure 3.27), the Si/Ti content of the Storegga and Trænadjupet

groups are similar: 0.1629 ± 0.0213, 0.1348 ± 0.014, respectively. This suggests a similar source for the Trænadjupet and Storegga groups, yet with a strong influence of heavy minerals and silicates for the Bear Island Group.

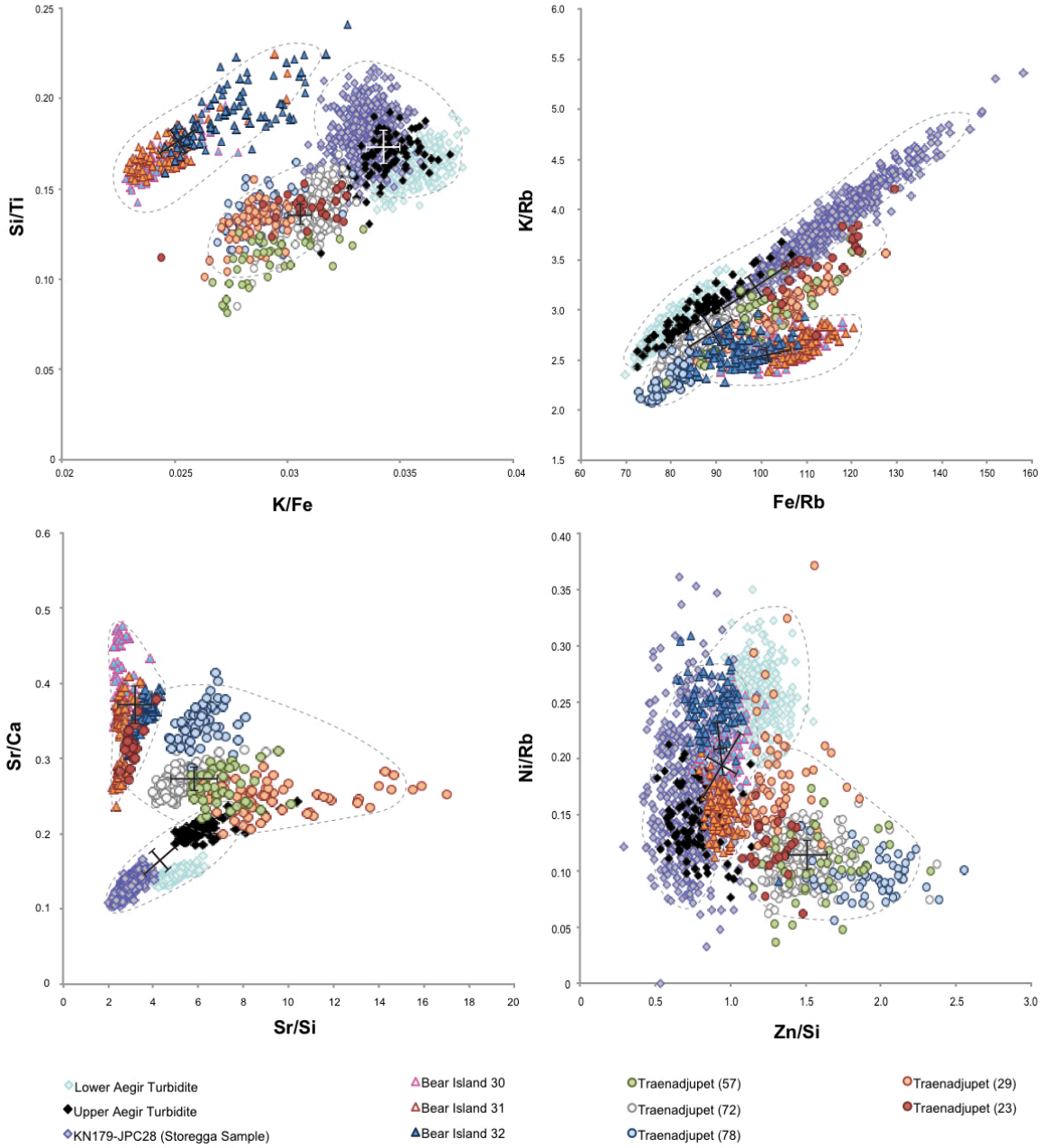

Figure 3.27: ITRAX composition of turbidite mud caps from the Ægir Ridge cores, the KN179-JPC28 sample from the central Storegga mud pond (see Figure 3.3) and comparison clusters of the Trænadjupet turbidite (3.4-2.6 Cal BP (Allin, thesis)) and the Bear Island Clusters detailed in Pope et al. (2016).

3.8.2.2 K/Rb vs. Fe/Rb

Fe/Rb has been interpreted to represent grain size related fractionation (Richter *et al.*, 2006), this is responsible for the elongate field of the groups within cross plots (Figure 3.27). Both K and Fe are commonly associated with turbidite muds as products of weathering of both continental and volcanic products. The relationship between the K and Fe when normalised

to Rb provides insight to provenance of the turbidites. There is distinct composition for both the Bear Island and Trænadjupet groups, and significant overlap of both Ægir turbidites with the KN179-JPC28 sample, indicating they are sourced from a similar region.

3.8.2.3 Ca/Si vs. Sr/Si

The Bear Island group show the highest Sr content (mean 7,495.3 ± 1,422) whilst Ca content (21,420 ± 4,569, Figure 3.27) is comparable to Trænadjupet and Storegga groups (19,747 ± 10,766, 17,563 ± 6,250, respectively). This implies a shallower water source for the failed material with high silica content. The Bear Island Fan deposited an estimated 4200 km^2 of material during MIS 2, sourced from the Barents Sea and Svalbard (Dowdeswell *et al.*, 1996; Vorren *et al.*, 1998; Pope *et al.*, 2016). This potentially explains the shallow water signature, given that the Barents Sea does not exceed 500 m water depth, and previous work has linked the composition of ice sheet deposits to those from eastern Svalbard (Pope *et al.*, 2016). The offset between the KN179 Storegga sample and the Upper and Lower Ægir could be attributed to Ca rich hemipelagic material incorporated into the flow as it moves along the sea bed.

3.8.2.4 Ni/Zn vs. Fe/K

A crossplot of Ni/Zn vs Fe/K highlights the difference in concentrations of ore elements from the Norwegian Caledonides that have been preserved in turbidite muds (Figure 3.27, Hanski *et al.,* 2011). Within the composition of turbidite groups variation in metallurgic sulphides can be seen. The Bear Island group display the highest concentrations of Ni (1,219 cps ± 244) and Zn (2,384 cps ± 249). The lowest concentrations of Ni and Zn are within the Storegga Group (386 ± 265 cps and 841 ± 436 cps, respectively), with intermediate Ni and high Zn values in the Trænadjupet Group of turbidites (373 ± 98 cps and 1219 ± 165 cps). This increased concentration of metal sulphides within turbidites of a more northerly provenance accurately reflects the macro geology of the region, and supports the interpretation of provenance from different sectors of the Norwegian Margin.

3.8.3 Sub bottom profile Results

Two acoustically transparent units were present along the ridge, albeit showing a variable thickness, suggesting a series of larger homogenous units. Figure 3.28 (Line 66, Line 40, Line 15 and Line 04, an enlarged print of this figure is available in Appendix 1) highlights the lines detailed in Figure 3.4. The seismic reflection lines illustrate the continuous repetition of a deeper acoustically transparent unit (purple unit, Figure 3.28) between 3-5 times thicker (average 3.4 times) than the uppermost acoustically transparent unit interpreted to be the

Ægir Turbidite/Holocene Storegga Slide (green unit, Figure 3.27). The purple unit represents the Lower Ægir Turbidite and may have a volume of 9,600-16,000 km^3. Bathymetric deep areas adjacent to the ridge show a detailed stratigraphy consisting of three or more acoustically transparent beds. The increasing bed thickness from line 66 to line 4 is consistent with a general bathymetric deepening of the ridge towards the southwest. Coring positions for this study are highlighted on line 15, which crosses the coring area. Line 40 shows an additional acoustically transparent unit below the Lower Ægir Turbidite within the central ridge valley (purple unit, Figure 3.28). This suggests there is another older turbidite deposited before the Lower Ægir Turbidite. The thickness of this unit was measured in mm, on line 40. Line 40 demonstrates these three units, fully penetrated by the 3.5 KHz. This older slide may have a volume 13 times greater than that of the Holocene Storegga Slide (2400-3500 km^3, Haflidason *et al.,* 2005), a potential volume of up to 41,000 km^3.

Table 3.8: Thickness (mm) of the two Ægir Ridge transparent units observed in cores 88 and from 3.5 kHZ data. Thickness was measured on interpretative sketches in mm. Volume estimate is based on the difference to the thickness of the Upper Ægir Ridge turbidite, the distal Storegga deposit. The volume used is the minimum (2,500 km^3) and maximum (3,400 km^3) estimates detailed in Haflidason et al. (2005)

Position	Upper turbidite mm (Green)	Lower Turbidite mm (Purple)	Size compared to Upper turbidite (Storegga)	Volume estimate min (km^3)	Volume estimate max (km^3)	Deeper Turbidite mm (blue)	Size compared to Upper turbidite (Storegga)	Volume estimate (based on Storegga 3500 km^3)
A	2.703	7.366	2.725	6,813	9,540			
B	2.499	6.862	2.746	6,865	9,611			
C	2.084	5.831	2.798	6,995	9,793			
D	0.435	1.374	3.159	7,898	11,057	6.062	13.936	34,840 - 48,776
E	0.628	2.439	3.883	9,708	13,591			
F	0.449	2.678	5.964	14,910	20,874			
G	0.878	2.394	2.727	6,818	9,545			
H	1.675	5.210	3.110	7,775	10,885			
Av.	1.441	4.583	3.389	8,473	11,862			

Comparing the thickness of the hemipelagic deposits in sections d and f allows an approximation of age. Based on the hemipelagite thickness between the Upper and Lower Ægir Turbidite (0.821 and 0.549 mm respectively), taken to represent 46,000 years between the two events, a projected age of between 79 and 115 ka BP could be estimated for the deeper slide deposit. The data does not consistently penetrate deep enough to fully resolve this issue.

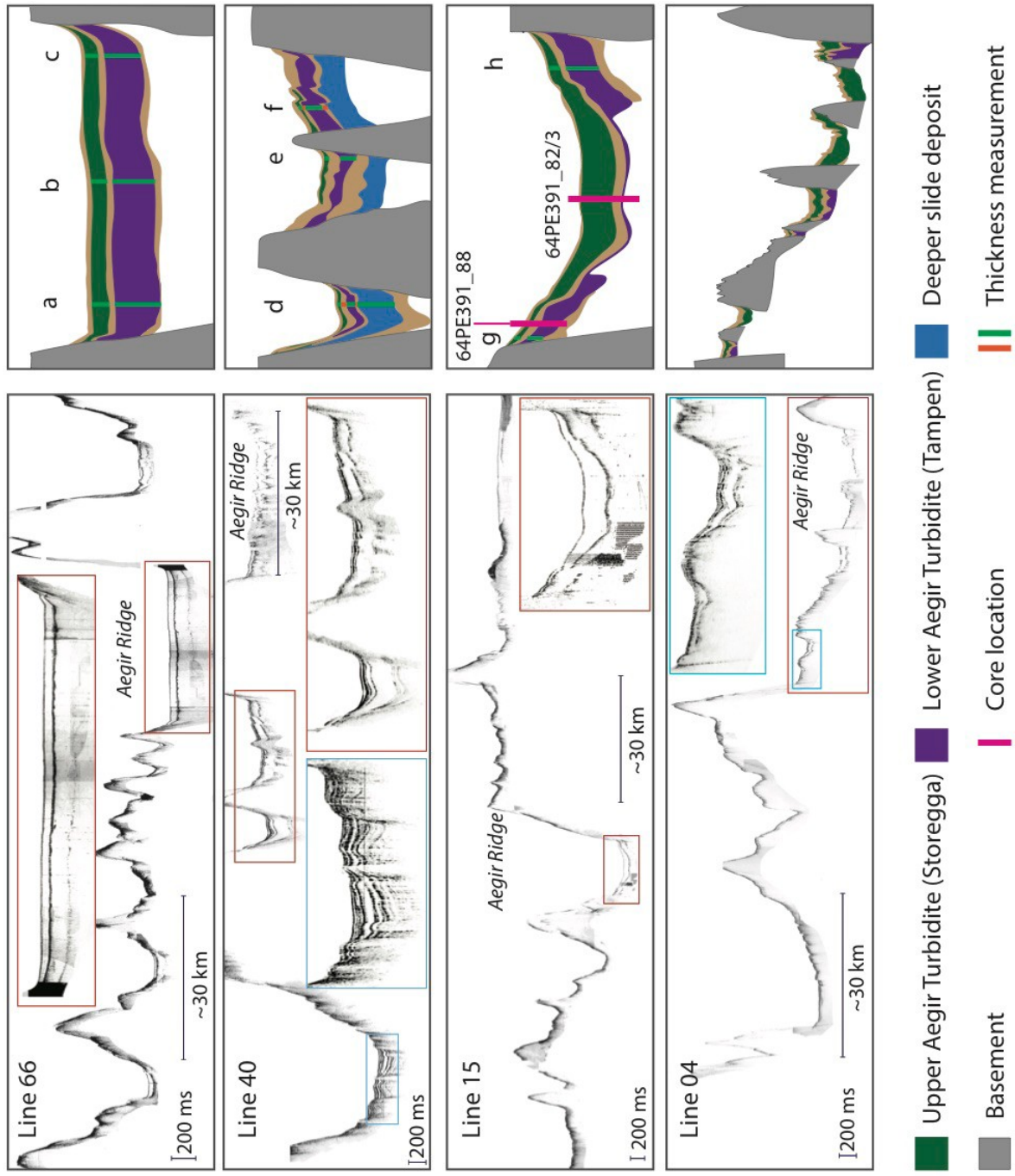

Figure 3.28: Selected 3.5 KHz lines across the Ægir Ridge from cruises EW9006 and EW9007 showing the consistent presence of two mega-turbidites along the ridge. Sketch taken from region of ridge highlighted in red, blue boxes denote additional areas of interest. Pink bars represent sediment cores, green bars indicate location of measurements of unit thickness discussed in Table 3.8. Line 66 is closest to the Storegga Slide scar, Line 4 is just north of the Faroes Ridge (see Figure 3.4). A larger verion of this figure is included in Appendix A.

3.8.4 Provenance

Turbidite mudcap composition is a reliable indication of source area and is predominantly dictated by the composition of materials involved in the original landslide (Pearce and Jarvis, 1995; Rothwell *et al.*, 2006; Hunt *et al.*, 2011, 2015a). Previous work has demonstrated that

turbidites maintain a signature of their original tectonic setting represented in the ratio of their REEs (McLennan *et al.*, 1993). The Ægir Ridge turbidites have been constrained as sharing an old upper continental crust origin on the basis of their Eu/Eu* anomaly and Th/Sc ratio. This considerably limits the provenance of the failure to the Norwegian continental margin. Whilst Kuijpers *et al*. (2000) document the presence of turbidites from the Faroes Islands along the Faroe margin, and highlight the potential for large mass wasting events, the regional geology and tectonic setting is discernible in the trace element geochemistry. A failure from the Faroes Platform, predominantly composed of Tertiary basaltic lavas, would demonstrate substantially different REE concentration than the results presented from these Ægir turbidites (Taylor *et al.*, 2000; Kuijpers *et al.*, 2001; Evans *et al.*, 2005; Keser *et al.*, 2005). The LREE enrichment and Eu/Eu* anomaly eliminate Iceland, the Faroes or the Mid-Ocean Ridge system as the source of the slides. The remaining potential source for the Ægir turbidites is the Norwegian continental slope. The REE profile is consistent with a felsic source. Therefore, the Ægir turbidites are interpreted here to represent failures of the Quaternary Naust formation, which was derived from the erosion of the felsic Norwegian continent through repeated ice sheet advances (Evans *et al.*, 2002; Ottesen and Rise, 2009; Rise *et al.*, 2010; Chand *et al.*, 2011).

The Storegga Slide Complex is the most proximal known slide scar. Alternate sources along the Norwegian margin were tested. The changes in the basement geology of the Norwegian Caledonides provide suitable differentiation in turbidite composition demonstrated in the ITRAX geochemical compostions. These data accurately distinguish between the Bear Island and Trænadjupet slides. The turbidite groups analysed from the Bear Island Fan and the Trænadjupet/Nyk complex demonstrate the consistent geochemical compositions of deposits from these sources (Figure 3.27). The KN179 Storegga Slide sample was taken from the centre of the Norwegian Basin and deposited at the same time as the Holocene Storegga Slide, and is used as a type-composition for failures from the Storegga Slide Complex (Paull *et al.,* 2010). When compared to the KN179 Storegga Slide sample, both Upper and Lower Ægir turbidites demonstrate excellent agreement of the K/Rb vs. Fe/Rb and the Zn/Si vs. Ni/Rb ratios illustrating they are from the same source region. The combination of the REE analysis confirming the Norwegian slope, and the ITRAX analyses imply provenance from the Storegga Slide Complex. While the Upper Ægir Turbidite is interpreted to represent the Storegga Slide at 8.17 ka BP (Paull *et al.*, 2010; Bondevik *et al.*, 2012), the Lower Ægir Turbidite represents a preceding failure from the Storegga Slide Complex, known as the Tampen Slide.

3.8.4.1 Slide Chronology

The established theory for the generation of slides from the Storegga Slide Complex relates the timing of failures to deglaciations (Evans *et al.*, 1996, 2005; Haflidason *et al.*, 2005; Hjelstuen *et al.*, 2005; Solheim *et al.*, 2005). The five previously identified slides broadly correlate to glacial terminations over the last 500 kyr: Storegga, 8.17 ka BP (MIS 2 termination), Tampen: 125 ka BP (MIS 6 termination), Slide R, 300 ka BP (MIS 10 termination), Møre Slide, 400 ka BP (MIS 12 termination) and Slide S, 500 ka BP (MIS 14 termination [Lisiecki and Raymo, 2004]). Additional older slide deposits identified within the Norwegian Basin (Slide U and Slide W, figure 1.5) have estimated volumes exceeding 20,000 km^3 (Hjelstuen and Andreassen, 2015). Dating through seismic correlation suggested an age of 2.74–0.5 Ma, with a recurrence interval of at least 370,000 years between events.

Here, an age of 56 ± 4 ka is provided for the Lower Ægir Turbidite, which is interpreted to represent the Tampen Slide. The new age for the Tampen Slide is 70,000 years younger than the previously suggested age. The dates for older slides (Slide R, Møre Slide and Slide S) may require similar adjustment when dated using sediment core material as opposed to the seismic correlation method (Bryn *et al.*, 2005; Solheim *et al.*, 2005). The suggested ages were applied through correlation of seismic packages to borehole cuttings, with a recovery of 10-20% (Bryn *et al.,* 2005) a method associated with considerable uncertainty. On the basis of these seismic investigations, the slide preceding the Holocene Storegga Slide is the Tampen Slide, with a projected date of 125 ka BP; shortly after the termination of glacial period MIS 6 (Saalian [Lisiecki and Raymo, 2004]), while the Lower Ægir Turbidite is dated to 56 ± 4 ka This has two possible interpretations: the error associated with seismic dating are substantial (70,000 years), or an additional failure from the Storegga Slide Complex exists between Storegga and the previously identified Tampen. The prospect of an additional failure is unlikely, because in excess of 100,000 km of seismic lines have been taken across the Storegga Slide scar and a failure of this size (2.6-3.4 times larger than Storegga) should have been identified. Therefore this work shows the Tampen Slide to have been previously incorrectly dated, and the revised date to be 56 ±4 ka BP.

The dating methods applied to sediment core 88 have taken a robust multiproxy approach. Dating the Tampen Slide to 55,900 ± 4000 years BP is in close agreement with earliest assessments of the age, size and volume of the Storegga Slide Complex (Bugge *et al.*, 1987; Jansen *et al.*, 1987; Evans *et al.*, 1996). Bugge *et al.* (1987) identified three Storegga Slides through a combination of coring across the slide and complimentary seismic reflection surveys. Bugge *et al.* (1987) initially divided the recent slide history of the Storegga Slide Complex into three slides: the First, Second and Third Storegga Slides (Bugge, 1983; Bugge *et*

al., 1987; Jansen *et al.*, 1987). The nomenclature of the First, Second and Third Storegga Slides was revised in Haflidason *et al.* (2004), and the First and Second events were recognised as one retrogressive failure (the Holocene Storegga Slide). The Third Storegga Slide was identified on seismic lines, but not reached with the coring campaign. The projected age of the Third Storegga Slide was 30-50,000 years ago. This date was estimated by extrapolating the sedimentation rate beyond radiocarbon limits to top of the turbidite using the depth estimated from seismic reflection profiles. This Third Storegga Slide of Bugge *et al.* (1987) is likely equivalent to the Tampen Slide dated at 55,900 ± 4000 years BP in this work.

Based on the re-evaluation of the Tampen Slide date, the suggested date of Slide R; 300 ka BP; should be interpreted with caution. Slide R failure likely represents the third turbidite identified in sub bottom reflection profiles (figure 3.28), which is crudely dated to 110-146 ka based upon seismic stratigraphy of the present study.

The evidence presented here, shows the established theory of the frequency of slides to be incorrect: slides of the Storegga Slide Complex are not limited to 100,000 years cycles. Both Storegga and Tampen occur 5-7 ka after the termination of a glacial period, suggesting a common period of maximum risk. The start date of MIS 5e is 130 ka BP, and the maximum age reached in the core is c.127 ± 15 ka BP, therefore whilst a slide within MIS 5e was absent within this core, its occurrence cannot be ruled out or confirmed on the available evidence.

3.8.5 Fennoscandian Ice Sheet during MIS 4/3

The new date for the Tampen Slide (56 ± 4 ka BP) does not align with a major glacial termination, but does occur with the onset of a MIS 3 warmth (57-29 ka BP). Figure 3.28 summarises the changing climatic conditions in Fennoscandia over the late Quaternary. The Lower Ægir turbidite was emplaced shortly after a substantial warming period from the peak MIS 4 glaciation within the Bø Interstadial (56-40 ka BP, Figure 3.30).

The extent of each ice sheet prior to MIS 2 over the continental shelf is poorly constrained. At the transition between MIS 4 and MIS 3, Recent work on MIS 3 terrestrial environmental reconstructions has challenged the traditional theory that central Fennoscandia was glaciated throughout MIS 3 (Helmens and Engels, 2010; Van Meerbeeck *et al.*, 2011); such that it is suggested that parts of Finland were ice free (Wohlfarth and Näslund, 2010). Central European climate reconstructions from the Eifel maars record a period of 7,000 years in early MIS 3 (57,000–49,000 ka) of intense warming, and pollen assemblages similar to modern. At the time of triggering of the Tampen Slide, the central European climate was therefore similar to the mid-Holocene, when the Storegga Slide was triggered.

This intense warming in MIS 3 is echoed in marine sediment studies from the Faroes, where a prolonged period of enhanced NSOW strength, coincident with especially low values of $\delta^{18}O$ indicative of warm surface waters is observed. IRD records show substantial ice rafting across the Vøring Plateau, associated with the end of the Karmoy Advance at 72–56 ka BP (Brendryen *et al.*, 2010). This is immediately prior to the deposition of the Tampen Slide. The magnitude of this change is comparable in palaeoclimatic records to the changes observed between the last glacial (MIS 2, Weichselian Glaciation) and the Holocene. These changes can be summarised as eustatic sea level change exceeding 90 m, and a retreat from a shelf edge glaciation, to mountain ice caps (Kandiano and Bauch, 2003; Lisiecki and Raymo, 2005; Mangerud *et al.*, 2011; Grant *et al.*, 2012). Thus, the MIS 4-3 transition represents a significant and rapid temperature change, and is identified in core PC88 6 cm below the Tampen Slide deposit. This implies that changing environmental conditions are important in slide preconditioning and triggering.

This alternative interpretation of MIS 3 as a warm period for central Europe, is important in the context of the new date for the Tampen Slide. MIS 3 is not regarded as a full interglacial, as it does not fall within the 100,000-year cyclicity of glacial-interglacial changes that has characterised the previous 500 ka (Lisiecki and Raymo, 2005). The significance of this is that a global climatic change is important in preconditioning the Norwegian continental slope to fail, but that change is not limited to the 100,000 year glacial cycles, therefore slides could occur during interglacials previously interpreted as cool, such as MIS 3. The previous interglacial period, MIS 5e, does conform to this cyclicity, and was preceded by the loss of the massive MIS 6 (Saalian) ice sheet (Jakobsson *et al.*, 2013), it is unclear if a slide occurred during this period on the available evidence.

The new date is incorporated into a revised model summarized in Figure 3.30. The novel contribution of this Ph.D. thesis is to show that while climate transitions are key to preconditioning continental slopes to fail, a full glacial- interglacial transition is not required. It is possible for smaller changes in climate, such as the MIS 4 to MIS 3 transition, to precondition the slope, and for more than one slide to occur per 100,000 year climate cycle.

3.8.6 Potential triggers for the Tampen and Storegga slides

The retreat of a significant volume of ice induces changes on the continental slope that may be capable of triggering a slide through changes to pore pressure from sediment loading, glacio-isostatic adjustment induced earthquakes and the destabilisation of methane clathrate. This model is adjusted here to include this new date (Figure 3.30). These

previously identified potential triggers are discussed below with regard to new dates following the processes outlined in Bryn *et al.* (2005):

Sediment Loading

Excess pore pressure refers to a sudden increase in pore pressure within sediments resulting from rapid sedimentation above impermeable horizons. Approximately 100 m of sediment was deposited during the Weichselian glaciation (110,000-11,700 years BP) on the upper continental slope in the region of the Storegga headwall (Bryn *et al.*, 2005). The interglacial clay horizons in the Storegga region have been extensively modelled to predict pore pressure across the profile of the slide (Kvalstad *et al*., 2005). Deposition rates vary substantially across the slide, with the highest rates in the slide scar region, decreasing towards the toe of the slide. These excess pore pressures have been suggested to be 20-30% at the time of the Holocene Storegga Slide (Masson *et al.*, 2006; Leynaud *et al.*, 2007; Leynaud *et al.*, 2009). In this example, the model demonstrated a considerably higher increase in pore pressures in the toe of the slide, resulting in eventual swelling and unloading. This higher excess pore pressure takes several thousand years to fully develop in comparison to the timing of maximum deposition rates, and may explain the delay between ice sheet retreat and slide triggering.

Earthquakes

Earthquakes triggered by isostatic rebound after glacial retreat have been assumed to reach ≥7 Mw (Bungum *et al.*, 2005; L'Heureux *et al.*, 2013). The ground acceleration from a magnitude 7 earthquake is capable of destabilising the continental slope, providing a trigger for large submarine slides. The rate of uplift today in Fennoscandia is exceeded only by that of the Himalaya, following the last glacial period uplift rates vary significantly, reaching a peak rate c. 10,000 years Cal BP (Mörner, 1990; Morner, 1991). The rate of uplift decreases exponentially from 10,000-4,500 years Cal BP. This relationship is similar for the ice sheet retreat proposed at the time of the Tampen Slide that occurs five thousand years after deglaciation commenced. Furthermore, associated sea level rise that occurs during deglacials has been modelled as sufficient to increased vertical load and reactivate faults in the seafloor and larger basement faults at depth (Brothers *et al.*, 2013). The Storegga Slide Complex is near the Jan Mayen Fracture Zone, which extends from Jan Mayen into the Storegga headwall. The Jan Mayen microcontinent is tectonically active and movement along this fracture zone combined with high sediment loads and glacio-isostatic rebound play an important role in triggering sliding (Hjelstuen and Andreassen, 2015).

Methane Clathrates

The relationship between methane clathrates and submarine landslides is unclear and widely debated. Changing ocean bottom temperatures could cause instability in clathrates contained in sediment below the Gas Hydrate Stability Zone (GHSZ) and sudden melting could trigger a submarine slide as the sediment looses internal cohesion and liquefies (Maslin *et al.*, 2004; Lee, 2009). It is also possible that large submarine slides would destablise clathrates through the removal of overburden.

The new date for the Tampen Slide contributes to the interpretation of preconditioning factors. The retreat of the MIS 4 ice sheet during the Bo Interstadial represents a significant loss of mass from the continental shelf, immediately following a period of rapid glacial sediment deposition. This implicates preconditioning through sediment loading, and triggering relating to ice-sheet retreat, linked to isostatic rebound and seismicity. The significant increase in North Atlantic temperatures resulting from ice-sheet retreat could contribute to clathrate dissociation, but this cannot be determined through the available evidence (Maslin *et al.*, 2004; Dawson *et al.*, 2011).

Recent work suggests that modern hydrate dissociation has not been detected in the atmosphere, and that the ocean-atmosphere transition is influenced by stratification, the depth of the hydrates in the sediment and the strength of the water column/sediment sink (Ruppel and Kessler, 2016).

The potential to resolve clathrate dissociation as a trigger for slides rests on evidence of a carbon isotopic excursion below a Slide deposit as seen in the Santa Barbara basin record. Hydrates are present in the region of the Storegga headwall within the Nyegga pockmark field (Micallef *et al.*, 2009; Plaza-Faverola *et al.*, 2011; Hill *et al.*, 2012). To date, a $\delta^{13}C$ record from an undisturbed sediment core close to the Storegga slide slide scar have not been attempted. The Storegga Slide removed much of the material from the Nyegga pockmark field that could contain this evidence: as such a definitive result is unlikely.

Attempts to link potential dissociation events as a result of the Storegga slide to methane concentration in the atmospheric record of the Greenland Ice cores have not been successful (Maslin *et al.*, 2004). This has been interpreted as evidence of no significant release of methane in the Northern Hemisphere at the time of the Storegga slide, however it is possible smaller volume methane escape events could be recorded in the carbon isotopic concentration within benthic foraminifera in sediment cores close the SSC. Methane has a very low $\delta^{13}C$, which can been detected in sediments where methane escapes have occurred (Berndt *et al.*, 2014; Panieri *et al.*, 2014).This hypothesis can be tested with further sediment coring targets close to the SSC to evaluate if such an event occurred before the Storegga Slide.

3.8.6.1 A revised history of Norwegian Slides.

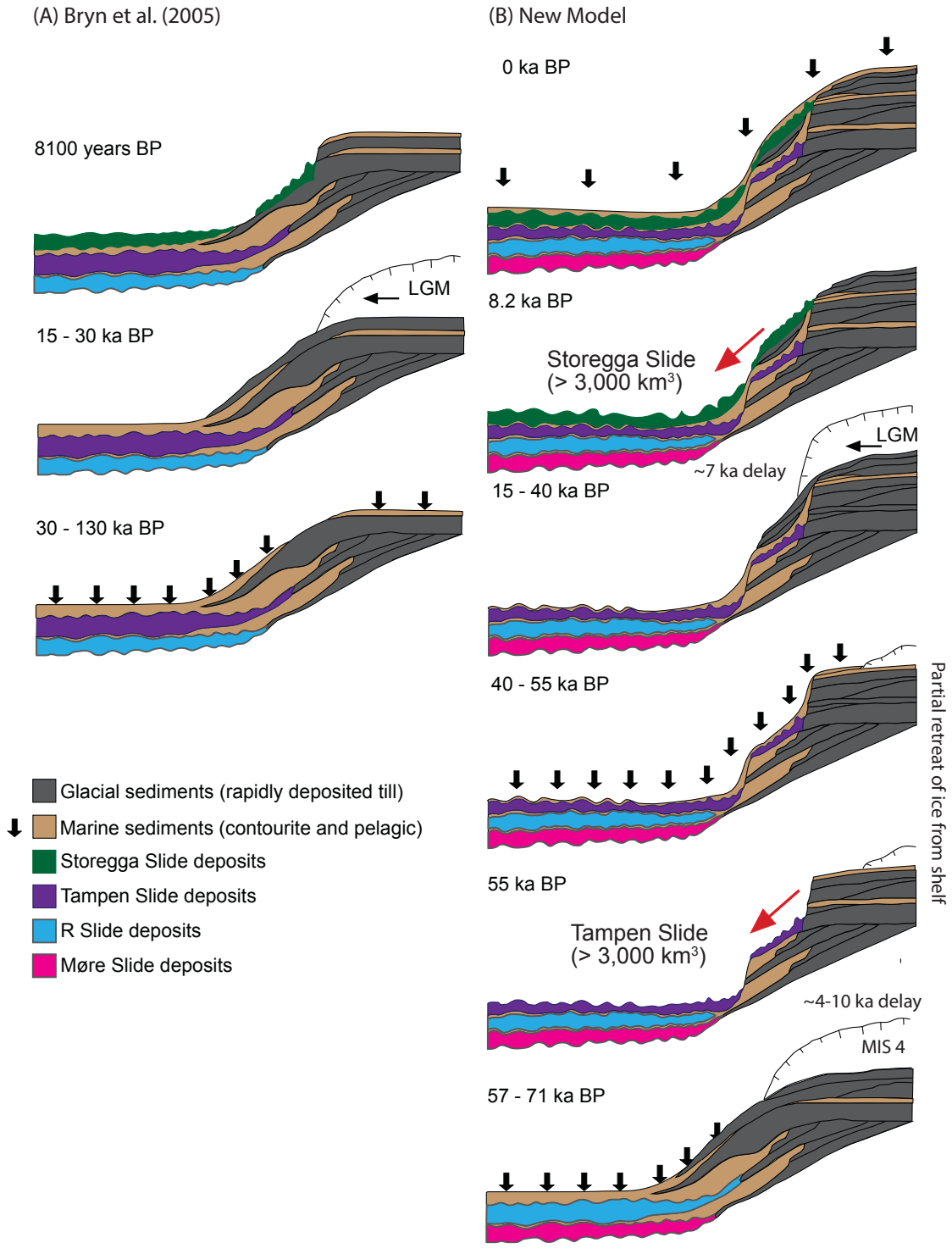

Figure 3.29: Comparison of the Bryn et al, (2005) model of the Storegga Slide Complex (A) to a new model accounting for the younger date of the Tampen Slide (B). Colours of slides relate to the stratigraphy detailed in Figure 3.6.

The Storegga Slide Complex has been shown here to have produced two massive slides in the last 60,000 years, this is a significant change in previous interpretations of the history of

slides from this complex, which limited frequency to 1/100,000 years. Additional slide complexes in the Nordic Seas demonstrate similar behaviour, which has already been documented, such as the Trænadjupet and Nyk slides, both of which have been triggered since the LGM from the same slide scar (3,400-2,600 years Cal BP and 21-19,000 Cal BP respectively (Lindberg *et al.*, 2004; Allin *et al.*, in prep)). This work highlights that more than one slide can occur per glacial cycle from the Storegga Slide Complex, as well as other Norwegian continental slope slide complexes (Figure 3.28). Submarine slides do show some correlation with deglaciation, indicating that a recently deglaciated slope is at the greatest risk of failure within 7,000 years of deglaciation.

3.8.6.2 Implications of the 56 ka Tampen Slide for tsunami hazards

Whilst each slide is potentially tsunamigenic, few tsunami deposits have been identified within this period. Slides of the volume of Storegga have the potential to generate a tsunami, but modelling work has shown smaller slides are also tsunamigenic, with a volume of 60km^3 being sufficient to generate a wave (Berndt *et al.*, 2009). The new date of 55.9 ± 4 ka BP has significant implications for northern European Coastlines. The potential volume of the Tampen Slide and considerable turbidite volume, suggests the slide behaved in a comparable manner to the 8.17 ka BP Storegga Slide. The rapid evacuation of the Holocene Storegga Slide is known to have generated a large tsunami capable of traversing the North Atlantic. Seismic reflection interpretations within the Storegga Slide Complex identified the Tampen Slide scar as overlapping with the Holocene Storegga Slide scar, and extending for more than 200 km further to the south (King *et al.*, 1996; Bryn *et al.*, 2003; Solheim *et al.*, 2005; Reiche *et al.*, 2011). Where present in seismic reflection profiles, the Tampen Slide headwall height is less than 220 m in comparison to the 250 m height of the Storegga Slide headwall (Bryn *et al.*, 2005; Solheim *et al.*, 2005). The volume of sediment involved in the Tampen Slide failure has been estimated at 1500 km^3 to 3000 km^3 (Evans *et al.*, 1996; Nygård *et al.*, 2005). Evidence from core 88 and from seismic reflection profiles across the turbidite deposits in the Ægir Ridge, suggest that the Tampen Slide is three-to-five times larger than the Storegga Slide. The impacts of tsunamis wave from the Storegga Slide have been mapped on Norwegian, Faroe, Greenland and UK coastlines (Bondevik *et al.*, 1997; Grauert and Bjo, 2001; Bondevik *et al.*, 2005; Wagner and Bennike, 2007; Bondevik *et al.*, 2012; Vasskog *et al.*, 2013). It cannot be proven that the Tampen Slide generated a tsunami, the scouring action of the MIS 2 ice sheets has removed the majority of coastal sediments > 29 ka Cal BP, but records of coastal or shallow marine sediments dating from MIS 3 should be re-examined for evidence of a tsunami. The much larger size of the Tampen Slide volume suggests a larger potential tsunami hazard compared to a repeat of the Storegga Slide.

3.9 Future work

Further research is needed to accurately date previous slides from the Storegga Slide Complex and surrounding the Lofoten Basin. Accurate dating using a multiproxy approach across the late Quaternary will allow the glacial transition hypothesis to be tested.

The thickness of the Storegga and Tampen deposits prohibits deeper piston coring in the proximal areas, yet the 3.5 KHz data suggests that off-rift zones to the west of the main Ægir Ridge may contain a condensed record of late Quaternary turbidites. The approach taken here should allow discovered turbidites to be assigned a provenance from the Norwegian continental slope.

3.10 Conclusions

The age of the penultimate slide from the Storegga Slide Complex, has been dated to 55,900 ± 4,000 years Cal BP. This re-assessment of slides from the Storegga Slide Complex has reduced the estimated recurrence interval from one slide per 100,000 years to two in last 60,000 years. This is consistent with the Trænadjupet/Nyk slide complex, which has seen at least two failures in the last 25,000 years. The new date challenges the original interpretation of preconditioning and triggering of mega-slides requiring a full glacial-interglacial transition between slides. The Storegga Slide Complex has failed twice within the last glacial cycle. Both slides occur within 2-7,000 years after the retreat of ice streams from the shelf edge and rapid sedimentation ceased.

A tsunami of the magnitude of the 8.2 ka BP Storegga event today, would represent a serious geohazard to northern European coastlines. The combined effects of damage to coastal populations, offshore infrastructure, and coastal Nuclear Power Stations would be catastrophic to the UK and Norway, with significant damage expected in locations where the Storegga tsunami has been detected. This includes low lying coastal areas such as the Netherlands and Denmark, coastal settlements of East Greenland, the Faroe Islands and Iceland.

This new date of the Tampen Slide has important implications for the UK, as the slide frequency now exceeds the threshold of 1/100,000 years for consideration in the UK risk register. In particular, this highlights the ongoing risk to glacially influenced margins worldwide. This new date provides important further evidence of a potential climate change role in the preconditioning of passive continental slope failures, but cannot provide a definitive cause. Further accurate dates within the context of local environmental changes are necessary for submarine slides across the Lofoten Basin and Svalbard. Particular attention

should be paid to regions currently experiencing rapid glacial retreat and ocean warming, where no recent significant slide has occurred, such as Svalbard and East Greenland.

Chapter 4 The climatic and environmental conditions preceding the Storegga and Tampen Slides: examining the relationship with global climatic change.

4.1 Abstract

Submarine landslides from the Storegga Slide complex are amongst the largest slope failures worldwide, and generate trans-oceanic tsunamis. The most recent failure from the Storegga Slide Complex occurred concurrently with the coldest period of the 8.2 ka climate event: a brief interruption to otherwise continual Northern Hemisphere warming since the Last Glacial Maximum (LGM, 26-19 ka BP). Of the five known slides of the Storegga Slide Complex, the Holocene Storegga Slide and the Tampen Slide are the only slides to have been dated from sedimentary archives. Dates for the older slides rely on seismic correlation, and were discussed in chapter 3. The new date for the Tampen Slide from a marine sediment core revised the projected age from 125 ka BP, to 55.9 ± 4 ka BP. This new date placed the slide in the early stages of MIS 3, a comparatively warm period across Europe and Scandinavia, suggesting a previously proposed theory of slide generation linking deglaciation to preconditioning is valid, but the magnitude of environmental change required is less than the deglacial changes observed from MIS 2-1. This chapter evaluates the environmental records contained within the sediment core from the Ægir Ridge, in addition to the wider environmental changes in the Arctic and Sub-Arctic regions. These analyses place the Tampen Slide in an environmental scenario that is found to be similar to the Holocene Storegga Slide. Both slides are found to occur within 2-10 ka of terrestrial deglaciation, within a climate comparable to the modern. Both also occurred in association with oceanic anomalies that are linked to significant surface water freshening, potentially both as a result of glacial lake outbursts generated by the decay of ice lakes. The Tampen Slide is placed here within Greenland Interstadials 14-17, a period of notable rapid and significant temperature changes between 7-12.5°C occurring over cycles of 200-600 years. These similarities suggest that regions known to be vulnerable to failure and that have not failed throughout the deglacial or Holocene should be identified in order to assess current risk to infrastructure and populations. The timing of the Tampen failure suggests that significant and rapid environmental changes are an important indicator of enhanced risk to Arctic slopes. Locations with slide scars with a history of repetitive failures, where the slide scar that has had suitable time to recharge with sediment and have undergone later deglaciation (5-6 ka BP), pose the greatest risk of modern failure under our current climatic regime.

4.2 Introduction

The Norwegian, Greenland and Icelandic seas play a crucial role in the Atlantic Meridional Overturning Circulation System (AMOC) and are sensitive to Milankovitch induced climate changes (Fronval and Jansen, 1997). During glaciations these high latitude ocean basins are surrounded by continental ice sheets and are the most northerly limit of the North Atlantic thermohaline circulation. Foraminifera extract oxygen and carbon from the ocean and combine with calcium ions to produce the carbonate in the tests. Thus, the foraminifera carbonate records the $\delta^{18}O$ of the ocean of the time. Changes in the $\delta^{18}O$ of past foraminiferal tests preserved in continually-accumulating hemipelagic sediments on the seafloor record past changes in the $\delta^{18}O$ of sea water in high latitude ocean basins. Changes in ocean $\delta^{18}O$ are primarily controlled by the volume of global ice sheets, ocean temperature and salinity (Bauch *et al.,* 1996; Fronval and Jansen, 1996, 1997; Bauch and Weinelt, 1997; Jansen *et al.,* 2000; Kandiano *et al.,* 2004; Risebrobakken *et al.,* 2005).

A key control over North Atlantic climate is the passage of surface Atlantic Water into the Arctic Ocean and the outflow of Norwegian Sea Deep Water (NSDW) formed in the Nordic seas , which are a major component of the North Atlantic Deep Water (NADW) across the Iceland Scotland Ridge (Andruleit and Baumann, 1998; Rasmussen and Bäckström, 2002; Risebrobakken *et al.,* 2005; Bauch and Erlenkeuser, 2008; Giraudeau *et al.,* 2010; Aagaard-Sørensen *et al.,* 2014). Variable ocean current circulation strength during the late-Glacial and Holocene, in addition to duringMIS 6-to-4 has been demonstrated in previous studies (Bauch *et al.,* 2001; Bauch and Erlenkeuser, 2008; Telesiński *et al.,* 2015). During the Last and Penultimate Glacial Maximums (LGM (MIS 2) and PGM (MIS 6), respectively), landmasses surrounding the Nordic seas hosted massive ice sheets, enriched in the lighter $\delta^{16}O$ isotope (Rasmussen *et al.,* 2006). The current circulation mode supports the mild climate of western Europe, representing a typical interglacial climate mode. This mode of circulation has been periodically interrupted by short lived stadial (cold) events, associated with weakened circulation, the most recent of which occurred c. 8200 years Cal BP, hereafter referred to as the 8.2 ka climate event. During this period, temperature reconstructions from the Nordic seas indicate a cooling of c. 3°C for approximately 70 years (Alley and Agustsdottir, 2005; Risebrobakken *et al.,* 2005). The 8.2 ka climate event was most likely caused by the final catastrophic drainage of a large ice-dammed lake that bordered the remnants of the Laurentide Ice Sheet (LIS), known as the pro-glacial Lake Agassiz-Ojibway, which released c. 100,000 km^3 of cold, fresh water into the North Atlantic. This outburst-flood event inhibited sinking of dense, salty water during ocean current circulation, and slowed the AMOC (Clarke *et al.,* 2004; Hillaire-Marcel *et al.,* 2007; Kleiven *et al.,* 2008; Lewis *et al.,* 2012).

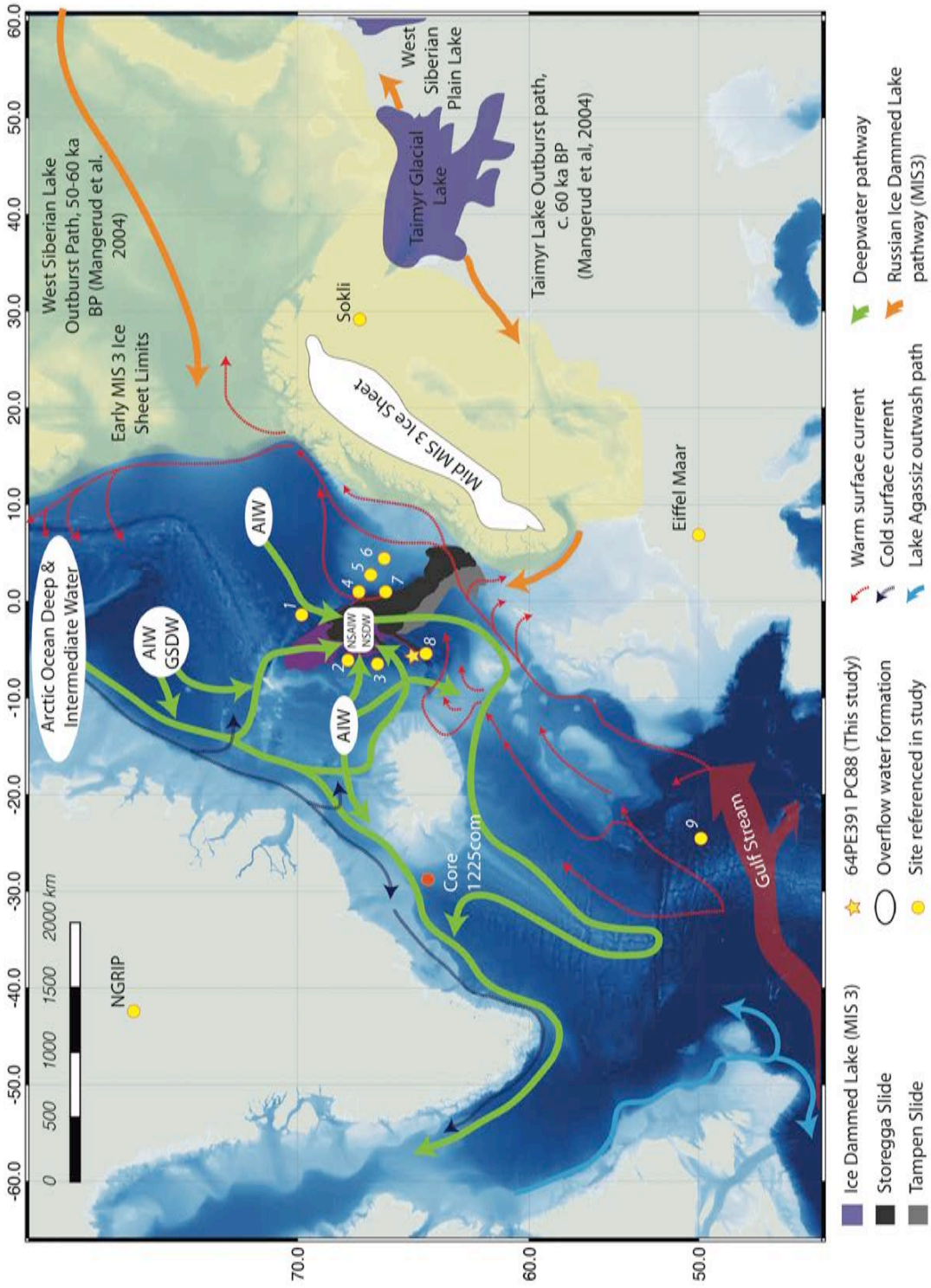

Figure 4.1: Map showing location of the sediment cores used in this study (64PE391 PC88), the location of the Storegga and Tampen slides (adjusted from Haflidason et al. (2005), Bugge et al. (1987), Belanger and Streeter (1982) and this study. Orange circle indicates core JM96-1225com, yellow circles relate to cores referenced in this chapter: 1- DSDP 345, 2 – VM28-56 (Kellog, 1977), 3 – ODP 985, 4 – ODP 643, 5 –ODP 642, 6 – ODP 644, 7 – VM27-86, 8 – DSDP 337, 9 – DSDP 609/U1308. Deep currents (solid lines) and surface currents adapted from Rudels et al.(1991), Hansen et al.(2000) and Blindheim et al.(2004), North Greenland Ice Core Project (NGRIP), Glacial Lake outburst flood pathways from Mangerud et al.(2004) and Hillaire-Marcel et al.(2007).

The 8.2 ka climate event is of interest in landslide-tsunami studies due to the remarkable coincidence of the timing of the coldest excursion of the 8.2 ka climate event with the timing of the Storegga Slide and tsunami (Bondevik *et al.,* 2012). The possibility of a relationship between past rapid climate change events, such as the 8.2 ka climate event, and landslide triggering requires attention, given the potential analogue to present-day accelerated global warming. The 8.2 ka climate event sits within a longer period of cooling between 8.65 and 8.00 cal ka BP (Rohling and Pälike, 2005), with a pronounced cold excursion at 8.15-8.05 cal ka BP (North Greenland Ice Core Project (NGRIP) $\delta^{18}O$ record; Rohling and Pälike, 2005). The date of the drainage of Lake Agassiz-Ojibway is estimated as 8.33 cal ka BP (range 8.04-8.49 cal ka BP), based on detrital carbonate layers accumulated within the Hudson Strait (Figure 4.1). The dates of the excursion show that the Storegga Slide occurred during this climate anomaly, yet a better approach to assess the temporal relationship between the 8.2 ka event and the Storegga Slide is to develop a climate record from a core in which the landslide deposit has been preserved. This would allow a precise comparison between the date of the onset of climate anomalies and slide triggering. If the older Tampen Slide (55.9 ± 4 cal ka BP, chapter 3) is shown to have occurred during a similar past climate anomaly, this would present strong evidence to suggest a causal link between rapid climate change and tsunamigenic landslides.

The new date of the Tampen Slide (55.9 ± 4 cal ka BP, chapter 3) dates the slide to early Marine Isotope Stage 3 (MIS 3 defined here as between 57 and 29 cal ka BP; Lisiecki and Raymo, 2005). During this time period, relative climate warming extended over much of western Europe (Helmens *et al.,* 2007; Sirocko *et al.,* 2015). Modelling the stability of ocean currents shows the AMOC to be more sensitive to freshwater perturbations during MIS 3 than MIS 1 (Zhang *et al.,* 2014). The effect of this heightened AMOC sensitivity is evident in the NGRIP $\delta^{18}O$ climate record, expressed during late MIS 4 to early MIS 3 (64-38 ka BP) as nine rapid and significant temperature fluctuations of 8-15°C, which occur over short timescales of 200-to-2,000 years (Huber *et al.,* 2006). Climate records extending to the last interglacial have shown evidence of comparable freshwater melt outbursts from the LIS during MIS 5e (123-109 ka BP (Nicholl *et al.,* 2012)), with further MIS 3 and 4 freshwater melt outbursts reported from Europe/Russia (Valen *et al*. 1995; Mangerud *et al.,* 2001; Mangerud 2004; Svendsen *et al.,* 2004; Larsen *et al.,* 2009; Helmens *et al.,* 2009; Astakhov 2014).

This chapter will examine the $\delta^{18}O$ stratigraphy of a sediment core from the Ægir Ridge containing the turbidite from the Tampen Slide, and examine the climatic context of environmental change preceeding and post-dating the deposition of both turbidites from the Storegga and Tampen slides. The $\delta^{18}O$ in foraminiferal tests reflect the ocean water conditions at the time the organism lived. Ocean water isotopic composition in turn reflects global ice volume changes, temperature and salinity. Through the identification of short and long term cycles in the $\delta^{18}O$

record of planktic and benthic foraminifera within the core, conditions at time of deposition of two mega-turbidites can be placed into a climatic context (Lekens *et al.,* 2006; 2009; Rabassa and Ponce, 2013). This analysis will allow the relative timing of deglaciation and the slides to be assessed, and the uncertainty of the date for the Tampen Slide reduced, by identifying the shifts from cold, glacial conditions (MIS 2, 4 and 6) to warm interglacials (MIS 1, 3 and 5).

Furthermore, significant regional climate events in the Nordic and Arctic seas preceeding both slides are discussed with reference to preconditioning the continental slopes for failure. Stable isotope analysis shows a reconstruction of the dominant ocean currents, sea surface temperatures and ice sheet volumes. Examining the similarities between the preceding environmental conditions before both the Tampen and Holocene Storegga slides allows an assessment of the potential preconditioning and triggering factors.

4.3 Aims

This chapter addresses two key questions: (1) did the Tampen Slide occur during glacial or interglacial conditions; and (2) how similar are the palaeoclimatic conditions (temperature, ice volume and dominant ocean currents) surrounding both the Tampen and Holocene Storegga slides. The comparison of the ratios of $\delta^{18}O$ and $\delta^{13}C$ provide proxies for changes in sea surface temperature and salinity, and the origin of deep-water water masses at the time of each slide. This is the first study to analyze the palaeoenvironmental conditions preceding two mega-slides from the Storegga Slide Complex, and allows an assessment of the preconditioning factors for both events. The identification of characteristic sea surface and deep-water conditions at the time of these slides may offer insights into current analogous seafloor regions at risk from slope failure surrounding the North Atlantic and Arctic oceans.

4.4 Background

The Ægir Ridge was chosen as a location to core non-erosive, distal turbidites from mega-slides originating from the Storegga Slide Complex (SSC) and to capture an environmental record of past climate change from the hemipelagic sediments. The dating of these turbidites is described in chapter 3. Slides from the Storegga Slide Complex, a 270 km long stretch of the Norwegian continental margin, have been extensively investigated (Bugge *et al.,* 1987; Evans *et al.,* 1996, 2005; Haflidason *et al.,* 2005). Five slides have been identified, and ages assigned to them on the basis of correlating seismic reflection packages into the slide scar, which are tied to boreholes on the Norwegian continental margin (Bryn *et al.,* 2005; Solheim *et al.,* 2005).

The suggested timing of these slides has been correlated to the retreat of major ice sheets, approximately in phase with major Northern Hemisphere glaciations with an estimated slide recurrence interval of 100 ka (Solheim *et al.,* 2005). Each slide was suggested triggered following a delay after deglacation, during which time post-glacial seismicity would be highest, and the continental slopes preconditioned with heavy sediment load during the glacial period (Evans *et al.,* 1996; Bryn *et al.,* 2003; 2005). The only slide to have been accurately dated is the Holocene Storegga Slide, from marine records of the slide (Bugge, 1983; Bugge *et al.,* 1987; Jansen *et al.,* 1987; Haflidason *et al.,* 2004; Paull *et al.,* 2010) and terrestrial records of the resulting tsunami (Bondevik *et al.,* 1998; Wagner and Bennike, 2007; Romundset and Bondevik, 2011; Vasskog *et al.,* 2013; Long *et al.,* 2016). The theory of slide preconditioning has not been sufficiently tested with respect to the four older slides: the Tampen Slide (~150-130 ka BP), Slide R (~300 ka BP), Møre Slide (~ 400 ka BP) and Slide S (~500 ka BP), which were dated through correlation of slide deposits identified in seismic reflection profiles tied to a dated drill-core (Solheim *et al.,* 2005). The distal turbidite from the Tampen Slide was successfully penetrated in a sediment core collected from the Ægir Ridge, and the deposit dated to 55.9 ± 4 ka BP (chapter 3), almost 70 ka younger than anticipated.

Benthic foraminiferal carbonates record an isotopic composition that reflects the composition and temperature of bottom waters (Waelbroeck *et al.,* 2002; Lisiecki and Raymo, 2005; Grant *et al.,* 2014). Records of temporal variations in benthic foraminifera $\delta^{18}O$ have been stacked to highlight global trends in climate known as the LR04 stack (Lisiecki and Raymo, 2005). This data stack was created to allow any benthic $\delta^{18}O$ record to be temporally aligned to this record. This record provides dates for transitions between MIS stages, and the timing of glacial-interglacial transitions and can be used to place the turbidites representing the Storegga mega-slides in the context of glacial and interglacial changes.

A spliced, dual species profile of benthic oxygen is necessary in the Nordic seas (Bauch *et al.,* 1996, 2000; Billups *et al.,* 2011; Telesiński *et al.,* 2015). A spliced profile is required as different species are present during glacial and interglacial periods, with very limited overlap: *Cibicidoides wuellerstorfi* is typical of the Nordic seas assemblage during periods of ice free summers (Belanger and Streeter, 1980; Streeter *et al.,* 1982; Cortijo *et al.,* 1997; Vidal *et al.,* 1998); whereas the glacial period $\delta^{18}O$ is represented by *Oridorsalis umbonatus*. Isotopic analyses of different species can be mathematically corrected either through the use of a standard offset, or the use of a least squares regression of results from the two species studied. Standard offsets are well established for $\delta^{18}O$, but is more complex for $\delta^{13}C$, for which a regression is preferred (Katz *et al.,* 2003).

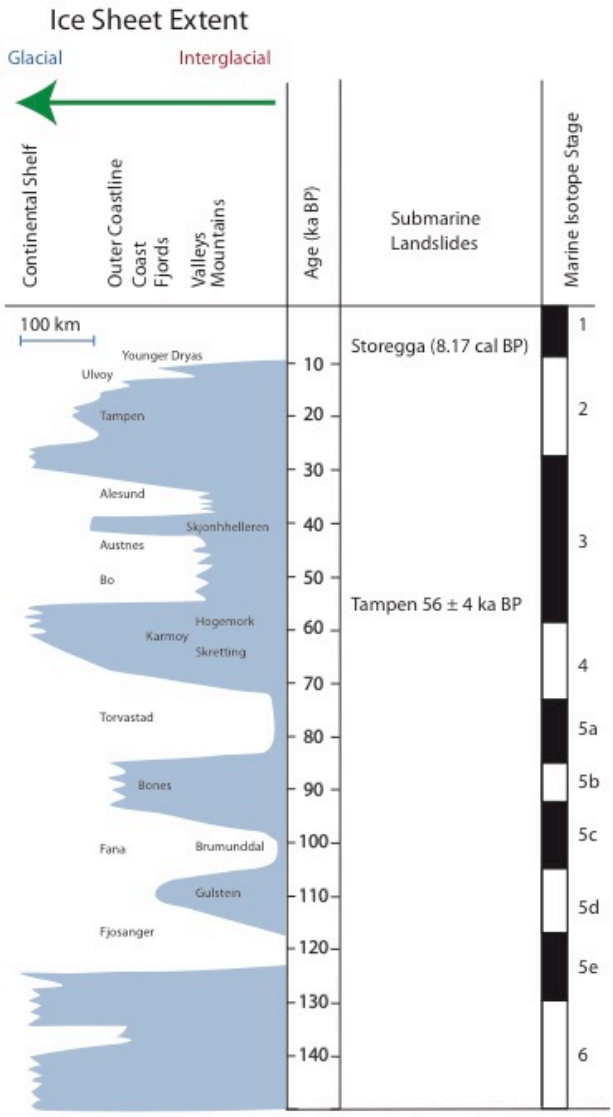

Figure 4.2: The glacial history of Fennoscandia (Mangerud et al. (2011), including the previously estimated dates of the Storegga and Tampen Slides (Solheim et al. (2005). MIS Boundaries from Lisieki and Raymo (2004).

4.5 Material and Methods

4.5.1 Piston cores PC88 and PC84

This study utilises two piston cores recovered in 2014 during the 64PE391 cruise on the *RV Pelagia*. This cruise collected 88 cores across the Norwegian and Lofoten basins. Cores PC84 and PC88 were selected from a collection of seven adjacent cores taken at the south-western tip of the Ægir Ridge. The coring sites were targeted on the basis of previous cruise JR50, which collected the acoustic sub-bottom profiler image in figure 3.5 (collected in 2001, R. Larter, *pers comm.)* that documented two large acoustically transparent units interbedded within thin stratified sequences, believed to be the deposits of the last two submarine slides from the Storegga Slide Complex. The analysis and initial dating of these beds is documented

in chapter 3. Core OC 84 contains an additional unit only present in this core. The unit is a 13 cm thick section of hemipelagite above the Tampen Slide deposit an below the debrite bed. This unit is included in the stratigraphy as it demonstrates the palaeoenvironmental conditions in the Nordic seas immediately following the Tampen Slide.

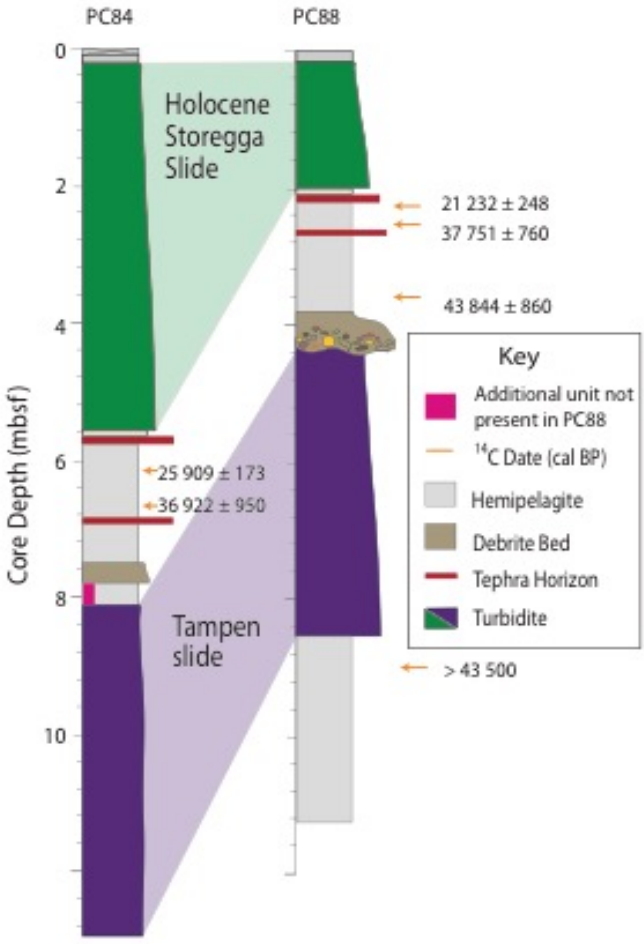

Figure 4.3: Lithological log to show the units discussed in this chapter from PC84 and PC88. The green unit represents the Holocene Storegga Slide in both core PC88 and PC84, the purple unit represents the Tampen Slide in both cores, as identified in chapter 3. Note the additional unit in PC84 immediately above the Tampen turbidite which is used in the stable isotope reconstruction.

4.5.2 Core logging and scanning

Cores were visually logged for variations in colour and grain-size using a visual grain-size comparator (Figure 4.3). Particular focus was applied to identifying mass transport deposits (glacigenic debris flows and turbidites) and hemipelagic sediments. This is critical when constructing palaeoenvironmental records, as sediments deposited as turbidites cannot be used to interpret environmental parameters, and are removed from the record to study climate change. This is detailed in chapter 3.

XRF element counts from the ITRAX core scanner (BOSCORF) are considered reliable indicators of major elements (Croudace *et al.,* 2006). Calcium counts are a well-established proxy for $CaCO_3$ content, which is a useful high-resolution tool to aid the analysis of the hemipelagic carbonate content that can be correlated to planktic foraminfera isotope stratigraphy in the North Atlantic (Richter *et al.,* 2006; Brendryen *et al.,* 2010). High-resolution ITRAX down-core analysis can identify sub-cm geochemical variations, which can be correlated to temporal variations in the NGRIP $\delta^{18}O$ record. This proxy is reliant on the relationship between productivity in Nordic Seas surface waters, and changing temperature conditions on the Greenland Ice Sheet. Interglacial cycles and Greenland Interstadials are characterized by warmer surface ocean conditions, and higher productivity/biogenic carbonate production. This is typically represented in the sedimentary record by lighter, coarser-grained hemipelagite and has been successfully used as a correlative tool to the dated NGRIP record (Lekens *et al.,* 2006; Richter *et al.,* 2006; Brendryen *et al.,* 2010; Hibbert *et al.,* 2010). An additional proxy useful in the identification of rapid climate changes is the ratio of Ti/K. The erosion and transport of magnetic minerals from the Iceland-Scotland Ridge is enhanced during cold periods (Lekens *et al.,* 2006; Richter *et al.,* 2006; Brendryen *et al.,* 2010). This results in an antiphase correlation between Ca and Ti/K records that has been used to define the boundaries of Greenland Interstadials in the Nordic seas (Richter *et al.,* 2006; Brendryen *et al.,* 2010). During warm periods, the concentration of Ti/K is diluted by enhanced biogenic carbonate flux. Full downcore ITRAX data are available in digital Appendix 2b.

Operating conditions for all ITRAX analyses were 30 kV and 30 mA with a dwell time of 30 seconds. The resolution for core PC88 was 500 µm, and core PC84 was 200 µm. These two records were spliced together to capture the hemipelagic unit directly above Unit 9 (chapter 3), which is only present in core PC84.

4.5.3 Stable isotope analysis

To create a down-core record of stable isotope variations, samples were taken every 1 cm down core through the hemipelagic units in cores PC84 and PC88, and dried at 40°C for 48 hours. The dried samples were weighed and washed through a 63 µm sieve. From each 1 cm^3 washed sample 8 specimens of the planktic species *Neogloboquadrina pachyderma sinistral (NPS*) with a size between 150-212 µm were selected for analysis of stable carbon and oxygen isotopes ($\delta^{13}C_{plank}$ and $\delta^{18}O_{plank}$). This analysis allows an interpretation of sea surface temperature/salinity. For benthic analyses to indicate water mass provenance, three specimens of epifaunal *Cibicidoides wuellerstorfi* or 6-18 specimens of the infaunal species *Oridorsalis umbonatus* were selected from the same samples.

All stable isotope samples were analysed at the NERC Isotope Geosciences Laboratory, British Geological Survey in England. Analyses were performed using an IsoPrime dual inlet mass spectrometer plus Multiprep device. Samples were loaded into glass vials and sealed with septa. The automated system evacuates the vials and delivered anhydrous phosphoric acid to the carbonate at 90°C. The evolved CO was collected for 15 minutes, cryogenically cleaned and passed to the mass spectrometer. Isotope values ($\delta^{13}C$, $\delta^{18}O$) are reported as per mille (‰) deviations of the isotopic ratios ($^{13}C/^{12}C$, $^{18}O/^{16}O$) calculated to the VPDB scale using a within-run laboratory standard calibrated against NBS-19 (McCrea, 1950). The calcite-acid fractionation factor applied to the gas values is 1.00798 (Friedman and O'Neil, 1977). Due to the long run time of 21 hours a drift correction is applied across the run, calculated using the standards that bracket the samples. The Craig correction is also applied to account for $\delta^{17}O$ (Craig, 1957). The average analytical reproducibility of the standard calcite (KCM) is 0.05‰ for $\delta^{13}C$ and $\delta^{18}O$. Full data for the stable isotope analysis can be found in the digital Appendix 2c.

Both carbon and oxygen isotope values in benthic foraminfera require correction to account for the quantified departure from the established isotopic calcite equilibrium for $\delta^{18}O_{benth}$ in both *C. wuellerstorfi* and *O. umbonatus*, a correction of +0.64 and 0.36 ‰ (respectively) was applied to the benthic $\delta^{18}O$ results (Duplessy *et al.,* 1988). For correction of the $\delta^{13}C_{benth}$ values to account for differences in infaunal and epifaunal habitats, sample depths yielding both species were identified at 19 sample depths. Results from these analyses were used to establish a relationship using linear regression to allow *O. umbonatus* to be corrected to comparable values demonstrated by *C.wuellerstorfi* specimens (Figure 4.7).

4.5.4 Chronology

An accurate chronology is required before interpreting the palaeoenvironmental proxies, as it allows the submarine slides to be confidently discussed within an independent stratigraphic chronology. A chronology for this core was created using a multiproxy approach, with methodologies applicable to the last 500 ka BP. A full discussion of the chronology of the core can be found in chapter 3.

4.5.4.1 Radiocarbon

AMS radiocarbon dating offers a well-tested approach to dating marine sediments NPS from cores PC88 and PC84 were dated using Accelerator Mass Spectrometry (AMS). Radiocarbon ages were converted to calibrated ages using the online Oxcal program with the Marine13 database (Reimer, 2013). Dates were calibrated using the suggested regional reservoir correction of 20 ± 30 years (Mangerud *et al.,* 2006). Uncertainty surrounds the radiocarbon reservoir correction, in particular surrounding Heinrich Events, where it has been estimated

at 1,200 years (Voelker *et al.,* 1998b; Waelbroeck *et al.,* 2001). This study does not address this uncertainty directly due to the low sedimentation rate of the core (2.6 cm/ka).

4.5.4.2 Coccolith

Coccolith abundance and changing species dominance has been used across the Nordic seas as a chronological tool that extends beyond the radiocarbon limit (Gard, 1988). An established record of variations in relative abundance and barren zones of coccoliths has been successfully used to provide datum horizons in cores from the Nordic seas (Gard, 1988; Backman *et al.,* 2009; Pope *et al.,* 2016). Within MIS 1-6, six species are used to define datum horizons: *Emiliania huxleyi, Gephyrocapsa mullerae, Gephyrocapsa caribbeanica, Gephyrocapsa apperta, Calcidiscus leptoporus* and *Coccolithus pelagicus*. These horizons and their defining characteristics are detailed in table 2-1, p80. Relative abundances were determined from $1mm^3$ of hemipelagic sediment smeared across an SEM stub. Species were counted using a *Hitachi* TM1000 scanning electron microscope (SEM) in BOSCORF. The high magnification of 1,000-10,000x allows rapid capture of high-resolution images for species identification. Species were counted across 15 fields of view at 2,000x magnification to a total of at least 300 specimens (Hunt *et al.,* 2013).

4.5.4.3 Tephra

Marine sediments of the North Atlantic preserve a record of Icelandic and Jan Mayen tephra (Lacasse *et al.,* 1996). Each eruption has a unique geochemical composition relative to other eruptions from the same province, and volcano (Haflidason *et al.,* 2000). When combined with existing stratigraphic information an accurate chronology can be established through a technique called tephrochronology. Tephrochronology offers an additional approach to dating marine and terrestrial sediments beyond the radiocarbon limit. The identification of tephra horizons within cores that can be linked to known and dated tephra horizons in marine, terrestrial or ice core records, provide isochronous age markers across the Northern Hemisphere. Tephra grains were identified from the > 150 μm fraction of the samples taken for stable isotope analysis. Full analysis of the tephra results can be found in chapter 3. Every other cm through the cores, a fraction of the sample was counted for IRD and tephra grains. Where peaks in IRD or tephra were identified, counting frequency was increased to every cm. Count numbers per sample were converted to number of grains/shards per dry gram of sediment to identify peaks in concentration. Those tephra identified were classified by colour as rhyolitic or basaltic shards.

Tephra shards were selected from identified concentration peaks, mounted on glass slides and ground down to reveal c. 20 shards on the exposed surface. Electron probe micro-analysis (EPMA) was performed using the *Cameca* SX100 at the Tephra Analysis Unit (TAU),

University of Edinburgh. For full details of analytical conditions see Hayward (2012). The major element concentrations were used in association with stratigraphical data from the cores to identify a volcanic provenance and likely source eruption.

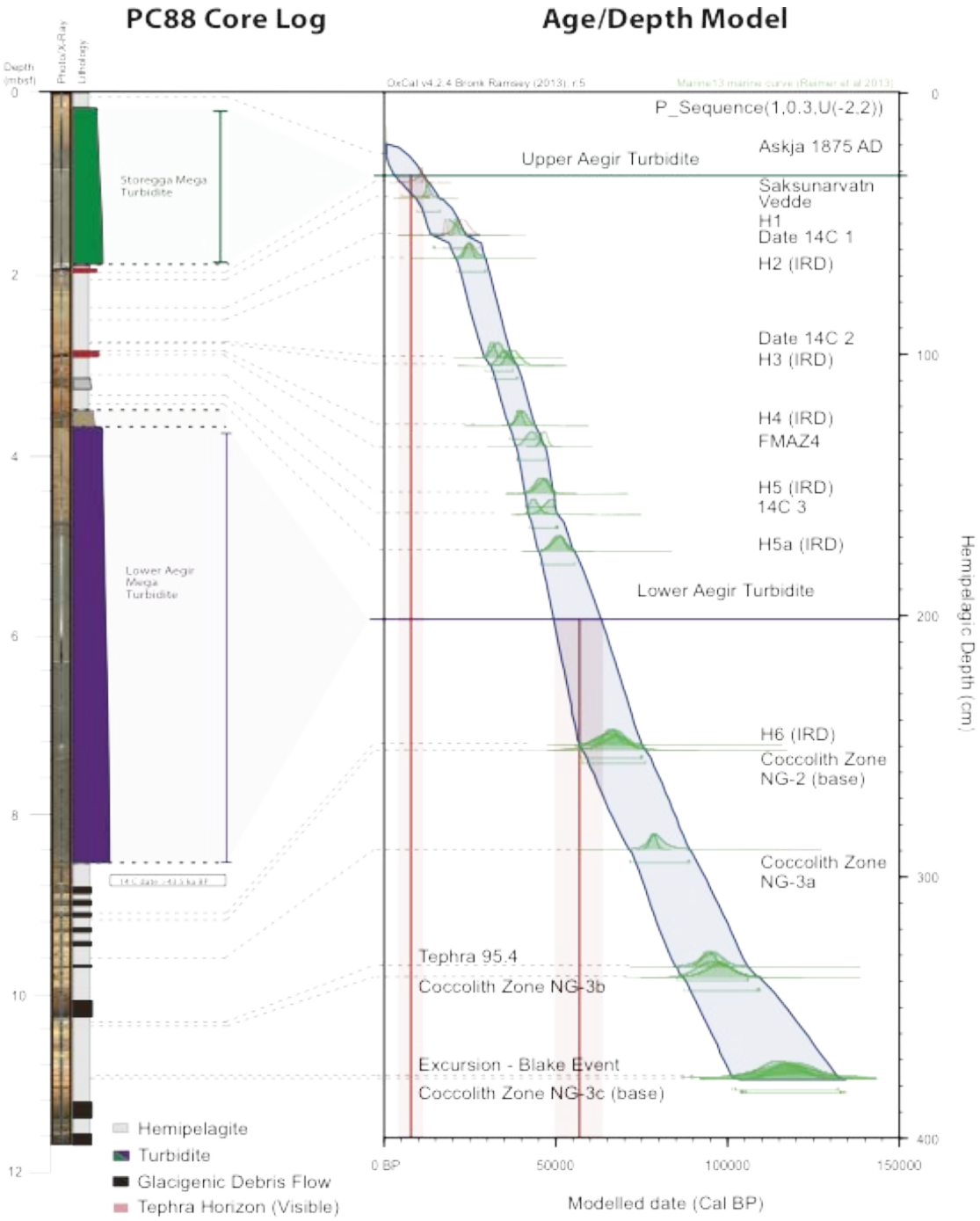

Figure 4.4: Age model for core PC88 showing identified chronological markers in Chapter 3, and the relative position of the Storegga and Tampen turbidites.

4.5.4.4 IRD

Ice Rafted Debris (IRD) is coarse grained (> 150 μm) sediment deposited by the melting of icebergs. Icebergs have been released from the Northern Hemisphere ice sheets during glacial and deglacial periods, and as a result horizons of IRD have developed across the North Atlantic as far south as 40° (Heinrich, 1988; Bond and Lotti, 1995; Hemming, 2004). These

events are broadly synchronous between the Fennoscandian and Greenland ice sheets and are labelled Heinrich Events. These Heinrich Events provide both datum horizons and an indication of ice sheet retreat.

4.5.4.5 Magnetics

Identification of magnetic excursions within marine sediments has been widely used in the North Atlantic to provide datum horizons beyond the radiocarbon limit (Nowaczyk and Baumann, 1992; Nowaczyk and Frederichs, 1999; Laj *et al.,* 2004; Lekens *et al.,* 2009). Fine-grained sediments retain a record of the intensity of the Earths' geomagnetic field, in addition to the angles of inclination and declination. Magnetic inclination undergoes significant changes over both long (Ma) and short-term (Ka) timescales. The short-lived fluctuations in inclination are termed magnetic excursions (Laj *et al.,* 2004; Thouveny *et al.,* 2004), and are globally synchronous. Magnetic inclination was measured on the 2G Enterprises magnetometer at the University of Southampton. Measurements were performed continuously down core at 1 cm intervals throughout PC88, significant changes in inclination were assessed in the context of additional stratigraphic information to confirm their correlation to dated excursions.

4.6 Results

4.6.1 Chronology

A full discussion about the dating sediment cores PC88 and PC84 is found within chapter 3. The core PC88 contains a hemipelagic sequence interbedded with two megaturbidites which represent the distal deposits of large submarine landslides. The younger turbidite is identified as the Holocene Storegga Slide. The older turbidite is interpreted as the penultimate slide from the Storegga Slide Complex, the Tampen Slide (chapter 3). Chapter 3 details the chronology of the core, and assigns an age of 55.9 ± 4 ka BP to the Tampen Slide, substantially younger than the age of 125 ka BP suggested by earlier works (Bryn *et al.,* 2005; Solheim *et al.,* 2005). Three ash horizons were identified between the two turbidites in core PC88: Saskunarvatn (10,290 years BP (Andrews *et al.,* 2002; Gudmundsdóttir *et al.,* 2011; Lohne *et al.,* Mangerud and Birks, 2013)), Vedde (12,100 years Cal BP (Davies *et al.,* 2001; Lane *et al.,* 2012)) and the Faroe Marine Ash Zone 4 (46,800 years BP (Wastegård and Rasmussen, 2016)). The correlation of major element oxide concentrations to known eruptions is discussed in chapter 3. Each horizon is regionally extensive and can be correlated to similar horizons in marine and terrestrial sediments.

Radiocarbon dates were calibrated using the standard 400-year marine reservoir correction in the Marine13 database, in addition to a 20 ± 30-year regional correction (Mangerud *et al.,* 2006; Reimer, 2013). The deepest radiocarbon date at 288 cm total core depth (43,540 ± 1,660 Cal BP). This date is considered at the limit of radiocarbon dating, and conflicts with the identification of Heinrich Event 5 and Faroe Marine Ash Zone 5 (46,000 ± 1,500 Cal BP and 46,800 ± 1,000 Cal BP respectively), both stratigraphically above the radiocarbon sample depth (Figure 4.3). Heinrich Events 1-6 are identified within the hemipelagic units of PC88 and correlated to previously dated North Atlantic sediment cores with well-dated Heinrich layers (as detailed in Sarnthein *et al.,* 1995; Svensson *et al.,* 2008). Beyond the radiocarbon limit (45.5 ka BP) and Heinrich Event 6 (66,500 years Cal BP) dating is achieved through the identification of coccolith datum horizons and the Blake geomagnetic excursion (117-112 ka BP).

Dating of the Holocene Storegga and Tampen turbidites was achieved through interpolation of the horizon at which they were found in the core between chronological markers. This was modelled in OxCal and illustrated in figure 3. The projected age for the upper turbidite is 8 ± 2.1 ka BP, consistent with dates of terrestrial deposits of the Storegga Slide (8.17 ka BP, Bondevik *et al.,* 2012). The older slide has been identified as the Tampen Slide, sourced from the same slide scar as the Storegga Slide, and dated to 55.9 ± 4 ka BP (see chapter 3).

4.6.2 Oxygen Isotope Stratigraphies

Figure 4.5 shows the corrected $\delta^{18}O$ benthic ($\delta^{18}O_{benth}$) values plotted against hemipelagic depth, in comparison to the global benthic $\delta^{18}O$ curve for the last 130,000 years from the LR04 stack (Lisiecki and Raymo, 2004). Chronological tie points identified in chapter 3, used to date the hemipelagic stratigraphy, are shown on Figure 4.5. The positions of the two turbidites are highlighted with a green line (Storegga, 8.2 ka BP) and Tampen with the purple line (55.9 ± 4 ka BP). Significant environmental changes can be identified within the core PC88 benthic isotope profile. Planktic $\delta^{18}O$ (Figure 4.6) reflects variations in surface temperature and salinity, with depleted values representing warmer and fresher surface waters.

The deepest section of the core is complex, with a series of short-lived fluctuations between *O. umbonatus* and *C. wuellerstorfi reflected in the* $\delta^{18}O_{plank}$ record as values fluctuating between 4.2 and 2.8 ‰. The core stratigraphy dates this period to between 123 and 71 ka BP, as such these shorter glacial/interglacial changes are identified as MIS 5, which is subdivided into well defined warm and cold periods of between 5,000 and 10,000 years long (Lisiecki and Raymo, 2004). Of particular interest are the depths between 379-368 cm, which are dominated by *O. umbonatus*

yet display lighter values than expected for a glacial period (< 3.9 ‰) due to the depletion in surface ocean productivity, and increased sea ice cover.

A pronounced enrichment in $\delta^{18}O_{benth}$ values is observed between 269 and 207 cm, throughout which no *O. umbonatus* are observed and $\delta^{18}O_{benth}$ values are > 4.9 ‰. During this period $\delta^{18}O_{plank}$ values decrease to a minima of 4.95 ‰, *indicating cold and saline surface conditions.* This is consistent with glacial conditions and a substantial Northern hemisphere ice sheet. This cold period is interrupted by a short-lived light isotope excursion at 259 and 251 cm in the $\delta^{18}O_{benth}$ record, within this period $\delta^{18}O_{benth}$ values are < 3.8 ‰. This suggests an additional period of anomalously warm/fresh bottom water.

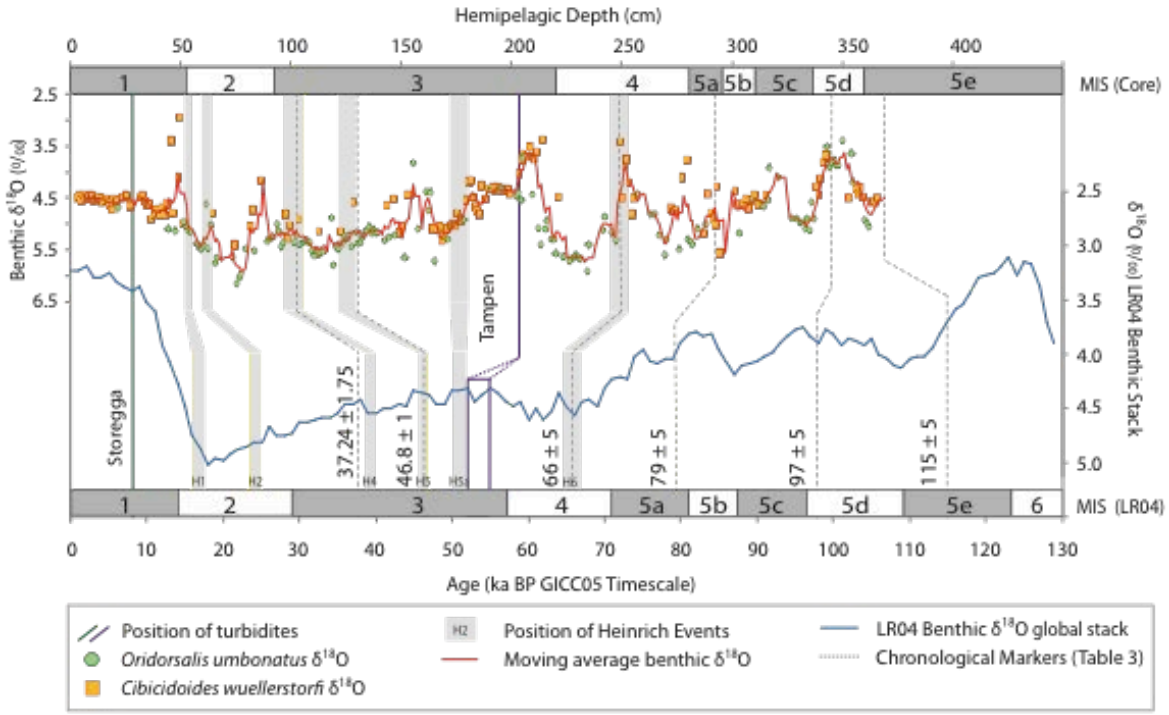

Figure 4.5: Benthic oxygen profile of core PC88 in comparison to the stacked global benthic record of Lisiecki and Raymo (2004). Tie points are taken from dating horizons illustrated in Figure 3.25.

Between core depths 207 and 154 cm, the faunal assemblage is dominated by *C. wuellerstorfi,* and typified by light (c. 4.5 ‰ $\delta^{18}O_{benth}$) isotopic values, consistent with interglacial values. The core depth between 207 and 184 cm is unusually light, with $\delta^{18}O_{benth}$ values as low as 3.2 ‰. Lower $\delta 18O_{benth}$ values indicate an anomalously warm or fresh period. Between 208 – 184 cm an unusually light $\delta^{18}O_{plank}$ isotopic peak is detected, with values consistently below 2.6 ‰. Within this period there is a sharp increase in $\delta^{18}O_{plank}$ values at 199 and 203 cm. This is important for interpreting the climatic context of the Tampen Slide which was deposited at 201 cm, the decrease in $\delta^{18}O_{plank}$ of 0.7 ‰ may be interpreted as a surface freshening or significant decrease in surface temperatures. Both $\delta^{18}O_{plank}$ and $\delta^{18}O_{benth}$ data are consistent with interglacial climates.

The older of the two turbidites, found at 201 cm hemipelagic depth, and represents the Tampen Slide, was deposited during this warm period, 6 cm above the identified glacial-interglacial transition. This demonstrates that the Tampen Slide was triggered following a significant deglaciation. The transition from *O. umbonatus* to *C. wuellerstorfi* at 207 cm is linked to the MIS 4/3 transition (57 ka BP) based on the presence of Heinrich Event 6 at 249 cm (dated to 66 ka BP). This transition is linked to substantial ice sheet retreat in Fennoscandia.

Heavy isotopic values are observed between 64 and 53 cm depth in the $\delta^{18}O_{plank}$ record, ranging from 4.7-4.9 ‰. This correlates to the LGM, dated within the core to 24-16 ka BP, consistent with chronological estimates of maximum ice sheet advance and retreat (Waelbroeck *et al.,* 2001, 2002; Clark and Mix, 2002; Thornalley *et al.,* 2010).

At 50cm hemipelagic depth a clear transition from *O. umbonatus* to *C. wuellerstorfi* is observed (Fig. 4.4). This is in preceeded by a decrease in $\delta^{18}O_{benth}$ values from 5.5 to 4.5 ‰ between 75- and-50 cm. These lighter $\delta^{18}O_{benth}$ values indicate fresher, and warmer bottom waters. The combination of *O. umbonatus* and heavy $\delta^{18}O_{benth}$ are typical of cold water conditions, and persist to 55 cm hemipelagic depth, with a few, lighter isotopic excursions observed in *C. wuellerstorfi* throughout this period. These changes indicate a transition from glacial to interglacial conditions at 50 cm. Immediately before this transition (53-51 cm), Heinrich Event 1 was identified in the core, along with a radiocarbon date 14C1 (54 cm, 20.69 ± 0.4 Cal ka BP, figure 4.3). It is suggested this change correlates to the MIS 2/1 transition, referred to as the last deglacial. Short-lived light isotope events may be generated by short lived warm periods (interstadials) within glacial periods, as detected in the Greenland ice core record; although these events are better detected in the planktic records (Section 4.6.1, Figure 4.6). Numerous short-lived light isotope peaks are visible within the $\delta^{18}O_{plank}$ record between 155 and 50 cm (c. 46 to 18 ka BP), in agreement with the glacial conditions identified from the $\delta^{18}O_{benthic}$ record; whereby excursions in both records are synchronous, reflecting large-scale ocean changes.

A further pronounced cold period is evident at 44 cm depth as a 0.6 ‰ increase to 4.36 ‰**.** This perturbation in an otherwise warming trend is dated in the core to c. 12,100 ka BP, the same horizon as the Vedde tephra, and is also consistent with age estimates for the Younger Dryas of 12,710 ± 52 to 11,546 ± 59 years Cal BP (Bondevik *et al.,* 2006; Bradley and England, 2008; Lohne *et al.,* 2013).

The Holocene section of the core (0-40 cm) displays consistently depleted values of $\delta^{18}O_{plank}$, indicating a period of relative sea surface temperature warmth and stability. Immediately before the deposition of the Storegga Turbidite (green line), a short interval of increased

$\delta^{18}O_{plank}$ is observed (37-35 cm, figure 4.6). This may represent the early stage of the 8.2 ka BP cold event (Alley and Agustsdottir, 2005; Lewis *et al.,* 2012; Long *et al.,* 2012).

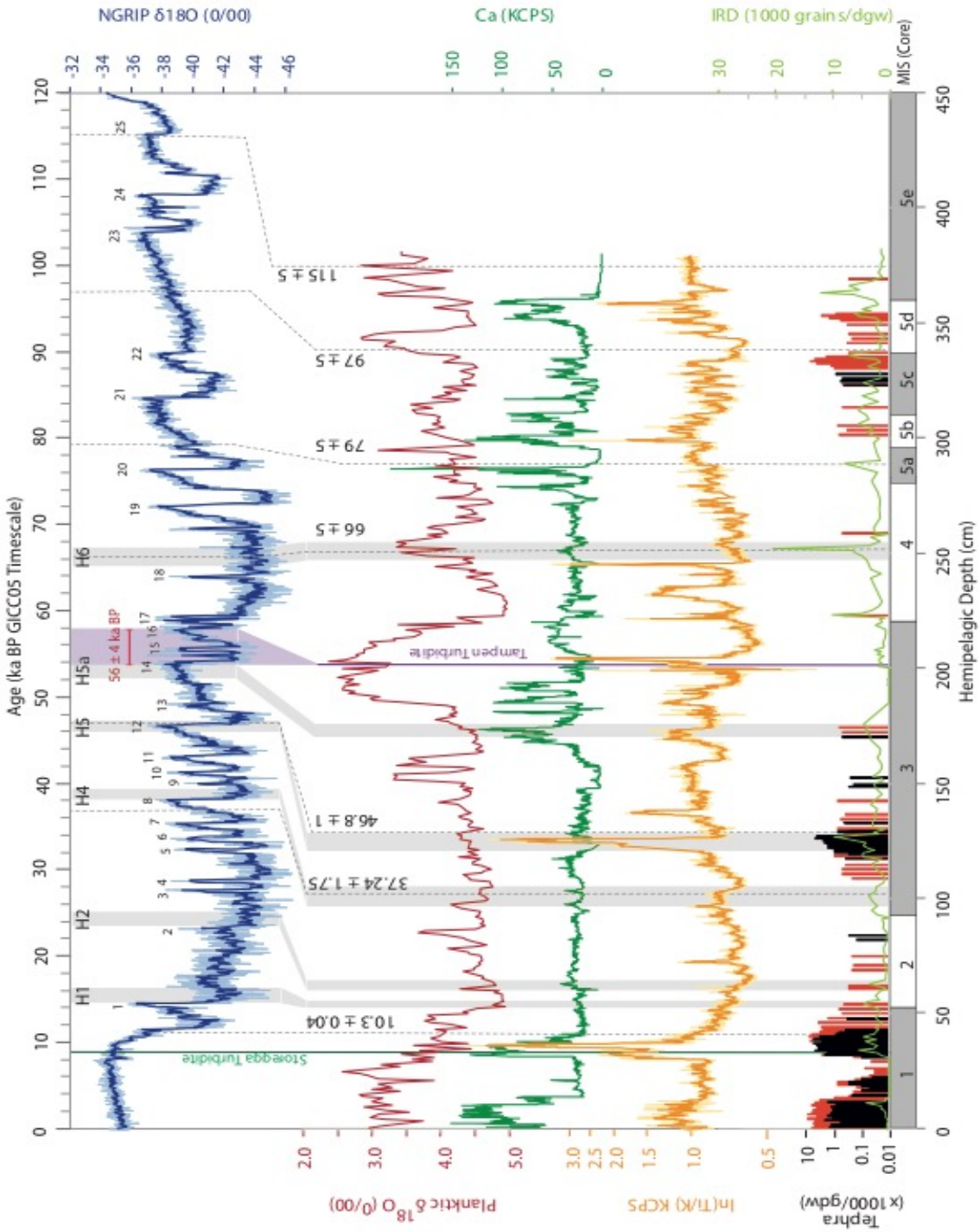

Figure 4.6: Planktic oxygen isotope profile for core PC88 alongside the NGRIP $\delta^{18}O$ record (Rasmussen et al., 2014), the Ca ITRAX data, and the Ti/K record to illustrate glacial period climate changes (after Brendryen et al., 2009). Dashed grey lines indicate age markers detailed in chapter 3. Green line indicates position of Storegga turbidite in the core, and associated uncertainty. Purple line indicates the Tampen turbidite in the core and the associated uncertainty for dating described in chapter 3. Tephra shard counts are shown in black (basaltic) and red (rhyolitic). MIS boundaries taken from Lisiecki and Raymo, 2004. Planktic $\delta^{18}O$ reflects variations in surface temperature and salinity, with depleted values representing warmer and fresher surface waters. Ca is a proxy

for surface ocean productivity, largely driven by the changes in temperature and ice cover of the Nordic Seas. Ti/K is used as a substitute for Ca during cold periods and reflects the increased transport of terrigenous materials during ice ages. Gray dashed lines and dates are the ages established in chapter 3 that are used to tie the proxy record from core PC88 to the NGRIP climate record (Rasmussen et al., 2014), with the estimated uncertainty.

4.6.3 Ca and Ti/K

Positive and negative excursions of the down-core ITRAX Ca record (Figure 4.6) show good correlation to the $\delta^{18}O_{plank}$ profile. Between 155-50 cm and 240-215 cm the Ca profile is relatively stable with values limited to < 25,000 KCPS (Figure 4.6). This is correlated with the periods described for the MIS 4 and MIS 2 glacial periods from the $\delta^{18}O_{plank}$ profile, respectively. Throughout the glacial periods, surface productivity is substantially reduced, reflected here as reduced Ca detection, and thus reduced Ca KCPS. The core depths between 50-0 cm and 210-155 cm show greatly enhanced counts, albeit with considerable variability.

The Ca record demonstrates greater variability than the stable isotope profiles due to greater resolution. The short-lived increases in Ca KCPS throughout the core likely relate to shorter-lived warm periods that temporally increased local productivity above the core site. Down-core variations in the Ti/K ratio are commonly used as an alternative proxy for near-bed bottom water current strength during glacial periods. During glacial and stadial periods, Ca is reduced due to colder surface waters and increased ice cover that influence the productivity of coccolithophores and their delivery to the seafloor. Increased Ti/K reflects the enhanced transport of weathered terrigenous material from the continental shelf during glacial periods (Richter *et al.,* 2006; Brendryen *et al.,* 2011). Both visible tephra units (Units 5 and 7, Figure 3.8) are clearly reflected within the Ti/K ratio (129 cm and 34 cm). The Ti/K ratio generally follows the Ca profile; both proxies show a marked increase at 200 and 48 cm, prior to the deposition of the Storegga and Tampen turbidites. This is a strong indication of the slide occurring after a significant loss of regional ice sheet mass and increased supply of weathered products to the continental slopes. Immediately before the Tampen Slide, there is a short-lived reduction in Ca and Ti/K (203-195 cm). This indicates a short-lived but significant cooling, which interrupts the overall warming trend from 210 cm, supportive of the observed increase in $\delta^{18}O_{plank}$.

Following the Tampen Slide, the Ca record shows the greatest variation for the whole core record. A series of short-lived, high amplitude fluctuations are visible. This may be interpreted as significant changes to sea surface temperature and/or salinity, and potentially correlate to Greenland Interstadial (GI) 14-16, dated to 49,600 ± 2051 to 56,500 ± 2430 years Cal BP. This is in excellent agreement with the projected date of the Tampen deposit from the age model

developed in chapter 3 of 55.9 ± 4 ka BP. The observed patterns in the Ca and Ti/K profiles demonstrate a consistent pattern of early MIS 3 warmth, interrupted by a brief cooling episode prior to the triggering of Tampen.

4.6.4 Carbon Isotopes

Carbon isotopes from benthic species were corrected using a least-squares regression which resulted in an R^2 of 0.25 between the two species, and the regression equation has been used to adjust the *O. umbonatus* $\delta^{13}C$ to *C. wuellerstorfi* values to produce a continuous carbon isotope profile (Figure 4.7).

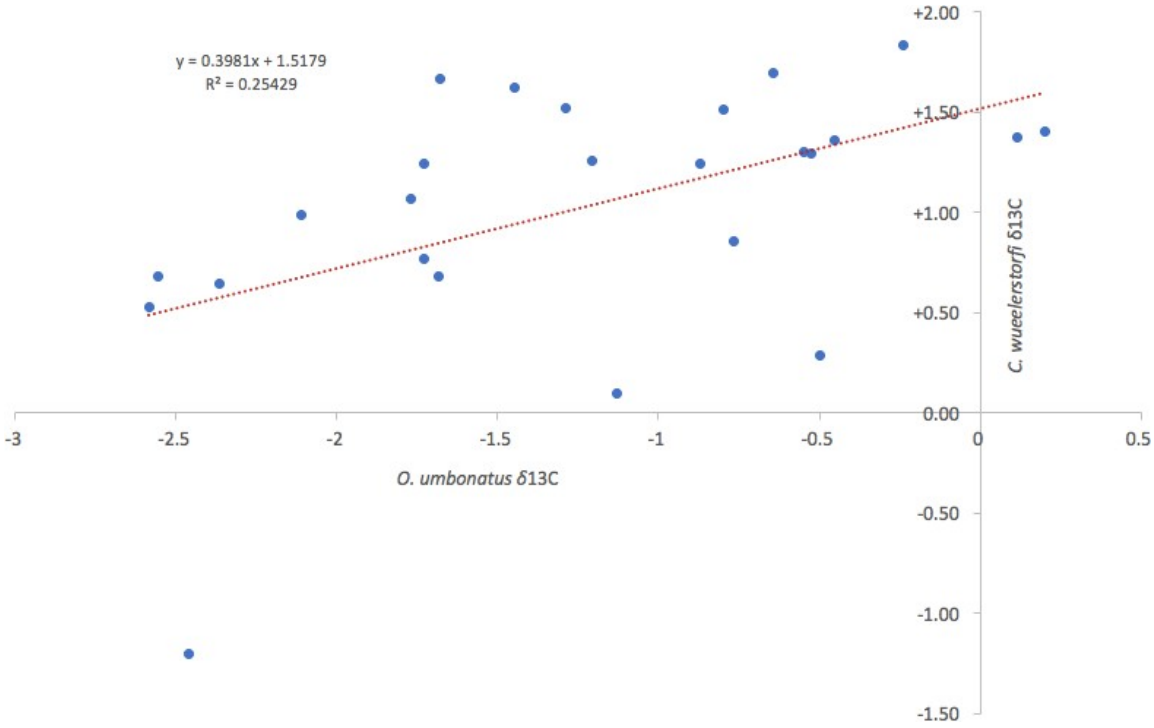

Figure 4.7: Calibration of $\delta^{13}C$ values for O. umbonatus against C. wuellerstorfi showing R^2 and the equation used to calibrate the species.

A regression calibration is limited by the assumption of a normal distribution of standard errors, and does not accurately reflect outliers, as such; the interpretation of corrected *O. umbonatus* values is treated with caution. For comparison, the corrections suggested by Shackleton (1987) and Katz (2003) were applied to *O. umbonatus* (Figure 4.8). Using the correction factors resulted in a systematically lower $\delta^{13}C$ from *O. umbonatus* than *C. wuellerstorfi* where dual samples were available. Over interpretation of *O. umbonatus* data is avoided on the basis of the low R^2 value. MIS 1, 3, 5a, 5c and 5e planktic $\delta^{13}C$ values are above 0.25 ‰. The down-core planktic record shows a good agreement with the Ba/Rb record from the ITRAX, a ratio that reflects surface productivity (Figure 4.9). There are departures from this agreement at the hemipelagic depths of both basaltic tephra horizons (10.3 ka BP and

46.8 ka BP, Figure 4.9), this is suggested to be a significant response to ocean surface fertilisation by basaltic tephra.

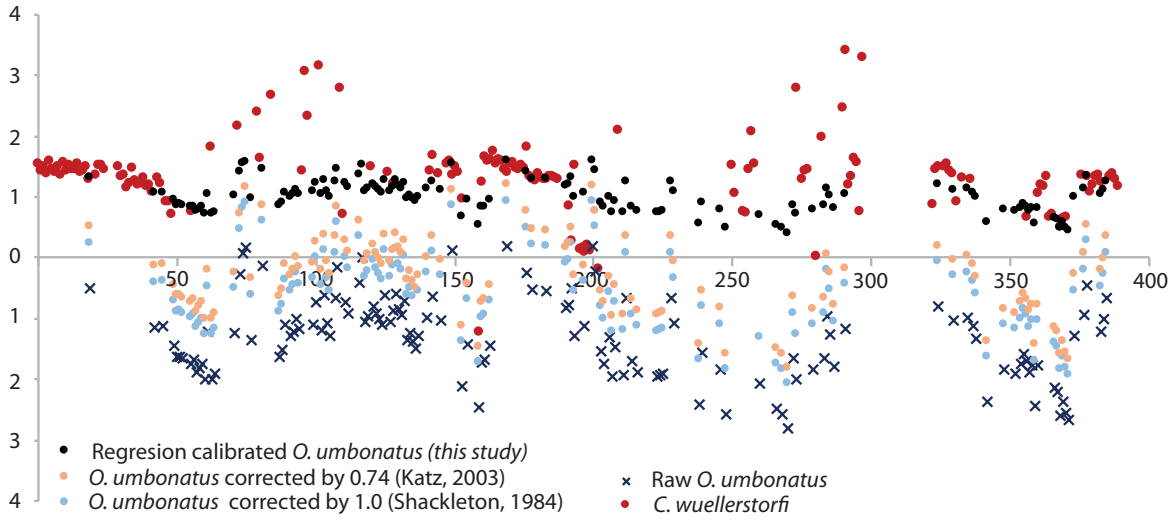

Figure 4.8: Comparison of correction factors discussed in the text for producing a combined O.umbonatus/C. wuellerstorfi benthic $\delta^{13}C$ profile.

Below the Tampen turbidite, between 259-251 cm, the core is dominated by *O. umbonatus* interrupted by brief lighter $\delta^{18}O$ and heavier $\delta^{13}C$ periods (Figure 4.10). These isotopic events are likely to relate to the transfer to the benthos of cold and/or fresh water, normally associated with short-lived warm interstadials (Hagen and Hald, 2004); this interpretation is reflected in the planktic data (section 4.6.3).

Immediately prior to the deposition of the Tampen turbidite (207-195 cm), a $\delta^{13}C$ anomaly is observed. Across this interval the *C. wuellerstorfi* $\delta^{13}C$ values are anomalously depleted to 0.14 ‰, this is the only occurrence of a sustained period of depleted benthic $\delta^{13}C$ in the *C. wuellerstorfi* record. This is replicated in the benthic $\delta^{18}O$ values, as a period of exceptionally light $\delta^{18}O$. This is a further indication of anomalous ocean conditions preceding the deposition of the Tampen turbidite.

The Holocene Storegga slide was deposited during a period dominated by *C. wuellerstorfi*, with $\delta^{13}C$ values consistently above 1.5 ‰, which are considered representative of Holocene (interglacial) values for this site. The MIS 3 data contains two anomalies clearly represented in both planktic and benthic values. At between 162-151 cm hemipelagic depth a continuous profile of *C. wuellerstofi* throughout MIS 3 is interrupted by a short-lived period of *O. umbonatus* dominance, and lighter $\delta^{13}C$ in the planktic record. This is interpreted as a change to glacial/stadial conditions, supported by the heavy $\delta^{18}O$ values at the same time.

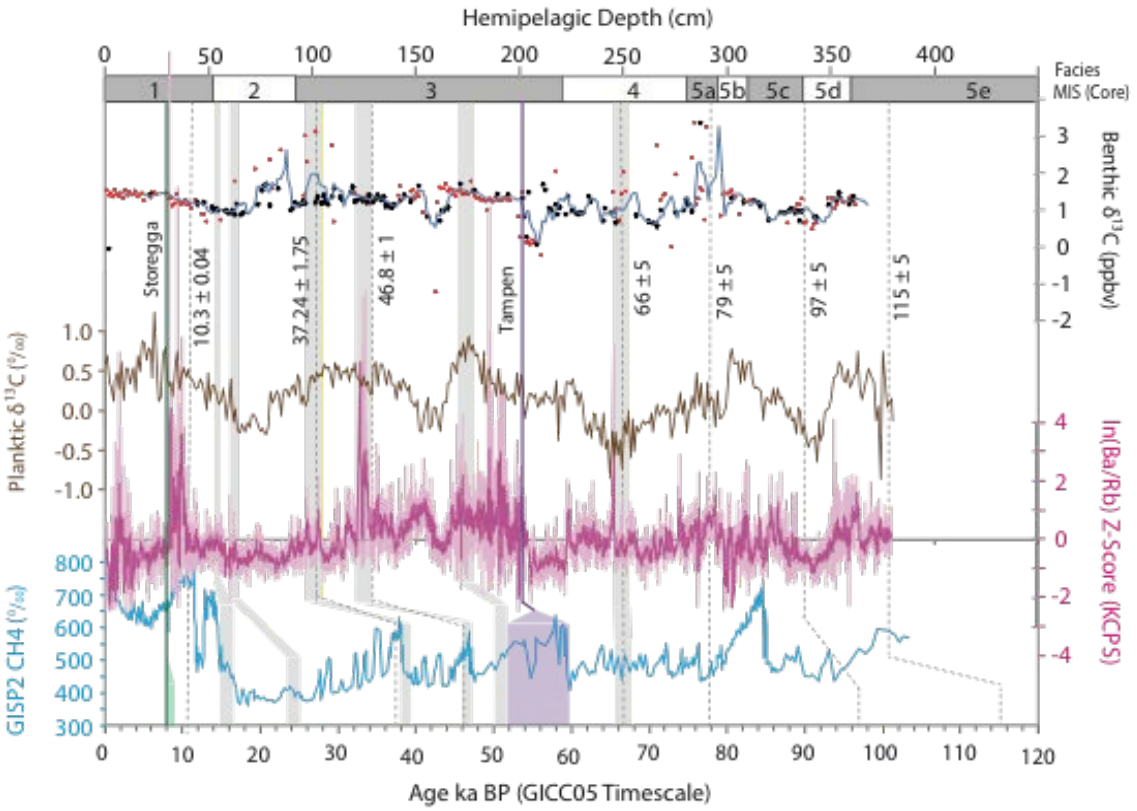

Figure 4.9: Carbon isotope stratigraphy for core PC88 compared to the ITRAX generated Ba/Rb curve, and the GISP 2 methane record (Brook et al., 1996). Grey bars represent Heinrich Events; dashed grey lines represent chronological tie points identified in chapter 3. Red diamonds represent C. wuellerstorfi, black circles represent O. umbonatus $\delta^{13}C$.

4.7 Discussion

This paper presents the first reconstruction of surface and deep-water conditions (temperature and salinity), and the volume of ice sheets from a core containing two turbidites sourced from the Storegga Slide Complex. Oceanographic conditions preceding each slide are remarkably similar, and indicate a strong link between deglaciation and preconditioning for slides. A further similarity is observed in the potential involvement of rapid climate change events, which can be observed immediately before each slide occurs. The new date for the Tampen Slide, 55.9 ± 4 ka BP, established in chapter 3, places the Tampen Slide in MIS 3 (57–29 ka BP), or late MIS 4. The stable isotope stratigraphy refines this to after the start of MIS 3, following a period of ice sheet retreat and surface freshening. The climatic conditions at the start of MIS 3 have been established as comparable to the Holocene across much of Europe, and are examined here in comparison to the conditions surrounding the Holocene Storegga Slide (Huber *et al.,* 2006; Sirocko *et al.,* 2015). The leading theory of slide preconditioning and triggering relates rapid deposition within the slide scar during the preceding glacial period, the isostatic uplift following retreat and associated low level seismicity, to each of the five landslides from the Storegga Complex (Berg *et al.,*

2005; Bryn *et al.,* 2005; Solheim *et al.,* 2005). The following discussion details the climate conditions before and after the slides, and how the environmental conditions may have contributed to slide triggering.

4.7.1 MIS 3

MIS 3 is notable for the instability demonstrated in both the palaeoclimatic reconstructions from the Greenland ice cores and North Atlantic sediments (Bond *et al.,* 1992; Kissel *et al.,* 1999; Rasmussen *et al.,* 1999; Shackleton *et al.,* 2000; Huber *et al.,* 2006; Steffensen *et al.,* 2008; Svensson *et al.,* 2008). Between 29-57 ka BP (D-O 3-17), 14 Dansgaard-Oeschger (D-O) events are synchronous with Greenland temperature increases of 8-16°C occurring over a few decades (Huber *et al.,* 2006; Steffensen *et al.,* 2008; Van Meerbeeck *et al.,* 2008). A central problem to resolving climatic variation and event chronologies in MIS 3 lies within dating methodologies. The limit of the AMS radiocarbon method lies within this period, with dates older than 43,500 ^{14}C years BP commonly exceeding the calibration limit (Reimer 2013; Alexanderson *et al*. 2011; Dalton *et al*. 2016). At the upper limit of the method a 0.2% contamination of modern carbon in a 45,000 year old sample results in an incorrect measured age of 40,000 years old (Olsson and Eriksson, 1972). A further complication arises from the preservation potential of MIS 3 deposits as a result of the MIS 2 glaciation. The large Weichselian ice sheets scoured much of the terrestrial material deposited before MIS 2 from the geological record, as such few terrestrial records from this time period are preserved. The reliance of terrestrial records on relative dating methodologies such as pollen and insect assemblage analysis to identify successive glacial or interglacial periods, as opposed to absolute dating methods such as tephra or AMS radiocarbon which can be directly linked to an independent chronology, raises the possibility of incomplete stratigraphies and chronological misinterpretations (Kjaer *et al.,* 2006; Larsen *et al.,* 2006; Astakhov, 2013, 2014). Where possible, multiple methods of dating should be applied where samples are available (Alexanderson *et al.,* 2011), this study uses multiple marine chronological methods that can be stratigraphically aligned to the NGRIP chronology, additional marine sediment core records and terrestrial sites. This chronology is robust, and the interpretation of the climatic conditions at the time of triggering of both slides can be used to assess conditions that may contribute to future risk.

Previous work in the Nordic seas has shown the early MIS 3 period as exhibiting a vigorous NSDW current, with notable variations in flow intensity (Kuijpers *et al.,* 1998), summer sea surface temperatures comparable to modern values (Kandiano *et al.,* 2004), extensive continental deglaciation across the Laurentide Ice Sheet (Dalton *et al.,* 2016b) and Fennoscandian Ice Sheet (Alexanderson *et al.,* 2008; Engels *et al.,* 2008; Helmens, 2008; Helmens and Engels, 2010), and

fossil pollen reconstructions from Central Europe with assemblages comparable to modern-day (Sirocko *et al.,* 2016). These reconstructions suggest that climate at the time of deposition of the Tampen Slide, in early MIS 3 was similar to climate at the time of the Storegga Slide. These common climatic conditions are essential to furthering our understanding of the link between climate change and slide preconditioning and triggering, and this work indicates a probable link between warming northern hemisphere temperatures and submarine landslides from the Storegga Slide Complex.

Sea level reconstructions for MIS 3 vary. Work by Grant *et al*. (2014) suggested no substantial eustatic rise in sea level, where Rohling *et al*. (2008) identified a sharp peak in relative sea level (R.S.L) rise at 52-53 ka BP. Recent work has partially resolved the debate through modelling sea level for MIS 3 using a reduced extent of the Laurentide Ice Sheet (reducing the extent by 700 km in the south- eastern sector), and incorporating geological markers from the Hudson River Lowlands that suggest regional relative sea level was within -0.9 m of the present day (Dalton *et al.,* 2016b; Creveling *et al.,* 2017).This uncertainty within MIS 3 sea level reconstructions is important as it highlights a significant unknown factor in slide preconditioning that is not yet resolved for the timing of the Tampen Slide.

MIS 3 has been shown to have climatic conditions comparable to modern day, and more akin to those of MIS 5e and early MIS 1 (Huber *et al.,* 2006; Sirocko *et al.,* 2016). The reason for this MIS 3 warm period that is punctuated by severe D-O cycles lies within long-term orbital changes. The insolation peak for MIS 3 is very narrow in comparison to MIS 1 and 5, which explains the short-lived duration of the warm period, which is restricted to the early part of MIS 3. Modelling work has illustrated that the MIS 3 locations of deep-water formation move northwards from the Atlantic into the Nordic and Labrador seas, where deep-water formation is more susceptible to freshwater input such as glacial outburst floods (Licciardi *et al.,* 1999; Jennings *et al.,* 2006; Thornalley *et al.,* 2010; Zhang *et al.,* 2014; Lohmann *et al.,* 2016). These conditions are broadly comparable to the early Holocene/Late deglacial periods with respect to ice shelf retreat, isostatic rebound and warming oceans. The implication of this is that these conditions are the same for the time periods preceding both the Holocene Storegga and Tampen slides, and that restricted ice sheet cover, rapid climate changes, a high latitude foci of deep-water formations and high relative sea levels are indicators of periods of enhanced risk of slides.

This interpretation of early MIS 3 as a period quite comparable to the early Holocene, is supported by the stable isotope stratigraphy of core PC88, which provides clear evidence that the last two submarine slides from the SSC were both triggered during an early interglacial climate,

shortly after a significant regional warming. Therefore, significant global climate changes may be an important preconditioning factor for large landslides in the sub-Arctic.

4.7.2 Stable isotopes and environmental interpretation

The $\delta^{18}O_{plank}$ record for core PC88 clearly demonstrates late stage deglacial conditions prior to both the Storegga and Tampen slides. The $\delta^{18}O_{plank}$ decrease from 4.8 to 2.6 ‰ between 62 and 59 ka BP, suggests significant surface freshening and regional warming prior to the Tampen Slide. However, the position of the Tampen Slide within this record is within a 0.5 ‰ increase in $\delta^{18}O$ during this otherwise warming period, which starts 2 cm below the slide. This could be interpreted as evidence of a short-lived cooling event at this time, during what was otherwise a warming period. Similar conditions exist before the Holocene Storegga Slide, a decrease from maximum glacial values of 4.6 ‰ at the LGM (18 ka BP) to 3.4 ‰ immediately before the slide. Therefore, both the Holocene Storegga and Tampen slides occurred during short term cold excursions within a warm, interglacial period. This is not evidence that all short-lived excursions in northern hemisphere temperatures are synchronous with submarine slides, but that temperature excursions may be an important preconditioning factor.

The benthic $\delta^{18}O$ and $\delta^{13}C$ records present a complimentary story. Hagen and Hald (2004) used the co-variations in benthic $\delta^{18}O$ and $\delta^{13}C$ to interpret the dominant deep-water currents across the Denmark Strait (watermass characteristics highlighted by coloured horizontal bars in Figure 4/10). The two overflows are affected by water from very similar source regions (Figure 4.1). The NSDW is the dominant deep-water mass in the Nordic seas, and forms from deepwater in the Greenland, Icelandic and Lofoten basins, as well as water exported from the Arctic. Deep-water convection occurs as the surface currents lose their heat to the surrounding atmosphere, become colder, and saltier, and sink. During glacial periods, the locus of deep-water formation shifts south of the Denmark and Iceland-Scotland overflows, with a much-reduced contribution from the Nordic seas to the North Atlantic, and is termed Glacial North Atlantic Intermediate Water (GNAIW). Indications of these water masses were identified in a benthic stable isotope profile in Hagen and Hald (2002). They identified a different isotopic composition characteristic of each water mass being dominant in the North Atlantic, where NADW values are lighter $\delta^{18}O$ (3.4-4.8 ‰) than GNAIW (4.2-5.2 ‰), GNAIW are enriched in nutrients and $\delta^{13}C$ (NADW: 0.9-1.3 ‰ to GNAIW 1.4-1.8 ‰). Within core PC88, Holocene MIS 1 and MIS 5e values for NADW are close to the values suggested as typical of the Holocene (Hagen and Hald, 2002), and are represented in this study as $\delta^{18}O$: 4-4.8 ‰ (Pink bar, Figure 4.10) and $\delta^{13}C$ 1.1-1.8 ‰ (Pink bar, Figure 4.10). A typical expression of

glacial period waters (e.g. MIS 2) also show a more enriched value, ranging from 1.8-3 ‰ $\delta^{13}C$ (Hagen and Hald, 2002Figure 4.10 purple bar)).

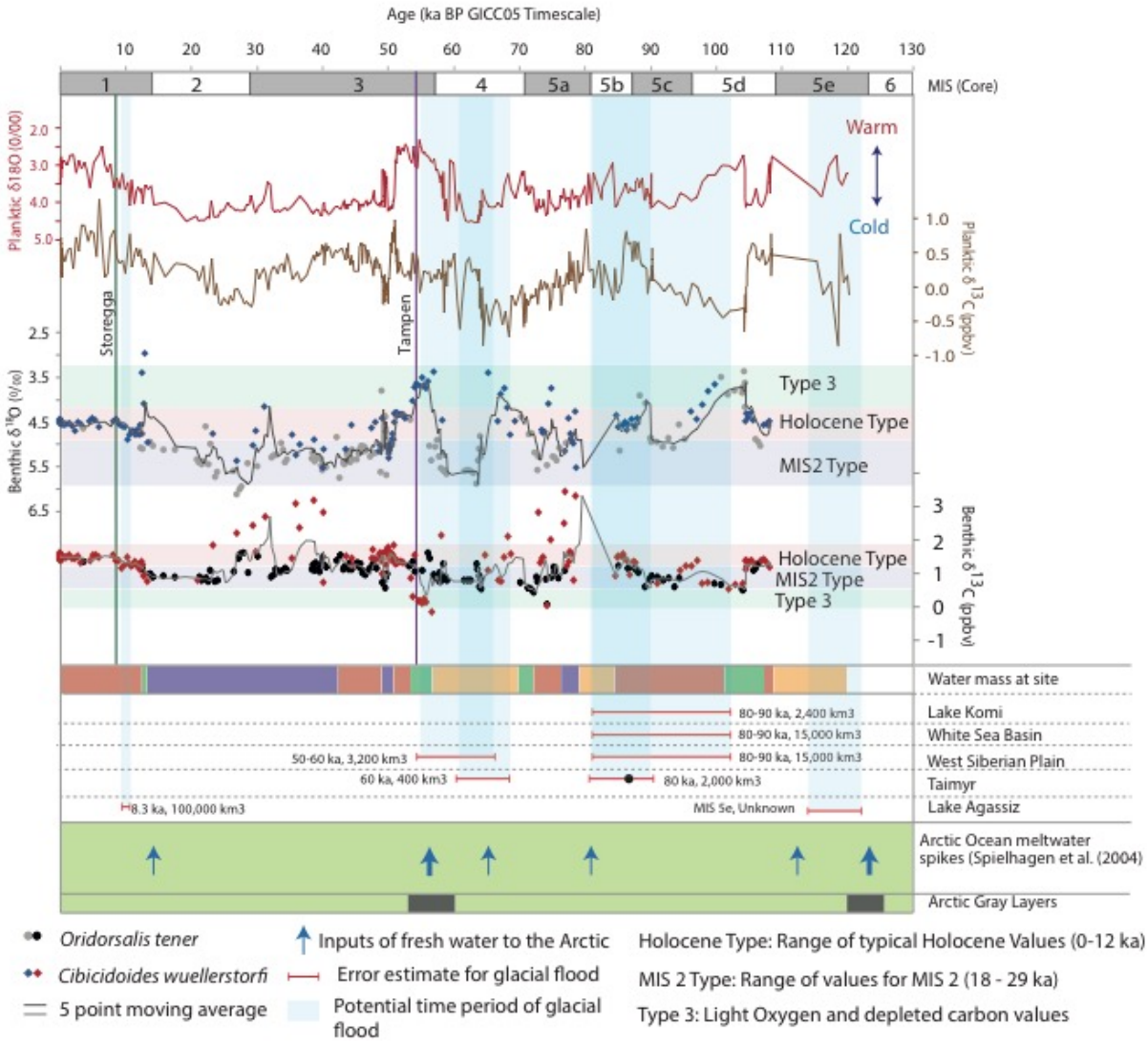

Figure 4.10: Stable isotope data plotted against calculated age from the Oxcal age model detailed in Figure 4.3. Horizontal colour bars indicate the water-mass passing over the site at the time of deposition based on modified values of Hagen and Hald (2004) discussed in section 4.7.2. Heinrich events shown for reference, significant glacial lake outbursts and associated errors on dating are from Mangerud et al. (2004) and Barber et al. (1999). MIS 5e outburst of Lake Agassiz from Nicholl et al. (2012). Position of the Storegga and Tampen turbidites are shown in green and purple respectively, estimates on dating error are found in Figure 4.3. Gray layers are documented in Jakobbson et al. (2001) and discussed with reference to freshwater input in Spielhagen et al. (2004).

A third water type can also be identified (Type 3, Figure 4.10 green bar), Figure 4.11). In limited sections of the core used in this study, a highly depleted $\delta^{13}C$ and exceptionally light $\delta^{18}O$ (3.2-4 ‰***)*** is observed. The observations are also made on *Cibicidoides wuellerstorfi*, the more reliable indicator of benthic $\delta^{13}C$, and offer an insight to either water mass source or salinity. There are two potential interpretations of this data. Southern Ocean Water (SOW) is

known to be richer in nutrients, and therefore strongly depleted in $\delta^{13}C$. Its incursion into the North Atlantic is associated with a slowdown in the AMOC, resulting in the northward progression of SOW to contribute to the NADW. (Oppo and Lehman, 1995; Hagen and Hald, 2002). An incursion of SOW to account for these changes would require a change of c. 5°C globally, for which there is no evidence at this time (Hagen and Hald, 2002).

The second explanation for these values is deep-water formation by brine rejection. In this process, cold surface waters freeze, creating plumes of cold fresh water, which rapidly sink. The observed surface freshening in PC88 is also observed in records from the Denmark Strait. This pattern of depleted $\delta^{18}O$ and $\delta^{13}C$ in PC88 is dated to between 56 and 54 ka BP. This is in good agreement with the same situation observed in core 1225com dated at 54 ka BP from the Denmark Strait, suggesting an ocean-wide change increase in surface freshness at this time (Hagen and Hald, 2002). The formation of deep water by this process (brine rejection) is commonly associated with terrestrially sourced freshwater discharges (outburst floods from ice dammed lakes), which result in the transfer of isotopically light $\delta^{18}O$ from the surface to the benthos. The Tampen and Holocene Storegga slides were both deposited within core depths characterised by these waters, suggested surface freshening could play a role in slide triggering.

4.7.3 Collapse of Ice Dammed Lakes

The most probable source of freshwater discharges detected in North Atlantic cores results from the collapse of ice dammed lakes. The timing of deposition of the Tampen Slide is coincident with the dates of suggested flood events have been hypothesized for MIS 3 (Channell *et al.,* 2012; Nicholl *et al.,* 2012; Galaasen *et al.,* 2014). These studies have suggested analogous conditions to the Laurentide Ice Sheet throughout the Late Quaternary, with further sources of freshwater outbursts in Russia and Northern Europe (Mangerud *et al.,* 2001; Mangerud *et al.,* 2001; Mangerud, 2004; Jensen *et al.,* 2011; Astakhov, 2014).

Two of the largest of these glacial lake drainage events were dated to early MIS 3 (Mangerud *et al.,* 2001; Mangerud, 2004; Lambeck *et al.,* 2006; Helmens *et al.,* 2009). The White Sea Lake had an estimated volume of c. 4800 km^3 (Jensen *et al.,* 2011), the lake formed at the ice margins of the Barents Sea, shortly following the significant marine transgression identified in North Russia (the Meezen Transgression) that occurred 60-65 kyr ago with an estimated 37 m eustatic sea level rise within 3-4,000 years (Kjaer *et al.,* 2006; Astakhov, 2014). This rise triggered a rapid collapse of the shelf ice in the Barents Sea, and has been related to the final outburst of freshwater from the White Sea Lake into the Arctic Ocean at c. 52 ka BP (Spielhagen, 2004). Optically Stimulated Luminescence (OSL) dating of terrestrial deposits have suggested timing of these outburst floods

from the Taimyr and West Siberian Lakes as 50-60 ka BP (Mangerud *et al*., 2001; Jensen *et al*., 2011).

The Middle Weichselian Glaciation (MIS 4) in the Arctic is a notable horizon in the majority of Arctic Ocean sediment cores. First identified in the work of Jakobsson *et al*. (2001), an anomalous dark gray sediment horizon has been dated to c. 53 ± 4 ka BP. This horizon has been linked to Arctic Ocean freshening following a significant ice sheet retreat at the MIS 4 termination (Spielhagen, 2004). Although this is not unique amongst periods of enhanced freshwater flux, it is one of only two such grey horizons identified between MIS 1 and MIS 8 (Jakobsson *et al.,* 2001; Spielhagen, 2004; Löwemark *et al.,* 2014; Löwemark, Regan and Hanebuth, 2016). The clay composition of this layer has been linked to the Barents and Kara seas (based on high smectite and kaolinite content (Spielhagen, 2004). The most significant freshwater spike has been dated to the terminal stages if the MIS 4-3 glacial retreat, with a date of 53 ± 4 ka BP applied in Spielhagen *et al*. (2004), and consistent with the surface freshening detected in PC88. A notable low salinity event had also been previously recorded in the Nordic seas by several authors (Baumann, 1995; Sarnthein and Altenbach, 1995; Spielhagen, 2004; Svendsen *et al.,* 2004). This has been postulated as a consequence of the drainage of ice dammed lakes from Northern Russia (see discussion above). The above listed works highlight the number of potential freshwater sources that impacted the Nordic seas and may explain the isotopic anomaly detected in core PC88 which occurred immediately prior to the triggering of the Tampen Slide.

Zhang *et al*. (2014) highlighted a less stable AMOC throughout MIS 3, indicating the potential for these freshwater inputs to have perturbed the global interglacial circulation is significant. Which is of note as early MIS 3 is characterised by several rapid climatic fluctuations directly comparable to the 8.2 ka event. Terrestrial records have consistently shown that the Storegga Slide occurred during the coldest period of the 8.2 ka BP climate anomaly (Bondevik *et al.,* 2012). The final collapse of the Laurentide Ice Sheet expelled > 1,014 km^3 of freshwater into the Labrador Sea, and was argued to be a major factor in the 8.2 ka BP cold event (Barber *et al.,* 1999; Sallun *et al.,* 2012). This event triggered sub-decadal, hemispheric-wide decreases in ocean surface temperatures of 1.5° to 3° C, and Greenland atmospheric temperatures decreased by 7.4 °C, culminating at 8.15 ka BP (Barber *et al.,* 1999; Alley and Agustsdottir, 2005; Alley *et al.,* 2010). A causal link between the 8.2 ka BP outburst flood and associated cooling, and the Storegga Slide has been inconclusively investigated (Bondevik *et al.,* 2012). It should be noted that discrepancies exist with regard to the date of the onset of the 8.2 ka event. High resolution records date the onset of the cold period in the North Atlantic to 8.38 ka BP (Kleiven *et al.,* 2008), and some identify a longer lived cooling starting c. 8,600 years BP (Rohling and Pälike, 2005). However, no study has been able to identify both the Holocene Storegga Slide and the 8.2 ka BP climate anomaly in the same record, hindering our understanding of which

occurred first. The stable isotope records discussed in this chapter indicate the onset of the 8.2 event cooling occurred before the Storegga Slide.

These studies show that there is evidence of ocean-wide changes in salinity at the time of the deposition of the Tampen Slide and the Storegga Slide, that may play a role in preconditioning and triggering of submarine slides. Such widespread freshening from glacial lake drainage should be compared to that of freshwater input from modern ice sheet melt to assess current and future risks.

4.7.4 A comparison of the oceanographic and ice sheet conditions prior to the two slides

Conditions preceding both slides are similar, and are summarized in table 4.1. The Holocene Storegga Slide has been dated from both marine and terrestrial records to 8.17 ka BP, falling within the coldest decades of the 8.2 ka climate anomaly (Bondevik *et al.,* 2012). The stable isotope reconstruction in this work shows the slides to have occurred during established interglacial conditions, which had persisted for 3-5 ka before the emplacement of the turbidite. The 8.2 ka BP climate anomaly is poorly defined within the benthic $\delta^{18}O$ record, which may be explained by its short duration, the low sedimentation rate and the Laurentide source for the outburst flood. The planktic $\delta^{18}O$ record does indicate a short increase in $\delta^{18}O$ values immediately preceeding the slide, interpreted here as the main phase of the 8.2 ka event cooling before the Storegga Slide was triggered. Here, the resolution in the sediment core PC88 is not sufficient to identify if the slide was triggered during the deepest cooling, or rapid warming following the cold event.

The Tampen Slide, dated in chapter 3 to 55.9 ± 4 ka BP, had an age uncertainty that could have correlated it in late MIS 4 or early MIS 3. This work suggests that an early MIS 3 scenario is most likely, with planktic and benthic $\delta^{18}O$ values typical of interglacial periods several thousand years before the slide. The short-lived increases in planktic $\delta^{18}O$ immediately before the Tampen Slide suggest a similar climate scenario to the Storegga Slide and the 8.2 ka BP event. The Tampen Slide is placed within Greenland Interstadials (GI) 14-16 (49,600 ± 2,051 to 55,800 ± 2,392 years BP), which represent a series of five rapid Greenland interstadial to stadial (GS) transitions, with an accompanying estimated 9-12° C temperature change in central Greenland for each event (Huber *et al.,* 2006). This indicates the Tampen Slide occurred during a period of rapid climate change.

The stratigraphy of this time period is regionally well established through the presence of the North Atlantic Ash Zone 2 {NAAZ2) eruption (55.35 ± 1.2 ka BP (Austin *et al.,* 2004; Brendryen *et al.,* 2011)). This tephra is present in cores across the Nordic seas and south of Iceland as a visible tephra horizon up to 20 cm-thick. Core PC88 was collected within the zone believed to be

covered by the ash cloud for this tephra, but this significant regional tephra marker is absent (Kvamme *et al.,* 1989; Rasmussen *et al.,* 2003; Austin *et al.,* 2004; Wastegård *et al.,* 2005). Tephra from within the turbidite were sampled, with a potential correlation to the NAAZ2 (chapter 3). This raises the possibility that the NAAZ2 eruption, the MIS 4/3 deglaciation, glacial lake drainage and the Tampen Slide occurred within a short time period (early MIS 3), further work on the tephra within the turbidite would be needed to confirm this. If NAAZ2 tephra is confirmed from within the Tampen Slide deposit, the tephra was either eroded and entrained by the turbidite, with the slide occurring shortly after the eruption, or the two were contemporary.

Table 4.1: Summary of environmental proxies and interpretations for conditions immediately before the Storegga Slide (8.17 ka BP) and the Tampen Slide (55.9 ± 4 ka BP)

Proxy	Pre-Storegga	Interpretation	Pre-Tampen	Interpretation	Analogous conditions
Benthic $\delta^{18}O$	Light (c. 4.5) for 4 ka, have decreased from c. 5.7	Interglacial, warming evident for 4 ka before slide	Exceptionally light (c. 3.5) for 3 ka, have decreased from c. 5.5	Interglacial, warming evident for 3 ka before slide, additional fresh water input	Yes
Benthic species	*C. wuellerstorfi* for c. 4 ka	Interglacial	*C. wuellerstorfi* for c. 3 ka	Interglacial	Yes
Planktic $\delta^{18}O$	Light: c. 4.0 for 6 ka, short-lived increase < 1 ka before slide	Warm and fresh surface water, rapid cooling before slide	Light: c. 2.7 for 4 ka. Significant increase < 1 ka before slide	Warm and anomalously fresh surface water, rapid cooling before slide	Yes
Benthic $\delta^{13}C$	Typical NADW, c. 1.3 ppbv for 5 ka	Bottom water consistent with interglacial NADW	Depleted (0.2 ppbv) for 3 ka	Bottom water unusually depleted – anomalously fresh. Interglacial conditions before Storegga, unusual conditions before Tampen	Yes
Ca ITRAX	High for c. 3 ka	Productive interglacial surface waters	High for c. 7 ka, decreasing values immediately before slide	Productive interglacial surface waters, interrupted by brief cooling immediately before slide	Yes
Ti/K ITRAX	Increasing from 8 ka before the slide	Vigorous bottom current activity	Increasing from 5 ka before slide	Vigorous bottom current activity	Yes
NGRIP record	8.2 event – rapid change coincident with slide	Resolution of core cannot infer if cooling or warming after 8.2 is coincident with the slide	GI 14-15: 3 periods of rapid cooling and warming, each of 10-12° C	Cannot resolve if slide occurs on warming or cooling, rapid climate change linked to slide	Yes

Glacial lake outburst	Aggasiz (8.34 ka BP)	West Siberian Plain (50-60 ka BP) and Taimyr (c. 60 ka BP)	Yes
Volcanic Eruptions	Vedde (12 ka BP), Saksunarvatn (10.3 ka BP), Suderoy (8.05 ka BP)	NAAZ 2 (55.4 ± 2.4 ka BP)	Yes
Arctic Freshwater pulse	c. 12 ka BP + input from Lake Agassiz at 8.34 ka BP	c. 55-53 ka BP	Yes

There is a potential link between timing of the Tampen Slide and suggested timing of two large glacial lake outbursts from Russia. The West Siberian Lake has been dated to 50-60 ka BP, and the Taimyr Lake to c. 57 ka BP (Spielhagen, 2004) and the estimated date for the freshwater period in core PC88 is 55-65 ka BP. The resolution from terrestrial dating is not sufficient to tie either outburst to the slide, but the anomalously fresh signal in both the benthic and planktic $\delta^{18}O$, and heavily depleted benthic $\delta^{13}C$ support a significant freshening of the Nordic seas immediately prior to the Tampen Slide. Therefore, a link is suggested between glacial lake outbursts from Fennoscandia potentially preconditioning the Norwegian continental slope for massive submarine landslides. This hypothesis should be tested with other slides in the Nordic seas, but may indicate sediment laden slopes where significant recent freshwater discharges have been observed should be identified as at higher risk of failure.

4.8 Conclusion

The comparison of the palaeoclimatic conditions preserved in the sedimentary record from the Aegir Ridge site, at the time of both the Storegga and Tampen slides, reveals both slides occurred shortly after substantial ocean and climatic warming. This chapter gives a comprehensive assessment of both the Storegga and Tampen slides with relation to local oceanographic variations, and relates the timing of these slides to the wider Arctic and Sub-Arctic glacial history. From the available evidence, both slides occurred under similar criteria: slides occur following a delay from a significant deglacial/warming period, with a potential link to freshwater discharges into the Arctic and Sub-Arctic regions, and when the North Atlantic circulation was operating in a mode comparable to today. Importantly, a short-lived rapid climate change may have been present before both slides. This evidence is supportive of a link between slide preconditioning/triggering and deglaciation, with a variable delay of between 1,500-5,000 years after the retreat of the ice sheet from its most seaward extent, and may support the notion of post-glacial seismicity triggering these slides. This palaeoclimatic and chronological data for the Storegga and Tampen slides could be used to identify slopes that are currently at most risk of failure. Slide complexes that have suffered repeated failure over the last 500 kyr, which have recently deglaciated (< 5 ka BP), and are

currently located in regions of enhanced deglaciation and post- glacial seismicity would be most at risk. This suggests slopes surrounding Svalbard, Jan Mayen and the Arctic should be assessed as risks to the UK and Northern Europe. The Tampen Slide is only the second of the five Slides from the Storegga Slide Complex to be dated and placed within a reliable climatic/oceanographic context. Further work should be performed to test these hypotheses and assess if the deglacial relationship is true for older slides, and other slide complexes.

Chapter 5 A previously undocumented landslide deposit from the Lofoten Contourite Drift, Norwegian continental margin

5.1 Abstract

The Nordic seas are host to several submarine landslide scars, notably from the 8.17 ka BP Storegga Slide, and the 2.9-3.6 ka BP Trænadjupet Slide. Slides of this scale can generate tsunamis capable of traversing the ocean basin, which would cause substantial damage to coastal settlements and offshore infrastructure. Whilst large slides such as Storegga and Trænadjupet have been well dated and probable tsunamis have been modelled, smaller slides still pose a significant risk to local shorelines and offshore infrastructure. Many smaller slides remain undated along the Norwegian Margin. This work dates a previously identified small landslide deposit perched upslope of the Lofoten Contourite Drift. Here we show the Lofoten Contourite Drift turbidite predates the adjacent Trænadjupet Slide by 2000 years, and assesses the limitations of correlating turbidites and tsunami deposits through radiocarbon chronologies. The date applied to the Lofoten Contourite Drift turbidite is 5.5 ka BP, but this is complicated by considerable erosion at the base of the deposit and the unconstrained local radiocarbon reservoir effect. This eliminates the possibility of synchronicity between the Lofoten Contourite Drift turbidite and the Trænadjupet Slide, but does not eliminate a potential earthquake trigger for either slide.

5.2 Introduction

5.2.1 Large-scale landslides on the Norwegian continental margin

The Norwegian continental margin has experienced several prodigious submarine landslides, including the Holocene Storegga and Tampen slides (Figure 5.1), which represents the largest known submarine landslide since the Penultimate Glacial Maximum (Evans *et al.*, 1996; Haflidason *et al.*, 2004, 2005; Bondevik *et al.*, 2012). The Holocene Storegga Slide occurred c. 8,170 years ago and mobilized 2,500-3,400 km^3 of sediment, generating a widespread tsunami in the Nordic seas (Bondevik *et al.*, 1998; Grauert and Bjo, 2001; Smith *et al.*, 2004; Wagner and Bennike, 2007; Long *et al.*, 2016). The Holocene Storegga Slide was not an isolated event, as many more large-volume landslides have been identified along the Norwegian continental margin (Chapter 1, Figure 1.7). Geophysical data provide evidence for at least four additional

landslides of similar-scale within the last 500 kyr sourced from the same location as the Holocene Storegga Slide (Evans *et al.*, 1996; King *et al.*, 1996; Haflidason *et al.*, 2004; Bryn *et al.*, 2005; Solheim *et al.*, 2005). Further along the Norwegian margin, north of the Vøring Plateau, the Trænadjupet Slide (2.6-3.4 ka BP [Allin, thesis]) overlies the older Nyk Slide (c. 19 ka BP), which have a combined volume of 1,200 km^3 (accurate individual volumes are disputed [Figure 5.1; Laberg *et al.,* 2002; Lindberg *et al.,* 2004]). Despite the number of large recurrent landslides along the Norwegian continental margin, the limitations of age-dating techniques are such that the importance of localised effects is often unclear, especially when compared to regional controls for landslide triggering.

Previous work suggests that the timing of large-volume submarine landslides on the Norwegian continental margin was related to the deglaciation of Fennoscandia (Bryn *et al.,* 2005). Fennoscandia comprises the Scandinavian peninsular, the Kola peninsula, Finland and Denmark, which have experienced significant environmental changes associated with Quaternary glaciations. This hypothesis was challenged in chapter 3 by the dating of a pre-Holocene submarine landslide from the Storegga Slide Complex known as the Tampen Slide, and is further challenged by dating of the Trænadjupet and Nyk Slides. Both the Trænadjupet and Nyk slides initiated from the same slide scar, and both during the last deglacial period without the need for sediment recharge between the Nyk and later Trænadjupet Slide (Laberg *et al.*, 2002). Therefore, the relationship between deglaciation and slide triggering is more complex than previously thought. Slopes are thought to be preconditioned to failure by rapid sediment loading during and following glacial periods, and triggered by isostatically-induced seismicity following rapid ice sheet retreat (Bryn *et al.*, 2005; Solheim *et al.*, 2005; Lee, 2009). The available geochronological control for large-volume submarine landslides on the Norwegian continental margin has large uncertainties, preventing robust testing of this hypothesis. In particular, it is unclear whether landslides were triggered synchronously as might be expected in response to regional earthquake or sea level hydraulic effects (Adams, 1990; Goldfinger *et al.*, 2003; Gutierrez-pastor *et al.*, 2009; Goldfinger *et al.*, 2013; Sumner *et al.*, 2013). A more complete understanding of the relationship between global temperature changes and slide triggering is essential for predicting the likelihood and timing of future submarine slides and associated potential tsunamis.

5.2.2 Regional versus local triggers for submarine landslides

Sediment core data recently acquired from the Nordic Seas provide an opportunity to determine submarine landslide timing and provenance to better understand when and how these slides occur. In this chapter, the Lofoten Contourite Drift is studied (Figure 5.1), where a ponded landslide run-out deposit, previously imaged by industry seismic data, is cored for

the first time. Given its close proximity to the large Trænadjupet Slide, located 40 km to the south of the coring site, we test whether this new landslide was: i) triggered at the same time and from a similar location to the nearby and well-dated Trænadjupet Slide; or ii) if it represents a previously undocumented landslide. If the former statement is correct, then this may suggest that a major regional earthquake triggered synchronous landslides across this region, whereas if the latter case is true it may implicate a more local trigger (Goldfinger *et al.,* 2003). Both points are key uncertainties that inhibit a robust understanding of landslide and tsunami hazard.

5.2.3 The Lofoten Contourite Drift

Since the mid-Miocene, along-slope thermohaline currents have sculpted the elongate Lofoten Contourite Drift (LCD) on the northern Norwegian continental margin, adjacent to the Lofoten Islands (Figure 5.1; Laberg *et al*., 2002; Laberg & Vorren 2004; Amundsen *et al*. 2015). The drift extends for 90 km along the base of a steep (7.5°) upper continental slope in water depths of ~1,000 m (Figure 5.2). The presence of the Lofoten-Vesterålen Islands has acted as a barrier to sediment reaching the continental slope, and has caused sediments to be diverted north or south of the site. This has shielded the Lofoten Contourite Drift from extreme glacial-interglacial variations in sedimentation by effectively blocking terrestrial inputs (Løseth and Tveten, 1996; Laberg *et al.*, 1999, 2001). As a result, the sediments have a regionally unique character and are largely composed of reworked hemipelagic sediments (Baeten *et al*., 2013). The Lofoten-Vesterålen margin (Figure 5.1) is incised by numerous canyons and slide scars (Laberg *et al.*, 1999; Baeten *et al.*, 2013, 2014; L'Heureux *et al.*, 2013; Rise *et al.*, 2013; Amundsen *et al.*, 2015; Brendryen *et al.*, 2015). The core location is 40 km north east of the slide scar of the c. 2.6-3.4 ka BP Trænadjupet Slide (Baeten, 2013; Laberg & Vorren, 2000; Laberg *et al.,* 2002). The drift terminates towards the northeast, with an irregular slope to the northwest marked by escarpments, which are up to 50 m high (Rise *et al*., 2013).

5.2.4 Identification of landslide run-out deposit in the moat of the Lofoten Continental Drift

Seismic reflection studies show the sediments of the Lofoten Contourite Drift (LCD) to be largely well-stratified (Baeten *et al.,* 2013). An exception is found within a prominent moat at the southeastern limit of the drift (Rise *et al.,* 2013). A previous Topas sub-bottom profile survey identified an acoustically transparent unit (~40 m thick) that ponds and partially infills the moat. The moat is then draped by an overlying thin (< 2 m thick) sequence of well-stratified material (Rise *et al.,* 2013). The acoustically transparent nature and geometry of

this ponded unit is suggested to represent rapid emplacement of sediments as landslide run-out (Rise *et al.,* 2013; Figure 5.2). The specific age and provenance of this unit is unclear.

5.3 Aims

This study seeks to answer two main questions. First, do the ponded unit within the Lofoten Contourite Drift (LCD) moat and Trænadjupet Slide share the same source on the continental slope, and hence represent a distal expression of the same landslide event? We investigate the provenance of the ponded unit by comparing the major element geochemical composition of the ponded unit with the known composition of turbidites from the Trænadjupet Slide, and other landslides in the region. Second, does the ponded turbidite within the LCD moat represent an independent slide synchronous with the adjacent Trænadjupet Slide. Here, we use new ^{14}C dates above and below the turbidite ponded in the moat of the LCD and compare to those new dates of the Trænadjupet Slide. If the geochemical composition of the LCD turbidite and turbidites from the Trænadjupet Slide are different, but the timings are the same, this may suggest that a regional trigger, such as a large earthquake, caused synchronous failure of the continental slopes above the Trænadjupet Slide and LCD.

5.4 Regional Setting

The Lofoten Basin is an asymmetrical basin to the east of the Mohns Ridge, west of the Barents Sea continental slope, and north of the northern margin of the Vøring Plateau (Laberg *et al*., 1999; Laberg *et al.*, 2001; Laberg and Vorren, 2004; Laberg *et al.,* 2005; Raj and Nilsen, 2009; Rise *et al*., 2013; Latarius and Quadfasel, 2016). This basin forms the deepest part of the Nordic seas with water depths exceeding 3000 m depth.

The continental slope above the Lofoten Basin has an average 5-6° gradient, but reaches 10° in regions, and is steeper than the more southerly sectors of the Norwegian margin (Vorren *et al*., 1998; Rise *et al*., 2013). The region has not experienced substantive rates of glacial deposition as observed at other slide complexes, such as the Storegga Slide Complex. This is due to the aforementioned barrier created by the Lofoten Islands, which effectively diverted the large ice streams to the south west of the LCD (Løseth and Tveten, 1996; Laberg *et al*., 1999; Laberg *et al*., 2001).

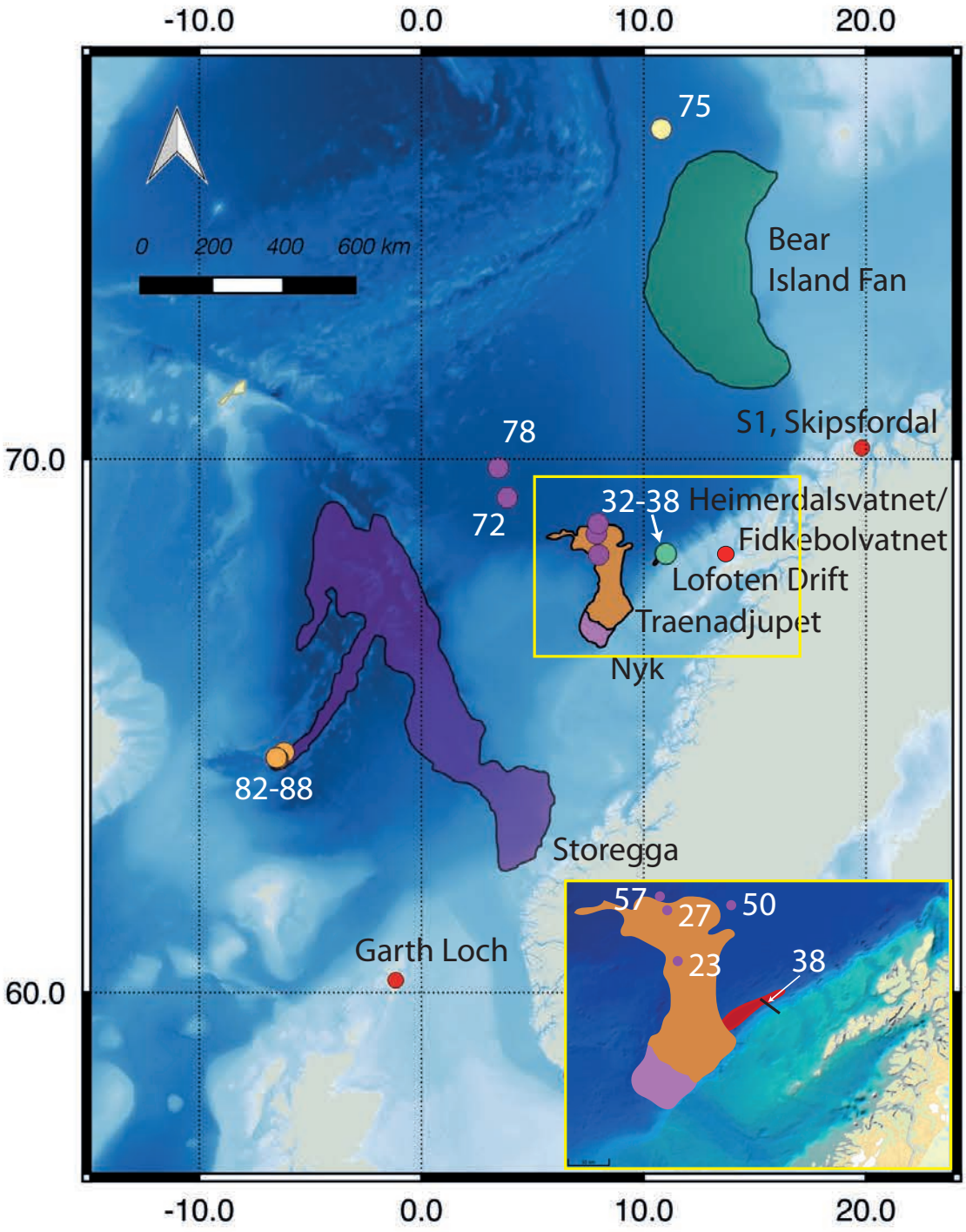

Figure 5.1: Regional map showing the location of the Lofoten Contourite Drift (red – expanded in inset) and the drift cores discussed in the text (cores PC32, PC35 and PC38 [green circle]). Additional cores (white text) used for geochemical comparison of slide composition from Storegga (82-88, deposit also confirmed in cores 72 and 78) and the Bear Island Fan (75). Inset shows Trænadjupet Slide (23, 27, 57), core 50 (Lofoten Basin core) and location of PC38 (Figure 5.2 for detail). Slide complexes and trough mouth fans highlighted: Storegga (purple), Trænadjupet (orange), Nyk (pink) and the Bear Island Fan (green). Red circles indicate the location of potential tsunami deposits.

The dominant source of sediment for the drift is along-slope transport by the surface and intermediate currents. Modern circulation has been interpreted by Laberg *et al*. (2005) to be broadly representative of current systems in place since the early-mid Miocene (Laberg *et al*.,

2005; Rise *et al*., 2013). The water bodies in the Lofoten Basin play a key role in the Atlantic Meridonial Overturning Circulation, and represents the largest ocean heat reservoir in the Nordic seas (Raj and Nilsen, 2009; Raj *et al*., 2015). Deep-water forms in a vortex in the centre of the Norwegian Basin before travelling south back towards the Iceland-Scotland Ridge and joining the North Atlantic Deep water (Rudels and Quadfasel, 1991; Hansen and Østerhus, 2000; Blindheim and Østerhus, 2005). Above 700m, the dominant water mass is the Norwegian Atlantic Water (NAW) sourced south of the Iceland-Scotland Ridge, which follows the Norwegian coastline northwards (Blindheim and Østerhus, 2005). The Lofoten Islands are to the north of the re-joining of the two branches of the Norwegian Atlantic Current (NAC).

The LCD is formed by the passage of the persistent Norwegian Atlantic Current, a topographically controlled contour current (Rebesco *et al*., 2014). Deposits from beneath these contour currents are known as contourites, which gradually accumulate sediments, and are sculpted into large geomorphological bodies known as drifts. These contourite drifts are widely investigated for records they preserve of variations in current strength, in addition to palaeoceanographic proxy records from microfossils. Contourite drifts are often interbedded with downslope deposits of mass wasting: turbidites. The LCD has developed into a separated drift, forming a distinct current-orientated mound, typical of steep slopes (Hunter *et al.*, 2007; Hernández-Molina *et al.*, 2008; Rebesco *et al.*, 2014). The mounded drift is separated from the continental slope by a moat, a pronounced depression between the drift and the base of the slope. It is this moat that contains the ponded turbidite proposed as representing a landslide from the slope (henceforth the LCD turbidite).

5.5 Methods and Methods

5.5.1 Material

Three sediment cores were collected during cruise 64PE391 (RV Pelagia, 2014), to establish the age and origin of the ponded turbidite unit within the moat of the LCD. This acoustically transparent unit, identified in a previous Topas sub-bottom profiles in Rise *et al.* (2013; Figure 5.5 inset) was targeted with piston and multi cores. The three cores were taken along the seismic line to target the centre (core PC35) and the edge (core PC38) of the unit for dating, and one core on the summit of the LCD (core PC32) to provide a continuous background record of sedimentation (core details are described in Table 5-1). PC38 was the only core to capture an upper and lower LCD turbidite boundary (interpreted to represent the ponded unit), and was chosen for further analysis. An additional core from the base of the slope, PC50 (Figure 5.2) was used to compare the composition of the turbidites.

Core PC38 (1300 m water depth) was 6.9 m long with excellent recovery (> 90%), and taken at edge of the transparent unit with the aim of penetrating the full thickness of the ponded unit for dating. The core was located on the northern edge of the Vøring Plateau (Figure 5.1). This coring site is approximately 40 km northeast of the Trænadjupet Slide. Radiographs taken of the core using the ITRAX at BOSCORF were used to aid with the interpretation of sedimentary units and bioturbation. The core recovered a turbidite interbedded with hemipelagite. Samples for ^{14}C dating were taken above-and-below the deposit.

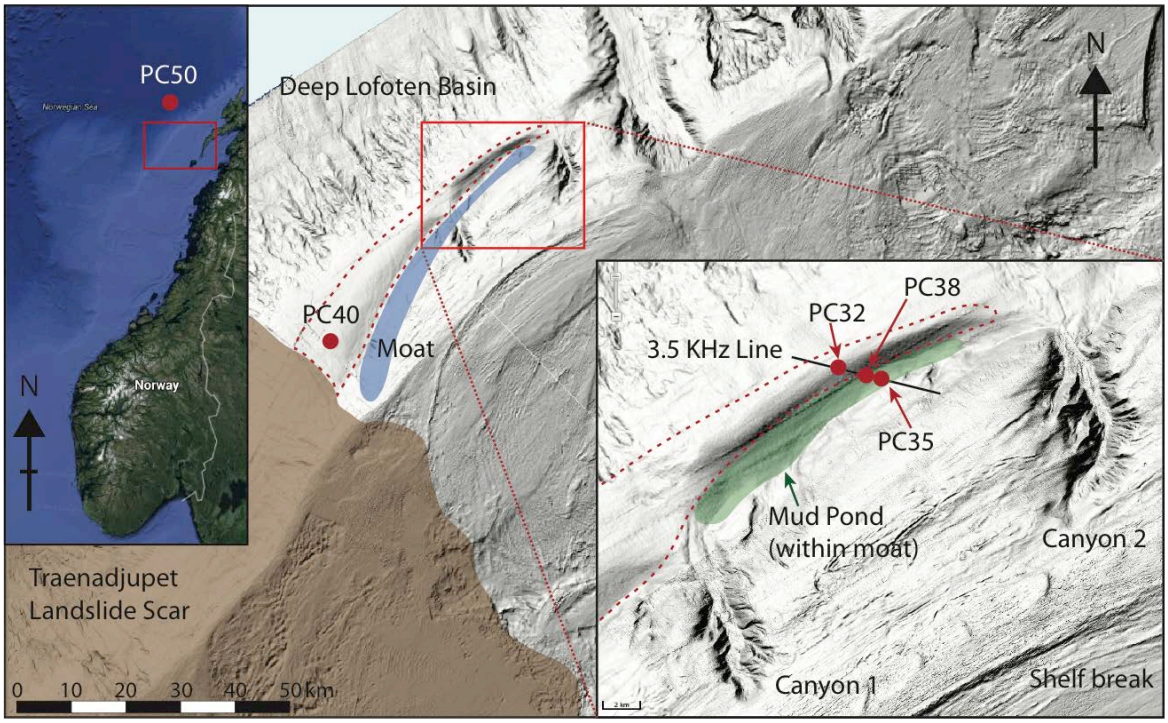

Figure 5.2: Shaded relief image from the Mareano database showing the location of the Lofoten Drift, the Trænadjupet Slide Scar and canyons 1 and 2 (Rise et al. 2013). The 3.5 KHz line used to place the cores (shown in Figure 5.5), and location of cores collected from the drift is highlighted in the inset, in addition to the interpreted extent of the mud pond. Brown shaded area indicates the location of the Trænadjupet Slide. PC 50 is only shown on the regional map inset (top left) as it is out of range of the Mareano database maps.

5.5.2 Bathymetry

This study utilises the Mareano (5 m resolution) databases and available bathymetry was annotated in line with the definitions in Rise *et al*. (2013). Bathymetric data are used to interpret the surface extent of both the ponded turbidite, which forms a broad, flat region within the moat, and escarpments on the slope above that may represent potential sources of the turbidite. The continental slope from the Vøring Plateau into the Lofoten Basin is relatively steep, estimated in Laberg *et al.* (1999) as 7.5 ° (Line VB-32-89, Figure 5.5), and an average of 3-5° in Rise *et al.* (2013).

5.5.3 Age model development

The age of a turbidite can be established from the sedimentation rate of the hemipelagite recovered in the core, the depth of the turbidite within the background hemipelagite, and the closest radiocarbon dates to the top of the turbidite (Urlaub *et al.,* 2013). To establish an age of the LCD turbidite, samples of foraminifera were taken from the hemipelagite above-and-below the LCD turbidite to establish the time of deposition by radiocarbon accelerator mass spectrometer (AMS) methods (Urlaub *et al.,* 2013). AMS radiocarbon dating is a widely used method for the late Quaternary, up to 43.5 ka BP, which is the limit of detection of radioactive carbon (Bronk Ramsey, 2007; Reimer, 2013). The age model for core PC38 was constructed using AMS radiocarbon dates from five samples of mono-specific *Neogloboquadrina pachyderma* sinistral (NPS) in the 125-250 µm fractions. All AMS radiocarbon measurements were made at the Natural Environment Research Council (NERC) Radiocarbon Laboratory at the Scottish Universities Environment Research Centre (SUERC) AMS Facility, East Kilbride. AMS radiocarbon dates must be calibrated using a marine radiocarbon calibration curve (Marine13), which accounts for variations in the age of surface waters, and were calibrated here using the OxCal 4.0 software (Ramsey, 2008) and the suggested reservoir correction age from Mangerud *et al.*, (2006) of 20 ± 30 years, using the Marine13 curve (Reimer, 2013). The radiocarbon reservoir is unconstrained in the study region and potentially highly variable due to the influence of polar waters (Voelker *et al.*, 1998; Bondevik *et al.,* 1999; Laberg *et al.*, 2002). For comparison to published ages of the Trænadjupet Slide and late Holocene climatic changes all dates have been calibrated using the suggested values for the Holocene of ΔR 20 ± 30 (Mangerud *et al.,* 2002). These data are presented in Table 5.2.

The age of the LCD turbidite was determined through the calculation of a hemipelagic sedimentation rate using two dates taken from an uninterrupted unit of hemipelagic sediments below the turbidite (LCD 3 and 4) and two dates were taken from above the LCD turbidite 10 cm apart (LCD 1 and 2). The upper boundary of the LCD turbidite is more difficult to determine due to considerable bioturbation across the boundary, whilst the lower boundary is steeply inclined and clearly erosional.

5.5.4 Turbidite provenance

To establish the provenance of the LCD turbidite within core PC38, the major element geochemical composition of the turbidite mud cap was compared to established geochemical compositions of turbidites of known origin in the Lofoten and Norwegian basins, discussed in chapter 3. Cores were scanned using the ITRAX XRF core scanner at the British Ocean

Sediment Core Research Facility, Southampton (BOSCORF). The ITRAX provides a continuous profile for numerous elements that are compared against one another and can be used as provenance indicators (Hunt *et al*. 2015). The ITRAX data assisted in the definition of the upper contact of the LCD turbidite that was oxidised and harder to identify from visual logging against the background hemipelagite. A suitable section of unoxidised turbidite mudcap was chosen to analyse and compare to the turbidite compositions of other slides along the margin (Pearce and Jarvis, 1992, 1995; Rothwell *et al.*, 2006; Hunt *et al.*, 2011, 2013). Oxidation commonly occurs at the top of turbidites, and can be identified through colour change (grey to dark orange) and Fe and Mn increases from ITRAX data (Jarvis and Higgs, 1987; Middelburg and De Lange, 1988). Comparing only the mud cap sections of the turbidites minimises the effects of grain size variation and water content, and has been successfully used in chapter 3 to distinguish provenance of distal turbidites (Hunt *et al.* 2013, 2015; MacLachlan *et al.,* 2015). The composition of the LCD turbidite is compared to that of slides from the Trænadjupet, Storegga or Bear Island provinces to deduce its likely provenance.

5.6 Results

5.6.1 Core sedimentology

Visual inspection of the split core and radiographic images reveal the LCD turbidite to be clearly distinguished from hemipelagic diamicton deposited above and below the event bed. The turbidite and hemipelagic facies were distinguished by grain size, colour and microfossil content and are listed in Table 5.1. Units 1 and 6 are classified as hemipelagic diamicton (HPC) facies, and are composed of clay and sands with frequent ice rafted debris, occasional tephra and abundant intact foraminifera. The colour of units 1 and 6 is variable, with Unit 6 showing two distinct dark brown horizons. These units are interpreted as hemipelagic sediments that have accumulated slowly on the drift beneath the Norwegian Atlantic Current. The coarse nature of the sediments potentially reflects the higher current strengths passing over the drift at the time of deposition.

The steeply inclined and erosional nature of the boundary between the clean sands at the base of the LCD turbidite and the HPC below indicates a loss of hemipelagic material beneath the LCD turbidite (Figure 5.3, Table 5.1). The LCD turbidite is composed of a base of clean coarse sands (<15 % mud classified as turbidite clean sands facies [TCS, figure 5.3]), with a distinct change to a muddy sand supported clast rich debrite facies [MSD figure 5.3, table 5-1]). The debrite facies grades to muddy sands which fine upwards from coarse to fine, and are capped by a clay and fine silt turbidite mud cap (TMC, figure 5.3). The LCD turbidite is

interpreted as a proximal debrite deposit, deposited upslope of the drift. Above the LCD turbidite a thin drape of hemipelagic diamicton represents a return to gradual sedimentation from ocean currents. The boundary between the turbidite mud cap and hemipelagic diamicton is highly bioturbated and difficult to determine. The limited thickness of hemipelagic drape above the turbidite suggests a recent age.

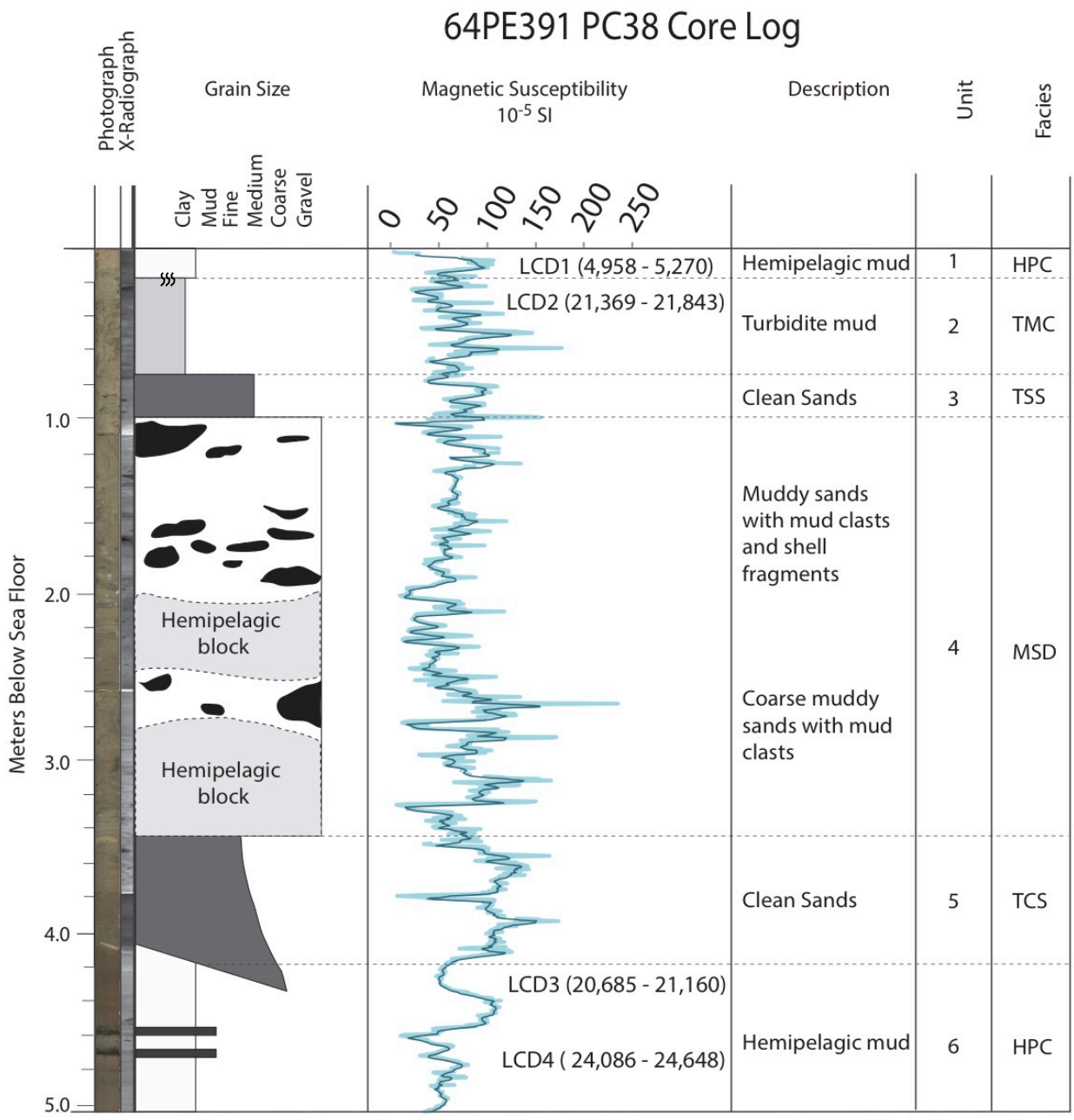

Figure 5.3: Core log, photograph and x-ray of core 63PE391_PC38 showing magnetic susceptibility, lithofacies (Table 5-1) and radiocarbon dates (cal years BP (Table 5.2)). Facies codes HPC – Hemipelagic Diamicton, TMC – Turbidite Mud Cap, TSS – Turbidite Silts, MSD – Muddy Sand Debrite, TCS – Turbidite Clean Sands. Facies interpretations are found in Table 5.1.

5.6.2 Was the Lofoten Contourite Drift deposit sourced from the same locationas Trænadjupet Slide?

The geochemistry of the LCD turbidite is distinct from the turbidite associated with the Trænadjupet Slide (Figures 5.1 (map) and 5.5). The most significant differences are the variations in Ca and Sr (Figure 5.4). The Trænadjupet Slide shows a lower Ca content (TP = 17564 ± 6250 counts per second (CPS), LCD Mud Pond 27120 ± 2080 CPS) and a higher Sr content (TP = 4760 ± 1360 CPS, LCD Mud Pond 5430 ± 490 CPS). The higher Sr content is indicative of a shallow water (< 200 m (Richter *et al.*, 2006)) source for the deposit, as higher Sr/Ca values indicate higher aragonite content more typical of shallow marine sediments (Rothwell *et al.,* 2006). Furthermore, the geochemical composition is also distinct from other landslide-triggered turbidites from the Bear Island Fan, the Storegga Slide Complex and elsewhere in the Lofoten Basin (Figure 5). Therefore, the LCD turbidite is not a distal deposit from the Trænadjupet Slide, nor from any other known landslides. The LCD turbidite therefore relates to a previously undocumented landslide on the Norwegian continental margin.

Table 5.1: Description and interpretation of facies observed in core PC38.

Sed. Units	Structure	Colour	Texture	Boundaries	Interpretation (code)
Unit 1 & 6	Clay and sands , occasional IRD and abundant foraminifera. Laminations visible in part, some evidence of bioturbation	Variable medium brown colour with occasional dark brown/black horizons and pale brown-yellow horizons.	Sandy silts and clays, IRD present, occasional tephra's.	Sharp boundary to unit 5 from unit 6, gradational between unit 2 to 1 and heavily bioturbated.	Hemipelagic diamicton (HPC)
Unit 2	Fine grained bioturbated muds.	Pale-medium grey-brown	Fine, devoid of microfossils	Poorly defined at base, bioturbated upper contact to unit 1	Turbidite mud cap (TMC)
Unit 3	Weakly laminated silts and fine sands, occasional lenses of sands	Grey-Brown	Moderately well sorted, no evidence of bioturbation	Poorly defined at base, overlying contorted rafts of hemipelagite in the debrite unit, gradational to muds at top	Turbidite silts (TSS)
Unit 4	Poorly sorted mud rich sands, evidence of rafted hemipelagic blocks of sediment. Penetrated blocks vary from flat lying to 90° to bedding. Sands are fine to medium (125-500 um) and mud rich.	Grey muddy sands with variable coloured blocks of hemipelagite	Poorly sorted	Abrupt boundary to unit E below. Upper boundary grades to fine sands and silts.	Muddy sand debrite with large clasts of hemipelagite (MSD).

Unit 5	Massive coarse sands (750 um), limited evidence of grading at top of unit, clean sands with low mud content, sands are moderately sorted, contain fragmented foraminifera.	Pale brown	Coarse, angular grains and fragmented microfossils	Sharp base, clearly erosive, abrupt boundary at top to clast rich unit 4.	Turbidite Clean Sands (TCS)

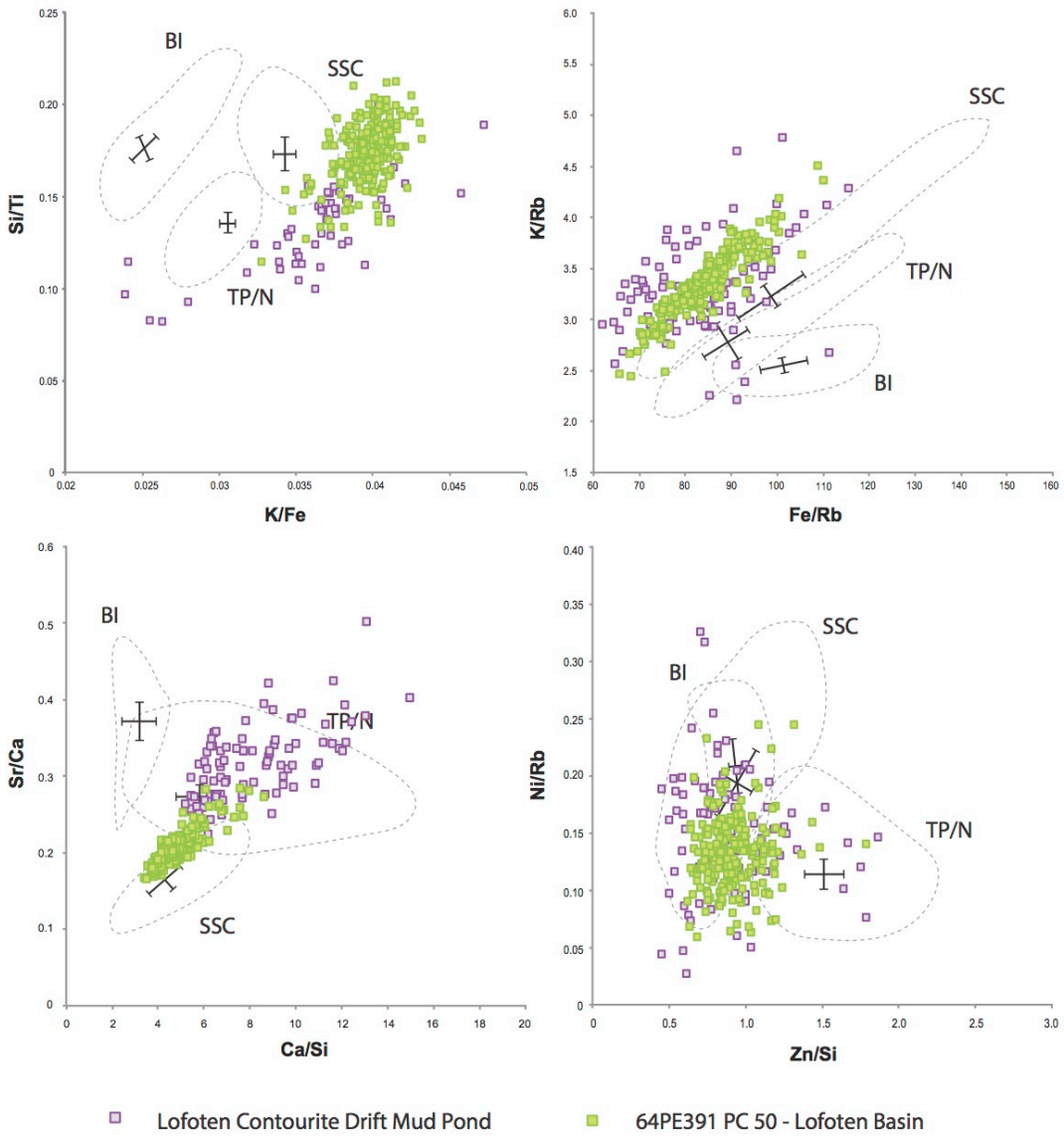

Figure 5.4: Comparison of the composition of the mud cap from the Lofoten Contourite Drift mud pond, the turbidite in core PC50 (Lofoten Basin, see Fig. 5.1). Composition fields represent the Storegga Slide Complex (SSC), the Bear Island Fan (BI) and the Trænadjupet/Nyk slide complex (TPN). Black crosses show average composition and standard deviation for each field. Compositional fields refer to those defined by this thesis in chapter 3.

The higher Ca and K content (TP 8,780 ± 995 CPS, LCD 10,415 ± 850 CPS) relates to the regional geology of the Lofoten-Vesterålen region. The Lofoten Islands are dominated by monzonitic gneisses with anomalously high MgO, CaO and K_2O values (Green *et al.,* 1972; Markl *et al.,* 2001). The barrier effect of the Lofoten- Vesterålen Margin and the narrow shelf create a shorter transport distance from source to sink for shelf sediments, as such the composition of failures from the Lofoten continental margin are geochemically distinct from the wider Norwegian continental margin. The turbidites sourced from the Lofoten continental margina re characterised by higher Si (LCD: 1,160 ± 150 CPS, TP: 825 ± 120 CPS) and lower Mn (LCD: 2,400 ± 280 CPS, TP: 4,155 ±2,137 CPS), typical of a higher-grade metamorphic geology.

There is a clear visual similarity between the mud pond and the turbidite in PC 50, suggesting the same source for the turbidites in both cores (Figure 5.4). This suggests a potential association between the LCD turbidite and turbidites from the floor of the Lofoten Basin (PC 50), further dates from PC 50 are required to prove this connection (Figure 5.6).

5.6.3 Was the emplacement of the ponded unit synchronous withthe Trænadjupet Slide?

Chronological constraints on the LCD turbidite are provided by five AMS ^{14}C radiocarbon dates. All dates were performed on monospecific samples of *Neogloboquadrina pachyderma sinistral*. Four of the AMS ^{14}C dates are from the piston core, and one from the paired multicore. These samples were chosen to try to correlate between the piston and multicores, and assess loss of sediment in the multicore.

AMS radiocarbon-dating of turbidites is preferably performed on samples from the upper boundary between mudcap and hemipelagite, removing the uncertainty of variable erosion at the base of the deposit (Urlaub *et al.,* 2013). Sample LCD 2 was taken too close to the upper turbidite boundary and was potentially contaminated with older foraminiferal carbonate; this is reflected in the older and out of sequence age and is rejected.

The date of LCD 1 comes from 5 cm above the boundary the turbidite mud cap and hemipelagic diamicton, and is calibrated to 4,958-5,270 Cal years BP. This provides an upper age limit for deposition of the unit and yields a sedimentation rate between dates LCD 3 and 4 of 9.28 cm/ka.

Table 5.2: Radiocarbon Dates for core 64PE391 PC38. Ages are calibrated using a ΔR of 20 ± 30 and the Marine13 curve (Ramsey, 2008; Reimer, 2013)

Sample Code	Stratigraphic position (cm)	HP Depth	^{14}C Age (yrs BP)	+/- 1σ (^{14}C yrs BP)	Calibrated Age	
LCD 1	0.05-0.07	6	4841	36	4958	5270
LCD 2	0.14-0.16	15	18256	61	21369	21843
LCD 3	4.15-4.17	25	17770	57	20685	21160
LCD 4	4.47-4.49	54	20729	75	24086	24648

Dates LCD 3 and 4 provide a maximum age constraint of the deposit of 20,685-21,160 Cal years BP. However, a key issue with dating turbidite deposits is estimating the amount of underlying hemipelagite sediment removed through erosion. The inclined erosive contact at the base of unit 5 is suggestive of sediment loss through erosion. Turbidites are therefore preferably dated from the oldest hemipelagite above the mudcap. Therefore, sample LCD 1 (4,958-5,270 Cal years BP) is the most reliable age with respect to this deposit (Urlaub *et al.,* 2013). Using the calculated sedimentation rate (9.28 cm/ka) and projecting this rate downwards from the date of LCD 1 by 5 cm, an estimate for the upper surface of the turbidite is calculated at 5,498 – 5,810 Cal BP. The Trænadjupet Slide is dated to 2,600-3,400 Cal BP; therefore, these two events are not synchronous.

5.6.4 What are the possible sources for the ponded unit?

The results of the geochemical and geochronological analyses demonstrate that the LCD turbidite was triggered at a different location and at a different time to the Trænadjupet Slide. The LCD slide was also not linked to any other slide in the adjacent Lofoten Basin. The local bathymetry from the Mareano database is used to investigate alternative source locations. The bathymetry highlights the shelf break at c. 600 m water depth (Figure 5.5), where canyons 1 and 2 form and deepen downslope (Rise *et al.*, 2013). Canyon 1 feeds into the mud pond (green), which is shown here as approximately 18 km long, and averages 1.5 km wide. The 3.5 KHz image (inset figure 5.5) suggests a maximum depth of the mud pond as 40 m. The position of the core is highlighted demonstrating the location of the coring site at the edge of the mud pond.

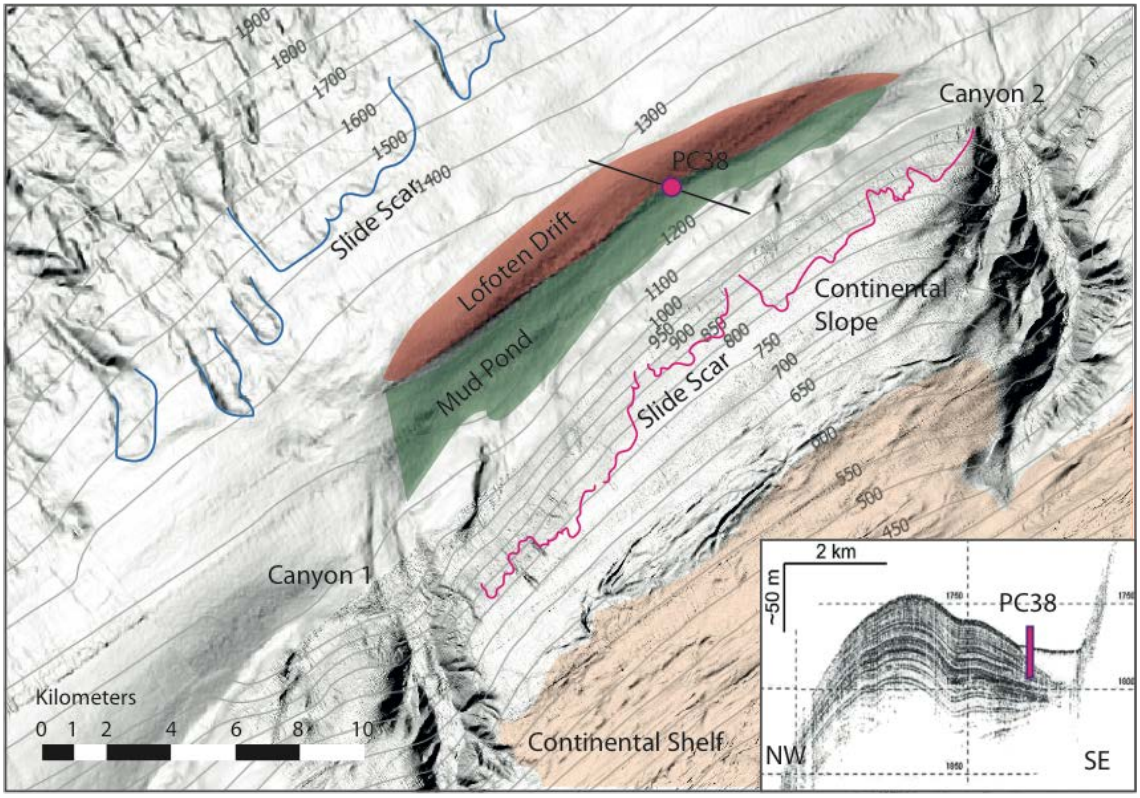

Figure 5.5: Annotated shaded bathymetry map of the Lofoten Drift and potential sources for the slide deposits. Red indicates the mounded Lofoten Drift, Green is the location of the mud pond, identified by flat topography between the slope and the drift. Pink lines indicate landslide scars as per the Mareano database. Blue lines to the top left highlight deeper slide scars on the basin side of the drift, suggestive of a potential larger failure. Inset: Topaz sub-bottom profile from Rise et al. (2013) showing the acoustically transparent mud pond between the drift (left) and the continental slope (right) pink bar indicates approximate position of PC38. Core PC50 is beyond the north western edge of this map but can be seen in Figure 5.1.

A potential source for the LCD slide is the shallow slide scars (pink scar outlines, figure 5.5) along the steepest section of the slope between 700 and 900 m water depth. This potential source is in close proximity to the LCD turbidite which is consistent with the large blocks of intact hemipelagite in the deposit suggesting minimal transport (Figure 5.3). No dates currently exist for the failure planes of these smaller slides from these scars. This would be a suitable target for future coring, and allow the slide scar dates, and the LCD turbidite dates detailed here to be directly compared, and confirm these scars as the source of the LCD turbidite. The inset shows the sub-bottom profile discussed in Rise *et al.* (2013) used to site the cores.

5.7 Discussion

5.7.1 A previously undocumented submarine landslide on the Norwegian continental margin

Analysis of sediments from the LCD slide identified by Rise *et al.* (2013) reveals a significantly different composition to any slides along the Norwegian margin, as established in chapter 3 (figure 5.4). We suggest the slide is locally triggered, and not related to the either the adjacent Trænadjupet or Nyk slides, the Storegga Slide, or failures from the Bear Island Fan. The bathymetry shows near continuous slide scars immediately above the mud pond, located at c. 750-850m water depths. These scars extend between canyons 1 and 2, about 200 m below the shelf break. Further slide scars downslope have not been dated but could be synchronous with slides from high up on the slope, and therefore contribute more mass to the overall failure deposit. This would have to be tested with further work, and dating the deposits in core PC 50, within the Lofoten Basin.

The available data do not allow for an accurate measurement of deposit volume; however, a first order estimate can be made from its extent as observed on bathymetric data and its depth measured on the 2D seismic reflection profile. The mud pond is 18 km long, and 1.5 km wide. Using the maximum depth of the mud pond, and assuming constant thickness throughout, this yields a volume of 1.08 km^3. This maximum volume indicates the slide was unlikely to have been regionally tsunamigenic (Tappin, 2010). However, relatively small slides have been documented to generate local tsunamis, for instance, the Nice Harbour tsunami of 1979 was triggered by a failure of 0.1 km^3, generating waves of 2-3 m high locally (Dan *et al.,* 2007; Labbé *et al.*, 2012). The Palos Verdes debris avalanche (c. 7,500 years BP) also involved a small 0.34 km^3 volume, but modelled to produce a locally 10 m-high wave (Locat *et al.*, 2004; Tappin, 2010). Therefore, the proximity of the deposit to the Lofoten Islands highlights the potential hazard posed by an equivalent future event to local onshore population and infrastructure.

5.7.2 Assessing the importance of local effects versus regional triggering

The 2,000-year difference in age between the Trænadjupet Slide and the LCD slide clearly illustrates that the two events were not synchronous. Whilst this does not rule out a separate earthquake trigger for each event, it does indicate local rather than regional factors may be more important in triggering these slides. The age of the Trænadjupet Slide was determined via multiple dates above and below the bed in cores across the Trænadjupet Slide and Lofoten Basin.

Preconditioning of submarine slopes for failure has been extensively studied in glacial regions, and the causes can be broadly split into five contributing factors (Lee, 2009; Leynaud *et al*., 2009; Urlaub *et al*., 2013): (1) sedimentation rates are highly variable in glacial regions, both in type and quantity. During glacial periods, large amounts of coarse sediment are dumped at rates of up to 36m / ka, on top of fine grained interglacial clays (Solheim *et al*., 2005; Leynaud *et al*., 2009). This rapid sedimentation loads the shelf with significant quantities of sediment; (2) throughout the glacial period, the locus of sedimentation is also shifted seaward, onto the steeper continental slope (Lee, 2009); (3) the high latitudes contain significant quantities of methane clathrate, which can be destabilised by changing temperatures and pressures. Destabilising clathrate ice forms free gas which will destabilise the sediment column above (Maslin *et al*., 2004; Lee, 2009); (4) the retreat of large ice sheets alters the isostatic pressure on the continental slope and shelf, and can trigger moderate earthquakes (Lee, 2009); and (5) changes in groundwater flow can be driven by ice sheet loading, affecting the pore water pressure within the marine sediments, priming the slope for failure (Lee, 2009). Distinguishing between potential preconditioning and triggers is an area of on-going research, and relies on accurate dating of turbidite deposits (Urlaub *et al*., 2013). Should multiple slides be found to be of the same age, this may be interpreted as implying a regional trigger, such as a large earthquake (Goldfinger *et al*., 2010; Pouderoux *et al*., 2012). This approach must be used with extreme caution in regions such as the Lofoten Basin, where the ^{14}C reservoir effect is unconstrained, and highly variable (Voelker *et al*., 1998a). Furthermore, closely spaced failures on a scale of tens of years, are unlikely to be resolved using the AMS radiocarbon method.

The similarities in composition between the Lofoten Drift turbidite and the turbidite recovered in core PC50 imply a similar source and may represent a larger failure or series of failures on this section of the continental slope. Bathymetric features support smaller landslides involving the lower slope of the drift, as well as failures higher up on the slope. The potential involvement of the lower slope raises the possibility of this being a larger submarine slide; thus, under this scenario the generation of a small tsunami is more probable.

Both the Trænadjupet Slide and the ponded unit occur several thousand years after the retreat of the Fennoscandian Ice Sheet, which was complete by 12,700 years Cal BP (Vorren *et al.*, 1988, 2015; Rise *et al.*, 2013; Brendryen *et al.*, 2015). The timing of slides from the Storegga Slide Complex is presumed to have occurred several thousand years after peak deglaciation, during a period of maximum uplift and post-glacial seismicity (Bryn *et al.*, 2005; Solheim *et al.*, 2005). Chapters 3 and 4 discussed the timing of the Holocene Storegga and Tampen slides, placing each 5-7,000 years after peak deglaciation. This is slightly longer for the both Trænadjupet and the LCD turbidite, and substantially shorter for the older Nyk Slide

(c. 19 ka BP), which occurred towards the end of the Last Glacial Maximum (LGM). This suggests that during deglaciation, the associated environmental changes: sea level rise, isostatic rebound, a change in sedimentation style and rate, are relevant preconditioning factors for glacially influenced submarine slides, however, each slide complex responds at a different rate to these environmental changes.

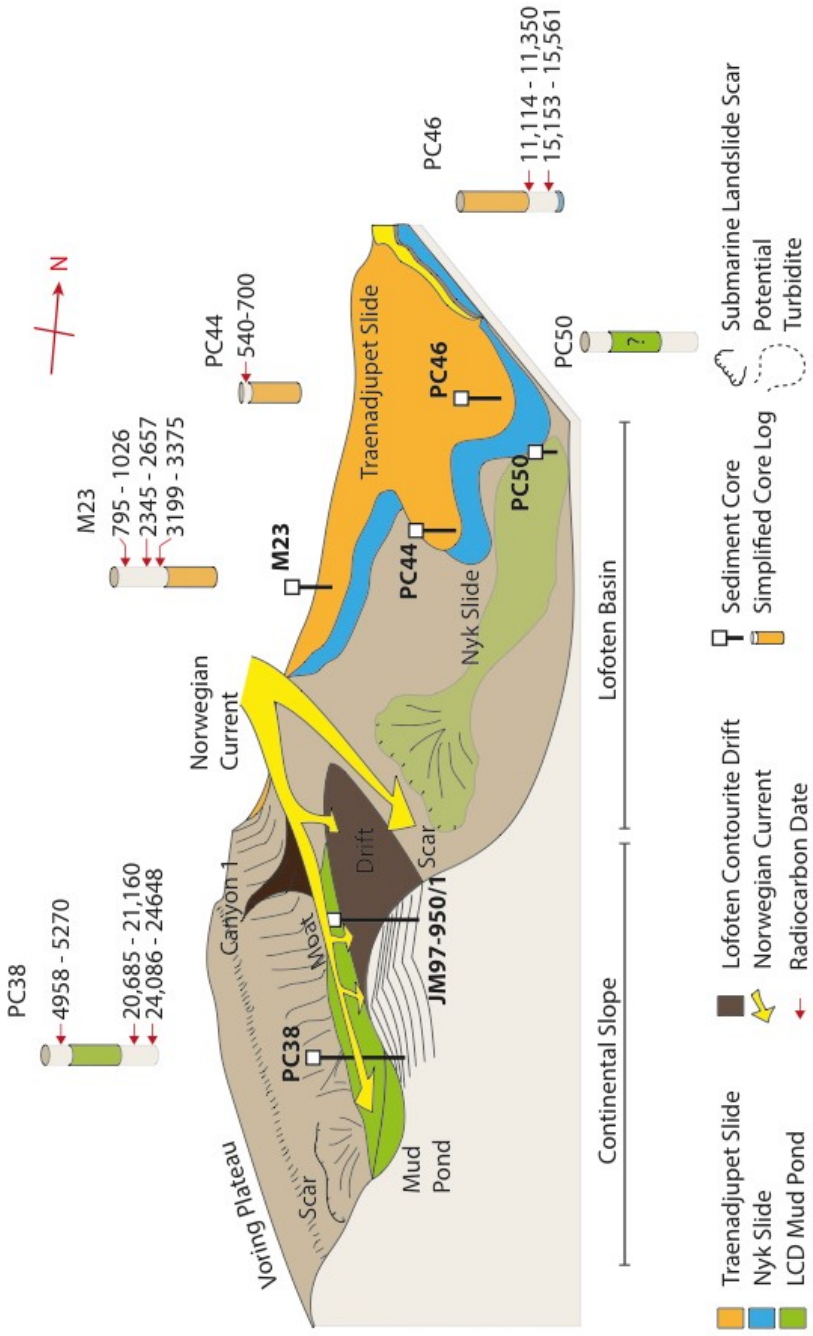

Figure 5.6: 3D cartoon showing the relative position of cores used for the geochemical comparison, the Lofoten Contourite Drift and mud pond, and landslide scars identified in Figure 5.5. All dates are given in calibrated age ranges; colours refer to dated turbidites (Allin, 2016).

The timing of the deposition of the LCD turbidite is coincident with a notable sea level change along the Lofoten coastline. Between 8,000 to 6,500 years Cal BP, relative sea level change

along the Lofoten coastline was occurring at its greatest rate, with a total 14 m change over 1,500 years, yet reaching a stillstand between 6,500-4,00 years Cal BP (Moller, 1984; Balascio *et al.*, 2011). This suggests the maximum sea level change ceased c. 1,000 years before the LCD slide was emplaced. Modelling work has suggested rapid sea level rise can reactivate shallow normal fault systems, and create an increase in seismicity that can trigger submarine slides (Brothers *et al., 2013*). The range of environmental changes identified prior to the triggering of this slide suggests a net-sum effect may be the most likely scenario for triggering the LCD slide, whereby a combination of factors together finally triggered the failure.

5.7.3 A regional underestimation of landslide frequency

This work has provided evidence of a newly identified landslide that is unique in age and source to previously documented slides on the Norwegian continental margin. This means that existing databases of submarine slides are incomplete and features a likely under-representation of smaller mass movements (Baeten, 2013; Urgeles and Camerlenghi, 2013). Small slides are often missed during surveys due to issues with data resolution, and yet these still pose a potential risk to local shorelines and offshore infrastructure.

Further evidence of underestimation of the submarine landslide tsunami risk can be identified in the onshore record of tsunami deposits. Garth Loch on Shetland records three tsunami deposits, one at 8,200 years Cal BP, relating to the Storegga Tsunami, and two younger deposits dated to c. 5,500 Cal BP and 1,500 Cal BP. The 5,500 Cal BP tsunami was locally significant, despite no source having been identified as yet. The tsunami height was reconstructed as being 10 m above sea level (3 m above modern sea-level; relative sea level at the time was 7 m lower), with a very limited geographical extent. This height was reconstructed from a local relative sea level change curve, built using radiocarbon dates of submerged peat on Shetland (Bondevik *et al*., 2005). Given the dimensions of the LCD slide, it is considered unlikely that a slide of $< 1km^3$ could generate a tsunami capable of reaching Shetland from Lofoten (Tappin, 2010). A small local submarine slide remains a likely source for the 5,500 Cal years BP tsunami deposit on the Shetland Islands. No potential source has been identified for the 1,500 Cal BP tsunamite, and this deposit has only been located at Garth Loch, suggesting a local trigger is most plausible. These examples illustrate the incomplete nature of the existing landslide tsunami catalogue offshore Norway, which is likely to be representative of most global landslide databases.

5.8 Conclusions

In this chapter, a new submarine landslide from the Nordic Seas has been dated to c. 5,500 Cal BP. Geochronological and provenance evidence demonstrate this slide is not related to

the large Trænadjupet slide failure, 40 km to the south. The slide has a maximum volume of 1 km^3, and is therefore unlikely to have generated a regional tsunami. However, based on comparisons to other small submarine landslides known to have generated tsunamis, the possibility of a local tsunami cannot be ruled out. This study highlights further work is needed to date, and accurately estimate the tsunamigenic potential of smaller slides from passive margins, which still pose a risk to populations and infrastructure.

Chapter 6 Conclusions and Future Work

The revised timeline of slides presented in this thesis has considerable implication for the UK and Europe with regards to managing and mitigating the potential risk posed by submarine landslides. This Chapter addresses the key questions posed in the introduction.

6.1 Question 1: What is the timing of mega-slides from the Storegga Slide Complex and how accurately can this be constrained?

The marine sediment core recovered from the Ægir Ridge captured two mega- turbidites, both geochemically constrained as sourced from the Storegga Slide Complex. The younger turbidite represents the deposit of the Holocene Storegga Slide, and the date generated from the core stratigraphy (8,020 ± 2,000 years BP) is in excellent agreement with the proposed date from terrestrial deposits of the Storegga tsunami (8,170 ± 200 years BP). The older turbidite has been interpreted here as a deposit from the Tampen Slide. This slide was estimated to have occurred c. 130,000 years ago. The core stratigraphy places this slide at 55,000 ± 4,000 years BP. This substantial revision moves the slide from an MIS 5 age, to an MIS 3 age. This suggests that the theory of deglaciation playing a role in the preconditioning of the slope is correct, but importantly, that the Storegga Slide Complex can generate massive failures, without a full glacial cycle to precondition, or a full deglacial to trigger the slide. This suggests the required amount of climatic change in the Northern Hemisphere is less than previously thought, and that smaller changes may still have a significant impact.

The level of error for the date of the Tampen Slide is considerable, but unlikely to be further resolved numerically. The stable isotope stratigraphy demonstrates that the slide occurred following a warming period, early in the relatively warm MIS 3 period. If further work were to be undertaken on this core, a cryptotephra search for the NAAZ 2 tephra (55,350 ± 1184 BP) would provide furtherconstraint for the turbidite. This tephra is located within the NGRIP record and therefore offers the best hope of further refining the age.

6.2 Question 2: What are the implications of submarine mega slide recurrence intervals for the UK National Risk Register?

This thesis provides evidence that the risk from the Storegga Slide Complex exceeds the minimum criteria for inclusion in the UK Risk Register. There have been two massive submarine landslides from this slide complex in the last 55,000 years. In addition, although not all submarine slides generate tsunamis, there are many other slide complexes with the

ability to generate massive failures. Whilst many have not been as accurately dated as the Storegga and Tampen Slides, the Fugloy, Andoya, the Faroes, Trænadjupet and Nyk Slides are all post glacial (since 22 ka BP). Slides from the Hinlopen complex are equivalent in size to Storegga, and dated to c. 30 ka BP. The potential for slides from Jan Mayen has been noted, although they are currently undated. Modelling has shown that a slide that exceeds 60 km^3 could generate a small tsunami along our northern coastlines (Berndt *et al.*, 2009). Although wave heights would be limited, we are still an unprepared population with significant coastal infrastructure. The likely risk therefore probably far exceeds the new frequency of slides from the Storegga Slide Complex established in this thesis. The Storegga Slide Complex has been shown here to generate two massive (>3,000 km^3) slides in the last 100,000 years, both would be tsunamigenic. There are numerous other submarine slide complexes in the Nordic Seas which have not been dated, but are known to have deglacial/Holocene triggered slides. On this basis, tsunamigenic submarine landslides should be discussed for inclusion in the UK Risk Register.

6.1 Question 3: How is the timing of mega-slides related to periods of environmental and climatic change?

Both the Storegga and Tampen Slides were triggered during a period of warmth, following a significant loss of mass from the Northern Hemisphere ice sheets. Whilst there is continued debate over the comparative warmth of MIS 3, the stable isotope profile from core 88 shows that there is a delay after the onset of interglacial warming of a few thousand years (5-10). There are broader similarities between the two slides. A significant surface freshening and slow down of the AMOC is well documented from the time of the Holocene Storegga Slide, which is coincident with the 8.2 climatic event. This rapid cooling, and subsequent warming has been related to the final drainage of the proglacial Lake Agassiz.

The Tampen Slide is broadly coincident with the drainage of large proglacial lakes in Northern Russia. These lakes drained into the Arctic Ocean and are linked with significant freshwater signals from the Arctic Ocean cores.

Further similarities are observed prior to the Tampen Slide, where a brief cooling interrupts the warming period preceding the slide, which suggests the slide may have occurred during an intense climate oscillation. This suggestion requires further testing with additional slides across the Nordic Seas.

6.3 Question 4: Was the landslide within the Lofoten Contourite Drift triggered at the same time as the adjacent Trænadjupet Slide

The challenges of dating marine deposits using radiocarbon mean that relating adjacent cores is limited by the radiocarbon reservoir effect. Cores that are located in regions with an unconstrained reservoir, are especially limited. If an event dated in two cores is closer than the maximum estimate of the radiocarbon reservoir (i.e. 400 years as a global average), the two events cannot be conclusively determined as synchronous. If the events are temporally greater than 1200 years apart (the maximum reservoir estimate for the Lofoten Basin), they can confidently be ruled as non-synchronous. Where possible, chronological tools such as tephra should be used to tie events together, as tephra is rapidly deposited over 1-5 years, which represents a greater degree of accuracy than radiocarbon.

Provenance is a more straightforward analysis, the dual use of Rare Earth Elements and ITRAX geochemistry allows for an accurate assessment of the different potential sources within the Nordic Seas. Rare Earth Elements of the source region are well preserved in turbidites, and can be used to asses the tectonic provenance. This narrows the source of sediments to being derived from young volcanic sources, old continental crust or subduction zones. Each source region is also affected by the local geology, such as volcanogenic massive sulphides and regional metamorphism.

6.4 Future Work

6.4.1 The Storegga Slide Complex

To further refine the preconditioning and triggering of the Storegga Slide Complex, longer sediment core records are required. The revised date of the Tampen Slide suggests the older slides from this complex would benefit from new dates from more precise dating using sediment cores. Only through this method can the theory of the slides being linked to deglaciations be thoroughly tested. This thesis represents a significant step forward, but the number of well dated slides from this complex is still limited to two, which is insufficient for statistical testing. The 3.5 kHZ data does suggest that some areas adjacent to the Ægir Ridge may contain thinner turbidite deposits, which could be penetrated with piston cores. To penetrate the slide deposits within the ridge, or closer to the centre of the basin would require a drill ship. Of particular interest is why there are no documented slides prior to 2.74 Ma. The Nordic Seas have been in their current configuration for c. 25 Ma, if no slides occurred between 25-2.74 Ma, this would be clear evidence of the importance of glaciations.

The core collection can be used for additional work. Examining the cryptotephra record from the cores will both refine the stratigraphy, and provide new data for the tephra community. If is of particular interest why some horizons are so well represented in this core, such as FMAZ4, but others are absent (i.e. FMAZ 2 and 3). Locating further tephra horizons will aid in the estimation of frequency and magnitude of ash cloud hazards.

Of particular interest with respect to tephra and turbidites, is the notable increase in abundance of foraminifera following the deposition of significant tephra. This can be quantified with an assessment of the Benthic Foraminiferal Accumulation Rate (BFAR), which calculates the flux of benthic forams, and is a proxy for benthic productivity. Tephra and turbidites provide an influx of nutrients to the benthos, as well as the surface ocean, as evidence by the plankton blooms that occur after eruptions. The effect of this has not been assessed quantitatively, and with turbidites of the size of the Storegga and Tampen Slide deposits, represent a significant impact on the benthos. The visible changes in abundance of forams and quite remarkable, and quantifying this change will allow for a more comprehensive interpretation of the impact of these events.

6.4.2 The Lofoten Basin

The more northerly Lofoten Basin was comprehensively cored as part of the 64PE391 cruise. Two transects of cores across the basin have been collected, and partially dated. Assessing the source for these slides is an on-going process, but early analysis suggests it is possible to identify the source region from cores from the central basin. This basin records slides from the Bear Island Fan, the Andoya and Trænadjupet complex, and potentially Jan Mayen. Interestingly, both the Storegga and Tampen Slides are detected within the basin, with consistent age estimates from the Ægir Ridge. The core stratigraphy for this basin has been extended to c. 350 ka with the identification of a large tephra horizon dated elsewhere to 305 ka. This raises the possibility of detecting older slides from the Storegga Slide Complex (Slide R and the Møre Slide), and potentially the Sklinnadjupet slide (c. 250 ka BP). Developing a stable isotope stratigraphy for these cores will also allow a comprehensive assessment of the role ofdeglaciation in slide preconditioning and triggering.

Appendix A Appendices for chapter 3

Digital Appendices available

A.1 Appendix 1a: Tephra shard geochemistry

A.2 Appendix 1b: Rare Earth Element data for turbidite provenance

A.3 Appendix 1c: Database of turbidite compositions from across the Nordic seas

Paper appendices included

A.4 Enlargement of Figure 3.28 page 97

Appendix B Appendix B Appendices for chapter 4

Digital Appendices available

B.1 Appendix 2a: Hemipelagic depth referenced data for stable isotope analysis and IRD counts

B.2 Appendix 2b: Downcore ITRAX data for core PC88 and PC84

List of References

Aagaard-Sørensen, S. *et al.* (2014) 'A Late Glacial–Early Holocene multiproxy record from the eastern Fram Strait, Polar North Atlantic', *Marine Geology*. Elsevier B.V., 355, pp. 15–26.

Abbott, P. M. *et al.* (2011) 'Identification of cryptotephra horizons in a North East Atlantic marine record spanning marine isotope stages 4 and 5a (???60,000- 82,000 a b2k)', *Quaternary International*. Elsevier Ltd and INQUA, 246(1–2), pp. 177–189.

Abbott, P. M. *et al.* (2012) 'A detailed framework of Marine Isotope Stages 4 and 5 volcanic events recorded in two Greenland ice-cores', *Quaternary Science Reviews*. Elsevier Ltd, 36, pp. 59–77.

Abbott, P. M. *et al.* (2013) 'Cryptotephrochronology of the Eemian and the last interglacial-glacial transition in the North East Atlantic', *Journal of Quaternary Science*, 28(5), pp. 501–514.

Abbott, P. M. *et al.* (2014) 'Re-evaluation and extension of the Marine Isotope Stage 5 tephrostratigraphy of the Faroe Islands region: The cryptotephra record', *Palaeogeography, Palaeoclimatology, Palaeoecology*, 409, pp. 153– 168.

Abrantes, F. *et al.* (1998) 'Sediment fluxes along the northeastern European Margin: Inferring hydrological changes between 20 and 8 kyr', *Marine Geology*, 152(1–3), pp. 7–23.

Adams, J. (1990) 'Palaeoseismicity of the Cascadia Subduction Zone: Evidence from turbidites off the Oregon-Washington Margin', *Tectonics*, 9(4), pp. 569–583.

Alexanderson, H. *et al.* (2011) 'A multi-method approach to dating middle and late Quaternary high relative sea-level events on NW Svalbard – A case study', *Quaternary Geochronology*. Elsevier B.V, 6(3–4), pp. 326–340.

Alexanderson, H., Eskola, K. O. and Helmens, K. F. (2008) 'OPTICAL DATING OF A LATE QUATERNARY SEDIMENT SEQUENCE FROM SOKLI , NORTHERN FINLAND',32, pp. 51–59.

Alley, R. B. *et al.* (2010) 'History of the Greenland Ice Sheet: Palaeoclimatic insights', *Quaternary Science Reviews*. Elsevier Ltd, 29(15–16), pp. 1728–1756.

Alley, R. B. and Agustsdottir, A. M. (2005) 'The 8k event: Cause and consequences of a major Holocene abrupt climate change', *Quaternary Science Reviews*, 24(10–11), pp. 1123–1149.

Allin, J. R. (2016) *The timing and frequency of large volume landslides and turbidity currents along the North-Eastern Atlantic Margin*. University of Southampton.

Allin, J. R. *et al.* (2017) 'New insights into the age and emplacement dynamics of large (>100 km3) and weakly tsunamigenic submarine landslides on the Norwegian Margin', *in prep*.

Amundsen, H. B. *et al.* (2015) 'Late Weichselian – Holocene evolution of the high- latitude Andøya submarine Canyon, North-Norwegian continental margin', *Marine Geology*, 363, pp. 1–14.

Andrews, J. T. *et al.* (2002) 'Distribution, sediment magnetism and geochemistry of the Saksunarvatn (10 180 ± 60 cal. yr BP) tephra in marine, lake, and terrestrial sediments, northwest Iceland', *Journal of Quaternary Science*, 17(8), pp. 731– 745.

Andruleit, H. A. and Baumann, K. H. (1998) 'History of the last deglaciation and holocene in the Nordic seas as revealed by coccolithophore assemblages', *Marine Micropalaeontology*, 35(3–4), pp. 179–201.

Ascough, P., Cook, G. and Dugmore, A. (2005) 'Methodological approaches to determining the marine radiocarbon reservoir effect', *Progress in Physical Geography*, 29(4), pp. 532–547.

Astakhov, V. I. (2013) 'Pleistocene glaciations of northern Russia – a modern view', 42(Astakhov 2004), pp. 1–24.

Astakhov, V. I. (2014) 'The postglacial Pleistocene of the northern Russian mainland', *Quaternary Science Reviews*. Elsevier Ltd, 92, pp. 388–408.

Austin, W. E. N. *et al.* (2011) 'North Atlantic reservoir ages linked to high Younger Dryas atmospheric radiocarbon concentrations', *Global and Planetary Change*. Elsevier B.V., 79(3–4), pp. 226–233.

Austin, W. E. N. *et al.* (2012) 'The synchronization of palaeoclimatic events in the North Atlantic region during Greenland Stadial 3 (ca 27 . 5 to 23 . 3 kyr b2k)', *Quaternary Science Reviews*. Elsevier Ltd, 36, pp. 154–163.

Austin, W. E. N. *et al.* (2014) 'Marine tephrochronology: an introduction to tracing time in the ocean', *Geological Society, London, Special Publications*, pp. 1–5.

Austin, W. E. N. and Hibbert, F. D. (2012) 'Tracing time in the ocean: A brief review of chronological constraints (60-8 kyr) on North Atlantic marine event- based stratigraphies', *Quaternary Science Reviews*. Elsevier Ltd, 36, pp. 28–37.

Austin, W. E. N., Wilson, L. J. and Hunt, J. B. (2004) 'The age and chronostratigraphical significance of North Atlantic Ash Zone II', *Journal of Quaternary Science*, 19(2), pp. 137–146.

Backman, J., Fornaciari, E. and Rio, D. (2009) 'Biochronology and palaeoceanography of late Pleistocene and Holocene calcareous nannofossil abundances across the Arctic Basin', *Marine Micropalaeontology*. Elsevier B.V., 72(1–2), pp. 86–98.

Baeten, N. J. (2013) *Mass movements on the continental slope offshore Lofoten, Northern Norway.*

Baeten, N. J. *et al.* (2013) 'Morphology and origin of smaller-scale mass movements on the continental slope off northern Norway', *Geomorphology*. Elsevier B.V., 187, pp. 122–134.

Baeten, N. J. *et al.* (2014) 'Origin of shallow submarine mass movements and their glide planes - Sedimentological and geotechnical analyses from the continental slope off Northern Norway.', pp. 2335–2360.

Balascio, N. L. *et al.* (2011) 'A multi-proxy approach to assessing isolation basin stratigraphy from the Lofoten Islands, Norway', *Quaternary Research*.University of Washington, 75(1), pp. 288–300.

Barber, D. C. *et al.* (1999) 'Forcing of the cold event of 8,200 years ago by catastrophic drainage of Laurentide lakes', *Nature*, 400, pp. 344–348.

Barrie, C. D. *et al.* (2010) 'Pyrite deformation textures in the massive sulfide ore deposits of the Norwegian Caledonides', *Tectonophysics*. Elsevier B.V., 483(3–4), pp. 269–286.

Bauch, H. a. *et al.* (1996) 'Implications of Stratigraphic and Palaeoclimatic Records of the Last Interglaciation from the Nordic Seas', *Quaternary Research*, 46, pp. 260–269.

Bauch, H. a. *et al.* (2000) 'A palaeoclimatic evaluation of marine oxygen isotope stage 11 in the high-northern Atlantic (Nordic Seas)', *Global and Planetary Change*, 24(1), pp. 27–39.

Bauch, H. a. *et al.* (2001) 'A multiproxy reconstruction of the evolution of deep and surface waters in the subarctic Nordic seas over the last 30,000 yr', *Quaternary Science Reviews*, 20(4), pp. 659–678.

Bauch, H. a. and Erlenkeuser, H. (2008) 'A "critical" climatic evaluation of last interglacial (MIS 5e) records from the Norwegian Sea', *Polar Research*, 27(2), pp. 135–151.

Bauch, H. a. and Weinelt, M. S. (1997) 'Surface water changes in the Norwegian Sea during last deglacial and Holocene times', *Quaternary Science Reviews*, 16(10), pp. 1115–1124.

Baumann, K. (1995) 'Reflection of Scandinavian Ice Sheet Fluctuations in Norwegian Sea Sediments during the Past 150,000 Years', *Quaternary Research*, 43(2), pp. 185–197.

Belanger, Paul, E. (1982) 'Palaeo-oceanography of the Norwegian Sea during the past 130,000 years: coccolithophorid nd foraminiferal data', *Boreas*, 11, pp. 29– 36.

Belanger, P. E. and Streeter, S. S. (1980) 'Distribution and Ecology of Benthic foraminifera in the Norwegian Seag', *Marine Micropalaeontology*, 5, pp. 401–428.

Bendle, J. A. P. and Rosell-Melé, A. (2007) 'High-resolution alkenone sea surface temperature variability on the North Icelandic Shelf: implications for Nordic Seas palaeoclimatic development during the Holocene', *The Holocene*, 17(1), pp. 9–24.

Berg, K., Solheim, A. and Bryn, P. (2005) 'The Pleistocene to recent geological development of the Ormen Lange area', *Marine and Petroleum Geology*, 22(1–2 SPEC. ISS.), pp. 45–56.

Berndt, C. *et al.* (2009) 'Tsunami modeling of a submarine landslide in the Fram Strait', *Geochemistry, Geophysics, Geosystems*, 10(4), p. n/a-n/a.

Berndt, C. *et al.* (2014) 'Temporal constraints on hydrate-controlled methane seepage off Svalbard.', *Science (New York, N.Y.)*, 343(6168), pp. 284–7.

Billups, K., Rabideaux, N. and Stoffel, J. (2011) 'Suborbital-scale surface and deep water records in the subtropical North Atlantic: implications on thermohaline overturn', *Quaternary Science Reviews*. Elsevier Ltd, 30(21–22), pp. 2976–2987.

Bleil, U. and Gard, G. (1989) 'Chronology and correlation of Quaternary magnetostratigraphy and nannofossil biostratigraphy in Norwegian-Greenland Sea sediments', *Geologische Rundschau*, 78(3), pp. 1173–1187.

Blindheim, J. and Østerhus, S. (2005) 'The Nordic Seas, Main Oceanographic Features', *Geophysical Monograph Series*, 158, pp. 11–37.

Blockley, S. P. E. *et al.* (2014) 'Tephrochronology and the extended intimate (integration of ice-core, marine and terrestrial records) event stratigraphy 8– 128 ka b2k', *Quaternary Science Reviews*. Elsevier Ltd, 106, pp. 88–100.

Bond, G. *et al.* (1992) 'Evidence for massive discharges of icebergs into the North Atlantic ocean during the last glacial period', *Nature*, 360(6401), pp. 245–249.

Bond, G. C. and Lotti, R. (1995) 'Iceberg discharges into the north atlantic on millennial time scales during the last glaciation.', *Science*, 267(5200), pp. 1005– 1010.

Bondevik, S. *et al.* (1997) 'The Storegga tsunami along the Norwegian coast, its age and run up', *Boreas*, 26(April), pp. 29–53.

Bondevik, S. *et al.* (1999) 'Late Weichselian marine C-14 reservoir ages at the western coast of Norway', *Quaternary Research*, 52(1), pp. 104–114.

Bondevik, S. *et al.* (2005) 'Evidence for three North Sea tsunamis at the Shetland Islands between 8000 and 1500 years ago', *Quaternary Science Reviews*,24(14– 15), pp. 1757–1775.

Bondevik, S. *et al.* (2006) 'Changes in north Atlantic Radiocarbon Reservoir Ages During the Allerod and Younger Dryas', *Science*, 312(2), pp. 1514–1517.

Bondevik, S., Stormo, S. K. and Skjerdal, G. (2012) 'Green mosses date the Storegga tsunami to the chilliest decades of the 8.2 ka cold event', *Quaternary Science Reviews*. Elsevier Ltd, 45, pp. 1–6.

Bondevik, S., Svendsen, J. I. and Mangerud, J. (1997) 'Tsunami sedimentary facies deposited by the Storegga tsunami in shallow marine basins and coastal lakes, western Norway', *Sedimentology*, 44(6), pp. 1115–1131.

Bondevik, S., Svendsen, J. I. and Mangerud, J. (1998) 'Distinction between the Storegga tsunami and the Holocene marine transgression in coastal basin deposits of western Norway', *Journal of Quaternary Science*, 13(6), pp. 529–537.

Boudreau, B. P. (1994) 'Is burial velocity a master parameter for bioturbation?', *Geochimica et Cosmochimica Acta*, 58(4), pp. 1243–1249.

Bouma, A. H. (1962) *Sedimentology of some Flysch deposits: A graphic approach to facies interpretation*. Elsevier.

Bouma, A. H. (1964) 'Turbidites', *Developments in Sedimentology*, 3, pp. 247– 256.

Bouma, A. H. (1987) 'Megaturbidite: An acceptable term?', *Geo-Marine Letters*, 7(2), pp. 63–67.

Bourget, J. *et al.* (2013) 'Late Quaternary megaturbidites of the Indus Fan: Origin and stratigraphic significance', *Marine Geology*. Elsevier B.V., 336, pp. 10–23.

Bourne, A. J. *et al.* (2013) 'Revisiting the Faroe Marine Ash Zone III in two Greenland ice cores: Implications for marine-ice correlations', *Journal of Quaternary Science*, 28(7), pp. 641–646.

Bradley, R. S. and England, J. H. (2008) 'The Younger Dryas and the Sea of Ancient Ice', *Quaternary Research*, 70(1), pp. 1–10.

Brauer, A. *et al.* (2014) 'The importance of independent chronology in integrating records of past climate change for the 60-8ka INTIMATE time interval', *Quaternary Science Reviews*, 106, pp. 47–66.

Breivik, A. J. *et al.* (2006) 'Rates of continental breakup magmatism and seafloor spreading in the Norway Basin–Iceland plume interaction', *Journal of Geophysical Research*, 111(B7), p. B07102.

Brendryen, J. *et al.* (2015) 'Ice sheet dynamics on the Lofoten–Vesterålen shelf, north Norway, from Late MIS-3 to Heinrich Stadial 1', *Quaternary Science Reviews*, 119, pp. 136–156.

Brendryen, J., Haflidason, H. and Sejrup, H. P. (2010) 'Norwegian Sea tephrostratigraphy of marine isotope stages 4 and 5: Prospects and problems for tephrochronology in the North Atlantic region', *Quaternary Science Reviews*. Elsevier Ltd, 29(7–8), pp. 847–864.

Brendryen, J., Haflidason, H. and Sejrup, H. P. (2011) 'Non-synchronous deposition of North Atlantic Ash Zone II in Greenland ice cores, and NorthAtlantic and Norwegian Sea sediments: An example of complex glacial-stage tephra transport', *Journal of Quaternary Science*, 26(7), pp. 739–745.

Bronk Ramsey, C. (2007) 'Deposition Models for Chronological Records', (September 2006), pp. 1–42.

Bronk Ramsey, C. *et al.* (2014) 'Integrating timescales with time-transfer functions: A practical approach for an INTIMATE database', *Quaternary Science Reviews*. Elsevier Ltd, 106, pp. 67–80.

Bronk Ramsey, C. *et al.* (2015) 'Improved age estimates for key Late Quaternary European tephra horizons in the RESET lattice', *Quaternary Science Reviews*. Elsevier Ltd, 118, pp. 18–32.

Brothers, D. S., Luttrell, K. M. and Chaytor, J. D. (2013) 'Sea-level-induced seismicity and submarine landslide occurrence', *Geology*, 41(9), pp. 979–982.

Brook, E.J. *et al.* (1996) 'Rapid Variations in atmospheric methane concentration during the past 110,000 years', *Science* 273, 1087-1091

Bryn, P. *et al.* (2003) 'The Storegga Slide Complex; Repeated Large Scale Sliding in Response to Climatic Cyclicity', in Locat, J., Mienert, J., and Boisvert, L. (eds) *Submarine Mass Movements and Their Consequences: 1st International Symposium*. Dordrecht: Springer Netherlands, pp. 215–222.

Bryn, P. *et al.* (2005) 'Explaining the Storegga Slide', *Marine and Petroleum Geology*, 22(1–2), pp. 11–19.

Bugge, T. (1983) *Submarine slides on the Norwegian continental margin, with special emphasis on the Storegga area. IKU Publ 110, 152 pp.pdf*. The Norwegian Institute of Technology.

Bugge, T. *et al.* (1987) 'A giant three-stage submarine slide off Norway', *Geo- Marine Letters*, 7(4), pp. 191–198.

Bugge, T., Belderson, R. H. and Kenyon, N. H. (1988) 'The Storegga Slide', *Philosophical Transactions of the Royal Society A: Mathematical, Physical and Engineering Sciences*, pp. 357–388.

Bungum, H., Lindholm, C. and Faleide, J. I. (2005) 'Postglacial seismicity offshore mid-Norway with emphasis on spatio-temporal-magnitudal variations', *Marine and Petroleum Geology*, 22(1–2 SPEC. ISS.), pp. 137–148.

Chand, S. *et al.* (2011) 'Stratigraphic development of the south Vøring margin (Mid-Norway) since early Cenozoic time and its influence on subsurface fluid flow', *Marine and Petroleum Geology*, 28(7), pp. 1350–1363.

Channell, J. E. T. (2006) 'Late Brunhes polarity excursions (Mono Lake, Laschamp, Iceland Basin and Pringle Falls) recorded at ODP Site 919 (Irminger Basin)', *Earth and Planetary Science Letters*, 244(1–2), pp. 378–393.

Channell, J. E. T. *et al.* (2012) 'A 750-kyr detrital-layer stratigraphy for the North Atlantic (IODP Sites U1302 – U1303 , Orphan Knoll , Labrador Sea)', *Earth and Planetary Science Letters*. Elsevier B.V., 317–318, pp. 218–230.

Channell, J. E. T. (2014) 'The Iceland Basin excursion: Age, duration, and excursion field geometry', *Geochemistry Geophysics Geosystems*, 15, pp. 4920– 4935.

Channell, J. E. T., Hodell, D. A. and Lehman, B. (1997) 'Relative geomagnetic palaeointensity and δ18O at ODP Site 983 (Gardar Drift, North Atlantic) since 350 ka', *Earth and Planetary Science Letters*, 153(1–2), pp. 103–118.

Channell, J. E. T. and Xuan, C. (2009) 'Self-reversal and apparent magnetic excursions in Arctic sediments', *Earth and Planetary Science Letters*. Elsevier B.V., 284(1–2), pp. 124–131.

Channell, J. E. T., Xuan, C. and Hodell, D. A. (2009) 'Stacking palaeointensity and oxygen isotope data for the last 1.5 Myr (PISO-1500)', *Earth and Planetary Science Letters*. Elsevier B.V., 283(1–4), pp. 14–23.

Clark, P. U. and Mix, a. C. (2002) 'Ice sheets and sea level of the Last Glacial Maximum.', *Quaternary Science Reviews*, 21, pp. 1–7.

Clarke, G. K. C. *et al.* (2004) 'Palaeohydraulics of the last outburst flood from glacial Lake Agassiz and the 8200BP cold event', *Quaternary Science Reviews*, 23(3–4), pp. 389–407.

Corfu, F., Andersen, T. B. and Gasser, D. (2014) 'The Scandinavian Caledonides: main features, conceptual advances and critical questions', *Geological Society, London, Special Publications*, 390(1), pp. 9–43.

Cortijo, E., Labeyrie, L. and Vidal, L. (1997) 'Changes in sea surface hydrology associated with Heinrich event 4 in the North Atlantic Ocean between 40° and 60°N', *Earth and Planetary ….*

Craig, H. (1957) 'Isotopic standards for carbon and oxygen & correction factors for mass spectrometric analysis', *Geochemica et Cosmochimica Acta*, 12, pp. 133–149.

Creveling, J. R., Mitrovica, J. X. and Pico, T. (2017) 'Sea-Level records from the U.S and mid-Atlantic constrain Laurentide Ice Sheet extent during Marine Isotope Stage 3', *Nature Communications*. Nature Publishing Group, 8(May), pp. 1–6.

Crocker, A. J. *et al.* (2016) 'Geochemical response of the mid-depth Northeast Atlantic Ocean to freshwater input during Heinrich events 1 to 4', *Quaternary Science Reviews*. Elsevier Ltd, 151, pp. 236–254.

Cronan, D. S., Rothwell, R. G. and Croudace, I. W. (2010) 'An ITRAX Geochemical Study of Ferromanganiferous Sediments from the Penrhyn Basin, South Pacific Ocean', *Marine Georesources & Geotechnology*, 28(3), pp. 207–221.

Croudace, I. W., Rindby, a. and Rothwell, R. G. (2006) 'ITRAX: description and evaluation of a new multi-function X-ray core scanner', *Geological Society, London, Special Publications*, 267(1), pp. 51–63.

Dahlgren, K. I. T. and Vorren, T. O. (2003) 'Sedimentary environment and glacial history during the last 40 ka of the Vøring continental margin, mid-Norway', *Marine Geology*, 193.

Dahlgren, K. I. T., Vorren, T. O. and Laberg, J. S. (2002) 'The role of grounding- line sediment supply in ice-sheet advances and growth on continental shelves : an example from the mid-

Norwegian sector of the Fennoscandian ice sheet during the Saalian and Weichselian', 96, pp. 25–33.

Dalton, A. S. *et al.* (2016a) 'Constraining the Late Pleistocene history of the Laurentide Ice Sheet by dating the Missinaibi Formation , Hudson Bay Lowlands , Canada', *Quaternary Science Reviews*. Elsevier Ltd, 146, pp. 288–299.

Dalton, A. S. *et al.* (2016b) 'Constraining the Late Pleistocene history of the Laurentide Ice Sheet by dating the Missinaibi Formation , Hudson Bay Lowlands , Canada', *Quaternary Science Reviews*. Elsevier Ltd, 146, pp. 288–299.

Dan, G., Sultan, N. and Savoye, B. (2007) 'The 1979 Nice harbour catastrophe revisited: Trigger mechanism inferred from geotechnical measurements and numerical modelling', *Marine Geology*, 245(1–4), pp. 40–64.

Davies, S. M., Wastegård, S., *et al.* (2010) 'Tracing volcanic events in the NGRIP ice-core and synchronising North Atlantic marine records during the last glacial period', *Earth and Planetary Science Letters*. Elsevier B.V., 294(1–2), pp. 69–79.

Davies, S. M., Larsen, G., *et al.* (2010) 'Widespread dispersal of Icelandic tephra: How does the Eyjafj??ll eruption of 2010 compare to past Icelandic events?', *Journal of Quaternary Science*, 25(5), pp. 605–611.

Davies, S. M. *et al.* (2012) 'Integrating the INTIMATE records using tephrochronology: Rising to the challenge', *Quaternary Science Reviews*. Elsevier Ltd, 36, pp. 11–27.

Davies, S. M. *et al.* (2014) 'A North Atlantic tephrostratigraphical framework for 130-60kab2k: New tephra discoveries, marine-based correlations, and future challenges', *Quaternary Science Reviews*. Elsevier Ltd, 106, pp. 101–121.

Davies, S. M., Turney, C. S. M. and Lowe, J. J. (2001) 'Identification and significance of a visible, basalt-rich Vedde Ash layer in a Late-glacial sequence on the Isle of Skye, Inner Hebrides, Scotland', *Journal of Quaternary Science*, 16(2), pp. 99–104.

Davies, S. M., Wastegård, S. and Wohlfarth, B. (2003) 'Extending the limits of the Borrobol Tephra to Scandinavia and detection of new early Holocene tephra', *Quaternary Research*, 59(3), pp. 345–352.

Dawson, A. G., Bondevik, S. and Teller, J. T. (2011) 'Relative timing of the Storegga submarine slide, methane release, and climate change during the 8.2 ka cold event', *The Holocene*, 21(7), pp. 1167–1171.

Dawson, A. G., Long, D. and Smith, D. E. (1988) 'The Storegga Slides: Evidence from eastern Scotland for a possible tsunami', *Marine Geology*, 82(3–4), pp. 271– 276.

Dawson, S. and Smith, D. (2000) 'The sedimentology of middle Holocene tsunami facies in northern Sutherland, Scotland, UK', *Marine Geology*, 170, pp. 69–79.

Dokken, T. M. and Jansen, E. (1999) 'Rapid changes in the mechanism of ocean convection during the last glacial period', *Nature*, 401(September 1999), pp.458–461.

Dowdeswell, J. a. *et al.* (1999) 'Asynchronous depostion of ice-rafted layers in the Nordic seas and North Atlantic Ocean', *Nature*, 400(July), pp. 348–351.

Dowdeswell, J. A. *et al.* (1996) 'Large scale sedimentation on the glacier- influenced Polar North Atlantic margins: Long-range side-scan sonar evidence.', 23(24), pp. 3535–3538.

Dugmore, a. J., Larsen, G. r. and Newton, a. J. (1995) 'Seven tephra isochrones in Scotland', *The Holocene*, 5(3), pp. 257–266.

Duplessy, J. C., Labeyrie, L. and Blanc, P. L. (1988) 'Norwegian sea deep water variations over the last climatic cycle: Palaeo-oceanographical implications', in Wanner, H. and Siegenthaler, U. (eds) *Long and Short Term Variability of Climate*. Berlin, Heidelberg: Springer Berlin Heidelberg, pp. 83–116.

Eldholm, O. (1977) 'Evolution of the Norwegian-Greenland Sea', (70708).

Elger, J. *et al.* (2015) 'The Fram Slide off Svalbard: a submarine landslide on a low-sedimentation-rate glacial continental margin', *Journal of the Geological Society*, 172(2), pp. 153–156.

Elger, J. *et al.* (2016) 'Chronology of the Fram Slide Complex offshore NW Svalbard and its implications for local and regional slope stability', *Marine Geology*. Elsevier B.V.

Engels, S. *et al.* (2008) 'Environmental inferences and chironomid-based temperature reconstructions from fragmentary records of the Weichselian Early Glacial and Pleniglacial periods in the Niederlausitz area (eastern Germany)', 260, pp. 405–416.

Evans, D. *et al.* (2002) 'Along-slope variation in the late Neogene evolution of the mid-Norwegian margin in response to uplift and tectonism', *Exhumation of the North Atlantic Margin: Timing, Mechanisms and Implications for Petroleum Exploration*, 196, pp. 139–151.

Evans, D. J. A. *et al.* (1996) 'Evidence for long-term instability in the Storegga Slide region off western Norway', *Marine Geology*, 130(3–4), pp. 281–292.

Evans, D. J. A. *et al.* (2005) 'Palaeoslides and other mass failures of Pliocene to Pleistocene age along the Atlantic continental margin of NW Europe', *Marine and Petroleum Geology*, 22(9–10), pp. 1131–1148.

Evans, H. F. *et al.* (2007) 'Palaeointensity-assisted chronostratigraphy of detrital layers on the Eirik Drift (North Atlantic) since marine isotope stage 11', *Geochemistry, Geophysics, Geosystems*, 8(11), p. n/a-n/a.

Freire, F. *et al.* (2014) 'Acoustic evidence of a submarine slide in the deepest part of the Arctic, the Molloy Hole', *Geo-Marine Letters*.

Friedman, I. and O'Neil, J. R. (1977) 'Compilation of stable isotope fractionation factors of geochemical interest', in Fleischer, M. (ed.) *Data of Geochemistry,6th Edition*. 6th edn. Untied States Geological Survey.

Fronval, T. and Jansen, E. (1996) 'Rapid changes in ocean circulation and heat flux in the Nordic seas during the last interglacial period', *Nature*, pp. 806–810.

Fronval, T. and Jansen, E. (1997) 'Eemian and early Weichselian (140-60 ka) palaeoceanography and palaeoclimate in the Nordic seas with comparisons conditions Torben Fronval Hydrography and Core Locations', 12(3), pp. 443–462.

Fruergaard, M. *et al.* (2015) 'Tsunami propagation over a wide, shallow continental shelf caused by the Storegga slide, southeastern North Sea, Denmark', *Geology*, 43(12), pp. 1047–1050.

Galaasen, E. V. *et al.* (2014) 'Rapid reductions in North Atlantic Deep Water during the peak of the last interglacial period.', *Science (New York, N.Y.)*, 343(6175), pp. 1129–32.

Gard, G. (1988) 'Late Quaternary calcareous nannofossil biozonation, chronology and palaeo-oceanography in areas north of the faeroe-iceland ridge', *Quaternary Science Reviews*, 7(1), pp. 65–78.

Gartner, S. (1977) 'Calcareous nannofossil biostratigraphy and revised zonation of the Pleistocene', *Marine Micropalaeontology*, 2(C), pp. 1–25.

Gaudino, S. *et al.* (2007) 'The role of different soil sample digestion methods on trace elements analysis: A comparison of ICP-MS and INAA measurement results', *Accreditation and Quality Assurance*, 12(2), pp. 84–93.

Geissler, W. H. *et al.* (2016) 'Arctic megaslide at presumed rest', *Scientific Reports*. Nature Publishing Group, 6, p. 38529.

Giraudeau, J. *et al.* (2010) 'Millennial-scale variability in Atlantic water advection to the Nordic Seas derived from Holocene coccolith concentration records', *Quaternary Science Reviews*. Elsevier Ltd, 29(9–10), pp. 1276–1287.

Goldfinger, C. *et al.* (2010) 'Cascadia Great Earthquake Recurrence: Rupture Lengths , Correlations and Constrained OxCal Analysis of Event Ages', p. 97331.

Goldfinger, C. *et al.* (2013) 'Spatially limited mud turbidites on the Cascadia margin: Segmented earthquake ruptures?', *Natural Hazards and Earth System Sciences*, 13(8), pp. 2109–2146.

Goldfinger, C., Nelson, C. H. and Johnson, J. E. (2003) 'Holocene earthquake records from the Cascadia Subduction Zone and Northern San Andreas fault based on precise dating of offshore turbidites', *Annual Review of Earth and Planetary Sciences*, 31(1), pp. 555–577.

Grant, K. M. *et al.* (2012) 'Rapid coupling between ice volume and polar temperature over the past 150,000 years', *Nature*. Nature Publishing Group, 491(7426), pp. 744–747.

Grant, K. M. *et al.* (2014) 'Sea-level variability over five glacial cycles', *Nature Communications*. Nature Publishing Group, 5, p. 5076.

Grauert, M. *et al.* (2001) 'Storegga tsunami deposits in a coastal lake on Suduroy, the Faroe Islands', *Boreas*, 30(4), pp. 263–271.

Grauert, M. and Bjo, S. (2001) 'Storegga tsunami deposits in a coastal lake on Su D uroy , the Faroe Islands'.

Green, T. H., Brunfelt, A. O. and Heier, K. S. (1972) 'Rare-earth element distribution and K/Rb ratios in granulites, mangerites and anorthosites, Lofoten- Vesteraalen, Norway', *Geochimica et Cosmochimica Acta*, 36(2), pp. 241–257.

Griggs, A. J. *et al.* (2014) 'Optimising the use of marine tephrochronology in the North Atlantic: a detailed investigation of the Faroe Marine Ash Zones II, III and IV', *Quaternary Science Reviews*. Elsevier Ltd.

Gudmundsdóttir, E. R. *et al.* (2016) 'A new high-resolution Holocene tephra stratigraphy in eastern Iceland: Improving the Icelandic and North Atlantic tephrochronology', *Quaternary Science Reviews*, 150, pp. 234–249.

Gudmundsdóttir, E. R., Eiríksson, J. and Larsen, G. (2011) 'Identification and definition of primary and reworked tephra in Late Glacial and Holocene marine shelf sediments off North Iceland', *Journal of Quaternary Science*, 26(6), pp. 589– 602.

Gudmundsdóttir, E.R. *et al.* (2011) 'Two new Icelandic tephra markers: The Hekla O tephra layer, 6060 cal. yr BP, and Hekla DH tephra layer, 6650 cal. yr BP. Land-sea correlation of mid-Holocene tephra markers', *The Holocene*, 21(4), pp. 629–639.

Gudmundsdóttir, E. R., Larsen, G. and Eiríksson, J. (2012) 'Tephra stratigraphy on the North Icelandic shelf: extending tephrochronology into marine sediments off North Iceland', *Boreas*, 41(4), pp. 719–734.

Gutierrez-pastor, J. *et al.* (2009) 'Earthquake Control of Holocene Turbidite Frequency Confirmed By Hemipelagic Sedimentation Chronology on the Cascadia and Northern California Active continental margins', 92(92), pp. 179–197.

Guyodo, Y. and Valet, J.-P. (1996) 'Relative variations in geomagnetic intensity from sedimentary records: the past 200,000 years', *Earth and Planetary Science Letters*, 143(1–4), pp. 23–36.

Haflidason, H. *et al.* (2004) 'The Storegga Slide: architecture, geometry and slide development', *Marine Geology*, 213(1–4), pp. 201–234.

Haflidason, H. *et al.* (2005) 'The dating and morphometry of the Storegga Slide', *Marine and Petroleum Geology*, 22(1–2), pp. 123–136.

Haflidason, H. *et al.* (2007) 'Holocene sedimentary processes in the Andøya Canyon system, north Norway', *Marine Geology*, 246(2–4), pp. 86–104.

Haflidason, H., Eiríksson, J. and Van Kreveld, S. (2000) 'The tephrochronolgoy of Iceland and the North Atlantic region during the Middle and Late Quarternary: a review', *J. Quaternary Sci.*, 15(JANUARY), pp. 3–22.

Haflidason, H., Eiríksson, J. and Van Kreveld, S. (2000) 'The tephrochronology of Iceland and the North Atlantic region during the middle and Late Quaternary: A review', *Journal of Quaternary Science*, 15(1), pp. 3–22.

Haflidason, H., Gravdal, A. and Sejrup, H. P. (2003) 'The Northern Storegga Slide Escarpment --- Morphology and Features', in Mienert, J. and Weaver, P. (eds) *European Margin Sediment Dynamics: Side-Scan Sonar and Seismic Images*. Berlin, Heidelberg: Springer Berlin Heidelberg, pp. 45–53.

Hagen, S. and Hald, M. (2002) 'Variation in surface and deep water circulation in the Denmark Strait, North Atlantic, during marine isotope stages 3 and 2', *Palaeoceanography*, 17(4).

Hambach, U., Rolf, C. and Schnepp, E. (2008) 'Magnetic dating of Quaternary sediments, volcanites and archaeological materials: an overview', *Quaternary Science Journal*, 57(1–2), pp. 25–51.

Hansen, B. *et al.* (2003) 'The Iceland-Faroe inflow of Atlantic water to the Nordic Seas', *Progress in Oceanography*, 59(4), pp. 443–474.

Hansen, B. T. and Østerhus, S. (2000) 'North Atlantic–Nordic Seas exchanges', *Progress in Oceanography*, 45(2), pp. 109–208.

Hanski, E. J. *et al.* (2011) 'The Pechenga Ni-Cu Sulfide Deposits , Northwestern Russia : A Review with New Constraints from the Feeder Dikes', *Reviews in Economic Geology*, 17, pp. 145–162.

Harbitz, C. B. (1992) 'Model simulations of tsunamis generated by the Storegga Slides', *Marine Geology*, 105(1–4), pp. 1–21.

Hayward, C. (2012) 'High spatial resolution electron probe microanalysis of tephra and melt inclusions without beam-induced chemical modification', *The Holocene*, 22(1), pp. 119–125.

Heinrich, H. (1988) 'Origin and consequences of cyclic ice rafting in the Northeast Atlantic Ocean during the past 130,000 years', *Quaternary Research*, 29(2), pp. 142–152.

Helmens, K. F. *et al.* (2007) 'Ice-free intervals continuing into Marine Isotope Stage 3 at Sokli in the central area of the Fennoscandian glaciations', 79, pp. 17– 39.

Helmens, K. F. *et al.* (2009) 'Early MIS 3 glacial lake evolution, ice-marginal retreat pattern and climate at Sokli (northeastern Fennoscandia)', *Quaternary Science Reviews*, 28(19–20), pp. 1880–1894.

Helmens, K. F. and Engels, S. (2010) 'Ice-free conditions in eastern Fennoscandia during early Marine Isotope Stage 3: lacustrine records', *Boreas*, 39(2), pp. 399– 409.

Helmens, S. J. B. Æ. O. H. Æ. K. F. (2008) 'Chironomid-based palaeotemperature estimates for northeast Finland during Oxygen Isotope Stage 3', pp. 49–61.

Hemming, S. R. (2004) 'Heinrich events: Massive late Pleistocene ditritus layers of the North Atlanitc and their global cliamate imprint', *Reviews of Geophysics*, 42(2003), pp. 1–43.

Hennekam, R. and Lange, G. J. (2012) 'X-ray fluorescence core scanning of wet marine sediments : methods to improve quality and reproducibility of high- resolution palaeoenvironmental records', *Limnology and Oceanography: Methods*, 10, pp. 991–1003.

Hernández-Molina, F. J., Llave, E. and Stow, D. A. V (2008) 'Chapter 19 Continental Slope Contourites', in *Developments in Sedimentology*, pp. 379–408.

Hibbert, F. D. *et al.* (2010) 'British ice sheet dynamics inferred from North Atlantic ice-rafted debris records spanning the last 175 000 years', *Journal of Quaternary Science*, 25(4), pp. 461–482.

Hibbert, F. D. F. D. *et al.* (2014) 'Identification of a MIS 6 age (c. 180 ka) Icelandic tephra within NE Atlantic sediments: a new potential chronostratigraphicmarker', *Geological Society, London, Special Publications*, 398(1), pp. 65–80.

Hill, T. M., Paull, C. K. and Critser, R. B. (2012) 'Glacial and deglacial seafloor methane emissions from pockmarks on the northern flank of the Storegga Slide complex', *Geo-Marine Letters*, 32(1), pp. 73–84.

Hillaire-Marcel, C., de Vernal, A. and Piper, D. J. W. (2007) 'Lake Agassiz Final drainage event in the northwest North Atlantic', *Geophysical Research Letters*, 34(15), p. L15601.

Hjelstuen, B. O. *et al.* (2004) 'Late Quaternary seismic stratigraphy and geological development of the south Vøring margin, Norwegian Sea', *Quaternary Science Reviews*, 23(16–17), pp. 1847–1865.

Hjelstuen, B. O. *et al.* (2005) 'Late Cenozoic glacial history and evolution of the Storegga Slide area and adjacent slide flank regions, Norwegian continental margin', *Marine and Petroleum Geology*, 22(1–2), pp. 57–69.

Hjelstuen, B. O. and Andreassen, E. V. (2015) 'North Atlantic Ocean deep-water processes and depositional environments: A study of the Cenozoic Norway Basin', *Marine and Petroleum Geology*. Elsevier Ltd, 59, pp. 429–441.

Hjelstuen, B. O., Eldholm, O. and Faleide, J. I. (2007) 'Recurrent Pleistocene mega- failures on the SW Barents Sea margin', *Earth and Planetary Science Letters*, 258(3–4), pp. 605–618.

Hoff, U. *et al.* (2016) 'the Nordic seas 90 kyr ago to present'. Nature Communications, 7, pp. 12247

Hoogakker, B. A. A., Thornalley, D. J. R. and Barker, S. (2016) 'Millennial changes in North Atlantic oxygen concentrations', *Biogeosciences*, 13, pp. 211–221.

Houternmans, J. C. and Suess, H. E. (1973) 'Reservoir models and production rate variation of natural radiocarbon', *J. Geophys. Res.*, 78(12), pp. 1897–1908.

Huber, C. *et al.* (2006) 'Isotope calibrated Greenland temperature record over Marine Isotope Stage 3 and its relation to CH4', *Earth and Planetary Science Letters*, 243(3–4), pp. 504–519.

Hunt, E. J., Croudace, W. I. and MacLachlan, E. S. (2015) 'Use of Calibrated ITRAX XRF Data in Determining Turbidite Geochemistry and Provenance in Agadir Basin, Northwest African Passive Margin', in Croudace, W. I. and Rothwell, G. R. (eds) *Micro-XRF Studies of Sediment Cores: Applications of a non-destructive tool for the environmental sciences*. Dordrecht: Springer Netherlands, pp. 127–146.

Hunt, E. J., Wynn, B. R. and Croudace, W. I. (2015) 'Identification, Correlation and Origin of Multistage Landslide Events in Volcaniclastic Turbidites in the Moroccan Turbidite System', in Croudace, W. I. and Rothwell, G. R. (eds) *Micro-XRF Studies of Sediment Cores: Applications of a non-destructive tool for the environmental sciences*. Dordrecht: Springer Netherlands, pp. 147–172.

Hunt, J. E. *et al.* (2011) 'Sedimentological and geochemical evidence for multistage failure of volcanic island landslides: A case study from Icod landslide on north Tenerife, Canary Islands', *Geochemistry, Geophysics, Geosystems*, 12(12)

Hunt, J. E. *et al.* (2013) 'Frequency and timing of landslide-triggered turbidity currents within the Agadir Basin , offshore NW Africa : Are there associations with climate change , sea level change and slope sedimentation rates ?', *Marine Geology*. Elsevier B.V., 346, pp. 274–291.

Hunt, J. E. *et al.* (2013) 'Multistage collapse of eight western Canary Island landslides in the last 1.5 Ma: Sedimentological and geochemical evidence from subunits in submarine flow deposits', *Geochemistry, Geophysics, Geosystems*, 14(7), pp. 2159–2181.

Hunt, J. E. (2017) 'Identifying and quantifying erosion beneath the deposits of long-runout turbidity currents along their pathway', *Marine Geology*. Elsevier, 389(February), pp. 32–51.

Hunter, S. E. *et al.* (2007) 'Deep western boundary current dynamics and associated sedimentation on the Eirik Drift, Southern Greenland Margin', *Deep Sea Research Part I: Oceanographic Research Papers*, 54(12), pp. 2036–2066.

Imbrie, J. *et al.* (1984) 'The orbital theory of Pleistocene climate: Support from a revised chronology of the marine d18O record', *Milankovitch and Climate: Understanding the Response to Astronomical Forcing*, pp. 269–305.

Laj, C. *et al.* (2000) 'North Atlantic palaeointensity stack since 75ka (NAPIS-75) and the duration of the Laschamp event', *Philosophical Transactions of the Royal Society A: Mathematical, Physical and Engineering Sciences*, 358(1768), pp. 1009–1025.

Jakobsson, M. *et al.* (2001) 'Pleistocene stratigraphy and palaeoenvironmental variation from Lomonosov Ridge sediments, central Arctic Ocean', *Global and Planetary Change*, 31(1–4), pp. 1–22.

Jakobsson, M. *et al.* (2013) 'Arctic Ocean glacial history', *Quaternary Science Reviews*. Elsevier Ltd, 92, pp. 40–67.

Jakobsson, S. P., Jónasson, K. and Sigurðsson, I. a. (2008) 'The three igneous rock series of Iceland', *Jökull*, pp. 117–138.

Jansen, E. *et al.* (1987) 'Large submarine slides on the Norwegian continental margin: Sediments, transport and timing', *Marine Geology*, 78(1–2), pp. 77–107.

Jansen, E. *et al.* (2000) 'Pliocene-Pleistocene Ice Rafting History and Cyclicity in the Nordic Seas During the Last 3.5 Myr', *Palaeoceanography*, 15(6), pp. 709–721.

Jarvis, I. and Higgs, N. (1987) 'Trace-element mobility during early diagenesis in distal turbidites; late Quaternary of the Madeira Abyssal Plain, N Atlantic', *Geology and geochemistry of abyssal plains*, 31(31), pp. 179–214.

Jarvis, I. and Jarvis, K. E. (1985) 'Rare-earth element geochemistry of standard sediments: a study using inductively coupled plasma spectrometry',*Chemical Geology*, 53, pp. 335–344.

Jennings, A. E. *et al.* (2006) 'Freshwater forcing from the Greenland Ice Sheet during the Younger Dryas: evidence from southeastern Greenland shelf cores', *Quaternary Science Reviews*, 25(3–4), pp. 282–298.

Jennings, A. E. *et al.* (2014) 'Holocene tephra from Iceland and Alaska in SE Greenland Shelf Sediments', *Geological Society, London, Special Publications*, 398(1), pp. 157–193.

Jensen, M. A. *et al.* (2011) 'Ice-distal landscape and sediment signatures evidencing damming and drainage of large pro-glacial lakes , northwest Russia'. *Boreas*, Vol 40, pp. 481-497.

Johannsdottir, G. . (2007) *Mid-Holocene to late glacial tephrochronology in west Iceland as revealed in three lacustrine environments*. University of Iceland, Reykjavik.

Jouve, G. *et al.* (2013) 'Microsedimentological characterization using image analysis and μ-XRF as indicators of sedimentary processes and climate changes during Lateglacial at Laguna Potrok Aike, Santa Cruz, Argentina', *Quaternary Science Reviews*, 71, pp. 191–204.

Jovane, L. *et al.* (2013) 'Magnetic methods and the timing of geological processes', *Geological Society, London, Special Publications*, 373(1), pp. 1–12.

Jung, Woo- Yeol and Vogt, P. R. (1997) 'A gravity and magnetic anomaly of Aegir Ridge, Norwegian Sea', *Journal of Geophysical Research*, 102, pp. 5065–5089.

Kandiano, E. S. and Bauch, H. A. (2003) 'Surface ocean temperatures in the north- east Atlantic during the last 500 000 years: evidence from foraminiferal census data', *Terra Nova*, 15(4), pp. 265–271.

Kandiano, E. S., Bauch, H. A. and Müller, A. (2004) 'Sea surface temperature variability in the North Atlantic during the last two glacial-interglacial cycles: Comparison of faunal, oxygen isotopic, and Mg/Ca-derived records', *Palaeogeography, Palaeoclimatology, Palaeoecology*, 204(1–2), pp. 145–164.

Katz, M. E. *et al.* (2003) 'Early Cenozoic benthic foraminiferal isotopes : Species reliability and interspecies correction factors', 18(2), pp. 1–12.

Keser Neish, J. and Ziska, H. (2005) 'Structure of the Faroe Bank Channel Basin, offshore Faroe Islands', *Petroleum Geology: North-West Europe and Global Perspectives - Proceedings of the 6th Petroleum Geology Conference*, pp. 873– 886.

King, E. L. *et al.* (1996) 'Quaternary seismic stratigraphy of the North Sea Fan: glacially-fed gravity flow aprons, hemipelagic sediments, and large submarine slides', *Marine Geology*, 130(3–4), pp. 293–315.

Kissel, C. *et al.* (1999) 'Rapid climatic variations during marine isotopic stage 3: Magnetic analysis of sediments from Nordic Seas and North Atlantic', *Earth and Planetary Science Letters*, 171, pp. 489–502.

Kjaer, K. H. *et al.* (2006) 'Eurasian ice-sheet interaction in northwestern Russia throughout the late Quaternary °', *Boreas*, 35.

Kleiven, H. K. F. *et al.* (2008) 'Reduced North Atlantic deep water coeval with the glacial Lake Agassiz freshwater outburst.', *Science (New York, N.Y.)*, 319(5859), pp. 60–4.

Knies, J. *et al.* (2000) 'A multiproxy approach to reconstruct the environmental changes along the Eurasian continental margin over the last 150 000 years', *Marine Geology*, 163(1–4), pp. 317–344.

Kuhs, M. *et al.* (2014) 'Iceberg-rafted tephra as a potential tool for the reconstruction of ice-sheet processes and ocean surface circulation in the glacial North Atlantic', *Geological Society, London, Special Publications*, pp. 141–155.

Kuijpers *et al.* (2001) 'Late Quaternary slope instability on the Faeroe margin: Mass flow features and timing of events', *Geo-Marine Letters*, 20(3), pp. 149–159.

Kuijpers, A. *et al.* (1998) 'Norwegian Sea overflow variability and NE Atlantic surface hydrography during the past 150,000 years', *Marine Geology*, 152(1–3), pp. 75–99.

Kullerud, G., Padget, P. and Vikes, F. (1955) 'Sphalerite-Bearing Ores in the Caledonides of Northern', *Norsk Geologisk Tidsskrift*.

Kvamme, T. *et al.* (1989) 'Geochemistry of Pleistocene ash zones in cores from the North Atlantic', 69, pp. 251–272.

L'Heureux, J. S. *et al.* (2013) 'Stability, mobility and failure mechanism for landslides at the upper continental slope off Vesterålen, Norway', *Marine Geology*, 346, pp. 192–207.

Labbé, M. *et al.* (2012) 'Refined numerical modeling of the 1979 tsunami in Nice (French Riviera): Comparison with coastal data', *Journal of Geophysical Research: Earth Surface*, 117(1), pp. 1–17.

Laberg, J. S. *et al.* (2000) 'The Andøya Slide and the Andøya Canyon, north- eastern Norwegian–Greenland Sea', *Marine Geology*, 162(2–4), pp. 259–275.

Laberg, J. S. *et al.* (2001) 'Seismic analyses of Cenozoic contourite drift development in the Northern Norwegian Sea', *Marine Geophysical …*, pp. 401– 416.

Laberg, J. S., Vorren, T. O., Mienert, J., *et al.* (2002) 'Late Quaternary palaeoenvironment and chronology in the Trænadjupet Slide area offshore Norway', *Marine Geology*, 188, pp. 35–60.

Laberg, J. S., Vorren, T. O., Mienert, J., *et al.* (2002) 'The Trænadjupet Slide: A large slope failure affecting the continental margin of Norway 4,000 years ago', *Geo-Marine Letters*, 22(1), pp. 19–24.

Laberg, J. S., Vorren, T. O., *et al.* (2005) 'A modern canyon-fed sandy turbidite system of the Norwegian continental margin', *Norsk Geologisk Tidsskrift*, 85(4), pp. 267–277.

Laberg, J. S., Stoker, M. S., *et al.* (2005) 'Cenozoic alongslope processes and sedimentation on the NW European Atlantic margin', *Marine and Petroleum Geology*, 22(9–10), pp. 1069–1088.

Laberg, J. S. *et al.* (2013) 'A submarine landslide complex affecting the Jan Mayen Ridge, Norwegian–Greenland Sea: slide-scar morphology and processes of sediment evacuation', *Geo-Marine Letters*, 34(1), pp. 51–58.

Laberg, J. S. and Vorren, T. O. (1993) 'A Late Pleistocene submarine slide on the Bear Island Trough Mouth Fan', *Geo-Marine Letters*, 13(4), pp. 227–234.

Laberg, J. S. and Vorren, T. O. (2000) 'The Trænadjupet Slide, offshore Norway - Morphology, evacuation and triggering mechanisms', *Marine Geology*, 171, pp. 95–114.

Laberg, J. S. and Vorren, T. O. (2004) 'Weichselian and Holocene growth of the northern high-latitude Lofoten Contourite Drift on the continental slope of Norway', *Sedimentary Geology*, 164(1–2), pp. 1–17.

Laberg, J. S. and Vorren, T. O. (2006) 'Frequency and triggering mechanisms of submarine landslides of the North Norwegian continental margin', *NORSK GEOLOGISK …*, pp. 155–161.

Laberg, J. S., Vorren, T. O. and Knutsen, S.-M. (1999) 'The Lofoten contourite drift off Norway', *Marine Geology*, 159(1–4), pp. 1–6.

Lacasse, C. *et al.* (1996) 'North Atlantic deep-sea sedimentation of Late Quaternary tephra from the Iceland hotspot', *Marine Geology*, 129(3–4), pp. 207– 235.

Lacasse, C. and Garbe-Schönberg, C. D. (2001) *Explosive silicic volcanism in Iceland and the Jan Mayen area during the last 6 Ma: Sources and timing of major eruprtions*, *Journal of Volcanology and Geothermal Research*.

Laj, C. *et al.* (2000) 'North Atlantic palaeointensity stack since 75ka (NAPIS-75) and the duration of the Laschamp event', *Philosophical Transactions of the Royal Society A: Mathematical, Physical and Engineering Sciences*, 358(1768), pp. 1009–1025.

Laj, C., Guillou, H. and Kissel, C. (2014a) 'Dynamics of the earth magnetic field in the 10-75 kyr period comprising the Laschamp and Mono Lake excursions: New results from the French Chaîne des Puys in a global perspective', *Earth and Planetary Science Letters*. Elsevier B.V., 387, pp. 184–197.

Laj, C., Guillou, H. and Kissel, C. (2014b) 'the Laschamp and Mono Lake excursions : New results from the French Chaîne des Puys in a global perspective Questions ':

Laj, C., Kissel, C. and Beer, J. (2004) 'High Resolution Global Palaeointensity Stack Since 75 kyr (GLOPIS-75) Calibrated to Absolute Values', *Timescales of the Palaeomagnetic Field*, 145, pp. 255–265.

Lambeck, K. *et al.* (2006) 'Constraints on the Late Saalian to early Middle Weichselian ice sheet of Eurasia from field data and rebound modelling', *Boreas*, 35(3), pp. 539–575.

Lane, C. S. *et al.* (2012) 'Was the 12.1ka Icelandic Vedde Ash one of a kind?', *Quaternary Science Reviews*. Elsevier Ltd, 33, pp. 87–99.

Langereis, C. G. *et al.* (1997) 'Magnetostratigraphy and astronomical calibration of the last 1.1 Myr from an eastern Mediterranean piston core and dating of short events in the Brunhes', *Geophysical Journal International*, 129(1), pp. 75–94.

Larsen, E. *et al.* (2006) 'Late Pleistocene glacial and lake history of northwestern Russia'. *Boreas*. Vol.35, pp.394-424.

Larsen, N. K. *et al.* (2009) 'Late Quaternary ice sheet, lake and sea history of southwest Scandinavia - A synthesis', *Boreas*, 38(4), pp. 732–761.

Latarius, K. and Quadfasel, D. (2016) 'Water mass transformation in the deep basins of the Nordic Seas: Analyses of heat and freshwater budgets', *Deep Sea Research Part I: Oceanographic Research Papers*. Elsevier, 114, pp. 23–42.

Lawrence, G. W. M. and Cartwright, J. A. (2009) 'The initiation of sliding on the mid Norway margin in the M??re Basin', *Marine Geology*. Elsevier B.V., 259(1–4), pp. 21–35.

Lee, H. J. (2009) 'Timing of occurrence of large submarine landslides on the Atlantic Ocean margin', *Marine Geology*. Elsevier B.V., 264(1–2), pp. 53–64.

Lekens, W. a. H. *et al.* (2009) 'Sedimentation history of the northern North Sea Margin during the last 150 ka', *Quaternary Science Reviews*. Elsevier Ltd, 28(5–6), pp. 469–483.

Lekens, W. A. H. *et al.* (2006) 'Meltwater and ice rafting in the southern Norwegian Sea between 20 and 40 calendar kyr B.P.: Implications for Fennoscandian Heinrich events', *Palaeoceanography*, 21(3), p. n/a-n/a.

Lewis, C. F. M. *et al.* (2012) 'Lake Agassiz outburst age and routing by Labrador Current and the 8.2 cal ka cold event', *Quaternary International*, 260, pp. 83–97.

Leynaud, D., Mienert, J. and Vanneste, M. (2009) 'Submarine mass movements on glaciated and non-glaciated European continental margins: A review of triggering mechanisms and preconditions to failure', *Marine and Petroleum Geology*. Elsevier Ltd, 26(5), pp. 618–632.

Leynaud, D., Sultan, N. and Mienert, J. (2007) 'The role of sedimentation rate and permeability in the slope stability of the formerly glaciated Norwegian continental margin: The Storegga slide model', *Landslides*, 4(4), pp. 297–309.

Licciardi, J., Teller, J. T. and Clark, P. (1999) 'Freshwater routing by the Laurentide Ice Sheet during the last deglaciation', *Mechanisms of global …*.

Lindberg, B., Laberg, J. S. and Vorren, T. O. (2004) 'The Nyk Slide—morphology, progression, and age of a partly buried submarine slide offshore northern Norway', *Marine Geology*, 213(1–4), pp. 277–289.

Lindholm, C. *et al.* (2005) 'Probabilistic and deterministic seismic hazard results and influence of the sedimentary Møre Basin, NE Atlantic', *Marine and Petroleum Geology*, 22(1–2 SPEC. ISS.), pp. 149–160.

Lisiecki, L. E. and Raymo, M. E. (2005) 'A Pliocene-Pleistocene stack of 57 globally distributed benthic D 18 O records', 20(May), pp. 1–17.

Locat, J. *et al.* (2004) 'Numerical analysis of the mobility of the Palos Verdes debris avalanche, California, and its implication for the generation of tsunamis', *Marine Geology*, 203(3–4), pp. 269–280.

Lohmann, G., Zhang, X. and Knorr, G. (2016) 'Abrupt Climate Change Experiments : The Role of Freshwater , Ice Sheets and Deglacial Warming for the Atlantic Meridional Overturning Circulation', 85(June 2015), pp. 161–170.

Lohne, O. S., Mangerud, J. and Birks, H. H. (2013) 'Precise 14C ages of the Vedde and Saksunarvatn ashes and the Younger Dryas boundaries from western Norway and their comparison with the Greenland Ice Core (GICC05) chronology', *Journal of Quaternary Science*, 28(5), pp. 490–500.

Long, A. J. *et al.* (2016) 'Lateglacial and Holocene relative sea-level changes and first evidence for the Storegga tsunami in Sutherland, Scotland', *Journal of Quaternary Science*, 31(3), pp. 239–255.

Long, A. J., Roberts, D. H. and Dawson, S. (2006) 'Early Holocene history of the west Greenland Ice Sheet and the GH-8.2 event', *Quaternary Science Reviews*, 25(9–10), pp. 904–922.

Løseth, H. and Tveten, E. (1996) 'Post-Caledonian structural evolution of the Lofoten and Vesterålen offshore and onshore areas', (Dalland 1981).

Løvholt, F. *et al.* (2017) 'Some giant submarine landslides do not produce large tsunamis', *Geophysical Research Letters*.

Løvholt, F., Harbitz, C. B. and Haugen, K. B. (2005) 'A parametric study of tsunamis generated by submarine slides in the Ormen Lange/Storegga area off western Norway', *Marine and Petroleum Geology*, 22(1–2 SPEC. ISS.), pp. 219–231.

Lowe, J. *et al.* (2008) 'Synchronisation of palaeoenvironmental events in the North Atlantic region during the Last Termination: a revised protocol recommended by the INTIMATE group', *Quaternary Science Reviews*, 27(1–2), pp. 6–17.

Löwemark, L. *et al.* (2014) 'Arctic Ocean Mn-stratigraphy: genesis, synthesis and inter-basin correlation', *Quaternary Science Reviews*. Elsevier Ltd, 92, pp. 97–111.

Löwemark, L., Regan, M. O. and Hanebuth, T. J. J. (2016) 'Late Quaternary spatial and temporal variability in Arctic deep-sea bioturbation and its relation to Mn cycles', *Palaeogeography, Palaeoclimatology, Palaeoecology*. Elsevier B.V., 365– 366(May), pp. 192–208.

MacLachlan, E. S., Hunt, E. J. and Croudace, W. I. (2015) 'An Empirical Assessment of Variable Water Content and Grain-Size on X-Ray Fluorescence Core-Scanning Measurements of Deep Sea Sediments', in Croudace, W. I. and Rothwell, G. R. (eds) *Micro-XRF Studies of Sediment Cores: Applications of a non-destructive tool for the environmental sciences*. Dordrecht: Springer Netherlands, pp. 173–185.

Le Maitre, P. *et al.* (1989) *A classification of igneous rocks and glossary of terms : recommendations of the International Union of Geological Sciences, Subcommission on the Systematics of Igneous Rocks*. Edited by R. W. Le Maitre. International Union of Geological Sciences.

Malamud, B. D. *et al.* (2004) 'Landslide inventories and their statistical properties', *Earth Surface Processes and Landforms*, 29(6), pp. 687–711.

Mangerud, J. *et al.* (2001) 'The chronology of a large ice-dammed lake and the Barents - Kara Ice Sheet advances, northern Russia', *Global and Planetary Change*.

Mangerud, J. (2004) 'Ice-dammed lakes and rerouting of the drainage of northern Eurasia during the Last Glaciation', *Quaternary Science Reviews*, 23(11–13), pp. 1313–1332.

Mangerud, J. *et al.* (2006) 'Marine 14C reservoir ages for 19th century whales and molluscs from the North Atlantic', *Quaternary Science Reviews*, 25(23–24), pp. 3228–3245.

Mangerud, J. *et al.* (2011) 'Glacial history of Norway', *Developments in Quaternary Science*, 15, pp. 279–298.

Mangerud, J. A. N. *et al.* (2001) 'Huge Ice-age lakes in Russia', 16, pp. 773–777.

Markl, G. (2001) 'REE constraints on fractionation processes of massive-type anorthosites on the Lofoten Islands, Norway', *Mineralogy and Petrology*, 72(4), pp. 325–351.

Masarik, J. and Beer, J. (2009) 'An updated simulation of particle fluxes and cosmogenic nuclide production in the Earth's atmosphere', *Journal of Geophysical Research*, 114(D11), p. D11103.

Maslin, M. *et al.* (2004) 'Linking continental-slope failures and climate change: Testing the clathrate gun hypothesis', *Geology*, 32(1), pp. 53–56.

Masson, D. *et al.* (2006) 'Submarine landslides: processes, triggers and hazard prediction.', *Philosophical transactions. Series A, Mathematical, physical, and engineering sciences*, 364(1845), pp. 2009–39.

McCrea, J. M. (1950) 'On the Isotopic Chemistry of Carbonates and a Palaeotemperature Scale', *The Journal of Chemical Physics*, 18(6), pp. 849–857.

McDonough, W. F. and Sun, S. -s. (1995) 'The composition of the Earth', *Chemical Geology*. Elsevier, pp. 223–253.

McLennan, S. M. *et al.* (1993) 'Geochemical approaches to sedimentation, provenance, and tectonics', *GSA Special Paper*, 284, pp. 21–40.

McLennan, S. M. and Taylor, S. . (1990) 'Geochemical and Nd-Sr isotopic composition of deep-sea turbidites: crustal evolution and plate tectonic associations', *… et Cosmochimica Acta*, 54(7), pp. 2015–2050.

Van Meerbeeck, C. J. *et al.* (2011) 'The nature of MIS 3 stadial-interstadial transitions in Europe: New insights from model-data comparisons', *Quaternary Science Reviews*. Elsevier Ltd, 30(25–26), pp. 3618–3637.

Van Meerbeeck, C. J., Renssen, H. and Roche, D. M. (2008) 'How did Marine Isotope Stage 3 and Last Glacial Maximum climates differ? Perspectives from equilibrium simulations', *Climate of the Past Discussions*, 4(5), pp. 1115–1158.

Meland, M. Y. *et al.* (2008) 'Water mass properties and exchange between the Nordic seas and the northern North Atlantic during the period 23-6 ka: Benthic oxygen isotopic evidence', *Palaeoceanography*, 23(1).

Micallef, A. *et al.* (2009) 'Development and mass movement processes of the north-eastern Storegga Slide', *Quaternary Science Reviews*. Elsevier Ltd, 28(5–6), pp. 433–448.

Middelburg, J. J. and De Lange, G. J. (1988) 'Geochemical characteristics as indicators of the provenance of Madeira abyssal plain turbidites . A statistical approach', *Oceanologica Acta*, 11(2), pp. 159–165.

Mienert, J. *et al.* (2010) 'Norwegian margin outer shelf cracking: A consequence of climate-induced gas hydrate dissociation?', *International Journal of Earth Sciences*, 99(SUPPL. 1), pp. 207–225.

Mienert, J. and Posewang, J. (1999) 'Evidence of shallow- and deep-water gas hydrate destabilizations in North Atlantic polar continental margin sediments', *Geo-Marine Letters*, 19(1–2), pp. 143–149.

Minisini, D. *et al.* (2007) 'Morphologic variability of exposed mass-transport deposits on the eastern slope of Gela Basin (Sicily channel)', *BasinResearch*, 19(2), pp. 217–240.

Mjelde, R. *et al.* (2008) 'Magmatic and tectonic evolution of the North Atlantic', *Journal of the Geological Society*, 165(1), pp. 31–42.

Moller, J. J. (1984) 'Holocene shore displacement at Nappstraumen, Lofoten, north Norway.', *Norsk Geologisk Tidsskrift*, 64(1), pp. 1–5.

Morner, N.-A. (1991) 'Course and origin of the Fennoscandian uplift: the case for two separate mechanisms', *Terra Nova*, 3(4), pp. 408–413.

Mörner, N. A. (1990) 'Glacial isostasy and long-term crustal movements in Fennoscandia with respect to lithospheric and asthenospheric processes and properties', *Tectonophysics*, 176(1–2), pp. 13–24.

Mosar, J. *et al.* (2002) 'Greenland-Norway separation: a geodynamic model for the North Atlantic', *Norwegian Journal of Geology*, 82, pp. 281–298.

Mulder, T. (2011) 'Gravity processes and deposits on continental slope, rise and abyssal plains', *Deep-sea Sediments. Elsevier, UK*. 1st edn. Heiko Hneke and Thierry Mulder, 63(11), pp. 25–148.

Newton, A. M. W. and Huuse, M. (2016) 'Late Cenozoic environmental changes along the Norwegian margin', *Marine Geology*. Elsevier, (April), pp. 1–29.

Nicholl, J. a. L. *et al.* (2012) 'A Laurentide outburst flooding event during the last interglacial period', *Nature Geoscience*. Nature Publishing Group, 5(12), pp. 901– 904.

Nielsen, T. and van Weering, T.C. E. (1998) 'Seismic stratigraphy and sedimentary processes at the Norwegian Sea margin northeast of the Faeroe Islands', *Marine Geology*, 152, pp. 141–157.

Nowaczyk, N. R. *et al.* (1994) 'Magnetostratigraphic data from late Quaternary sediments From the Yermak Plateau, Arctic Ocean: evidence for four geomagnetic polarity events within the last 170 ka of the Brunhes Chron', *Geophys. J. Int.*, 117(2), pp. 453–471.

Nowaczyk, N. R. (1997) 'High-resolution magnetostratigraphy of four sediment cores from the Greenland Sea. II. Rock magnetic and relative palaeointensity data', *Geophysical Journal International*, 131(2), pp. 325–334.

Nowaczyk, N. R. (2003) 'Detailed study on the anisotropy of magnetic susceptibility of arctic marine sediments', pp. 302–317.

Nowaczyk, N. R. and Baumann, M. (1992) 'Combined high-resolution magnetostratigraphy and nannofossil biostratigraphy for late Quaternary Arctic Ocean sediments', *Deep Sea Research Part A, Oceanographic Research Papers*, 39(2 PART 1).

Nowaczyk, N. R. and Frederichs, T. W. (1999) 'Geomagnetic events and relative palaeointensity variations during the past 300 ka as recorded in Kolbeinsey Ridge sediments, Iceland Sea: Indication for a strongly variable geomagnetic field', *International Journal of Earth Sciences*, 88(1), pp. 116–131.

Nowaczyk, N. R. and Knies, J. (2000) 'Magnetostratigraphic results from the eastern Arctic Ocean: AMS 14C ages and relative palaeointensity data of the Mono Lake and Laschamp geomagnetic reversal excursions', *Geophysical Journal International*, 140(1), pp. 185–197.

Nygård, A. *et al.* (2005) 'The glacial North Sea Fan, southern Norwegian Margin: architecture and evolution from the upper continental slope to the deep-sea basin', *Marine and Petroleum Geology*, 22(1–2), pp. 71–84.

Oladottir, B. A. *et al.* (2011) 'Provenance of basaltic tephra from VatnajOkull subglacial volcanoes, Iceland, as determined by major- and trace-element analyses', *The Holocene*, 21(7), pp. 1037–1048.

Óladóttir, B. A. *et al.* (2008) 'Katla volcano, Iceland: Magma composition, dynamics and eruption frequency as recorded by Holocene tephra layers', *Bulletin of Volcanology*, 70(4), pp. 475–493.

Olsson, I. and Eriksson, K. (1972) 'Fraactionation studies of the shell of foraminifera', in *Etudes sur la Quaternaire dans le Monde*, pp. 921–923.

Oppo, D. W. and Lehman, J. (1995) 'Suborbital timescale variability of North Atlantic Deep Water during the past 200, 000 years that in association portions', 10(5), pp. 901–910.

Orvik, K. A. (2002) 'Major pathways of Atlantic water in the northern North Atlantic and Nordic Seas toward Arctic', *Geophysical Research Letters*, 29(19), p. 1896.

Osete, M.-L. *et al.* (2012) 'The Blake geomagnetic excursion recorded in a radiometrically dated speleothem', *Earth and Planetary Science Letters*, 353–354, pp. 173–181.

Ottesen, D. *et al.* (2005) 'The Vestfjorden-Trænadjupet palaeo-ice stream drainage system , mid-Norwegian continental shelf', 218, pp. 175–189.

Ottesen, D. *et al.* (2012) 'Large-scale development of the mid-Norwegian shelf over the last three million years and potential for hydrocarbon reservoirs in glacial sediments', *Geological Society, London, Special Publications*, pp. 53–73.

Ottesen, D. and Rise, L. (2009) 'Geological evolution of the Norwegian continental shelf between 61^{o}N and 68^{o}N during the last 3 million years', *Norwegian Journal of …*, (2005), pp. 251–265.

PAGES, P. I. W. G. of (2016) 'Interglacials of the last 800,000 years', *Reviews of Geophysics*, 54, pp. 162–219.

Panieri, G. *et al.* (2014) 'Record of methane emissions from the West Svalbard continental margin during the last 23.500yrs revealed by δ13C of benthic foraminifera', *Global and Planetary Change*. Elsevier B.V., 122, pp. 151–160.

Paull, C. K. *et al.* (2010) 'The tail of the Storegga Slide: insights from the geochemistry and sedimentology of the Norwegian Basin deposits', *Sedimentology*, 57(6), pp. 1409–1429.

Pearce, N. J. G. *et al.* (2004) 'The application of ICP-MS methods to tephrochronological problems', *Applied Geochemistry*, 19(3), pp. 289–322.

Pearce, N. J. G., Abbott, P. M. and Martin-Jones, C. (2014) 'Microbeam methods for the analysis of glass in fine-grained tephra deposits: a SMART perspective on current and future trends', *Geological Society, London, Special Publications*, 398(1), pp. 29–46.

Pearce, N. J. G., Bendall, C. A. and Westgate, J. A. (2008) 'Comment on "Some numerical considerations in the geochemical analysis of distal microtephra" by

A.M. Pollard, S.P.E. Blockley and C.S. Lane', *Applied Geochemistry*, 23(5), pp. 1353–1364.

Pearce, T. J. and Jarvis, I. (1995) 'High-resolution chemostratigraphy of Quaternary distal turbidites: a case study of new methods for the analysis and correlation of barren sequences', *Geological Society, London, SpecialPublications*, 89(1), pp. 107–143.

Pearce, T. and Jarvis, I. (1992) 'Applications of geochemical data to modelling sediment dispersal patters in distal turbidites: late Quaternary of the Madeira Abyssal Plain', *Journal of Sedimentary Research*, 62(6).

Peck, V. L. *et al.* (2006) 'High resolution evidence for linkages between NW European ice sheet instability and Atlantic Meridional Overturning Circulation', *Earth and Planetary Science Letters*, 243(3–4), pp. 476–488.

Peck, V. L. *et al.* (2007) 'The relationship of Heinrich events and their European precursors over the past 60ka BP: a multi-proxy ice-rafted debris provenance study in the North East Atlantic', *Quaternary Science Reviews*, 26(7–8), pp. 862– 875.

Pilcher, J. *et al.* (2005) 'A Holocene tephra record from the Lofoten Islands, Arctic Norway', *Boreas*, 34(2), pp. 136–156.

Piper, D. J. W. and Bau, M. (2013) 'Normalized rare earth elements in water, sediments, and wine: identifying sources and environmental redox conditions', *American Journal of Analytical Chemistry*, 2013(October), pp. 69–83.

Plaza-Faverola, A., B??nz, S. and Mienert, J. (2011) 'Repeated fluid expulsion through sub-seabed chimneys offshore Norway in response to glacial cycles', *Earth and Planetary Science Letters*. Elsevier B.V., 305(3–4), pp. 297–308.

Pope, E. L. *et al.* (2015) 'Are large submarine landslides temporally random or do uncertainties in available age constraints make it impossible to tell?', *Marine Geology*. Elsevier B.V., 369, pp. 190–33.

Pope, E. L. *et al.* (2016) 'Long-term record of Barents Sea Ice Sheet advance to the shelf edge from a 140,000 year record', *Quaternary Science Reviews*. ElsevierLtd, 150, pp. 55–66.

Pouderoux, H., Lamarche, G. and Proust, J. N. (2012) 'Building an 18 000-year- long palaeo-earthquake record from detailed deep-sea turbidite characterisation in Poverty Bay, New Zealand', *Natural Hazards and Earth System Science*, 12(6), pp. 2077–2101.

Prell, W. L. *et al.* (1986) 'Graphic correlation of oxygen isotope stratigraphy application to the Late Quaternary', *Palaeoceanography*, 1(2), pp. 137–162.

Pyles, D. R., Straub, K. M. and Stammer, J. G. (2013) 'Spatial variations in the composition of turbidites due to hydrodynamic fractionation', *Geophysical Research Letters*, 40(15), pp. 3919–3923.

Rabassa, J. and Ponce, J. F. (2013) 'The Heinrich and Dansgaard-Oeschger climatic events during Marine Isotopic Stage 3: Searching for appropriate times for human colonization of the Americas', *Quaternary International*. Elsevier Ltd and INQUA, 299, pp. 94–105.

Raj, R. P. *et al.* (2015) 'The Lofoten Vortex of the Nordic Seas', *Deep Sea Research Part I: Oceanographic Research Papers*, 96, pp. 1–14.

Raj, R. P. and Nilsen, J. E. Ø. (2009) 'General Circulation of the Norwegian Sea with a Deeper Look into the Lofoten Basin From Space', *Plateau*, (d), pp.197–198.

Ramsey, C. B. (2008) 'Deposition models for chronological records', *Quaternary Science Reviews*, 27(1–2), pp. 42–60.

Ramsey, C. B. and Lee, S. (2013) 'Recent and Planned Developments of the Program OxCal', *Radiocarbon*. New York, US: Cambridge University Press, 55(2), pp. 720–730.

Rashid, H., Piper, D. J. W. and Flower, B. P. (2013) 'The Role of Hudson Strait Outlet in Younger Dryas Sedimentation in the Labrador Sea', in *Abrupt Climate Change: Mechanisms, Patterns, and Impacts*. American Geophysical Union, pp. 93–110.

Rasmussen, S. O. *et al.* (2006) 'A new Greenland ice core chronology for the last glacial termination', *Journal of Geophysical Research Atmospheres*, 111(6), pp. 1– 16.

Rasmussen, S. O. *et al.* (2014) 'Dating, synthesis, and interpretation of palaeoclimatic records of the Last Glacial cycle and model-data integration: Advances by the INTIMATE (INTegration of Ice-core, MArine and TErrestrial records) COST Action ES0907', *Quaternary Science Reviews*. Elsevier Ltd, 106, pp. 1–13.

Rasmussen, T. L. *et al.* (1996) 'Rapid changes in surface and deep water conditions at the Faeroe Margin during the last 58,000 years', *Palaeoceanography*, 11(6), pp. 757–771.

Rasmussen, T. L. *et al.* (1999) 'Climate records and changes in deep outflow from the Norwegian Sea ~ 150-55 ka', *Terra Nova*, 11(2–3), pp. 61–66.

Rasmussen, T. L. *et al.* (2003) 'Stratigraphy and distribution of tephra layers in marine sediment cores from the Faeroe Islands, North Atlantic', *Marine Geology*, 199, pp. 263–277.

Rasmussen, T. L. and Bäckström, D. (2002) 'The Faroe–Shetland Gateway: Late Quaternary water mass exchange between the Nordic seas and the northeastern Atlantic', *Marine Geology*, 188.

Rasmussen, T. L. and Thomsen, E. (2008) 'Warm Atlantic surface waterinflow to the Nordic seas 34-10 calibrated ka B.P', *Palaeoceanography*, 23(1), pp. 1–13.

Rebesco, M. *et al.* (2000) 'Acoustic facies of Holocene megaturbidites in the Eastern Mediterranean', *Sedimentary Geology*, 135(1–4), pp. 65–74.

Rebesco, M. *et al.* (2013) 'Quaternary contourite drifts of the Western Spitsbergen margin', *Deep Sea Research Part I: Oceanographic Research Papers*. Elsevier, 79, pp. 156–168.

Rebesco, M. *et al.* (2014) 'Contourites and associated sediments controlled by deep-water circulation processes: State-of-the-art and future Considerations', *Marine Geology*.

Reiche, S. S., Hjelstuen, B. O. and Haflidason, H. (2011) 'High-resolution seismic stratigraphy, sedimentary processes and the origin of seabed cracks and pockmarks at Nyegga, mid-Norwegian margin', *Marine Geology*, 284(1–4), pp. 28– 39.

Reimer, P. (2013) 'IntCal13 and Marine13 Radiocarbon Age Calibration Curves 0– 50,000 Years Cal BP', *Radiocarbon*, 55(4), pp. 1869–1887.

Reimer, R. . and Reimer, P. (2006) 'Marine reservoir corrections and the calibration curve', *Pages News*, 14(3), pp. 12–13.

Richter, T. O. *et al.* (2006) 'The Avaatech XRF Core Scanner: technical description and applications to NE Atlantic sediments', *Geological Society, London, Special Publications*, 267(1), pp. 39–50.

Rise, L. *et al.* (2005) 'Large-scale development of the mid-Norwegian margin during the last 3 million years', *Marine and Petroleum Geology*, 22(1–2), pp. 33– 44.

Rise, L. *et al.* (2006) 'The Sklinnadjupet slide and its relation to the Elsterian glaciation on the mid-Norwegian margin', *Marine and Petroleum Geology*, 23(5), pp. 569–583.

Rise, L. *et al.* (2010) 'Late Cenozoic geological development of the south Vøring margin, mid-Norway', *Marine and Petroleum Geology*, 27(9), pp. 1789–1803.

Rise, L. *et al.* (2013) 'The Lofoten-Vesterålen continental margin, North Norway: Canyons and mass-movement activity', *Marine and Petroleum Geology*.Elsevier, 45, pp. 134–149.

Risebrobakken, B. *et al.* (2006) 'The penultimate deglaciation: High-resolution palaeoceanographic evidence from a north-south transect along the eastern Nordic Seas', *Earth and Planetary Science Letters*, 241(3–4), pp. 505–516.

Risebrobakken, B., Dokken, T. and Jansen, E. (2005) 'Extent and variability of the meridional Atlantic circulation in the eastern Nordic seas during Marine Isotope Stage 5 and its influence on the inception of the last glacial', *The Nordic Seas: An Integrated Perspective Oceanography, Climatology, Biogeochemistry, and Modeling*, 158, pp. 323–339.

Roberts, A. P. (2008) 'Geomagnetic excursions: Knowns and unknowns', *Geophysical Research Letters*, 35(17), pp. 1–7.

Roberts, A. P., Tauxe, L. and Heslop, D. (2013) 'Magnetic palaeointensity stratigraphy and high-resolution Quaternary geochronology: successes and future challenges', *Quaternary Science Reviews*. Elsevier Ltd, 61, pp. 1–16.

Rohling, E. J. and Pälike, H. (2005) 'Centennial scale climate cooling with a sudden cold event around 8,200 years ago', *Nature*, 434 (April).

Romundset, A. and Bondevik, S. (2011) 'Propagation of the Storegga tsunami into ice-free lakes along the southern shores of the Barents Sea', *Journal of Quaternary Science*, 26(5), pp. 457–462.

Roth, R. and Joos, F. (2013) 'A reconstruction of radiocarbon production and total solar irradiance from the Holocene 14C and CO2 records: Implications of data and model uncertainties', *Climate of the Past*, 9(4), pp. 1879–1909.

Rothwell, R. G. *et al.* (2006) 'Turbidite emplacement on the southern Balearic Abyssal Plain (western Mediterranean Sea) during Marine Isotope Stages 1-3: an application of ITRAX XRF scanning of sediment cores to lithostratigraphic analysis', (Haschke 2006), pp. 79–98.

Rothwell, R. G. and Croudace, I. w. (2015) 'Twenty Years of XRF Core Scanning Marine Sediments: What Do Geochemical Proxies Tell Us?', in Croudace, I. W. and Rothwell, R. G. (eds) *Micro-XRF Studies of Sediment Cores: Applications of a non- destructive tool for the environmental sciences*. Dordrecht: Springer Netherlands, pp. 25–102.

Rothwell, R. G., Thomson, J. and Kahler, G. (1998) 'Low-sea-level emplacement of a very large Late Pleistocene "megaturbidite" in the western Mediterranean Sea', 93(1996), pp. 1996–1999.

Ruddiman, W. . and Glover, L. K. (1972) 'Vertical Mixing of Ice-Rafted Volcanic Ash in North Atlantic Sediments', *Geological Society of America Bulletin*, 83(9), p. 2817 LP-2836.

Ruddiman, W. F. (1977) 'Late Quaternary deposition of ice rafted sand in the subpolar North Atlantic (lat 40^{o} to 65^{o} N)', *Geological Society of America Bulletin*, 88(71213), pp. 1813–1827.

Rudels, B. and Quadfasel, D. (1991) 'Convection and deep water formation in the Arctic Ocean-Greenland Sea system', *Journal of Marine Systems*, 2(1991), pp. 435–450.

Ruppel, C. and Kessler, J. D. (2016) 'The Interaction of Climate Change and Methane Hydrates', pp. 1–43.

Safronova, P. A. *et al.* (2015) 'Late Pliocene - early Pleistocene deep-sea basin sedimentation at high-latitudes; mega-scale submarine slides of the north- western Barents Sea margin prior to the shelf-edge glaciations', *Basin Research*,

Sallun, A. E. M. *et al.* (2012) 'Geochemical evidence of the 8.2ka event and other Holocene environmental changes recorded in palaeolagoon sediments, southeastern Brazil', *Quaternary Research*. University of Washington, 77(1), pp. 31–43.

Sarnthein, M. *et al.* (1995) 'Variations in Atlantic Surface Ocean Palaeoceanography, 50-Degrees-80-Degrees-N - a Time-Slice Record of the Last 30,000 Years', 10(6), pp. 1063–1094.

Sarnthein, M. *et al.* (2001) 'Fundamental Modes and Abrupt Changes in North Atlantic Circulation and Climate over the last 60 ky --- Concepts, Reconstruction and Numerical Modeling', in Schäfer, P. *et al*. (eds) *The Northern North Atlantic: A Changing Environment*. Berlin, Heidelberg: Springer Berlin Heidelberg, pp. 365– 410.

Sarnthein, M. and Altenbach, A. V (1995) 'Late Quaternary changes in surface water and deep water masses of the Nordic Seas and north-eastern North Atlantic : a review', *Geol Rundsch*, 84, pp. 89–107.

Scott, E. M., Cook, G. and Naysmith, P. (2007) 'Error and uncertainty in radiocarbon measurements', *Radiocarbon*, 49(2).

Sejrup, H. P. *et al.* (2005) 'Pleistocene glacial history of the NW European continental margin', *Marine and Petroleum Geology*, 22(9–10), pp. 1111–1129.

Shackleton, N. J. (1987) 'Oxygen isotopes, ice volume and sea level', *Quaternary Science Reviews*, 6(3–4), pp. 183–190.

Shackleton, N. J., Hall, M. a and Vincent, E. (2000) 'Phase relationships between millennial-scale events 64,000- 24,000 years ago', *Palaeoceanography*, 15(6), pp.565–569.

Shanmugam, G. (1997) 'The Bouma Sequence and the turbidite mind set', *Earth- Science Reviews*, 42(4), pp. 201–229.

Shanmugam, G. (2000) '50 years of the turbidite paradigm (1950s-1990s): Deep- water processes and facies models-a critical perspective', *Marine and Petroleum Geology*, 17(2), pp. 285–342.

Sier, M. J. *et al.* (2015) 'The Blake Event recorded near the Eemian type locality – A diachronic onset of the Eemian in Europe', *Quaternary Geochronology*, 28, pp. 12–28.

Sirocko, F. *et al.* (2015) 'The ELSA-Vegetation-Stack: Reconstruction of Landscape Evolution Zones (LEZ) from laminated Eifel maar sediments of the last 60,000??years', *Global and Planetary Change*. Elsevier B.V., 142, pp. 108–135.

Sirocko, F. *et al.* (2016) 'The ELSA-Vegetation-Stack : Reconstruction of Landscape Evolution Zones (LEZ) from laminated Eifel maar sediments of the last 60 , 000 years', *Global and Planetary Change*. Elsevier B.V., 142, pp. 108–135.

Smith, D. *et al.* (2004) 'The Holocene Storegga Slide tsunami in the United Kingdom', *Quaternary Science Reviews*, 23, pp. 2291–2321.

Smith, D. E., Cullingford, R. A. and Haggart, B. A. (1985) 'A major coastal flood during the {Holocene} in eastern {Scotland}', *Eiszeitalter und Gegenwart*, 35, pp. 109–118.

Solheim, A. *et al.* (2005) 'The Storegga Slide complex: repetitive large scale sliding with similar cause and development', *Marine and Petroleum Geology*, 22(1–2), pp. 97–107.

Spielhagen, R. F. (2004) 'Arctic Ocean deep-sea record of northern Eurasian ice sheet history', *Quaternary Science Reviews*, 23(11–13), pp. 1455–1483.

Steffensen, J. P. *et al.* (2008) 'High-Resolution Greenland Ice Core Data Show Abrupt Climate Change Happens in Few Years', (June).

Stoker, M. S. *et al.* (2005) 'Neogene stratigraphy and the sedimentary and oceanographic development of the NW European Atlantic margin', *Marine and Petroleum Geology*, 22(9–10), pp. 977–1005.

Stoner, J. S. *et al.* (2002) 'South Atlantic and North Atlantic geomagnetic palaeointensity stacks (0-80 ka): Implications for inter-hemispheric correlation', *Quaternary Science Reviews*, 21(10), pp. 1141–1151.

Stoner, J. S. and St-Onge, G. (2007) 'Chapter Three Magnetic Stratigraphy in Palaeoceanography: Reversals, Excursions, Palaeointensity, and Secular Variation', 1(7), pp. 99–138.

Stow, D. a. V. and Tabrez, a. R. (1998) 'Hemipelagites: processes, facies and model', *Geological Society, London, Special Publications*, 129(1), pp. 317–337.

Streeter, S. S. *et al.* (1982) 'Late Pleistocene palaeo-oceanography of the Norwegian-Greenland Sea: Benthic foraminiferal evidence', *Quaternary Research*, 18(1), pp. 72–90.

Stuiver, M. (1961) 'Variations in radiocarbon concentration and sunspot activity',

Journal of Geophysical Research, 66(1), pp. 273–276.

Sumner, E. J. *et al.* (2012) 'Facies architecture of individual basin-plain turbidites: Comparison with existing models and implications for flow processes', *Sedimentology*, 59(6), pp. 1850–1887.

Sumner, E. J. *et al.* (2013) 'Can turbidites be used to reconstruct a palaeoearthquake record for the central Sumatran margin ?', *Geology*, (41), pp. 763–766.

Sun, S. -s. and McDonough, W. F. (1989) 'Chemical and isotopic systematics of oceanic basalts: implications for mantle composition and processes', *Geological Society, London, Special Publications* , 42(1), pp. 313–345.

Svendsen, J. I. *et al.* (2004) 'Late Quaternary ice sheet history of northern Eurasia', in *Quaternary Science Reviews*, pp. 1229–1271.

Svensson, A. *et al.* (2008) 'A 60 000 year Greenland stratigraphic ice core chronology', *Climate of the Past*, 4(1), pp. 47–57.

Swindles, G., Vleeschouwer, F. De and Plunkett, G. (2010) 'Dating peat profiles using tephra: stratigraphy, geochemistry and chronology', *Mires and Peat*, 7, pp. 1–9.

Talling, P. J. *et al.* (2004) 'Beds comprising debrite sandwiched within co-genetic turbidite: origin and widespread occurrence in distal depositional environments', pp. 163–194.

Talling, P. J. *et al.* (2012) 'Subaqueous sediment density flows: Depositional processes and deposit types', *Sedimentology*, 59(7), pp. 1937–2003.

Talling, P. J. (2014) 'On the triggers, resulting flow types and frequencies of subaqueous sediment density flows in different settings', *Marine Geology*. Elsevier B.V., 352, pp. 155–182.

Talling, P. J., Amy, L. a. and Wynn, R. B. (2007) 'New insight into the evolution of large-volume turbidity currents: Comparison of turbidite shape and previous modelling results', *Sedimentology*, 54(4), pp. 737–769.

Talwani, M. and Eldholm, O. (1977) 'Evolution of the Norwegian-Greenland Sea', *Bulletin of the Geological Society of America*, 88(7), pp. 969–999.

Tappin, D. R. (2010) 'Mass transport events and their tsunami hazard', *Submarine Mass Movements and Their Consequences*, 28, pp. 667–684.

Tauxe, L. (1993) 'Sedimentary records of relative palaeointenstiy of the geomagnetic field: theory and practice', *Reviews of Geophysics*, 31(93), pp. 319– 354.

Taylor, J. *et al.* (2000) 'Morphology and Late Quaternary sedimentation on the North Faeroes slope and abyssal plain, North Atlantic', *Marine Geology*, 168(1–4), pp. 1–24.

Taylor, S. R. and McLennan, S. . (1985) 'The continental crust: Its composition and evolution', *McClennan, Blackwell Scientific Publications*, 21(1), pp. 85–86.

Telesiński, M. M. *et al.* (2015) 'Evolution of the central Nordic Seas over the last 20 thousand years', *Quaternary Science Reviews*, 121, pp. 98–109.

The UK Cabinet Office (2017) *National Risk Register of Civil Emergencies*, *National Risk Register of Civil Emergencies*.

Thordarson, T. (2014) 'The widespread ~10ka Saksunarvatn tephra is not a product single eruption', in *American Geophyiscal Union, Fall Meeting*. San Fransisco.

Thornalley, D. J. R. *et al.* (2011) 'The deglacial evolution of North Atlantic deep convection.', *Science (New York, N.Y.)*, 331(6014), pp. 202–5.

Thornalley, D. J. R., Mccave, I. N. and Elderfield, H. (2010) 'Freshwater input and abrupt deglacial climate change in the North Atlantic', *Palaeoceanography*, 25, pp. 1–16.

Thornalley, D. J. R., McCave, I. N. and Elderfield, H. (2011) 'Tephra in deglacial ocean sediments south of Iceland: Stratigraphy, geochemistry and oceanic reservoir ages', *Journal of Quaternary Science*, 26(2), pp. 190–198.

Thouveny, N. *et al.* (2004) 'Geomagnetic moment variation and palaeomagnetic excursions since 400 kyr BP: A stacked record from sedimentary sequences of the Portuguese margin', *Earth and Planetary Science Letters*, 219(3–4), pp. 377–396.

Thouveny, N. *et al.* (2008) 'Palaeoclimatic context of geomagnetic dipole lows and excursions in the Brunhes, clue for an orbital influence on the geodynamo?', *Earth and Planetary Science Letters*. Elsevier B.V., 275(3–4), pp. 269–284.

Timms, R. G. O. *et al.* (2016) 'A high-resolution tephrostratigraphy from Quoyloo Meadow, Orkney, Scotland: Implications for the tephrostratigraphy of NW Europe during the Last Glacial-Interglacial Transition', *Quaternary Geochronology*. Elsevier B.V, pp. 1–15.

Tooley, M. J. and Smith, D. (2005) 'Relative sea-level change and evidence for the Holocene Storegga Slide tsunami from a high-energy coastal environment: Cocklemill Burn, Fife, Scotland, UK', *Quaternary International*, 133–134, pp. 107– 119.

Torbjørn Dahlgren, K. I., Vorren, T. O. and Laberg, J. S. (2002) 'Late Quaternary glacial development of the mid-Norwegian margin-65 to 68°N', *Marine and Petroleum Geology*, 19(9), pp. 1089–1113.

Tric, E. *et al.* (1991) 'The Blake geomagnetic event: transition geometry, dynamical characteristics and geomagnetic significance.', *Earth Planet. Sci. Lett.*, 102(1), pp. 1–13.

Turney, C. S. M. (1998) 'Extraction of rhyolitic component of Vedde microtephra from minerogenic lake sediments', pp. 199–206.

Turney, C. S. M. *et al.* (2016) 'High-precision dating and correlation of ice, marine and terrestrial sequences spanning Heinrich Event 3: Testing mechanisms of interhemispheric change using New Zealand ancient kauri (Agathis australis)', *Quaternary Science Reviews*, 137, pp. 126–134.

Urgeles, R. and Camerlenghi, A. (2013) 'Submarine landslides of the Mediterranean Sea: Trigger mechanisms, dynamics, and frequency-magnitude distribution', *Journal of Geophysical Research: Earth Surface*, 118(4), pp. 2600– 2618.

Urlaub, M., Talling, P. J. and Masson, D. G. (2013) 'Timing and frequency of large submarine landslides: Implications for understanding triggers and future geohazard', *Quaternary Science Reviews*. Elsevier Ltd, 72, pp. 63–82.

Valen, V., Larsen, E. and Mangerud, J. A. N. (1995) 'High-resolution palaeomagnetic correlation of Middle Weichselian ice-dammed lake sediments in two coastal caves, western Norwav', *Boreas*, 24, pp. 141–153.

Valet, J.-P. (2003) 'Time variations in geomagnetic intensity', *Reviews of Geophysics*, 41(1), p. 1004.

Valet, J. P., Meynadier, L. and Guyodo, Y. (2005) 'Geomagnetic dipole strength and reversal rate over the past two million years', *Nature*, 435(7043), pp. 802– 805.

Valet, J. P., Plenier, G. and Herrero-Bervera, E. (2008) 'Geomagnetic excursions reflect an aborted polarity state', *Earth and Planetary Science Letters*, 274(3–4), pp. 472–478.

Vanneste, M., Mienert, J. and Bunz, S. (2006) 'The Hinlopen Slide: A giant, submarine slope failure on the northern Svalbard margin, Arctic Ocean', *Earth and Planetary Science Letters*, 245(1–2), pp. 373–388.

Vasskog, K. *et al.* (2013) 'Evidence for Storegga tsunami run-up at the head of Nordfjord, western Norway', *Journal of Quaternary Science*, 28(4), pp. 391–402.

Vidal, L., Labeyrie, L. and Van Weering, T. C. E. (1998) 'Benthic d18O records in the North Atlantic over the last glacial period (60-10 kyr): Evidence for brine formation', 13(3), pp. 245–251.

Voelker, A. H. L. and Haflidason, H. (2015) 'Refining the Icelandic tephrachronology of the last glacial period – The deep-sea core PS2644 record from the southern Greenland Sea', *Global and Planetary Change*, 131, pp. 35–62.

Voelker, A. L. *et al.* (1998a) 'Correlation of marine (super 14) C ages from the Nordic Seas with the GISP2 isotope record; implications for (super 14) C calibration beyond 25 ka BP.', *Radiocarbon*, 40(1), pp. 517–534.

Voelker, A. L. *et al.* (1998b) 'Correlation of marine (super 14) C ages from the Nordic Seas with the GISP2 isotope record; implications for (super 14) C calibration beyond 25 ka BP.', *Radiocarbon*, 40(1), pp. 517–534.

Vogt, P. R. and Jung, W. Y. (2009) 'Treitel Ridge: A unique inside corner hogback on the west flank of extinct Aegir spreading ridge, Norway basin', *Marine Geology*. Elsevier B.V., 267(1–2), pp. 86–100.

Vorren, T. O. *et al.* (1988) 'The last deglaciation (20,000 to 11,000 B. P.) on Andoya, northern Norway', *Boreas*, 17(1), pp. 41–77.

Vorren, T. O. *et al.* (1998) 'the Norwegian–Greenland Sea continental margins: Morphology and Late Quaternary Sedimentary Processes and Environment', *Quaternary Science Reviews*, 17(1–3), pp. 273–302.

Vorren, T. O. T. O. *et al.* (2015) 'Chronology and extent of the Lofoten-Vesterålen sector of the Scandinavian Ice Sheet from 26 to 16 cal. ka BP', *Boreas*, 44(3),

Waelbroeck, C. *et al.* (2001) 'The timing of the last deglaciation in North Atlantic climate records.', *Nature*, 412(6848), pp. 724–727.

Waelbroeck, C. *et al.* (2002) 'Sea-level and deep water temperature changes derived from benthic foraminifera isotopic records', *Quaternary Science Reviews*, 21(1–3), pp. 295–305.

Wagner, B. and Bennike, O. (2007) 'First indication of Storegga tsunami deposits from East Greenland', *Journal of Quaternary …*, 22(December 2006), pp. 321– 325.

Wallrabe-Adams, H. J. and Lackschewitz, K. S. (2003) 'Chemical composition, distribution, and origin of silicic volcanic ash layers in the Greenland-Iceland- Norwegian Sea: Explosive

volcanism from 10 to 300 ka as recorded in deep-sea sediments', *Marine Geology*, 193(3–4), pp. 273–293.

Wastegård, S. *et al.* (2000) 'New discoveries of the Vedde Ash in southern Sweden and Scotland', *Boreas*, 29(1), pp. 72–78.

Wastegård, S. (2002) 'Early to middle Holocene silicic tephra horizons from the Katla volcanic system, Iceland: New results from the Faroe Islands', *Journal of Quaternary Science*, 17(8), pp. 723–730.

Wastegård, S. *et al.* (2005) 'A tephra-based correlation between the Faroe Islands and the Norwegian Sea raises questions about chronological relationshipsduring the last interglacial', *Terra Nova*, 17(1), pp. 7–12.

Wastegård, S. *et al.* (2006) 'Composition and origin of ash zones from Marine Isotope Stages 3 and 2 in the North Atlantic', *Quaternary Science Reviews*, 25(17– 18), pp. 2409–2419.

Wastegård, S. and Rasmussen, T. L. (2016) 'Faroe Marine Ash Zone IV : a new MIS 3 ash zone on the Faroe Islands margin', pp. 81–93.

Weaver, P. P. E. and Kuijpers, a. (1983) 'Climatic control of turbidite deposition on the Madeira Abyssal Plain', *Nature*, 306(5941), pp. 360–363.

Van Weering, T. C. E. *et al.* (1998) 'Sediments and sedimentation at the NE Faeroe continental margin; Contourites and large-scale sliding', *Marine Geology*, 152(1– 3), pp. 159–176.

Weltje, G. J. and Tjallingii, R. (2008) 'Calibration of XRF core scanners for quantitative geochemical logging of sediment cores: Theory and application', *Earth and Planetary Science Letters*, 274(3–4), pp. 423–438.

Winkelmann, D. (2006) *Dynamic and timing of the Yermack/Hinlopen Slide, Arctic Ocean.*

Winkelmann, D. and Stein, R. (2007) 'Triggering of the Hinlopen/Yermak Megaslide in relation to palaeoceanography and climate history of the continental margin north of Spitsbergen', *Geochemistry, Geophysics, Geosystems*, 8(6).

Wohlfarth, B. and Näslund, J. O. (2010) 'Fennoscandian ice sheet in MIS 3 - Introduction', *Boreas*, 39(2), pp. 325–327.

Wynn, R. B. *et al.* (2010) 'Investigating the timing, processes and deposits of one the World^{1}s largest submarine gravity flows: the "Bed 5 event" off northwest Africa', 28, pp. 463–474.

Xuan, C. and Channell, J. E. T. (2009) 'UPmag: MATLAB software for viewing and processing u channel or other pass-through palaeomagnetic data',*Geochemistry, Geophysics, Geosystems*, 10(10), pp. 1–12.

Yoon, S. H. *et al.* (1991) 'Late Pleistocene sedimentation on the Norwegian continental slope between 67° and 71°N', *Marine Geology*, 99(1–2), pp. 187–207.

Zhang, X. *et al.* (2014) 'Instability of the Atlantic overturning circulation during Marine Isotope Stage', *Geophysical Research Letters*, 41(12), pp. 4285–4293.

Zillén, L. M., Wastegård, S. and Snowball, I. F. (2002) 'Calendar year ages of three mid-Holocene tephra layers identified in varved lake sediments in west central Sweden', *Quaternary Science Reviews*, 21(14–15), pp. 1583–1591.